

**Theory and Applications for Sulfur Chemistry:
Hydrogen from Hydrogen Sulfide**

by

Ryan J. Gillis

B.S., Brigham Young University (2015)

Submitted to the Department of Chemical Engineering
in partial fulfillment of the requirements for the degree of
Doctor of Philosophy in Chemical Engineering

at the

MASSACHUSETTS INSTITUTE OF TECHNOLOGY

September 2020

© Massachusetts Institute of Technology 2020. All rights reserved.

Author
Department of Chemical Engineering
July 30, 2020

Certified by
William H. Green
Professor
Thesis Supervisor

Accepted by
Patrick S. Doyle
Graduate Officer, Department of Chemical Engineering

Theory and Applications for Sulfur Chemistry: Hydrogen from Hydrogen Sulfide

by

Ryan J. Gillis

Submitted to the Department of Chemical Engineering
on July 30, 2020, in partial fulfillment of the
requirements for the degree of
Doctor of Philosophy in Chemical Engineering

Abstract

In this thesis, I explore the chemistry of reacting sulfur species computationally and experimentally. The computational work centers around creating the capability to automatically predict the thermochemical properties of arbitrary sulfur molecules and the kinetic parameters of reactions between these species. A demonstration of this enhanced capability is shown in the automatic creation of detailed chemical mechanism describing the partial oxidation of dimethyl sulfide. The experimental work focuses on a hydrogen generating chemical cycle that uses a hydrogen sulfide feedstock. Initially exploring the reactivity of hydrogen sulfide, water, and iodine mixtures to form hydroiodic acid, two competing pathways were discovered. The more interesting pathway involved the reaction of hydrogen sulfide with iodine and water to form hydroiodic acid and sulfur dioxide. A bench-top prototype was created demonstrating the creation of hydrogen gas from hydrogen sulfide through this pathway. Technoeconomic modeling of the proposed process was conducted, suggesting both commercial and environmental motivation for adoption. The thesis concludes with a brief discussion of future work.

Thesis Supervisor: William H. Green
Title: Professor

Acknowledgments

At the end of this doctoral work, it often seems to me both that I just arrived at MIT and that I have only hazy memories of my life before coming to Cambridge.

My wife is the most important person in my life. I often feel incomplete without her. Her patience as I spent long hours writing and in lab enabled any success found in these pages.

My son, Diego, is both the bane of my sleeping hours and the delight of my waking ones. Although the life of an often absent father is the only one that he has known, his shy smile and eager gurgles provide me with both the drive to create and hope for a better world.

My parents and siblings also deserve mention for the impact that they had through my formative years. The love of learning and sense of responsibility they instilled have led me to where I am today.

Perhaps most impactful on this work is my adviser, Bill. His kindness, knowledge, and willingness to let me work on problems that I felt were important have shaped my development as a scientist, engineer, and human being.

I have also been fortunate to have found a home in many different communities at MIT and in Cambridge. My time as a Graduate Resident Tutor at McCormick has enriched my life with the many wonderful students that have become dear and close friends. The Green research group has also provided a model of collaborative work and learning. Filled with individuals smarter than I, they have always been a willing resource for my many questions and thoughtful collaborators. Finally, my faith community in the local Latter-day Saint congregation has been a family to me despite the thousands of miles from my siblings and parents.

Contents

1	Introduction	25
1.1	Sulfur: An Element of Contrasts	26
1.2	Sulfur Chemistry in Nature	26
1.2.1	Occurrence	26
1.2.2	Similarities and Differences	28
1.3	Sulfur Chemistry in Industry	30
1.3.1	Sources of Sulfur	30
1.3.2	End Uses of Sulfur	32
1.4	Hydrogen from Hydrogen Sulfide	34
1.4.1	Hydrogen Sulfide's Properties	35
1.4.2	Motivation	36
1.5	Review of Lab Tested Methods	38
2	Advances in Mechanism Prediction for Sulfur Species	43
2.1	Introduction	43
2.2	Methods	45
2.2.1	Quantum Chemical Calculations and Dataset Creation	45
2.2.2	Mechanism Generation	46
2.3	Results	47
2.3.1	Benchmarking of the Calculation Procedure	47
2.3.2	Dataset	49
2.3.3	Thermochemistry Prediction	50
2.3.4	Dimethyl Sulfoxide Oxidation	51

2.4	Discussion	53
2.4.1	Discrepancies between the Model and Experiment	53
2.4.2	Sensitivity Analysis of Major Species	56
2.5	Conclusion	57
3	Hydrogen from Hydrogen Sulfide and Water	59
3.1	Introduction	59
3.1.1	Hydrogen from Hydrogen Sulfide	59
3.2	Methods	61
3.3	Results	64
3.3.1	<i>HI</i> Formation Rate at Low H_2S Concentrations	65
3.3.2	<i>HI</i> Formation Rate at High H_2S Concentrations	68
3.3.3	Concentration Regimes of the Branching Pathways	69
3.3.4	Experimental Characterization of the Sulfur Products	70
3.3.5	Computational Evidence	71
3.4	Discussion	74
3.4.1	H_2 production from H_2S and H_2O	74
3.4.2	Thermochemical H_2S Decomposition to Elemental Sulfur	77
3.5	Conclusion	78
3.6	Acknowledgment	78
3.7	Author Contributions	78
4	Prototype Construction and Testing	81
4.1	Introduction	81
4.2	Safety Considerations	81
4.3	System Inventory	83
4.3.1	Material Selection	85
4.3.2	Reactor Details	86
4.4	Analytic Techniques	88
4.5	Initial Testing Results	89
4.6	Conclusion and Next Steps	90

5 Techno-economic Modeling and Process Viability Examination	93
5.1 Introduction	93
5.1.1 Thermochemical Cycles	94
5.1.2 Aspen Plus Modeling	96
5.1.3 Experimental Methods	97
5.2 Hydrogen Productions from Hydrogen Sulfide with Elemental Sulfur Byproducts	97
5.2.1 Water Solvent Process Model	97
5.2.2 Solvent Substitution Experiments	101
5.2.3 Isopropyl Alcohol Solvent Process Model	103
5.2.4 Solvent Selection	106
5.2.5 Process Viability and Comparison	107
5.3 Hydrogen Productions from Hydrogen Sulfide with Sulfur Dioxide Byproducts	108
5.3.1 Flowsheet	108
5.3.2 Energy and Utilities	112
5.3.3 Results and Viability	113
5.4 Conclusions	116
6 Summary and Recommendations for Future Work	117
6.1 Summary	117
6.2 Recommendations for Future Work	118
6.2.1 Sulfur Chemistry Expansion	118
6.2.2 Sour Gas Processing	119
6.3 Final Conclusion	120
A Tables	121
A.1 Group Additivity Values	122
A.2 Molecule Dataset	140
A.2.1 Validation Set Comparison	140
A.2.2 Full Molecule List with Thermochemistry	142

A.3	Kinetics	166
A.3.1	High Pressure Rate Constant Expressions	166
A.4	Experimental Appendix	172
A.4.1	Experimental Conditions	172
A.4.2	Experimental Index	173
A.5	Computational Appendix	174
A.5.1	Gas Phase Thermochemistries	174
B	Figures	193
B.1	Table of Contents	193
B.1.1	Transition States	193
B.1.2	Additional Sensitivity Plots	215
B.2	Experimental Details	215
B.2.1	Side reactions	215
B.2.2	Kinetic Inference on the Iodine Concentration Dependence . .	217
B.2.3	Sulfur Product Analysis	218
B.3	Computational Details	224
B.3.1	Thermochemistries	224
B.3.2	Branching Points	225

List of Figures

1-1	Illustration of the biogeochemical interconversion pathways for sulfur[125]	27
1-2	Analogous sulfur and oxygen-centric molecules.	29
1-3	Examples of sulfur molecules that seemingly break the octet rule.	29
1-4	Sulfur sources in the U.S. and Internationally in 2017.[11]	33
1-5	Sulfur consumption by end us in the U.S. in 2017.[11]	34
2-1	The molecules in the validation set.	46
2-2	A histogram sorting the deviations between experiment and calculation for 49 sulfur and oxygen containing molecules. The two outliers were excluded when determining the BAC values.	48
2-3	Parity plots comparing the calculated thermochemical value and the linear model prediction	50
2-4	A diagram of the key reaction pathways for the oxidation of dimethyl sulfide by hydroxyl radicals. $CH_3S(O)OH$, OCS and CH_2O were observed but not quantified in the experiments[7][15].	52
2-5	A. Comparison of the experiment and model at 280K and 1 bar of synthetic air over the course of the experiment. B. Comparison of the terminal selectivities of the experiment and model at 260K, 270K, 280K, 290K, and 298K.	53
2-6	Pathways for dimethyl sulfone formation in the model. None fully explained the dimethyl sulfone formation observed in the experiments.	54

2-7 Top three most sensitive kinetic and thermodynamic parameters for dimethyl sulfone formation. Thermodynamic sensitivities are reported in units of $\frac{mol}{kcal}$.	55
2-8 Top three most sensitive kinetic and thermodynamic parameters for thioformaldehyde formation. Thermodynamic sensitivities are reported in units of $\frac{mol}{kcal}$.	55
2-9 Top three most sensitive kinetic and thermodynamic parameters for dimethyl sulfoxide formation. Thermodynamic sensitivities are reported in units of $\frac{mol}{kcal}$.	57
2-10 Top three most sensitive kinetic and thermodynamic parameters for sulfur dioxide formation. Thermodynamic sensitivities are reported in units of $\frac{mol}{kcal}$.	57
3-1 Experimental Apparatus	64
3-2 Measured ion concentrations over a single typical experiment with annotations marking changes in the reactor conditions A. Addition of I_2 dissolved in isopropyl alcohol: This leads to a slight increase in the ion concentrations as a minor amount of I_2 reacts with H_2O to create HOI and HI . B. Beginning of H_2S flow: Feeding H_2S leads to a steady increase in the amount of each ion. C. Depletion of I_2 : The complete consumption of one of the reactants stops the formation of ion products. D. Ending of H_2S flow: This starts the flow of inert and the stripping of any leftover H_2S from the reactor	64
3-3 Ion concentrations during H_2S flow at low H_2S concentrations with various reactor conditions: A. Base B. Added Zn ions C. Reactor pH = 3 D. Excess of I_2 E. Reactor pH = 0 F. 4 Molar KI	66

3-4 A. Observed product to reactant ratio across three reactant concentrations using an alcohol cosolvent. The amount of iodide generated is nearly equal to the amount of hydronium ion generated. B. Observed product to reactant ratio across a range of reactant concentrations using an alcohol cosolvent.	69
3-5 Gas chromatogram of the toluene extract from the reactor volume and mass spectra of sulfur dioxide observed at the marked peak in the chromatogram	71
3-6 A free energy diagram at 298.15 K limited to species expected to be part of the hypothesized SO_2 formation mechanism as well as the first and last steps of the elemental sulfur pathway. The gas phase geometries, frequencies and energies are calculated at BP86 and CCSD(T) levels of theory and then corrected with estimated solvation energies and dissociation constants. Transition states are not included. On the main pathway one mole of HI is formed in each intermediate step and I_2 and H_2O alternate as the additional reactant. On the competing pathways H_2S replaces H_2O . All the energies are zeroed with respect to H_2S and calculated at 298.15 K. The details of the calculations can be found in Appendix B.	74
3-7 A flow diagram describing a potential series of reactions and separations resulting in the formation of H_2 and SO_2 from H_2S and H_2O . . .	75
3-8 A depiction of how the proposed process would reduce carbon emissions in a refinery setting.	76
4-1 Key steps of the process cycle to be tested with the minimum viable experiment.	83
4-2 Labeled diagram to be used with table	85
4-3 Gas-liquid contact reactor for the reaction of hydrogen sulfide with dissolved iodine	87

4-4	Conversion versus contact time plots for HI decomposition reaction using 1 gm of NORIT ROX 0.8 as catalyst at different temperatures and feedings. Dots correspond to experimental values, lines to calculated ones (az $HI = HI - H_2O$ azeotropic solutions; pure HI = pure gaseous HI[47]	88
4-5	Hydrogen iodide decomposition reactor	88
4-6	Photograph of the minimum viable experiment to test for hydrogen generation from hydrogen sulfide	89
4-7	TCD detection of hydrogen in the process outlet stream.	90
4-8	Upgraded experimental apparatus	92
5-1	Experimental Apparatus	97
5-2	Water Solvent Process Flow Diagram	98
5-3	Experimental results confirming HI formation in a pure isopropyl alcohol solvent	102
5-4	Isopropyl Alcohol Solvent Process Flow Diagram	103
5-5	Hydrogen sulfide decomposition process flowsheet producing SO_2 as a byproduct	109
5-6	Modeled conversion of the HI decomposition reactor	110
B-1	Top three most sensitive kinetic and thermodynamic parameters for methylthiol formate formation. Thermodynamic sensitivities are reported in units of $\frac{mol}{kcal}$	215
B-2	The discrepancy between I^- and H^+ in excess I_2 experiments can be partially explained by the formation of I_3^-	219
B-3	Reaction rate as a function of I_2 concentration. The reaction rate drops less than a factor of 2 as the concentration of I_2 drops a factor of 20, then falls to near 0 as the I_2 concentration falls near zero.	219
B-4	Comparison between experiments performed at high and low concentrations, using the alcohol cosolvent	220
B-5	Sample PXRD spectra, consistent with orthorhombic S_8	220

B-6 Chromatogram for a mixture of species formed during the reaction of H_2S and I_2 in isopropyl alcohol	221
B-7 Mass spectra at 6.7 minutes, identified as SO_2	221
B-8 Mass spectra at 9.8 minutes, hypothesized to be isopropyl iodide . . .	222
B-9 Mass spectra at 24.7 minutes, hypothesized to have the formula $C_6H_8O_3S$	222
B-10 Mass spectra at 26.9 minutes, hypothesized to have the formula $C_6H_{12}O_2S$	223
B-11 Free energy change of the overall reaction $H_2S + 3I_2 + 2H_2O \rightarrow 6HI + SO_2$ in gas phase using BP86/def2-TZVPD level of theory. One mole of HI is formed in each intermediate step and is not considered to react in the subsequent step. All the energies are zeroed with respect to H_2S and calculated at 298.15 K.	224
B-12 The alternative pathway in gaseous phase is represented in the above figure. One mole of HI is formed in each intermediate step and is not considered to react in the subsequent step. a. H_2S , b. I_2 , c. HSI , d. $HSSH$, e. $HSSI$, f. $HSSH$, g. $HSSI$, h. HS_4H , i. HS_4I , j. HS_5H , k. HS_5I , l. HS_6H , m. HS_6I , n. HS_7H , o. HS_7I , p. HS_8H , q. HS_8I , r. S_8 . All the energies are zeroed with respect to H_2S , calculated at 298.15 K and the units used are kcal/mol. It can be seen that the free energy change for the overall alternative reactive, $:8H_2S + 8I_2 \rightarrow 16HI + S_8$ is 26.6 kcal/mol (or) 3.32 kcal/mol for the reaction, $H_2S + I_2 \rightarrow 2HI + 1/8S_8$	224
B-13 Free energy change of the overall reaction $H_2S + 3I_2 + 2H_2O \rightarrow 6HI + SO_2$ in gas phase using CCSD(T)/AVTZ level of theory. One mole of HI is formed in each intermediate step and is not considered to react in the subsequent step. All the energies are zeroed with respect to H_2S and calculated at 298.15 K.	225

List of Tables

2.1	Bond additivity corrections fit from the 47 molecules in the validation set (all values in $\frac{kcal}{mol}$)	47
2.2	Deviations between the calculated (CBS-QB3) and experimental enthalpy of formation values with and without the newly calculated sulfur BACs (all values in $\frac{kcal}{mol}$)	47
2.3	Summary statistics for the GAV fit to the calculated values (units of $\frac{kcal}{mol}$, $\frac{cal}{mol \cdot K}$)	50
4.1	Labeled components of the minimum viable experimental system . . .	83
4.1	Labeled components of the minimum viable experimental system . . .	84
4.1	Labeled components of the minimum viable experimental system . . .	85
5.1	Parameters taken from the process model	113
5.2	Calculated values from net present value analysis based on the parameters observed in the process model	113
5.3	Comparison between the proposed process and the current dominant market technologies	115
A.1	Sulfur-centered group additivity values. Enthalpies are given in $\frac{kcal}{mol}$. Entropies and heat capacities are given in $\frac{cal}{mol \cdot K}$	124
A.1	Sulfur-centered group additivity values. Enthalpies are given in $\frac{kcal}{mol}$. Entropies and heat capacities are given in $\frac{cal}{mol \cdot K}$	125
A.1	Sulfur-centered group additivity values. Enthalpies are given in $\frac{kcal}{mol}$. Entropies and heat capacities are given in $\frac{cal}{mol \cdot K}$	126

A.1	Sulfur-centered group additivity values. Enthalpies are given in $\frac{kcal}{mol}$. Entropies and heat capacities are given in $\frac{cal}{mol \cdot K}$	127
A.1	Sulfur-centered group additivity values. Enthalpies are given in $\frac{kcal}{mol}$. Entropies and heat capacities are given in $\frac{cal}{mol \cdot K}$	128
A.1	Sulfur-centered group additivity values. Enthalpies are given in $\frac{kcal}{mol}$. Entropies and heat capacities are given in $\frac{cal}{mol \cdot K}$	129
A.1	Sulfur-centered group additivity values. Enthalpies are given in $\frac{kcal}{mol}$. Entropies and heat capacities are given in $\frac{cal}{mol \cdot K}$	130
A.1	Sulfur-centered group additivity values. Enthalpies are given in $\frac{kcal}{mol}$. Entropies and heat capacities are given in $\frac{cal}{mol \cdot K}$	131
A.2	Oxygen-centered group additivity values. Enthalpies are given in $\frac{kcal}{mol}$. Entropies and heat capacities are given in $\frac{cal}{mol \cdot K}$	132
A.3	Carbon-centered group additivity values. Enthalpies are given in $\frac{kcal}{mol}$. Entropies and heat capacities are given in $\frac{cal}{mol \cdot K}$	133
A.3	Carbon-centered group additivity values. Enthalpies are given in $\frac{kcal}{mol}$. Entropies and heat capacities are given in $\frac{cal}{mol \cdot K}$	134
A.3	Carbon-centered group additivity values. Enthalpies are given in $\frac{kcal}{mol}$. Entropies and heat capacities are given in $\frac{cal}{mol \cdot K}$	135
A.3	Carbon-centered group additivity values. Enthalpies are given in $\frac{kcal}{mol}$. Entropies and heat capacities are given in $\frac{cal}{mol \cdot K}$	136
A.3	Carbon-centered group additivity values. Enthalpies are given in $\frac{kcal}{mol}$. Entropies and heat capacities are given in $\frac{cal}{mol \cdot K}$	137
A.3	Carbon-centered group additivity values. Enthalpies are given in $\frac{kcal}{mol}$. Entropies and heat capacities are given in $\frac{cal}{mol \cdot K}$	138
A.3	Carbon-centered group additivity values. Enthalpies are given in $\frac{kcal}{mol}$. Entropies and heat capacities are given in $\frac{cal}{mol \cdot K}$	139
A.4	All comparisons are in $\frac{kcal}{mol}$	140
A.4	All comparisons are in $\frac{kcal}{mol}$	141

A.5 A list of the molecules used in the study and their thermodynamic properties. Enthalpies are given in $\frac{kcal}{mol}$. Entropies and heat capacities are given in $\frac{cal}{mol \cdot K}$	143
A.5 A list of the molecules used in the study and their thermodynamic properties. Enthalpies are given in $\frac{kcal}{mol}$. Entropies and heat capacities are given in $\frac{cal}{mol \cdot K}$	144
A.5 A list of the molecules used in the study and their thermodynamic properties. Enthalpies are given in $\frac{kcal}{mol}$. Entropies and heat capacities are given in $\frac{cal}{mol \cdot K}$	145
A.5 A list of the molecules used in the study and their thermodynamic properties. Enthalpies are given in $\frac{kcal}{mol}$. Entropies and heat capacities are given in $\frac{cal}{mol \cdot K}$	146
A.5 A list of the molecules used in the study and their thermodynamic properties. Enthalpies are given in $\frac{kcal}{mol}$. Entropies and heat capacities are given in $\frac{cal}{mol \cdot K}$	147
A.5 A list of the molecules used in the study and their thermodynamic properties. Enthalpies are given in $\frac{kcal}{mol}$. Entropies and heat capacities are given in $\frac{cal}{mol \cdot K}$	148
A.5 A list of the molecules used in the study and their thermodynamic properties. Enthalpies are given in $\frac{kcal}{mol}$. Entropies and heat capacities are given in $\frac{cal}{mol \cdot K}$	149
A.5 A list of the molecules used in the study and their thermodynamic properties. Enthalpies are given in $\frac{kcal}{mol}$. Entropies and heat capacities are given in $\frac{cal}{mol \cdot K}$	150
A.5 A list of the molecules used in the study and their thermodynamic properties. Enthalpies are given in $\frac{kcal}{mol}$. Entropies and heat capacities are given in $\frac{cal}{mol \cdot K}$	151
A.5 A list of the molecules used in the study and their thermodynamic properties. Enthalpies are given in $\frac{kcal}{mol}$. Entropies and heat capacities are given in $\frac{cal}{mol \cdot K}$	152

A.5 A list of the molecules used in the study and their thermodynamic properties. Enthalpies are given in $\frac{kcal}{mol}$. Entropies and heat capacities are given in $\frac{cal}{mol \cdot K}$	153
A.5 A list of the molecules used in the study and their thermodynamic properties. Enthalpies are given in $\frac{kcal}{mol}$. Entropies and heat capacities are given in $\frac{cal}{mol \cdot K}$	154
A.5 A list of the molecules used in the study and their thermodynamic properties. Enthalpies are given in $\frac{kcal}{mol}$. Entropies and heat capacities are given in $\frac{cal}{mol \cdot K}$	155
A.5 A list of the molecules used in the study and their thermodynamic properties. Enthalpies are given in $\frac{kcal}{mol}$. Entropies and heat capacities are given in $\frac{cal}{mol \cdot K}$	156
A.5 A list of the molecules used in the study and their thermodynamic properties. Enthalpies are given in $\frac{kcal}{mol}$. Entropies and heat capacities are given in $\frac{cal}{mol \cdot K}$	157
A.5 A list of the molecules used in the study and their thermodynamic properties. Enthalpies are given in $\frac{kcal}{mol}$. Entropies and heat capacities are given in $\frac{cal}{mol \cdot K}$	158
A.5 A list of the molecules used in the study and their thermodynamic properties. Enthalpies are given in $\frac{kcal}{mol}$. Entropies and heat capacities are given in $\frac{cal}{mol \cdot K}$	159
A.5 A list of the molecules used in the study and their thermodynamic properties. Enthalpies are given in $\frac{kcal}{mol}$. Entropies and heat capacities are given in $\frac{cal}{mol \cdot K}$	160
A.5 A list of the molecules used in the study and their thermodynamic properties. Enthalpies are given in $\frac{kcal}{mol}$. Entropies and heat capacities are given in $\frac{cal}{mol \cdot K}$	161
A.6 A list of the radical species used in the study, their thermodynamic properties, and the source of the data. Enthalpies are given in $\frac{kcal}{mol}$. Entropies and heat capacities are given in $\frac{cal}{mol \cdot K}$	162

A.6 A list of the radical species used in the study, their thermodynamic properties, and the source of the data. Enthalpies are given in $\frac{kcal}{mol}$. Entropies and heat capacities are given in $\frac{cal}{mol \cdot K}$.	163
A.6 A list of the radical species used in the study, their thermodynamic properties, and the source of the data. Enthalpies are given in $\frac{kcal}{mol}$. Entropies and heat capacities are given in $\frac{cal}{mol \cdot K}$.	164
A.6 A list of the radical species used in the study, their thermodynamic properties, and the source of the data. Enthalpies are given in $\frac{kcal}{mol}$. Entropies and heat capacities are given in $\frac{cal}{mol \cdot K}$.	165
A.7 Rate expressions determined with transition state theory by the author. Prefactors (A) are provided in units of s^{-1} for unimolecular reactions and $\frac{cm^3}{mol s}$. Temperatures are provided in K.	167
A.7 Rate expressions determined with transition state theory by the author. Prefactors (A) are provided in units of s^{-1} for unimolecular reactions and $\frac{cm^3}{mol s}$. Temperatures are provided in K.	168
A.8 Rate expressions used in model generation that were taken from literature experiments or calculations. Prefactors (A) are provided in units of s^{-1} for unimolecular reactions and $\frac{cm^3}{mol s}$. Temperatures are provided in K.	170
A.8 Rate expressions used in model generation that were taken from literature experiments or calculations. Prefactors (A) are provided in units of s^{-1} for unimolecular reactions and $\frac{cm^3}{mol s}$. Temperatures are provided in K.	171
A.9	172
A.10 An index of experiments concerning the reaction of H_2S and I_2 .	173
A.11 Computed BP86, CCSD(T), and MRCI geometries of H_2S , I_2 , HSI , HI , H_2O , $HSOH$, $HOSI$, $HOSOH$, $HOS(O)I$ and SO_2 . Experimental numbers are provided wherever available from the NIST molecular database	174

A.12 Computed BP86, CCSD(T), Davidson corrected MRCI energies; and T1 diagnostics of H_2S , I_2 , HSI , HI , H_2O , $HSOH$, $HOSI$, $HOSOH$, $HOS(O)I$ and SO_2	177
A.13 Computed and available experimental frequencies of H_2S , I_2 , HSI , HI , H_2O , $HSOH$, $HOSI$, $HOSOH$, $HOS(O)I$ and SO_2	178
A.14 Energies, geometrical parameters, frequencies and zero point energies (ZPE) of $HSSH$, $HSSI$, $HSSSH$, $HSSI$, HS_4H , HS_4I , HS_5H , HS_5I , HS_6H , HS_6I , HS_7H , HS_7I , HS_8H , HS_8I , and S_8 computed at BP86/def2-TZVPD is listed below. The following convention is used for the larger molecules: In $HSSI$, rS(2)S(3) would refer to the distance between the second atom and the third atom(first sulfur and the second sulfur atom).	181
A.15 Computed and experimental rotational constants (GHz) of $HOSOH$	191

Chapter 1

Introduction

Chapter one introduces the reader to sulfur chemistry, its current position in the economy, spaces for innovation, and the principal impetus for the the work.

Chapter two describes advances in predictive chemistry for sulfur species. Specifically, it will focus on the automatic prediction of thermodynamic properties. As a demonstration of these enhancements the detailed chemical mechanisms of several sulfur systems will be presented.

Chapter three describes the initial experimental work characterizing the reactions between hydrogen sulfide and iodine to create hydrogen iodide. Variance in the observed products were explored.

Chapter four describes the building and testing of a prototype H_2S processing unit based on the aforementioned observations.

Chapter five describes the implications of the observations. Techno-economic modeling describing the economic and environmental motivators that might drive the adoption of newly proposed chemical processes based on the observed chemistry.

Chapter six will briefly overview the key implications of the work and the possible future directions for research on predictive sulfur chemistry and the production of hydrogen from hydrogen sulfide.

1.1 Sulfur: An Element of Contrasts

Sulfur occupies a rather peculiar position among the elements. One of the oldest of the identified elements, its history and nature is filled with contradiction. The central component of two amino acids (methionine and cysteine) and as such critical for countless proteins and life itself, sulfur is none-the-less often encountered in the form of noxious gases, lethal to humans in minute concentrations. Similarly, sulfuric acid is the highest produced commodity chemical by mass, crucial for the production of artificial fertilizers[120], and yet the disposal of hydrogen sulfide and sulfur dioxide, waste streams from energy producers, results in tens of billions of dollars in damages and mitigating expenditures.[21] This balance of the tremendous impact of feeding half the world's population with the capability in many forms of terrible destruction invites the study of sulfur chemistry.

These invitations have not gone unheeded, and through human history sulfur has found both imagined uses in the ancient arts of alchemy and practical application in medicine, agriculture, and warfare. It is into this legacy that this work finds its home: leveraging the uniqueness, mitigating the hazards, finding new value propositions, and understanding old mysteries pertaining to sulfur chemistry.

1.2 Sulfur Chemistry in Nature

1.2.1 Occurrence

Sulfur is the fifth most common element on earth, with two primary isotopes ^{32}S and ^{34}S as well as a bevy of less abundant and stable isotopes. These atoms were born deep in the belly of stars and are present on earth in a wide variety of configurations from the relatively inert sulfide and sulfate minerals to gases both organic and inorganic. Notably elemental sulfur, uncoupled from other elements, is also found in significant quantities particularly near geothermal or volcanic activity[106]

Naturally dynamic, sulfur moves between the crust, the oceans, and the atmosphere as it cycles between its mineral, organic, and inorganic forms. For example,

anaerobic biologic activity converts sulfate minerals into elemental sulfur. Elemental sulfur in contact with the atmosphere oxidizes to create sulfur oxides, especially sulfur dioxide gas. Sulfur dioxide will further oxidize in the microscopic water droplets of the atmosphere creating sulfuric acid which will rain down onto the crust, reacting with a variety of minerals to convert back into sulfate minerals. This highlights but one of a nearly infinitely variable chains by which sulfur shifts between its many forms as it moves through the natural world.

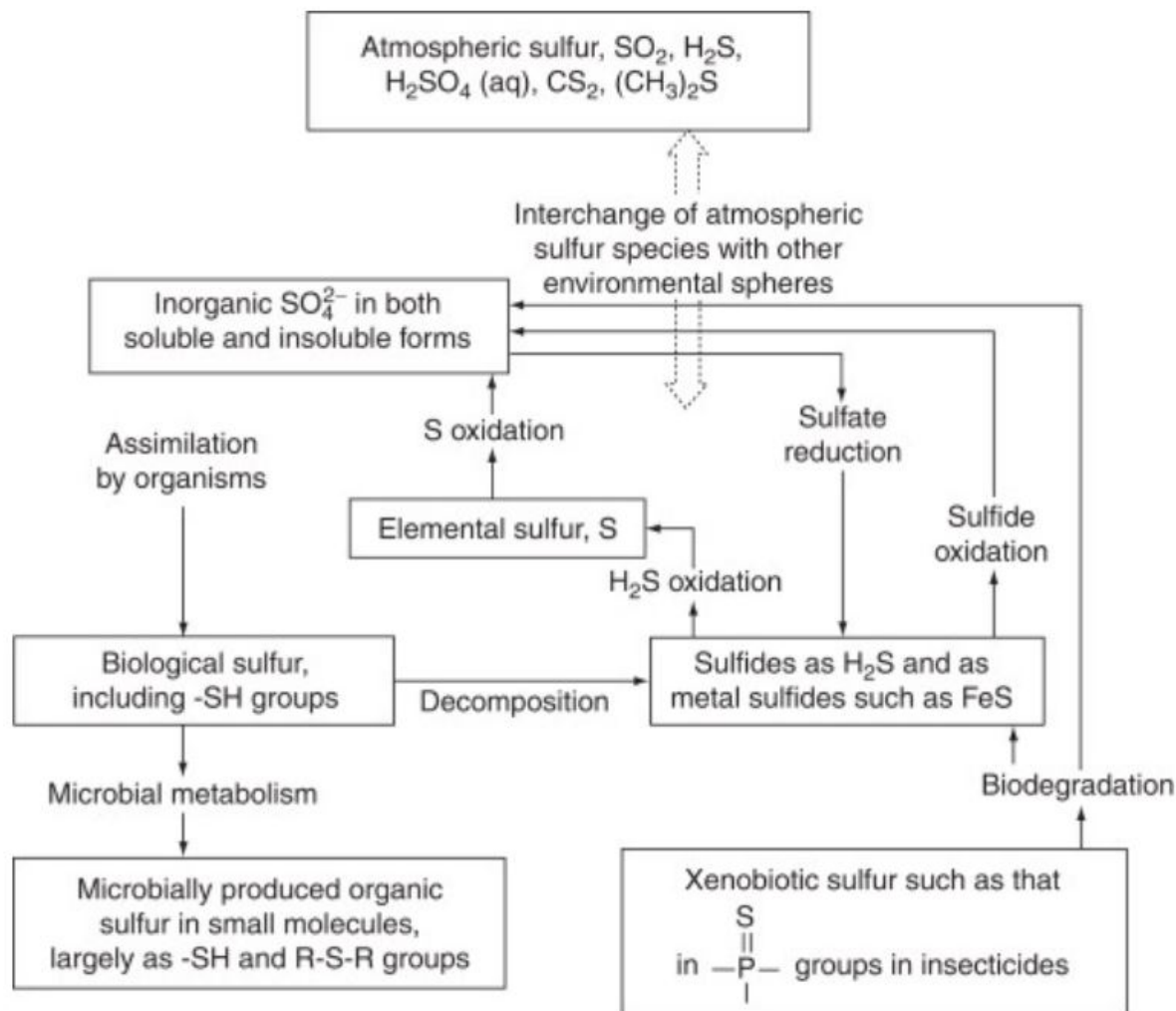


Figure 1-1: Illustration of the biogeochemical interconversion pathways for sulfur[125]

This flexibility in nature and ease of intra-conversion, as illustrated all around us in the natural world, hints at its potential for greater application. In a world filled with the detailed customization of designer molecules, each with an ultra-niche

purposes, sulfur stands as an extremely simple, yet flexible material.

1.2.2 Similarities and Differences

The nature of elements is rooted in their electronic structure. Sulfur is no exception and is located among the chalcogens in group 16 of the periodic table, positioned below oxygen and above selenium.

1 H Hydrogen 1.008	2 He Helium 4.003	3 Li Lithium 6.94	4 Be Beryllium 9.012	5 B Boron 10.81	6 C Carbon 12.011	7 N Nitrogen 14.007	8 O Oxygen 15.999	9 F Fluorine 18.998	10 Ne Neon 20.180
11 Na Sodium 22.990	12 Mg Magnesium 24.305	21 Sc Scandium 44.956	22 Ti Titanium 47.867	23 V Vanadium 50.942	24 Cr Chromium 51.996	25 Mn Manganese 54.938	26 Fe Iron 55.845	27 Co Cobalt 58.933	28 Ni Nickel 58.693
19 K Potassium 39.098	20 Ca Calcium 40.078	39 Y Yttrium 88.906	40 Zr Zirconium 91.224	41 Nb Niobium 92.906	42 Mo Molybdenum 95.95	43 Tc Technetium [97]	44 Ru Ruthenium 101.07	45 Rh Rhodium 102.906	46 Pd Palladium 106.42
37 Rb Rubidium 85.468	38 Sr Strontium 87.62	56 Cs Cesium 132.905	57 * 57 - 70	71 Lu Lutetium 174.967	72 Hf Hafnium 178.49	73 Ta Tantalum 180.948	74 W Tungsten 183.84	75 Re Rhenium 186.207	76 Os Osmium 190.23
87 Fr Francium [223]	88 Ra Radium [226]	103 Lr Lawrencium [262]	104 Rf Rutherfordium [267]	105 Db Dubnium [270]	106 Sg Seaborgium [269]	107 Bh Bohrium [270]	108 Hs Hassium [270]	109 Mt Moscovium [278]	110 Ds Darmstadtium [281]
*Lanthanide series									
89 Ac Actinium [227]	90 Th Thorium 232.038	91 Pa Protactinium 231.036	92 U Uranium 238.029	93 Np Neptunium [237]	94 Pu Plutonium [244]	95 Am Americium [243]	96 Cm Curium [247]	97 Bk Berkelium [247]	98 Cf Californium [251]
**Actinide series									
57 La Lanthanum 138.905	58 Ce Cerium 140.116	59 Pr Praseodymium 140.908	60 Nd Neodymium 144.920	61 Pm Promethium [145]	62 Eu Europium 150.36	63 Gd Gadolinium 151.964	64 Tb Terbium 157.25	65 Dy Dysprosium 162.500	66 Ho Holmium 164.930
67 Er Erbium 167.259	68 Tm Thulium 168.934	69 Yb Ytterbium 173.045	70 Lv Livermorium [293]	71 Fr Flerovium [289]	72 Nh Nharguni [286]	73 Mc Moscovium [289]	74 Lv Livermorium [293]	75 Ts Tennessine [293]	76 Og Oganesson [294]

A cursory glance shows that sulfur has 6 valence electrons and would be expected to behave similarly to oxygen. This is in fact often true with many analogues between stable oxygen and sulfur molecules (for example water and hydrogen sulfide) and between oxygen and sulfur functional groups (for example alcohols and thiols).

However, these are only the beginning of the nuanced characteristics of sulfur chemistry and it is the differences that lead to sulfur's unique characteristics. Perhaps the most striking bonding characteristic of sulfur is the sheer number of different bonding patterns sulfur compounds can have. With six valence electrons, it would be expected that sulfur would tend to have two bonds, similar to water and oxygen in general. However, in practice sulfur compounds have two, four, or six bonds in

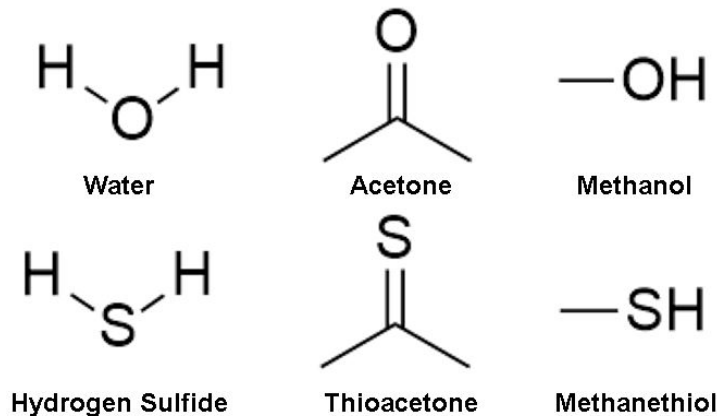


Figure 1-2: Analogous sulfur and oxygen-centric molecules.

a wide variety of arrangements seemingly with up to 12 valence electrons. The reasons for this flexibility are somewhat beyond the scope of this introduction, but the key idea is that highly resonant species with stable charges on the sulfur allow for both the preservation of the octet rule and more than two bonds.[94] For convenience throughout this work these types of species will be represented with these higher than expected bond numbers in accordance with historical precedent and convenience. Sulfur itself can exhibit an oxidation state of anywhere from -2 to +6. These flexibilities allow sulfur to exist both as sulfuric acid (H_2SO_4) and hydrogen sulfide (H_2S).

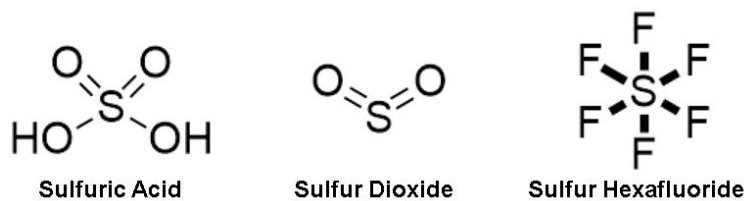


Figure 1-3: Examples of sulfur molecules that seemingly break the octet rule.

Another interesting chemical aspect of sulfur is its internal bonding capability. Significantly larger than oxygen, sulfur bonds to itself readily but not irreversibly. These "medium strength" internal bonds are one of their crucial biological features, with slight changes in *in vivo* conditions triggering coupling and uncoupling of sulfur atom pairs.[112] These coupling and uncoupling events can drastically change the conformation of the larger protein, often in ways key to its functionality.[55] Another

consequence of their looser, and as a consequence much more flexible, bonds is their ability to form long chains of sulfur atoms. In fact, elemental sulfur exists in a wide variety of allotropes shifting between optimally stable rings, crowns, and chains with slight changes in temperature and pressure. In some conditions chains of hundreds of thousands of sulfur atoms can form, creating liquids of extreme viscosity.[151]

Understanding the nature of sulfur atoms themselves form the foundation upon which thermodynamic, kinetic, and practical calculation and experimentation are based.

1.3 Sulfur Chemistry in Industry

To this point only cursory mention has been given to the sources and end uses of sulfur in our modern society. These will be briefly outlined here along with an estimate of their magnitude.

1.3.1 Sources of Sulfur

Hydrocarbon Processing

Over 75% of the sulfur enters the economy through the oil and gas industry.[11] The sulfur content of crude oil varies by source but can commonly exceed 2%. Natural gas can present even more extreme sulfur content with developed wells exceeding 20% hydrogen sulfide concentration. The production of sulfur in this way is more or less involuntary and scales with the production of fuels as firms are mandated to remove the sulfur from their products.

Production of sulfur from hydrocarbons processing has risen sharply in the last decade and is expected to continue to rise. This increase is driven by several long term market trends. First, the sulfur content of oil and gas extracts is rising. This is to be expected as firms deplete sweeter, higher value resources. Second, the allowable sulfur content in fuels is dropping dramatically due to regulations both regional and international. Notably the International Maritime Organization has reduced the al-

lowed sulfur content in bunker fuels by 85% in 2020.[3] U.S., European, and Chinese environmental agencies have also recently tightened their sulfur content limits.[1] The removal of sulfur from these previously very sour fuels is accelerating sulfur production at the processing sites. Third, the scale of fuel production in general is rising.[5] Excepting the recent and temporary reduction in consumption due to the 2020 recession, fuel consumption has dramatically increased in the past decade. Higher levels of fuel processing have thus led to greater amounts of sulfur production.

This increasing production is not universally met with increased consumption. Particularly in locations far from heavy chemical industry, the cost of transporting the material can lead to its accumulation. Hundreds of thousands of metric tons of sulfur, involuntarily produced in hydrocarbon processing are just dumped in giant pyramids. These stockpiles present hazards as their combustion would release catastrophically toxic amounts of sulfur dioxide into the atmosphere. Despite these risks, the pyramids to grow at locations around the world.

Before moving on to other, less significant sources of sulfur in our economy, I will briefly give a slightly more detailed description of the steps in sulfur production. As hydrocarbon extracts are processed, a key step is removing the sulfur content from the stream. In oil refining this is done primarily through hydrodesulfurization, a process by which chemically entrained organic sulfur is reacted with hydrogen over a catalyst to produce hydrogen sulfide and a lower sulfur content hydrocarbon.[130] This hydrogen sulfide is typically separated from other light gases using acid gas removal units, most commonly absorbing the hydrogen sulfide into aqueous solutions of alkyl amines.[127] This hydrogen sulfide stream is then converted to elemental sulfur with the Claus process, reacting with oxygen over a catalyst to produce steam and elemental sulfur.[78] Natural gas processing has a similar flow, separating the hydrogen sulfide from the natural gas stream and then producing elemental sulfur with a Claus unit. The elemental sulfur is then shipped from the refineries and gas processing sites to sulfuric acid production and other end users.

Smelting and Other Sources

After hydrocarbon processing, the next highest source of sulfur is as a byproduct of metal smelting. Notably copper, but also zinc, lead, and molybdenum are often mined as sulfide ores. Smelting these metals involves first roasting, or reacting the sulfide ore with oxygen at elevated temperatures to produce sulfur dioxide and the metal oxide, before these metal oxides are reduced to their purified metallic form. Similarly to oil and gas processing, this sulfur production is as a byproduct and scales with the production of the metal itself.

Note that while hydrocarbon processing produces elemental sulfur, this process produces sulfur dioxide. Firms are not able to ignore this byproduct as easily as the oil and gas processors can dump solid sulfur in piles. Sulfur dioxide atmospheric emissions are tightly regulated as they contribute significantly to acid rain and general respiratory health issues. As a result smelters convert the sulfur dioxide byproduct into sulfuric acid and it is this sulfuric acid that enters the market in this form.

Finally, elemental sulfur can also be directly extracted from the earth's crust. This typically happens through the Frasch process, where superheated water is used to melt sub-surface sulfur, pressurizing it back through a pipe as a liquid to the surface where it is cooled, collected and sold.[83] Near volcanic and other geologic activity more conventional mining occurs at a smaller scale. However, due largely to the increasing involuntary production of sulfur as a byproduct of hydrocarbon and metal production these sulfur extraction technologies are becoming less common.

1.3.2 End Uses of Sulfur

With the glut of sulfur entering the market involuntarily it is in strange symmetry that the highest consumption of any chemical in the world is sulfuric acid. Sulfuric acid is produced from either elemental sulfur or sulfur dioxide byproducts. In fact, almost all of the elemental sulfur is converted to sulfuric acid before use in other industries. This conversion is most commonly performed through the Contact process. Briefly, the elemental sulfur inlet is burned to form sulfur dioxide, then catalytically oxidized

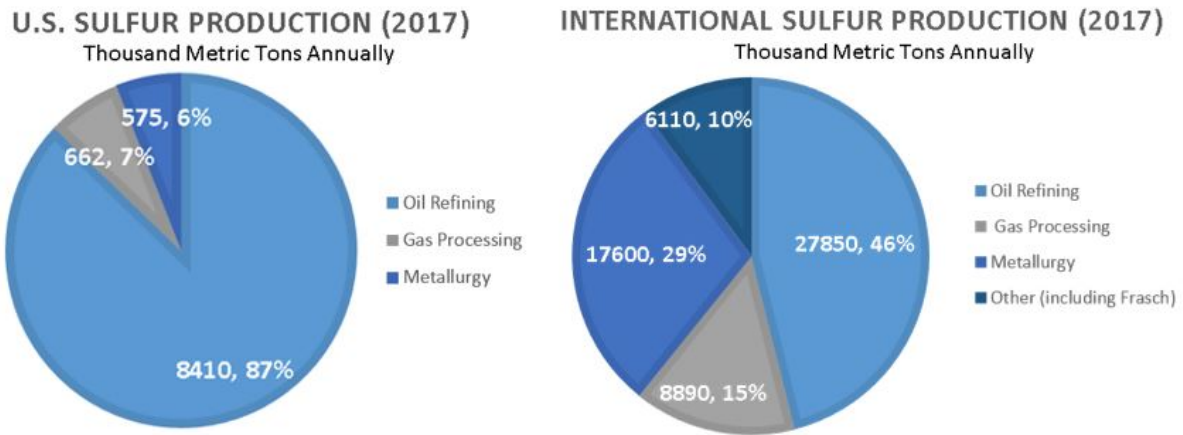


Figure 1-4: Sulfur sources in the U.S. and Internationally in 2017.[11]

to form sulfur trioxide. Next the sulfur trioxide is reacted with additional sulfuric acid to form oleum, before finally having water added to form highly concentrated sulfuric acid.[120]

Sulfuric acid has a wide range of applications and uses both used directly and as a feedstock into the production of other chemicals. In fact its consumption is so widespread and fundamental that it is often used as a proxy for the productivity of a developed country. The more sulfuric acid they consume, the higher their standard of living across a wide range of metrics.

The highest volume end use of sulfur is in fertilizers. In the U.S. alone over 5 million metric tons of sulfur are used annually to produce phosphatic and nitrogenous fertilizers.[11] These fertilizers are key to industrial farming and the high food production that sustains the world's growing population. It is estimated that half of the people alive today have food because of these synthetic fertilizers. [128] Sulfur also is a major component in most fungicides, herbicides, and insecticides.

Oil and gas refining are the next highest end use of sulfuric acid. This sulfuric acid is principally used to convert lighter hydrocarbons to high octane fuel additives in a process called alkylation.

Leaching is a type of metal extraction that require high volumes of strong acids like sulfuric acid. It is next on the list and works by dissolving metals from ores into sulfuric acid which is accumulated before recovery of the metals takes place. Copper,

uranium, and vanadium are the principal metals extracted this way.

There are a multitude of additional uses for sulfuric acid that I will only briefly touch on. The first step of paper production requires sodium sulfide to convert wood chips into wood pulp. Lead acid batteries, like the ones that start a majority of light duty vehicles, use sulfuric acid as the main electrolyte. Other newer batteries also use sulfur compounds as electrolytes. Steel production also requires sulfuric acid to remove impurities and sulfur forms a key component of many explosives.[11]

Sulfur is a key material in our economy crucial to the production of food, fuels, metals, building materials, energy storage devices, and electronics. It is unsurprising that it serves as a proxy for overall productivity and standard of living.

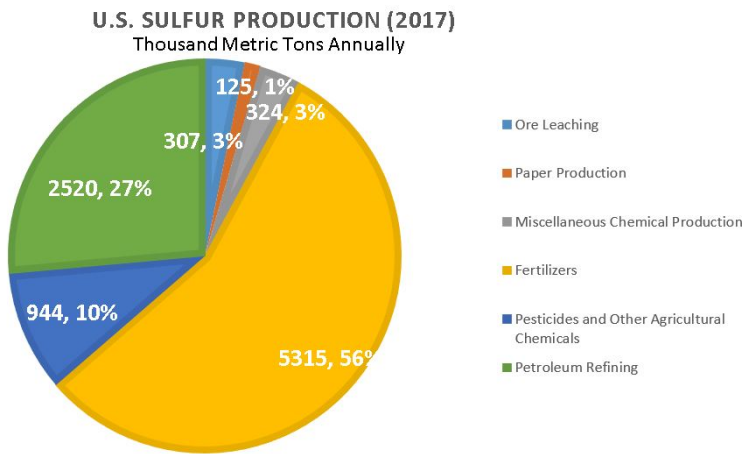


Figure 1-5: Sulfur consumption by end use in the U.S. in 2017.[11]

1.4 Hydrogen from Hydrogen Sulfide

Having introduced sulfur in general, I will now specifically highlight hydrogen sulfide, a toxic gas that is both naturally abundant and produced as an unwanted byproduct at high volumes in oil and gas processing. Particularly I will address current methods that extract value from this historically undesirable product. This will form the foundation and backdrop of later chapters' discussions of newly invented processes for hydrogen production from hydrogen sulfide.

1.4.1 Hydrogen Sulfide's Properties

Hydrogen sulfide is perhaps the simplest sulfur molecules comprised of just a single sulfur atom covalently bonded to two hydrogen atoms, in a structure analogous to water. Unlike water however, hydrogen sulfide is a colorless gas at temperatures above -60 Celsius. At ambient temperatures it has a density heavier than air at 1.36 kg/m^3 and a characteristic pungent odor, most similar to rotten eggs.

For human experimentalists the most pressing characteristic of this gas is its extreme toxicity. Binding with the iron in mitochondrial enzymes, hydrogen sulfide above a concentration of 0.1% causes instantaneous loss of consciousness at only the first breath. Lower concentrations can be equally deadly over long time periods with the U.S. Occupational Safety and Health Administration (OSHA) setting a maximum permissible concentration of 20 parts per million. Perhaps even more impressive than government standards is the fact that human noses have evolved to detect hydrogen sulfide at concentrations below 1 part per billion.

Despite the significant hazard that its toxicity holds, hydrogen sulfide is a byproduct of both the production of nature gas and the desulfurization of other heavier hydrocarbon extracts. The scale of both of these practices cause tens of millions of metric tons of hydrogen sulfide to enter our economy, demanding processing at huge scales. To give a sense of these scales, at an average U.S. oil refinery over 50,000 metric tons of hydrogen sulfide are produced each year[11], while large refineries dealing with especially sour crudes can exceed this factor by over an order of magnitude.

Hydrogen sulfide is also created when biomass is degraded in anaerobic conditions. Notably, this occurs at landfills and during wastewater treatment, both at the municipal level but more significantly in agricultural processing facilities.[116] As newer methods are developed for the generation of energy vectors from biomass, the creation of hydrogen sulfide from the decomposition will accelerate even further. Currently though, production from these sources are significantly lower than production from oil and gas operations.

As would be expected this industrial production is a major pain point for these

industries. Not only are they producing a volatile gas product with no value, but it is a gas product that is deadly at even relatively low concentrations. Even at concentrations below which it threatens human health, hydrogen sulfide has a pungent smell that makes working in such locations problematic. Human health aside, the gas also is a materials hazards, degrading all but the most highly alloyed metals. This introduces a materials and design challenge to systems that need to already be extremely over-designed because of their inherent hazards.

As mentioned previously, Claus processing represents that primary method by which hydrogen sulfide is converted to elemental sulfur at the large scale. However, if you are at a well-site or water treatment facility the scale of hydrogen sulfide production is mismatched to that which can be handled by the Claus process. A wide variety of processes have sprung up to fill these lower volume treatment needs, including the Lo-Cat, SulFerox, Thiopaq, and CrystaSulf branded methods. Among these Lo-Cat and SulFerox both use reaction with iron particles or ions to absorb and convert the hydrogen sulfide into elemental sulfur. Thiopaq is unique in that it uses thiophylic bacteria to convert solvated hydrogen sulfide into elemental sulfur. CrystaSulf avoids the materials and phase challenges of the aqueous methods by using sulfur solvating non-aqueous solvents for the reaction and regeneration steps. However, each of these methods, while scaling to smaller input volumes, are much more expensive. Operating costs for these specialty systems can be up to \$2000 per metric ton of sulfur treatment. These costs can be prohibitive and a major factor in the profitability of individual sour natural gas wells.

1.4.2 Motivation

It is the work of the latter half of this thesis to present the foundation of a new method for hydrogen production from hydrogen sulfide. Having provided a background in both the nature of hydrogen sulfide and the position of sulfur in our market, I will now argue the merit of such an advance.

Before I do this however, let me highlight the challenges. As previously stated hydrogen sulfide is an incredibly toxic material that requires extreme caution and

preventative measures when performing research. Further the corrosivity of the gas and other associated sulfur compounds multiplies this safety hazard, while introducing additional financial challenges. These problems are real and unavoidable when dealing with hydrogen sulfide. Chemistry deals with the essence of material, and the essence of hydrogen sulfide is pretty unfriendly to human interaction.

Despite these inherent challenges the production of hydrogen gas from hydrogen sulfide has many advantages as well. First, there is a market need for both hydrogen gas and hydrogen sulfide processing. Thus, new methods that create hydrogen from hydrogen sulfide simultaneously fill both of these market pain points, which are especially sharp at high volumes such as those created by oil refining firms. This dual functionality also provides additional flexibility for firms that might have a need for hydrogen sulfide treatment, but little use for hydrogen or the reverse. This would be the case at natural gas sites where hydrogen production is an upside with the primary motivation in low cost hydrogen sulfide processing.

Related to this is the fact that the processing of hydrogen sulfide is a cost to these firms, and if it could instead be used then it could be a potentially "free" feedstock for the production of hydrogen. The current market-dominant hydrogen production process is steam methane reforming. This method inherently requires natural gas as its inlet to produce hydrogen. In fact the majority of cost associated with producing hydrogen by this method is from the opportunity cost associated with procuring the natural gas feedstock.[r18] If hydrogen sulfide is used as a feedstock, then this, typically dominant, feedstock procurement cost drops to nothing.

The scale of hydrogen sulfide processing is also commensurate in scale with the demand for hydrogen at some refineries. This is unsurprising because one of the main uses for hydrogen gas at these facilities is in their desulfurization units. Restated, refineries purchase hydrogen gas to desulfurize fuels creating hydrogen sulfide. if the hydrogen sulfide can be converted back into hydrogen gas than a continuous recycle loop could be established, reducing or even eliminating the need for additional hydrogen procurement.

Hydrogen production is also a very carbon intensive process. As was mentioned,

the key feedstock for producing hydrogen is natural gas. Pulling hydrogen atoms off of carbons naturally fills our atmosphere with more carbon, which in turn contributes to climate change. In fact, some estimate that over 2.3% of all anthropogenic carbon emissions are the result of hydrogen production. This is more or less unavoidable as a nature of the hydrocarbon feedstock, and the difficult of capturing and storing carbon dioxide. Production of hydrogen from hydrogen sulfide in contrast lacks this inherent carbon production. This is not to say that its production will be carbon-free, as any chemical processing activity requires the manipulation of pressure and temperature, activities that require energy and thus cause carbon emissions. However, it is limited to these types of emissions, excluding emissions that are a result of the chemistry itself.

Finally, for those investigating low carbon hydrogen production, hydrogen sulfide presents an easier chemical barrier compared to water, another highly studied source of low carbon hydrogen. The free energy of formation of water is -54.6 kcal/mol compared to the -8.0 kcal/mol of hydrogen sulfide. This means that the unavoidable energy requirement for hydrogen production from hydrogen sulfide is approximately 1/7th that of water. Comparing to equivalent amounts of hydrogen production, this thermodynamic barrier is roughly equivalent to the production of hydrogen from methane. While this does not guarantee or directly inform on the utility costs of producing hydrogen by these methods, it does introduce a lower bound. Having that lower bound similar to steam methane reforming, rather than water electrolysis provides the possibility of a profitable process.

Overall, despite the challenges, the market need and underlying chemistry both provide encouragement in exploring new ideas for hydrogen production from hydrogen sulfide.

1.5 Review of Lab Tested Methods

To date, no method for producing hydrogen from hydrogen sulfide has been commercialized. However, scientists and researchers have been studying this possibility for at

least the last five decades and have explored a wide variety of options. A brief summary of some of these ideas will be presented, along with the barriers that prevented their adoption.

There are many ways to categorize different types of chemical processes. Here when describing the various methods that have been explored for producing hydrogen sulfide I will focus on the nature of the energy in the process. A thermodynamic price must be paid to convert lower energy reactants into higher energy products, but that price can be paid with heat, electricity, light, or some combination of these. I will first focus on thermal methods as they dominate the hydrogen production industry today and are generally accepted to scale better than either electric or photo based processes.

The simplest approach to producing hydrogen from hydrogen sulfide is thermal decomposition. As with most chemicals, if the temperature is high enough entropy effects dominate energetic stability and the hydrogen sulfide will decompose into hydrogen gas and sulfur vapors. For hydrogen sulfide this begins to occur around 1200 K with even higher temperatures required for significant conversion.[70] The kinetics of this process can be aided by various catalysts[95] [60] but the stumbling block of this approach is the high temperatures, and thus high energy requirement, and high carbon cost of producing hydrogen in this way.

Another thermal approach involves the use of thermochemical cycles. These are series of reactions that together amount to one overall, usually highly unfavorable reaction. For example, they have been extensively studied with relation to the decomposition of water.[156] While breaking these difficult reactions into steps does not change the overall energy requirements, it can ease separations and allow more efficient input of energy into the system. There are many different flavors of these cycles but I will briefly describe just two. First, we have two step adsorption/desorption cycles. The first step involves the adsorption of hydrogen sulfide onto a metal oxide or sulfide, commonly nickel[26] [74], iron[36], with more recent interest in zirconium to produce a metal sulfide and hydrogen gas. In the second step of this cycle the solid adsorbent is heated and reduced back to the oxide or lower order sulfide with

sulfur vapor evolved. These systems work, but are difficult to scale and suffer severe long term efficiency losses as the surface area of the absorbents rapidly drops. Another notable thermochemical cycle for the decomposition of hydrogen sulfide is a modified Bunsen cycle. The original Bunsen cycle was developed by General Atomics and used 3 chemical reaction steps to theoretically decompose water.[156] The hydrogen sulfide variant was proposed by Wang across a series of papers over the last decade.[145][146] [85] However, several well-known problems associated with the Bunsen cycle persist even in this hydrogen sulfide variant. However, its use of iodine intermediates, particularly hydrogen iodide as a precursor to hydrogen gas formation is of interest.

In general I would say that there are many technically viable methods to produce hydrogen gas from hydrogen sulfide. However, they each run into issues with their high temperatures negating any advantage, economic or environmental, that could be gained by these alternate hydrogen sulfide processing methods.

Non-thermal methods are generally grouped as electrolytic, photochemical or some combination. Electrochemical schemes dissolve the hydrogen sulfide typically in aqueous solutions and use electrical current to drive the dissociation of the sour gas into hydrogen and sulfur. Significant effort has gone into selecting just the right electrode surfaces, electrolytes, and conditions. However, non-soluble sulfur has a tendency to inhibit already questionable efficiency over the course of operation.[68] [69] Photochemical methods seem particularly appealing at first glance, as they require neither the high temperatures of thermal methods, nor the electricity costs of electrolytic methods. However, the issues arise in scaling these technologies out of the lab. For the chemistry to occur they have to have a certain incidence of specific types of radiation. In tanks making elemental sulfur light is quickly blocked, significantly inhibiting the efficiency of the processes. Despite these challenges significant work has gone into finding just the right catalysts that can provide just the right environment for the photolysis of hydrogen sulfide.[105] [25] [67] [129][32] Combinations of photolysis and electrolysis have also been explored.[87] [158]

While this is not an exhaustive list of every explored method for hydrogen sulfide

decomposition it should provide the reader a general sense of their function and why they have not achieved commercialization yet. Excellent reviews written by Chakma and Zaman[152] and more recently by Reverberi et al. [115] further explore this topic.

Chapter 2

Advances in Mechanism Prediction for Sulfur Species

2.1 Introduction

Before moving into more applied research into sulfur gas processing, I will first describe advances I have made in the automated modeling of sulfur species. This chapter is, in part, based on my publication in ChemSystemsChem, 2, e1900051, 2020, Ryan J. Gillis and William H. Green, Thermochemistry Prediction and Automatic Mechanism Generation for Oxygenated Sulfur Systems: A Case Study of Dimethyl Sulfide Oxidation.

Chemical systems often resist simplification because the number of important species and reactions far exceeds anyone's definition of simple. However in spite of the inherent complexity, understanding the detailed chemistry of reacting systems is crucial in a wide variety of pursuits, both academic and commercial. Entwined within this detailed chemistry lie key combustion characteristics such as the ignition delay[124], extinction strain rate[89], octane number[154], or flame speed[96]. Other natural systems are also better understood with a knowledge of the chemistry, including the formation pathways and fates of species in the atmosphere[133]. Similarly, biological systems are often described in complex reaction networks[44] that attempt to predict or describe the behavior of feedback loops [114] that control the behavior

of cells and organisms. Industrially, the conditions leading to desired products, such as a biocrude from biomass[139], and the conditions that lead to unwanted products, such as particulate matter[117] within a furnace or combustion engine, can be clarified with the detailed chemistry. These are just a few examples of the very practical knowledge that come from detailed chemical mechanisms.

Automatic reaction mechanism generation is a powerful tool to understand complex reactive systems and describe the detailed chemistry. The Reaction Mechanism Generator (RMG) software[54] is an implementation of this concept that allows the user to create detailed kinetic models for use in the design, optimization, or understanding of reactors, engines, or fuels.[53]

Sulfur chemistry is an area that is not well explored by automatic mechanism generation. There are many inherent challenges when modeling sulfur systems including their variable oxidation and valence, the unique reactions in which they participate, and the only limited experimental characterization of the kinetics and thermodynamics of sulfur species, especially radicals. Previous efforts have allowed for the modeling of low valence sulfur species,[141] [28] but many important systems involve highly oxidized, high and changing valence, sulfur species.

Automatic mechanism generation methods require rapid evaluations of the thermochemistry of individual molecules. Accurate quantum chemical calculations are far too time intensive to be practical in this setting, requiring other methods of predicting thermochemistry. An older relatively simple solution is to use a linear model known as Benson group additivity[17]. This method assigns each heavy atom thermochemical values based on its characteristics and the characteristics of the atoms to which it is bonded. A molecule's thermochemistry is then predicted by summing over each heavy atom. Newer, more nuanced machine learning methods promise greater predictive power, albeit with less transparency[118] [86].

This work describes the expansion of the RMG software to higher valence sulfur species, with an emphasis on thermochemistry prediction for high valence sulfur molecules. This focus involves the creation of a sulfur species database, and the implementation of a simple prediction method to estimate the thermochemistry for

an arbitrary molecule. The chapter closes with a case study demonstrating the new functionality, examining the partial oxidation of dimethyl sulfide. The validity of the automatically generated model was tested by comparing the model to experimental work that measured the concentration of major species during the hydroxyl radical initiated oxidation of dimethyl sulfide.[7]

2.2 Methods

2.2.1 Quantum Chemical Calculations and Dataset Creation

First, 47 sulfur species with experimentally measured enthalpies of formation were used to test the accuracy of the calculation methods.[97] [92] [102] [22] [90] [91] [93] [24] The molecules in this validation set were selected because they both had experimental measurements for enthalpy of formation and were comprised of 10 or fewer heavy atoms. An approach using b3lyp/CBSB7 for the geometry optimization, frequency calculation, and hindered rotor scans along with CBS-QB3 for the energy calculation was selected. The thermochemistry and rate calculations were performed using the rigid-rotor harmonic oscillator (RRHO) approximation with corrections for internal rotors, using the Arkane software in the RMG package[54]. Each rotating dihedral within the molecule was treated as a 1-dimensional independent rotor and stepped in 10 degree increments through the full rotation. An optimization constrained by the stepped dihedral was performed at each of these steps. Additional details on the hindered rotor treatment can be found in the work of Sharma et al[121]. Rate calculations were performed using conventional Transition State Theory (TST) with Eckart tunelling corrections.[42] Constraints on computational resources required the use of different versions of Gaussian for these calculations. The majority of the calculations used Gaussian03[49], with several exceptions noted in detail in Appendix A.[50][51] Bond additivity corrections (BAC) were determined with a least squares fit to the 47 validation molecules for C-S, S-S, S-H, S-O, and S=O bonds. All other BAC corrections came from the work of Paraskevas et al.[107]

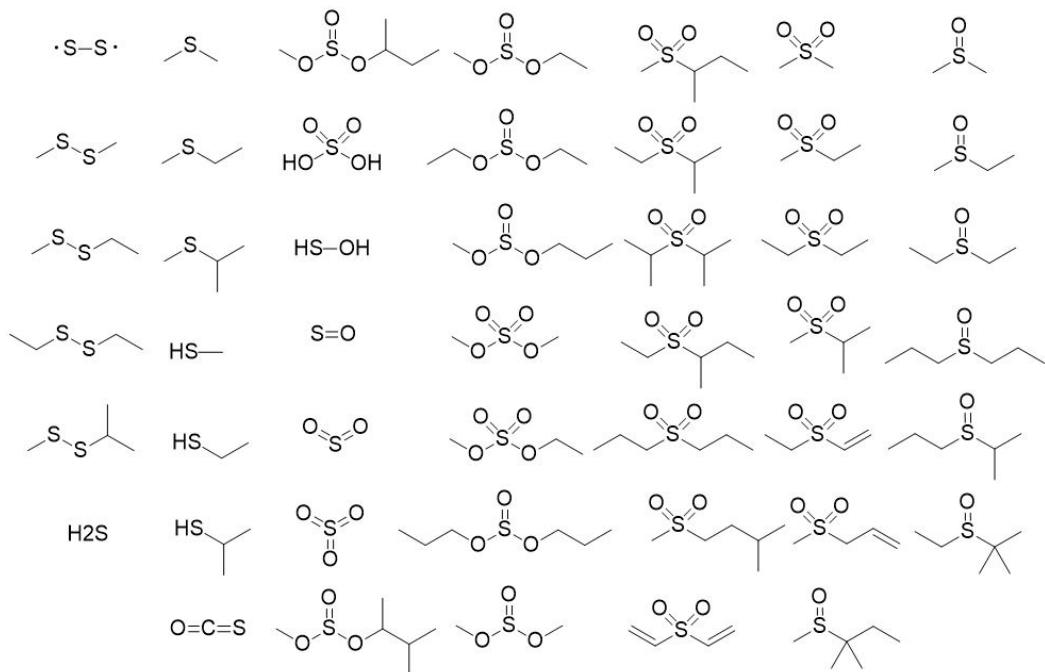


Figure 2-1: The molecules in the validation set.

The validated procedure was then used to calculate 255 oxygenated sulfur molecules. These 255 molecules were combined with 185 molecules from Class[27] and Vandeputte[139]. This combined list of 440 molecules was used to derive group additivity values for the prediction of the thermochemistry of sulfur containing molecules.

2.2.2 Mechanism Generation

The second section of the work uses the Reaction Mechanism Generator software with the augmented thermochemistry predictions to create a detailed kinetic model. The RMG software creates kinetic models by iteratively adding species and reactions, starting from user specified initial conditions. The reactions are automatically generated using known reaction templates and their corresponding kinetics are estimated using a hierarchical tree of rate estimation rules. The thermochemistry of each species is estimated using a combination of published libraries and group additivity methods. A detailed description of the algorithm can be found in the work of Gao. [54]

The detailed chemical mechanism was created based on the conditions studied by

Barnes et al.[7]. Specifically, a concentration of 25 ppm hydrogen peroxide and 15 ppm dimethyl sulfide in a bath of artificial air at 1 bar total pressure and a temperature of 298K was used in model generation. The input file annotated to include the RMG-Py and RMG-database version numbers used in mechanism generation is supplied in the Appendix A.

2.3 Results

2.3.1 Benchmarking of the Calculation Procedure

Before creating a dataset, we validated our methods for oxygenated sulfur molecules. This was done by comparing calculated enthalpies of formation to experimentally measured enthalpies for 47 molecules. The lack of experimental data precludes similar comparisons to entropies and heat capacities.

First, bond additivity corrections (BACs) for C-S, S-S, S-H, S-O, and S=O bonds were calculated using a least squares fitting from these 47 molecules. These BAC values were combined with those suggested by Paraskevas[107] for molecules containing carbon, hydrogen, and oxygen. The BAC corrections and their effect on the accuracy of the test set is shown in Tables 1 and 2.

Table 2.1: Bond additivity corrections fit from the 47 molecules in the validation set (all values in $\frac{kcal}{mol}$)

Bond Additivity Corrections (CBS-QB3)				
S-O	S=O	C-S	S-H	S-S
0.07	-1.03	1.08	-0.69	-1.46

Table 2.2: Deviations between the calculated (CBS-QB3) and experimental enthalpy of formation values with and without the newly calculated sulfur BACs (all values in $\frac{kcal}{mol}$)

Summary Statistics		
	w/out Sulfur BACs	w/Sulfur BACs
RMSD	1.70	1.23
MAD	1.42	1.08
Avg. Deviation	1.09	0.03

Naturally, the newly fit BACs lowered the deviation between calculated and experimental values. However, they also noticeably corrected a persistent overprediction of the enthalpy in oxygenated sulfur compounds by the CBS-QB3 method. A histogram of deviations between the calculations and experiment is shown below in Figure 2. A detailed list of the deviation between each experimental and calculated value is included in Appendix A.

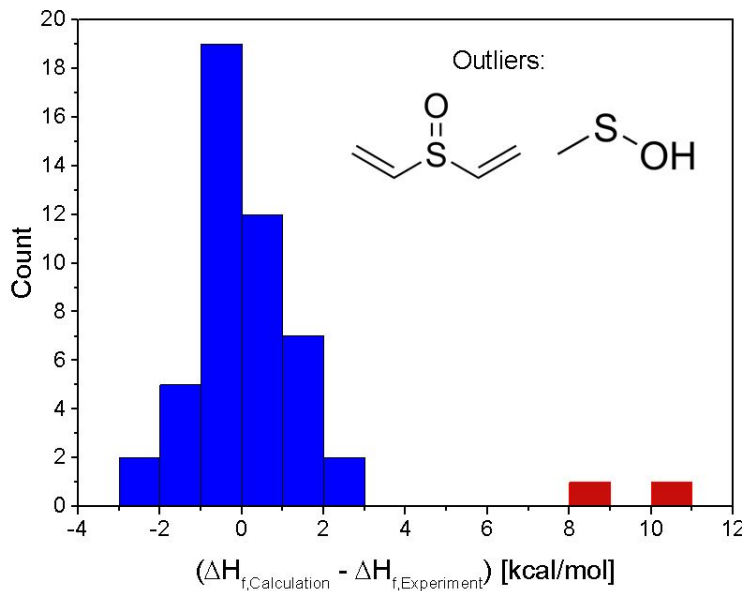


Figure 2-2: A histogram sorting the deviations between experiment and calculation for 49 sulfur and oxygen containing molecules. The two outliers were excluded when determining the BAC values.

This set of 47 molecules excluded 2 potential experimental data sources. Divinyl sulfoxide and methane sulfenic acid each had only a single experimental enthalpy measurement source[143] [136] and the measured value for each deviated wildly from our calculated values (8.33 and 10.15 kcal/mol off respectively). This could be due to a weakness of our calculation method or it could be from inaccurate experimental numbers. Either way, these values were excluded from the least squares fit for bond additivity corrections.

2.3.2 Dataset

Content with the accuracy of the method, we selected 255 primarily oxidized and high valence sulfur molecules to supplement existing sulfur species thermochemistry data. When considering what molecules should be included in this dataset, we balanced representation of typical highly oxygenated sulfur molecule motifs with very unstable, semi-randomly generated, molecules. The emphasis on unstable molecules might seem odd. However, thermochemistry prediction from a dataset is inherently limited by the nature of the molecules in the training data, and both experimental and computational studies often focus on relatively low energy molecules. In contrast, automatic mechanism generation, in combinatorial fashion, generates a wide range of structures, from the stable to the extremely unstable. If the datasets used to predict thermochemistry are disproportionately filled with low energy molecules, then the predictions for the energy will necessarily skew low. Thus, there is an important, and largely unfilled, gap in knowledge about the thermochemical nature of high energy and high valence sulfur species. For this reason, about 150 molecules that we calculated for this study were randomly generated, usually creating high energy structures. This was done by starting with a structure such as a sulfur atom double bonded to an oxygen atom and iteratively adding atoms in a semi-random manner.

Once a list of molecules was selected, their geometries, frequencies, hindered rotor scans, and CBS-QB3 energies (including BACs) were computed. The thermochemical descriptors (enthalpy, entropy, and heat capacities) were then calculated using the Arkane software as described in the Methods section. We combined these 255 molecules (240 stable, 15 radical) with the low valence sulfur thermochemistries calculated by Class[27] and Vandeputte[141] to create a dataset with 440 molecules (368 stable, 72 radical). Using this combined dataset a group additivity scheme was created and implemented in the Reaction Mechanism Generator software. The thermochemical descriptors of all 440 molecules in the dataset are found in Appendix A. Additionally, the 255 molecules that were calculated as a part of this work have their geometries, frequencies, and zero-point energies reported.

2.3.3 Thermochemistry Prediction

After compiling a dataset of sufficient size, we turned to the problem of predicting thermochemistry from this information. In this work we fit the data to a group additivity scheme, not because we believe it is the most accurate prediction method, but rather because it integrates well with the automated mechanism generating software that we will use in the creation of a dimethyl sulfide oxidation mechanism. However, the information provided could and should be integrated into more sophisticated prediction schemes. The 368 stable species were fit by adjusting 200 sulfur containing group additivity values.[81] Non-sulfur containing groups present in the molecules were assigned values according to the RMG-database used in mechanism generation. The 200 group values are included in Appendix A along with the anticipated uncertainties for their enthalpy component. Summary and fitting statistics are included in Table 3. The quality of the fit is emphasized in the parity plots comparing the calculated and fit enthalpy and entropy of formation shown in Figure 3.

Table 2.3: Summary statistics for the GAV fit to the calculated values (units of $\frac{kcal}{mol}$, $\frac{cal}{mol K}$)

	$\Delta H_f(298 K)$	$\Delta S_f(298 K)$	$C_p(300 K)$	$C_p(500 K)$	$C_p(1000 K)$
MAD	0.73	0.99	0.36	0.31	0.22
RMSD	1.18	1.62	0.59	0.49	0.39

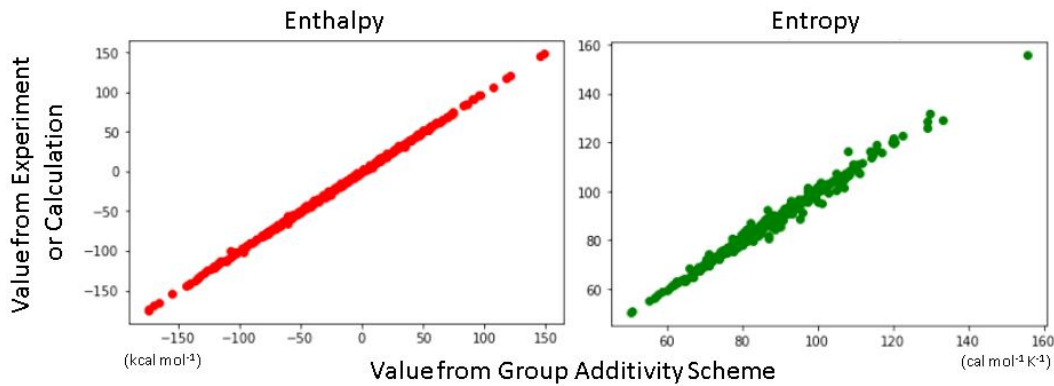


Figure 2-3: Parity plots comparing the calculated thermochemical value and the linear model prediction

The 72 radical species were used to generate hydrogen bond increment (HBI)

corrections as defined by Lay et al.[82] This information is organized in a tree structure in the version of RMG used in mechanism generation and conveniently accessible through the Molecule Search Tool at rmg.mit.edu. Together the stable species group additivity scheme and hydrogen bond increment corrections allow thermochemistry prediction for a variety of sulfur species.

2.3.4 Dimethyl Sulfoxide Oxidation

Experiment and Motivation

As a test for our new thermochemistry estimation scheme, we selected the OH initiated oxidation of dimethyl sulfide. This system was chosen because the primary products of the reaction span a wide range of highly oxygenated sulfur structures, from sulfoxides to sulfones to carbonyl sulfide and more. Further, this is an important system for understanding the formation of sulfuric acid in the atmosphere. Thus, this test case itself provides value and insight for pollutant formation. Finally, there are many experimental studies on this system which provide ample experimental validation and comparison for the system. [12] [7] [137] [19] [57] Among these the work by Albu, Barnes et al.[7] will be most rigorously compared, because they provide the largest amount of quantitative information about a variety of products across a range of temperature conditions. A review of the system by Barnes et al. provides a convenient aggregation of known kinetic and thermodynamic parameters of the system as well as a general reaction scheme with which to compare our automatically generated mechanism.[15]

While dimethyl sulfide oxidation seems an ideal comparison system, it does have challenges. Because the oxidation is at low temperatures small errors in estimates of transition state energies have large effects on the estimates of the rate constants. Further, there is some uncertainty about the efficiency of the hydrogen peroxide photolysis by the lamps used in the experiments. The lamp forces the reaction as it continuously creates hydroxyl radicals from hydrogen peroxide. To model this behavior the concentration of hydroxyl radical was held fixed while solving the concentra-

tion profiles. This precludes any validation of the time scale of reaction (dependent on the intensity of the lamps), but still allows product profiles and selectivities to be tested. This also creates uncertainty as the photolyzing lamps could have affected the chemistry of more than just the hydrogen peroxide species. The Appendix A has detailed information about the kinetic information, from literature or newly calculated, supplied in the mechanism generation process.

Dimethyl Sulfide Reaction Mechanism

The automatically generated mechanism contains 43 species and 122 reactions (included in full with the Appendix A). A limited set of the major reaction pathways are illustrated below in Figure 4. Consistent with previous studies the model identifies two primary pathways by which the dimethyl sulfide reacts. They differ in importance based on temperature, with low temperature conditions favoring the addition pathway and its production of dimethyl sulfoxide, and the high temperatures favoring hydrogen abstraction leading to sulfur dioxide products.

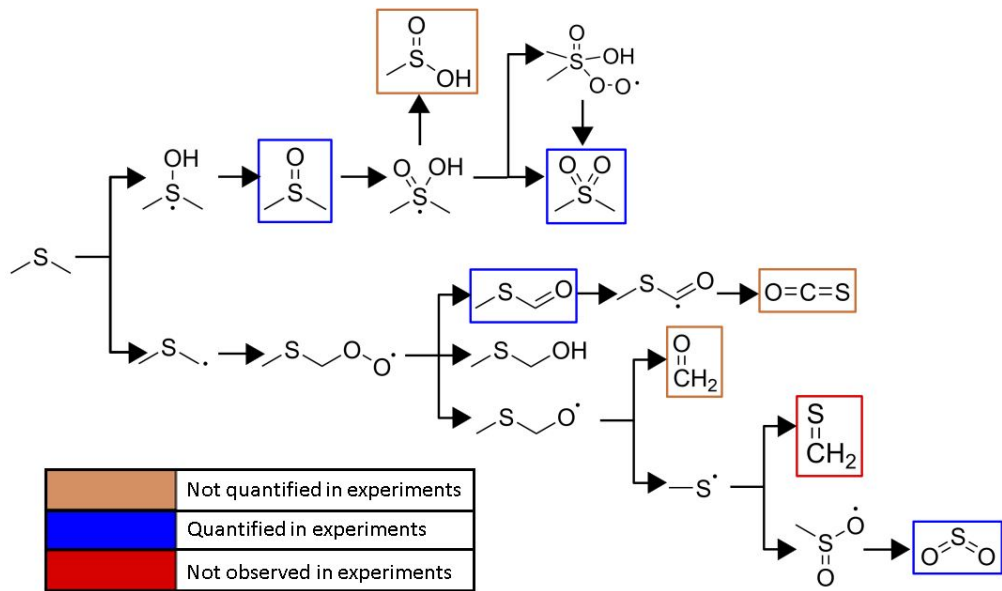


Figure 2-4: A diagram of the key reaction pathways for the oxidation of dimethyl sulfide by hydroxyl radicals. $\text{CH}_3\text{S(O)OH}$, OCS and CH_2O were observed but not quantified in the experiments[7][15].

Experimental Validation

The selectivity of the four major species observed and quantified by Albu, Barnes et al.[7] (dimethyl sulfoxide, dimethyl sulfone, sulfur dioxide, and methyl thiolformate) were compared to the model's predictions in Figure 5. Relatively good agreement is found between the experimental results and the model predictions for 3 of the 4 major species. The remaining sulfur-containing species that were observed but not quantified by Albu, Barnes et al.[7] also appeared in the model, e.g. carbonyl sulfide and methyl sulfenic acid. Many of the non-sulfur compounds observed but not quantified in the experiment also appeared in the model, including formaldehyde, methyl hydroperoxide, and carbon dioxide. The temperature dependence of the branching between the sulfur dioxide and dimethyl sulfoxide formation pathways also seems to be well captured by the model.

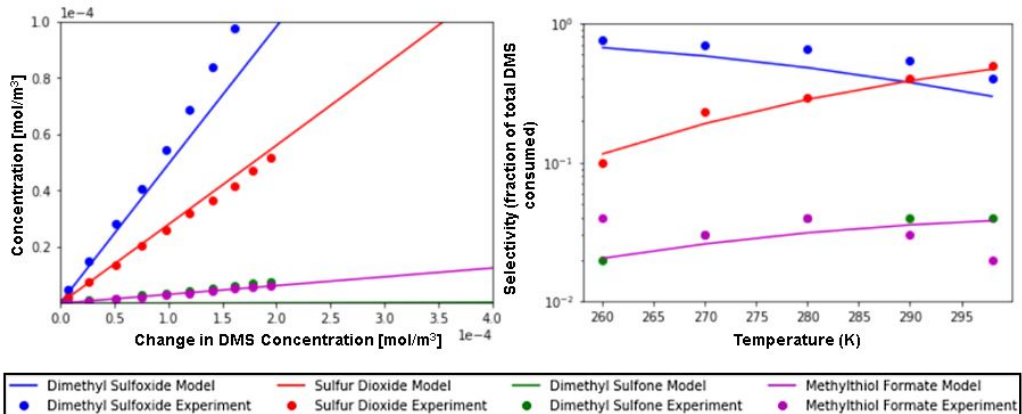


Figure 2-5: A. Comparison of the experiment and model at 280K and 1 bar of synthetic air over the course of the experiment. B. Comparison of the terminal selectivities of the experiment and model at 260K, 270K, 280K, 290K, and 298K.

2.4 Discussion

2.4.1 Discrepancies between the Model and Experiment

There are some aspects in which our automatically generated model does not agree with experiments. Most notably the model fails to predict significant formation of

dimethyl sulfone ($DMSO_2$), one of the major (2 – 4% selectivity) products. Many pathways to form dimethyl sulfone were explored in the model, but none proved to have a low enough barrier to lead to the level of dimethyl sulfone formation reported in the experiments. The pathways to dimethyl sulfone that appear in the model are illustrated in Figure 6 and the sensitivity analysis in Fig. 7. The transition states and kinetic details for each of the computed reactions along these pathways can be found in the Appendix A. Due to the low temperature of the reaction system, dimethyl sulfone formation is especially sensitive to barrier heights. Which, if any, of these paths to dimethyl sulfone is the significant pathway remains an ongoing question.

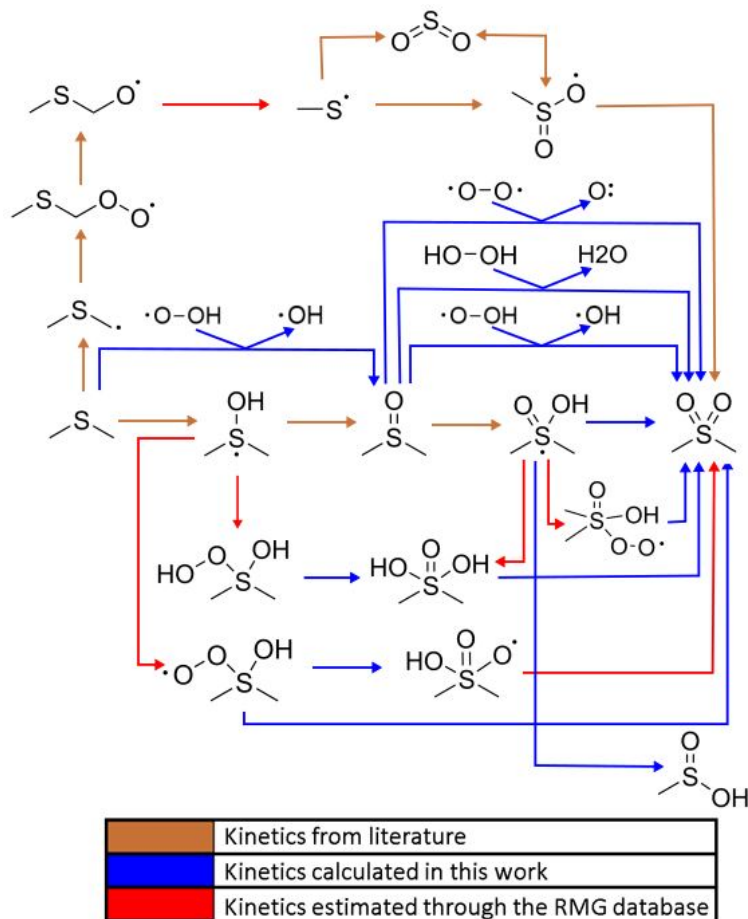


Figure 2-6: Pathways for dimethyl sulfone formation in the model. None fully explained the dimethyl sulfone formation observed in the experiments.

Additionally, the model predicts the formation of significant amounts of thioformaldehyde. This is a product that is not observed in any of the experimental

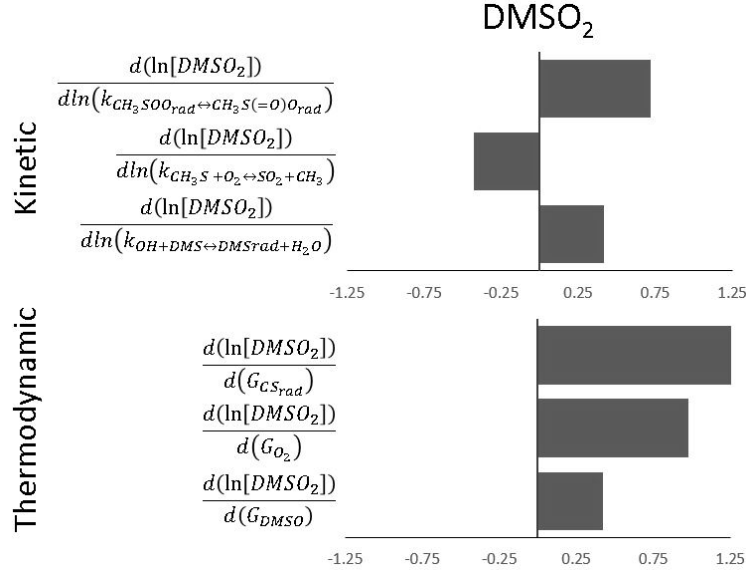


Figure 2-7: Top three most sensitive kinetic and thermodynamic parameters for dimethyl sulfone formation. Thermodynamic sensitivities are reported in units of $\frac{mol}{kcal}$.

works. [7] [12] [15] The sensitivity analysis (Figure 8) suggests that perhaps the hydrogen abstraction of methylthiyl radicals by O_2 is being significantly over-predicted. Alternatively, the reactivity of the CH_2S species could be underpredicted or the species could have been missed by the experimental analysis technique.

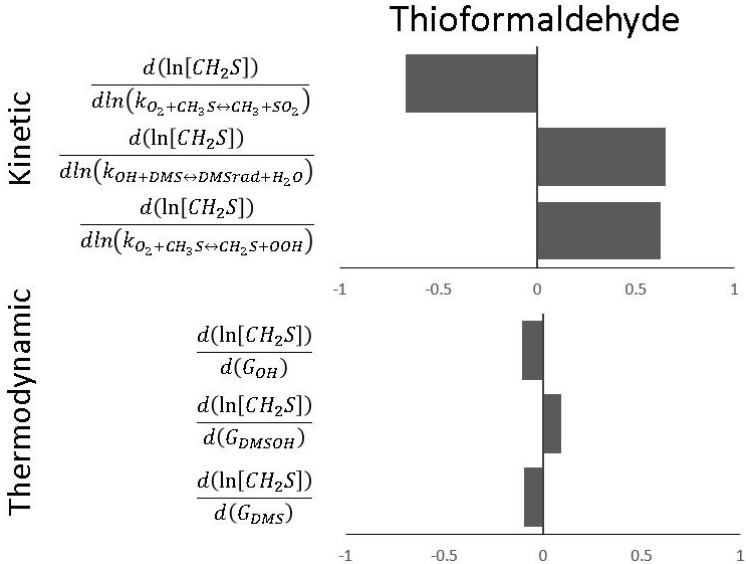


Figure 2-8: Top three most sensitive kinetic and thermodynamic parameters for thioformaldehyde formation. Thermodynamic sensitivities are reported in units of $\frac{mol}{kcal}$.

Finally, there are several minor discrepancies between the experiments and the model. For example, some experiments have suggested that sulfur dioxide is produced by both the hydroxyl addition and hydrogen abstraction pathways.[12] This is not reflected in our model, with the overwhelming majority of the sulfur dioxide formed through the hydrogen abstraction pathway. The missing addition pathways are thought to occur through the formation and decomposition of methanesulfonic acid.[15] Experiments performed in the absence of oxygen[7] are also not accurately represented by the model presented here as many of the crucial model oxidation pathways require molecular oxygen.

2.4.2 Sensitivity Analysis of Major Species

As has been seen with thioformaldehyde, sensitivity analysis provides insight into what kinetic parameters and species thermochemistries have the largest effects on the concentrations of model species. In Figures 9 and 10, sensitivity analysis reveals the most important species and kinetic factors for the highest concentration observable species, dimethyl sulfoxide and sulfur dioxide, respectively. The reactions and species on these lists of most sensitive parameters have either experimentally determined or explicitly calculated kinetics and thermochemistry. As such, we believe the uncertainties in their parameters to be relatively small.

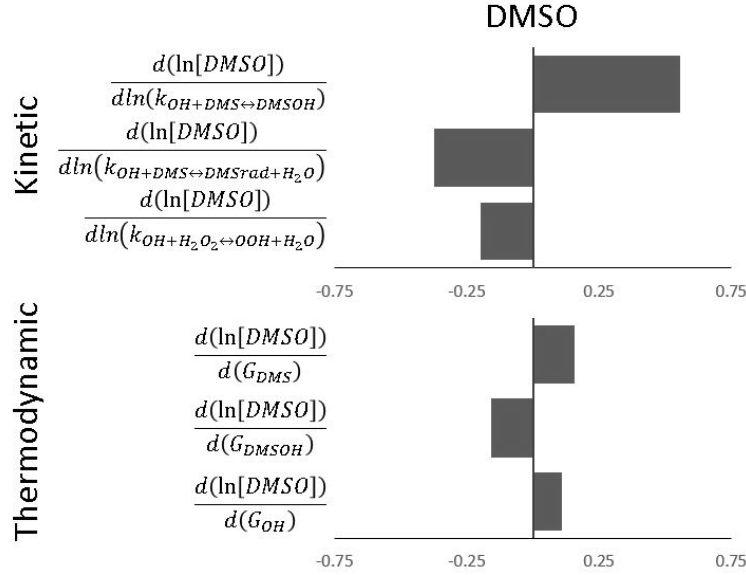


Figure 2-9: Top three most sensitive kinetic and thermodynamic parameters for dimethyl sulfoxide formation. Thermodynamic sensitivities are reported in units of $\frac{mol}{kcal}$.

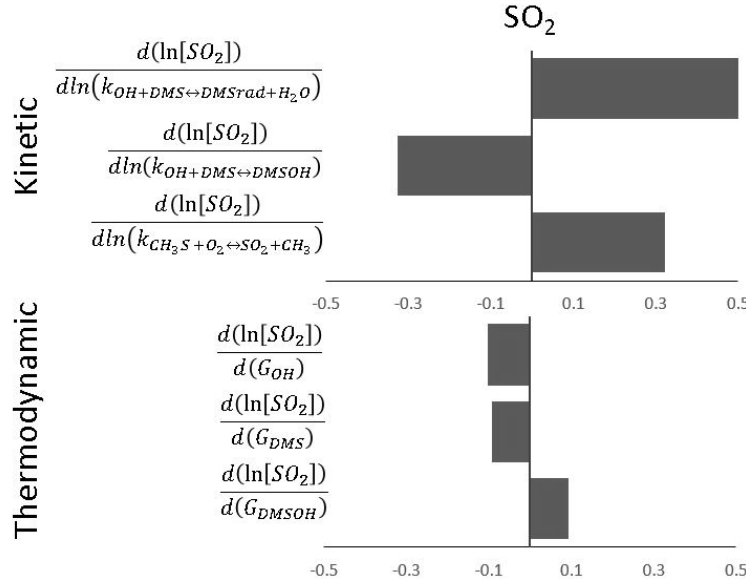


Figure 2-10: Top three most sensitive kinetic and thermodynamic parameters for sulfur dioxide formation. Thermodynamic sensitivities are reported in units of $\frac{mol}{kcal}$.

2.5 Conclusion

Methods for estimating thermochemical parameters for a wide range of C/H/O/S species were incorporated into the Reaction Mechanism Generator (RMG) software

suite. These results illustrate that RMG is now capable of automatically creating reasonable kinetic models for systems containing highly oxidized sulfur species. Further, this work illustrates how automatic mechanism generation software could be further expanded to other systems of interest.

A detailed kinetic model of dimethyl sulfide oxidation was also created and analyzed. While generally validated by experimental observations, a few discrepancies were observed. These discrepancies invite the creation of models of even further complexity, especially exploring the low temperature generation of dimethyl sulfone.

Acknowledgement

Financial support from the Gas Phase Chemical Physics Program of the US Department of Energy, Office of Basic Energy Sciences, Division of Chemical Sciences, Geosciences, and Biosciences (under award number DESC0014901) is gratefully acknowledged.

Chapter 3

Hydrogen from Hydrogen Sulfide and Water

3.1 Introduction

3.1.1 Hydrogen from Hydrogen Sulfide

This chapter is, in part, based on my publication in the ACS Sustainable Chemistry Engineering 2019, 7, 7, 7369–7377, by Ryan J. Gillis, Phalgun Lolur and William H. Green, *H₂* Generation from *H₂O* and *H₂S* through an Iodine Cycle.

Hydrogen has many unique properties that present both challenges and opportunities in its application as an energy vector and chemical feed stock. While potentially exciting as an energy vector, currently hydrogen is almost exclusively used as a chemical feedstock for hydrocarbon processing,[119, 66] ammonia generation,[31] and methanol production.[108] Although there are many ways in which hydrogen can be produced, 96% of hydrogen is currently generated from fossil fuels, primarily from natural gas reforming.[39] This practice is inherently carbon emitting, leading to the emission of hundreds of millions of metric tons of *CO₂* annually. A non-carbon based source of hydrogen could have significant economic and environmental value.

One potential source is *H₂S*, a toxic sulfur compound present in significant quantities in many natural gas reserves especially in southeast Asia, northwest Australia,

central U.S.A., the Middle East, and North Africa. [21] H_2S is also a major product of most oil hydrodesulfurization processes, created as H_2 reacts with sulfur-containing hydrocarbons over a catalyst such as $NiMo/Al_2O_3$ or $CoMo/Al_2O_3$. [66]

There are many potential methods that could produce H_2 from H_2S . These include direct[70] and catalyzed[95][60] thermal decomposition. These thermal decomposition methods scale well but requires high temperatures and thus high energy costs to produce significant amounts of hydrogen. Other methods, such as electrochemical[68][69], photochemical[105][25][67][129][32] or some combination[88][158] create H_2 at low temperatures but often are difficult to scale[20]. Another potential method of H_2S decomposition is through a thermochemical cycle. A modified Bunsen cycle has been examined extensively by Wang.[145][146][85] However, the separation challenges remained with H_2S instead of H_2O as a reactant. These are some of the wide range of H_2S based, H_2 generating schemes that have been examined, with reviews written by Chakma and Zaman[152] and more recently by Reverberi et al. [115]

Seeking a method that scales well and can be accomplished without reaching extreme temperatures, we initially explored a thermochemical cycle based on two reaction steps:



The second reaction is well studied due to its importance in some water splitting cycles,[47, 73, 147] so we focused on the first step, $H_2S + I_2$. At 25 degrees Celsius the reaction between H_2S and I_2 in the gas phase is extremely unfavorable with a $\Delta Grxn^\circ$ of 36.9 kJ/mol. However, if performed in water the complete dissociation of HI drives the reaction to consume the hydrogen sulfide. Restated, in the aqueous phase the thermodynamic limit of the reaction is the almost complete consumption of H_2S .

Qualitative descriptions of this reaction in aqueous conditions have been presented

by various authors[142, 40] but little detailed analysis is available. Many of these experiments observed the formation of a solid product within their reaction vessels, which was sometimes confirmed to be sulfur. Multiple authors have confirmed that HI is a major product, and indeed this reaction has been used to synthesize HI .[142, 68] Other researchers also find a fairly fast reaction at neutral or acidic conditions.[99] Mehra and Sharma quantitatively characterize the reaction of H_2S and I_2 in the context of using I_2 as an H_2S adsorbent.[99] In this characterization they measure the volumetric rate of adsorption of H_2S gas into an I_2 solution at ambient conditions. They find that the reactive absorption happens extremely quickly, measuring rates of 0.1 mol H_2S absorbed per m^2 gas-liquid interface per second. Kalina and Maas also observed the near complete conversion of H_2S (from 25% to less than 1 ppm) at a flow rate of $880\text{ cm}^3\text{min}^{-1}$ bubbling through an upright glass cylindrical reactor 30 cm high and 5 cm in diameter.[68] This Kalina and Maas experiment was conducted in basic conditions where iodine will be mostly oxidized to the iodate ion as was preferable for the electrochemical process they were exploring.

With only limited characterization of the reaction of H_2S and I_2 available in literature, this work aims to understand the chemistry of the sulfur and iodine species, especially in context of H_2 production schemes. As shown below, sometimes the chemistry forms the expected products described above, but at other reaction conditions different unexpected products can be formed, with much bigger potential to improve sustainability.

3.2 Methods

The primary reactants were H_2S in a balance of N_2 obtained from AirGas and 99.8% pure solid I_2 crystals obtained from VWR Chemistry. Several different sources of H_2S were used in the experiments. Due to safety concerns regarding the toxicity of H_2S , to the extent possible, a gas cylinder with the relatively low concentration of 30 ppmv H_2S in a balance of N_2 was used. This source had an estimated concentration uncertainty of +/- 0.8%. The concentration was confirmed using non-dispersive

ultraviolet spectroscopy comparing to calibration standards from Gas Measurements Instruments and Research Gas Mixtures. Another H_2S cylinder, containing 25 ppm H_2S in N_2 , prepared by Praxair was used for a single experiment and compared as expected with experiments that used the 30.16 ppm AirGas cylinder. In addition to these relatively low concentration sources, another AirGas cylinder with a concentration of 8.9 mole % H_2S in a balance of N_2 was used in experiments that required H_2S at a higher concentration. An iron oxide sulfur trap was used to remove any remaining H_2S in the effluent. The toxicity of the H_2S is severe and caution was taken to ensure that proper ventilation and emergency response procedures were in place to limit this significant hazard.

The general experimental procedure involved the continuous creation and measurement of dissolved HI . H_2S was bubbled through stirred a reactor filled with I_2 and H_2O and the amount of HI created was inferred from the continuously measured concentration of hydronium and iodide ions. The SevenExcellence ion concentration measurement system, the InLab Expert Pro pH probe, and the perfectION Combination Iodide Electrode were purchased from Mettler Toledo and used to continuously monitor the concentration of these products. Calibration standards at pH 1, 2, 3, 4, and 7 were purchased from VWR. A series of iodide concentration calibration standards were created by diluting an Iodide ISE standard purchased from Mettler Toledo from 1000 to 0.1, 1, 5, 10, 25, 50, 100, 500, and 850 mg/L. These standards were created regularly and calibrations were performed both before and after the experiment was performed.

The flow rates of the gas mixtures were controlled by a needle valve and glass tube flow meter with a tungsten carbide float. The flow meter was manufactured by VWR and had an estimated error of +/- 3%. This claim was confirmed with a DryCal DC-Lite primary volumetric flow meter that is expected to be accurate to within +/- 1%. Also, a pressure gauge was added between the reactor and the flow meter to ensure that the pressure remained ambient throughout the experiments.

Within the first several experiments it became clear that the experiment could be improved by taking steps to increase the solubility of the naturally only marginally

water soluble I_2 crystals. Uneven distribution of the I_2 through the reactor increased the noise in the ion measurements and lowered the amount of I_2 that reacted, which we hypothesize is due to mass transfer barriers. Two methods were used to dissolve the I_2 crystals leading to uniform ion concentration near the electrolytic probes and lowered mass transfer limitations. First, the I_2 crystals were predissolved in a small amount of isopropyl alcohol and then added to the aqueous reactor. After demonstrating that the small amount of isopropyl alcohol did not compromise the accuracy of the ion measurement probes, the alcohol cosolvent was used in the majority of the remaining experiments. In general, the amount of the cosolvent was minimized according to the amount of I_2 required by that experiment. This meant that the concentration of the cosolvent ranged from about 2vol% for the trials with less than 0.01 gm of I_2 to around 12.5vol% for experiments requiring greater than 1.5 gm of I_2 . Control experiments with constant I_2 level and varied concentration of the cosolvent confirmed this variation did not have any effect on the observed stoichiometry. An alternative method for solvating the I_2 without using any cosolvent was to add excess KI . The dissociated iodide ions solvate the I_2 through the formation of I_3^- . This method had the disadvantage of drowning out the measurement of the I^- ions. This means that estimations of HI formation in these experiments were based entirely on the pH measurements. A brief sketch of the experimental set-up is shown below in Figure 1. The data that supports the findings of this study are available from the corresponding author upon reasonable request.

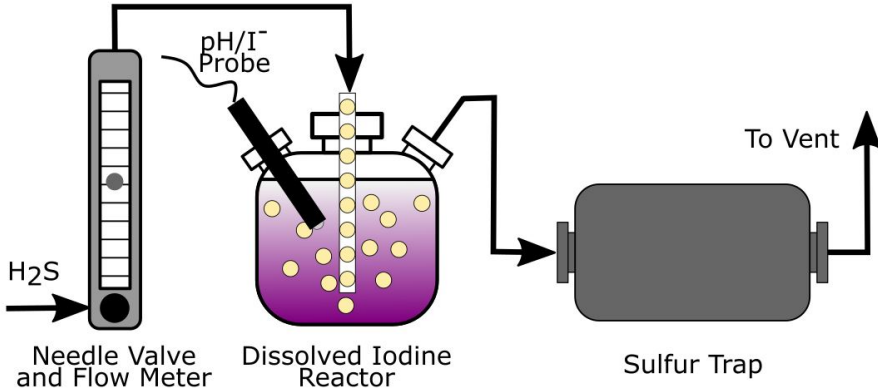


Figure 3-1: Experimental Apparatus

3.3 Results

From this apparatus a time series of proton and iodide concentrations is measured. An annotated example of this raw data is included below in Figure 2.

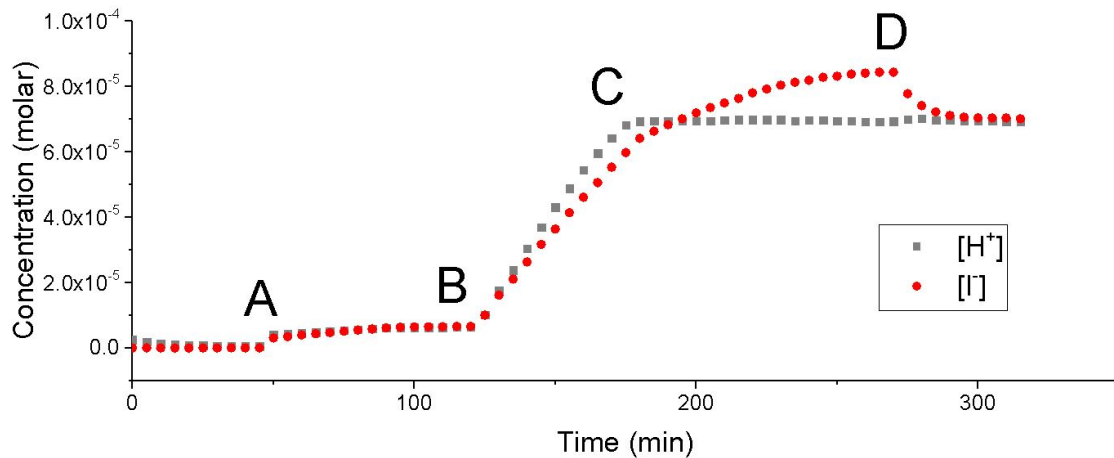


Figure 3-2: Measured ion concentrations over a single typical experiment with annotations marking changes in the reactor conditions A. Addition of I_2 dissolved in isopropyl alcohol: This leads to a slight increase in the ion concentrations as a minor amount of I_2 reacts with H_2O to create HOI and HI . B. Beginning of H_2S flow: Feeding H_2S leads to a steady increase in the amount of each ion. C. Depletion of I_2 : The complete consumption of one of the reactants stops the formation of ion products. D. Ending of H_2S flow: This starts the flow of inert and the stripping of any leftover H_2S from the reactor

The unusual shape of the I^- concentration curve was determined to be caused by

interaction between dissolved H_2S and the I^- electrolytic probe. Once H_2S flow is halted and purging N_2 restored, the aberrant signal disappears leaving very close ion concentration agreement between the pH and I^- ion probes. Additionally, experiments performed flowing H_2S through the reactor without I_2 replicated the shape and magnitude of this feature.

Key questions about the reaction between H_2S and I_2 can be answered from this time series of ion concentrations. First though, a severe inconsistency between our expected model and observed data was found.

3.3.1 HI Formation Rate at Low H_2S Concentrations

Our experiments showed that, surprisingly, the amount of HI produced for a given amount of H_2S reacted was much higher than originally predicted. In experiments where the I_2 was predissolved (either with isopropyl alcohol as a cosolvent or with excess KI forming soluble I_3^- ions) and H_2S was supplied at a concentration near 30 ppmv, rather than producing 2 HI per H_2S reacted as would be predicted by $H_2S + I_2 \rightarrow 2HI + S^0$, up to 6 HI were created. This can be seen in Figure 3 by analyzing the slope of the ion concentrations in the region of data where H_2S is reacting with dissolved I_2 .

Several hypotheses seeking to understand this discrepancy were tested by modifying the conditions of the reactor. These conditions included lowered pH, the presence of sulfide precipitating metal ions, and large excesses of I_2 . It was observed that these varied conditions did not affect the observed stoichiometry of the reacting system.

The unexpected stoichiometry remained consistent even at more extreme conditions meant to more closely approximate industrially-relevant H_2S decomposition conditions. Limited by the pH tolerance of the ion meter, the above experiments were repeated in two variations, first, measuring $[I^-]$ in solutions with a pH initially at 0 and, second, measuring pH in solutions with KI dissolved make the initial state of the reactor 4 molar $[I^-]$. In both high $[I^-]$ and low pH conditions the unexpected

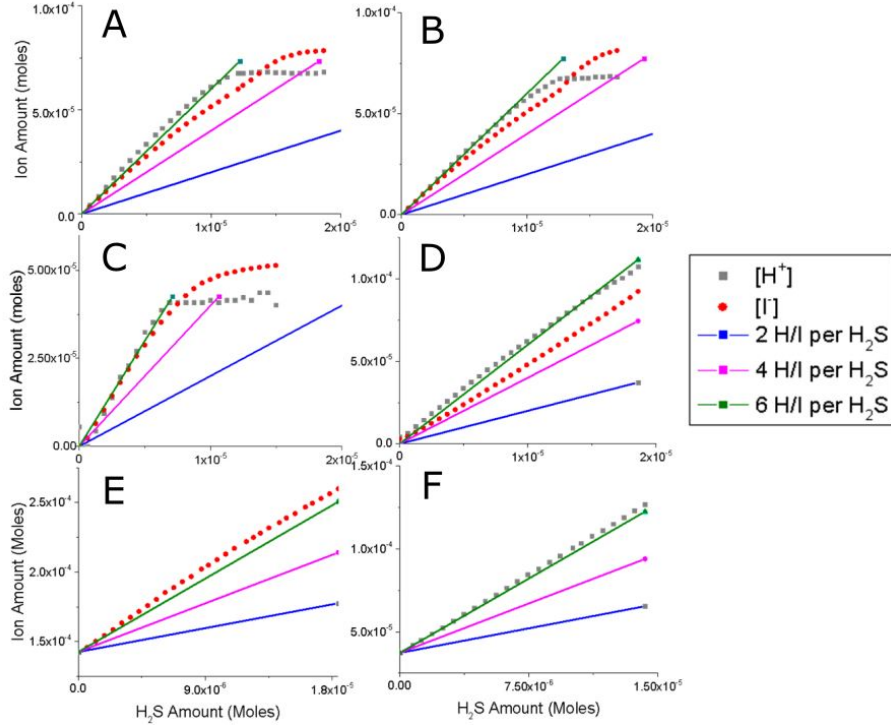


Figure 3-3: Ion concentrations during H_2S flow at low H_2S concentrations with various reactor conditions: A. Base B. Added Zn ions C. Reactor pH = 3 D. Excess of I_2 E. Reactor pH = 0 F. 4 Molar KI

stoichiometry persisted.

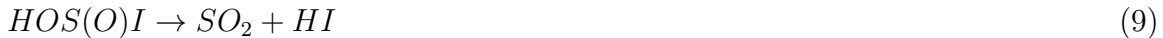
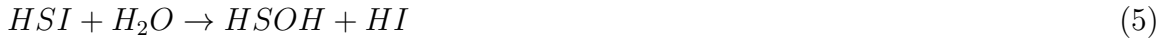
In addition to the measured ion concentrations, the depletion of I_2 also occurred at approximately triple the expected rate. Although there was no direct measurement of I_2 concentrations the moment of its depletion can be inferred both from the disappearance of the characteristic orange and brown color from the reactor and the halting of ion generation.

After repeated confirmation of these results, alternative reaction sequences were considered. One reason this stoichiometry is particularly surprising is that the additional hydrogen observed in excess the HI must be coming from water, as in the experiments with the KI solvation strategy there are no other sources of hydrogen in the system. One reaction sequence consistent with the observations and thermodynamically plausible involves the creation sulfur-iodine intermediates and their sequential oxidation to SO_2 . This is described by the overall reaction shown below.



The proposed step by step mechanism that most simply leads to this overall reaction stoichiometry involves the alternating reaction of sulfur or sulfur-oxygen species with I_2 and the newly formed iodine containing species with H_2O . Each of these reaction steps releases HI . The large solvation energy of HI is thought to drive the reaction forward.

SO_2 Pathway



The proposed mechanism draws inspiration from the work of previous chemists. Benson's demonstration of the gas phase reaction of H_2S and I_2 to produce HSI [65] and Kice's description of the typical reactions of sulfur molecules[72] provided a framework for the mechanism. The proposed reaction sequence also has many parallels to the conclusions of Danehy and Oester who observed over-oxidation of a variety of thiols by I_2 in the presence of HI .[35, 33, 34] They postulated that the overoxidation of these thiols led to the formation of sulfenic or sulfonic acids. Further they also observed a concentration dependence to this over-oxidation, with lower concentrations leading to a higher level of oxidation. Finally, the highest ratios that they observed (5.8 and 5.9 I/SH) match well with our low concentration experiments. Our results compare well with their previous findings on the over-oxidation of larger thiols, lending further support for the water consuming SO_2 formation mechanism.

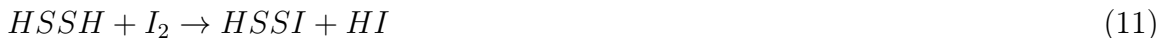
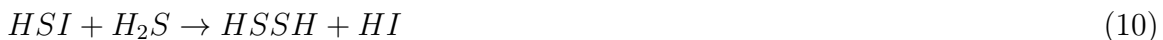
3.3.2 HI Formation Rate at High H_2S Concentrations

A key question to consider is why this experiment observes stoichiometry consistent with SO_2 formation while most other reported experiments combining H_2S and I_2 report solid elemental sulfur formation. There are several dramatic differences between this experiment and the conditions tested by other investigators. Most notably the concentration of H_2S used in the experiments reported here was 30 ppm as opposed to 25%[68, 69] or pure[99, 142] H_2S in experiments that observed elemental sulfur formation. This suggests that there is a branching point during the sulfur iodine reactions that is controlled by the concentration of H_2S .

To test this hypothesis we performed the same experiments at H_2S concentrations up to 8.9%. The ratio of ions formed per H_2S fed was determined for each experiment. The results diverged depending on which I_2 solvation strategy was used. When the alcohol cosolvent was used, the rates of HI formation fell dramatically at high H_2S concentrations, consistent with results observed by other researchers. However, when the KI solvation strategy was used, the stoichiometry remained unexpectedly high, regardless of concentration. The contrasting ratios between the experiments performed with 30.16 ppm H_2S and those performed at higher concentrations and an alcohol cosolvent are shown in figure 4 below.

In addition to the ratio of 2 HI formed per H_2S the high concentration experiments also created a clumped yellow solid, suspected to be elemental sulfur. The results supported our hypothesis that the HI formation rate was consistent with the formation of elemental sulfur. We suggest that a likely mechanism for this production involves the alternating reactions of H_2S and I_2 .

Elemental Sulfur Pathway





.....



3.3.3 Concentration Regimes of the Branching Pathways

This leads us to the surprising result that decreasing the concentration of the reactant H_2S can increase the amount of the primary product, HI , that is produced. Consider the following three trials, highlighted in Figure 4, that all used the same H_2S flow rate (5 ccm, or 1.22 moles/s), differing only in the degree to which they are diluted [one undiluted (89000 ppm), one diluted at a ratio of 20:1 (4450 ppm), and the final diluted at a ratio of 100:1 (890 ppm)].

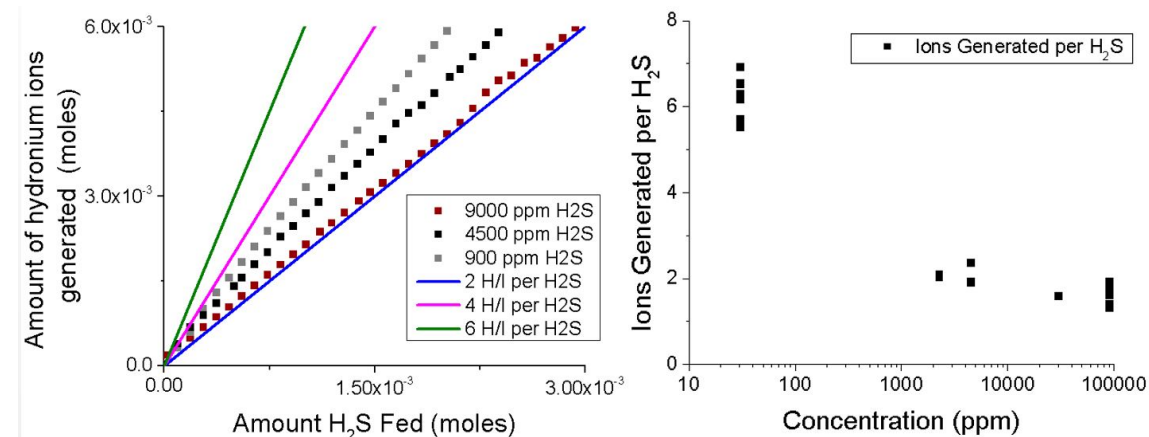


Figure 3-4: A. Observed product to reactant ratio across three reactant concentrations using an alcohol cosolvent. The amount of iodide generated is nearly equal to the amount of hydronium ion generated. B. Observed product to reactant ratio across a range of reactant concentrations using an alcohol cosolvent.

Curiously, in this case, despite the decreased reactor residence time, a greater amount of product is generated at the lower concentrations. A survey of concentrations and flow rates confirms this trend.

While the exact transition concentration is unclear, somewhere between 2300 and 30 ppm the chemistry shifts from favoring the elemental sulfur forming reaction 1 to the SO_2 forming reaction 3. Concentrations below this transition seem to be conducive to the observed water-splitting driven by the oxidation of H_2S .

3.3.4 Experimental Characterization of the Sulfur Products

Having observed a concentration dependent stoichiometry, further support for our hypothesized mechanism can be found by characterizing the sulfur products of these reaction pathways. When using the low concentration cylinder these sulfur products were below the detection limit of our analytical equipment. However, sulfur products were observed from the experiments that used high concentration H_2S . Among the products at high concentration was elemental orthorhombic sulfur, as confirmed by PXRD.

To be sure that any oxidized sulfur species observed was the result of the reaction with water rather than an alcohol cosolvent, experiments characterizing these products were performed by solvating the I_2 with KI not including any alcohol. After an extraction of the reactor fluid with toluene, a distinct SO_2 peak was observed, strongly supporting our suggested mechanism. The gas chromatogram is included with the mass spectra as Figure 5. No other significant non-solvent peaks were observed.

During experiments with an alcohol cosolvent in addition to SO_2 a white solid was observed to form. Based on the chromatogram and mass spectra the solid seems to be a mixture of oxidized organosulfur compounds. This suggests that during the alcohol cosolvent experiments some of the alcohol is likely reacting to form these compounds. These side reactions and their precipitating products likely preclude isopropyl alcohol as a cosolvent for a scaled up version of this reaction sequence. However, these bench-top experiments are still useful in demonstrating the HI formation stoichiometry and confirming the creation of sulfur dioxide. More detailed chromatograms and spectra are included in the Appendix B.

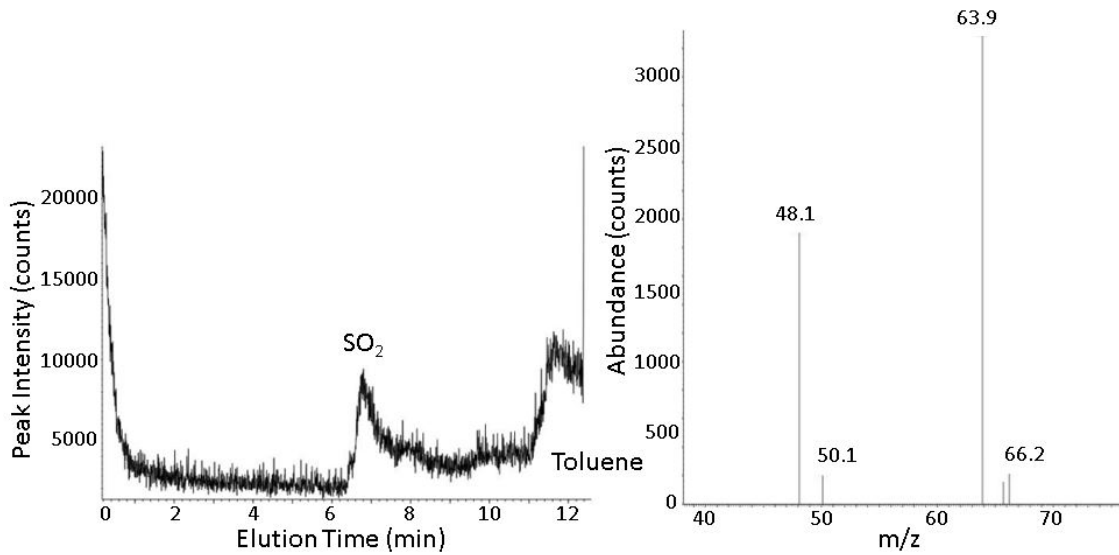


Figure 3-5: Gas chromatogram of the toluene extract from the reactor volume and mass spectra of sulfur dioxide observed at the marked peak in the chromatogram

One reaction that we thought we might observe, but did not, was the Bunsen reaction and the associated formation of sulfuric acid.



We tested for the presence for the sulfate ion by dissolving barium chloride in the reactor volume but observing no precipitate formation, we conclude that there is not significant formation of sulfuric acid. We also did not see any peaks in the gas chromatograph/mass spectra measurements that could match sulfuric acid.

3.3.5 Computational Evidence

To evaluate the reasonableness of the proposed SO_2 pathway, reaction thermochemistries for each species on this path were estimated computationally. Since solvation effects are crucial in understanding this system, special efforts were employed to estimate the solvation free energies of each species in water. One method to estimate solvation energies uses a COnductor-like Screening MOdel, often abbreviated to COSMO[75]. First proposed by Klamt et al in 1993, COSMO is a part of the Polarizable Con-

tinuum Model (PCM) family[132]. It's extension, COSMO-RS[76, 10, 9] (COSMO for realistic solvation) has been subsequently developed as a combination of COSMO with statistical thermodynamics treatment of interacting surfaces. Quantitatively, it is known to predict solvation free energies to about an accuracy of 0.4 kcal/mol (RMSE). By coupling geometry, frequency, and single point energy calculations with the COSMO-RS method we were able to estimate the thermochemistries of each species in both the elemental sulfur and SO_2 pathway.

Potential Energy Diagrams

To establish the level of theory and basis sets to be used for studying the system of reactions as proposed in the previous section, it is important to compare experimental data (wherever available) with the computational calculations. Thiohypiodous acid (HSI) formation is considered a key intermediate in the reaction between H_2S and I_2 . The reaction, $H_2S + I_2 \rightarrow HSI + HI$ was initially studied experimentally by Benson et al[65] in 1978 as a part of a study of divalent sulfur compounds and understanding the thermochemistry and kinetics of sulfur containing systems. The reaction has been used to test and benchmark the level of theory used for this computational study. Initially, density functional theory (DFT) was chosen as the level of theory for calculations for computational efficiency. Turbomole[135, 6] was used to compute the free energies and frequencies using the BP-86[16, 109] functional in gas phase at 298.15 K, and def2-TZVPD basis[149] was used for all the atoms and effective core potential (ecp) was used for the iodine[111] atoms. MOLPRO 2015[150] was used to perform the CCSD(T)/AVTZ calculations. Extra d orbitals were used in the basis to describe sulfur containing species - AV(T+d)Z. Pseudopotential bases developed by Kirk Peterson were employed to describe iodine species.[110, 111] For the above reaction we obtain a gas phase enthalpy change of 7.61 kcal/mol (BP-86) and 8.04 kcal/mol (CCSD(T)) respectively. This compares well with the experimental value of 6.28 +/- 0.67 kcal/mol.[65] It is worth noting that Ornellas et al. investigated the same reaction[62] in gas phase using CCSD(T) level of theory using triple, quadruple, and quintuple basis extrapolated to the complete basis set limit to obtain an enthalpy

change of 8.82 kcal/mol. Taking the scalar relativistic and core-valence effects into account, their value was further improved to 8.4 kcal/mol. With our methods comparing well to both the experimental values and other analyses, optimized geometries and frequencies were calculated for each species in the SO_2 pathway and for the first and last species in the elemental sulfur pathway. The detailed results of these calculations are included in Appendix B.

Moving to aqueous conditions from the gas phase requires both an estimation of solvation energies and dissociation constants. Turbomole was then used to generate the necessary COSMO files for calculating the solvation energies, using the optimized gas-phase geometries. COSMOthermX17[43] was then utilized to calculate the solvation energies using TZVPD-FINE level of theory. Since COSMOthermX17 does not directly take dissociation of HI into account, it was manually calculated using the relation, $\Delta G = 2.303RT \cdot pKa$. In our system, only the pKa of HI is known, estimated to have a value of -9.5[134]. For all other species it had to be estimated computationally. COSMOtherm employs a Linear Free Energy Relationship(LFER) method to estimate pKas of compounds in water and select solvents. This requires a COSMO file of the dissociated species, which was easily calculated with TURBOMOLE. It was discovered that the only other species that readily dissociates is $HOS(O)I$, with an estimated aqueous pKa of -6.36. The dissociation energy, was then calculated using the above mentioned equation and included in the total solvation energy.

The dissociation of HI is considered to drive the reaction forward and is accounted in our calculations using a hybrid experimental and computational determination of the pKa of HI in water. We expect additional reactions/interactions to take place between HI , I_2 and water which could further favor the formation of HI . The details of this secondary chemistry is outside the scope of this particular paper but it would be a good topic for future research.

While there are some endothermic steps the overall pathway to SO_2 is more exoergic than the pathway to elemental sulfur. The potential energy diagram shown in Figure 6 and our observation that the stoichiometry changes with H_2S concentration suggests a competition between the between the channel leading to SO_2 and

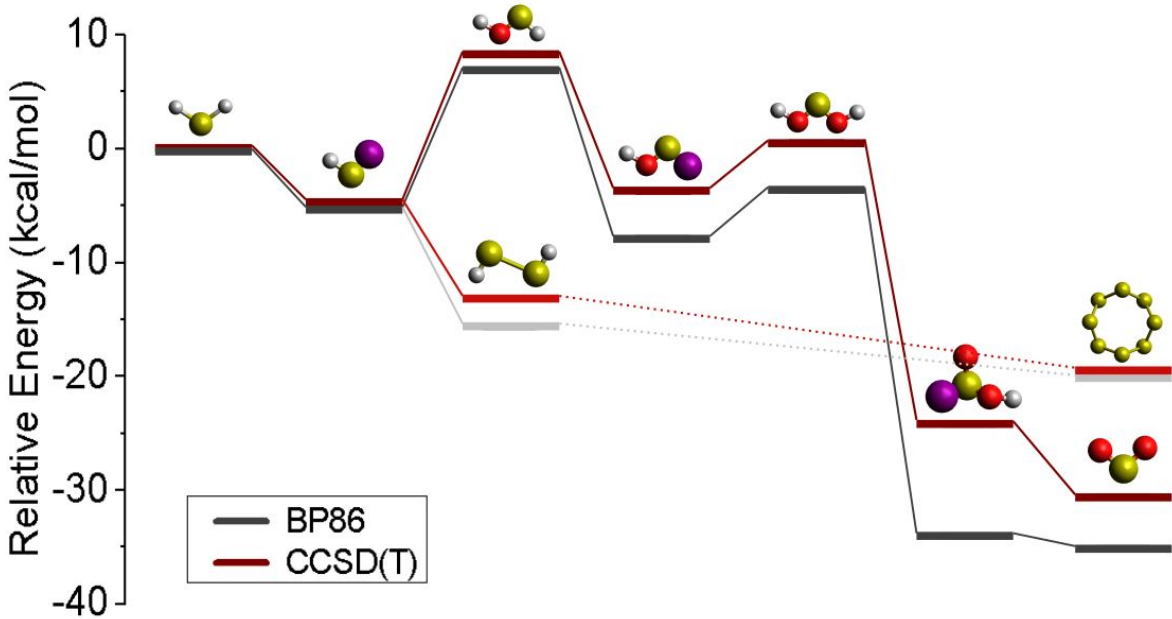


Figure 3-6: A free energy diagram at 298.15 K limited to species expected to be part of the hypothesized SO_2 formation mechanism as well as the first and last steps of the elemental sulfur pathway. The gas phase geometries, frequencies and energies are calculated at BP86 and CCSD(T) levels of theory and then corrected with estimated solvation energies and dissociation constants. Transition states are not included. On the main pathway one mole of HI is formed in each intermediate step and I_2 and H_2O alternate as the additional reactant. On the competing pathways H_2S replaces H_2O . All the energies are zeroed with respect to H_2S and calculated at 298.15 K. The details of the calculations can be found in Appendix B.

the channel leading to elemental sulfur. We hypothesize that the branching point between these channels occurs at the common intermediate HSI .

3.4 Discussion

3.4.1 H_2 production from H_2S and H_2O

The most striking implication of these results is that in certain concentration regimes water reacts with H_2S and I_2 to form HI which itself can be decomposed to H_2 . Across two reaction steps this accomplishes the splitting of water driven by the oxidation of H_2S into SO_2 . Figure 7 illustrates the key reaction and separation steps that could accomplish the generation of H_2 from H_2S and H_2O .

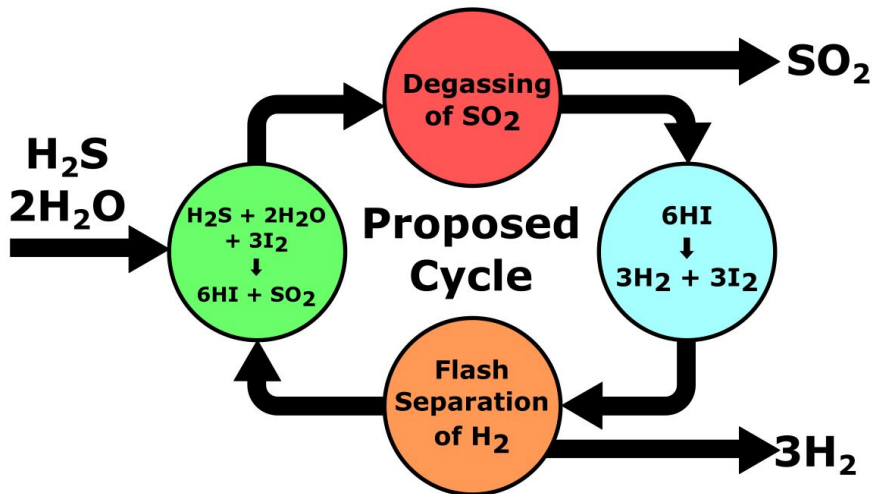


Figure 3-7: A flow diagram describing a potential series of reactions and separations resulting in the formation of H_2 and SO_2 from H_2S and H_2O .

This process is, of course, limited by the amount of sulfur that is available to be oxidized or that once oxidized can be processed or used. However, the amount of hydrogen sulfide processed in refineries is enough to have a significant impact on the world hydrogen economy. Approximately 40.6 million metric tons of sulfur were created as a byproduct of hydrocarbon extraction and processing via the Claus process in 2015.[2] Given the capability to produce H_2 from H_2S at a ratio of 3:1, this corresponds to the ability to produce $3.8E+9$ kmol or 7.6 million metric tons of H_2 per year. This represents more than 10% of the estimated 65 million metric tons of hydrogen produced in the world per year for any purpose, and billions of dollars per year in potential value.[120] A rough depiction of how this process would fit into a refinery setting and reduce CO_2 emissions is shown below in Figure 8.

The reduction in carbon emissions associated with the adoption of this process would also have significant social value. It is, however, difficult to anticipate precisely the degree to which adoption of this sulfur-based technology would reduce carbon emissions. This is because even though the chemistry of hydrogen gas production in this system is not inherently carbon emitting, energy, likely supplied from carbon intensive sources, would be needed to vaporize and condense the process streams, pressurize process streams to induce flow, and purify the product streams. A process

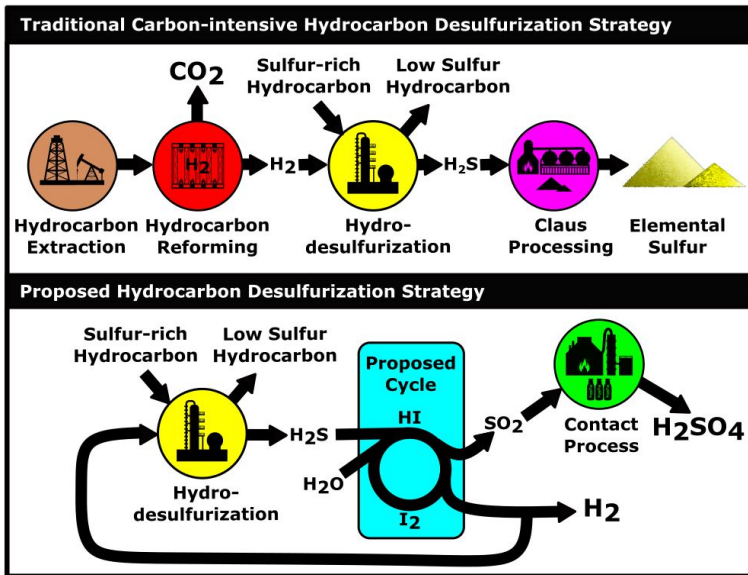


Figure 3-8: A depiction of how the proposed process would reduce carbon emissions in a refinery setting.

model was created to provide a rough estimate of the CO_2 emissions, allowing a comparison to other hydrogen generation methods. Details about the process model can be found in Chapter 5. We emphasize that this model was created to provide a general sense of the CO_2 emissions and that a much more rigorous engineering analysis would be required to make definitive conclusions on the financial costs of the process.

In an environment with other local heating requirements with which the proposed process can heat integrate, we estimate that this sulfur-based technology would produce about 1.2 kg of CO_2 per kg of H_2 created. This is less than 20% of the 7-10 kg of CO_2 per kg of H_2 created during steam methane reforming.[126, 41] In a less ideal situation, the CO_2 emissions per H_2 produced could be much higher, but are still expected to be less than from steam methane reforming. Using this strategy and re-examining the world market in 2015 we estimate that given full implementation, about 44 million metric tons of CO_2 emissions could have been avoided in that year. With a carbon social value between \$35 and \$220 per metric ton,[103] this would correspond to between \$1.5 and \$9.7 billion in social value created with the implementation of this process for the year 2015. This social value would increase over

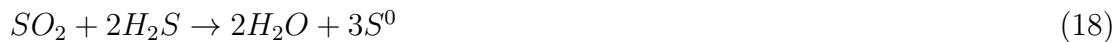
time as both the amount of hydrogen sulfide processed increases and the social cost of carbon emissions rises. While there are significant uncertainties in these estimations they suggest that further development of these ideas is warranted, with motivations both financial and ethical, if even a fraction of this value can be realized.

3.4.2 Thermochemical H_2S Decomposition to Elemental Sulfur

Along with the unexpected SO_2 forming, water-splitting pathway observed in reaction 3, the originally expected elemental sulfur forming pathway of reaction 1 was also seen at high H_2S concentrations. It might seem that it would always be preferable to form more H_2 so reaction 3 would always be preferred. However, SO_2 is harder to store and transport, poses a greater hazard, and is more difficult to separate from the other stream components than elemental sulfur. It is likely that both H_2 -generating pathways could be of use, depending on the demand for SO_2 for sulfuric acid production.

The economics of H_2S -decomposing thermochemical cycles based on reaction 1 have been studied.[56] Their viability is dubious in aqueous conditions due to the thermal requirements, but could be made viable with the use of alternate solvents or process designs. However, due to the observed side reactions, isopropyl alcohol is likely an unsuitable co-solvent for the scaled process. Other studies of H_2S splitting sequences have suggested that toluene may be an acceptable cosolvent.[153]

Note that one could achieve the same products and stoichiometry of reaction 1 by combining the new process, based on reaction 3, with the catalytic step of the Claus process,



By using some SO_2 to make sulfuric acid via the Contact process, and reacting some via reaction 17, one could achieve any desired ratio of co-products, albeit at the

cost of consuming more H_2S . With the advent of these processes H_2S can be viewed less as a toxic waste, and more as H_2 generation resource.

3.5 Conclusion

This work points out unexpected, potentially exploitable chemistry, and poses an explanation supported by computational calculations and experimental observation. Specifically, the reaction of H_2S and I_2 in H_2O is observed to form 6 HI and SO_2 . As the only other hydrogen containing species in the reactor during many trials, water must be participating in the reaction. The evidence supports a hydrogen generation scheme involving the splitting of H_2O driven by the oxidation of H_2S with iodine containing intermediates.

The expected pathway to elemental sulfur, reaction 1, was also observed at high H_2S concentration conditions. The nature of the sulfur product and amount of HI and thus H_2 generated by each pathway differs substantially. The merits of both chemistries are discussed along with the potential impact of such chemistries on the larger hydrogen market.

3.6 Acknowledgment

This work was supported in part under the Cooperative Agreement between the Masdar Institute of Science and Technology, Abu Dhabi, UAE and the Massachusetts Institute of Technology, Cambridge, MA, USA, Reference Number 02/MI/MIT/CP/11/07633/GEN/G/00

3.7 Author Contributions

Ryan J. Gillis is responsible for experimental design, execution, and interpretation as well as mechanism hypotheses and product analyses. Dr. Phalgun Lolur is responsible for all quantum chemical analyses. Dr. William H. Green is the corresponding author and responsible for guidance and oversight on all aspects of the work. MIT, the

employer of William H. Green, has filed a PCT patent application, PCT/US19/13018, on an invention related to this manuscript, listing Ryan J. Gillis and William H. Green as the inventors. Phalgun Lolur has no competing interest.

Chapter 4

Prototype Construction and Testing

4.1 Introduction

Donald Rumsfeld, an American Statesman, once said that in life there are known unknowns and unknown unknowns. He said that throughout history it was always unknown unknowns that proved the most difficult. While originally applied to geopolitics, this applies very well to chemical process scale-up. However a chemical engineer tries to anticipate and mitigate the challenges of moving a chemical process from a lab notebook or process model to reality, they are often thwarted.

As such, it is often most efficient to just build the simplest possible system, as quickly as possible, and see if it works. Doing so also helps to speedily identify the areas for additional focus rather than trying to anticipate them.

It is this approach that we have taken with testing the proposed chemical cycle for creating hydrogen gas from hydrogen sulfide and water through iodo-intermediates. The following chapter describes the minimum viable system to test the basic chemistry and reports the measurements of hydrogen production.

4.2 Safety Considerations

Any experiment with with hydrogen sulfide as a reactant or product must take strict and comprehensive precautionary measures to prevent injury or loss of life. It is

almost impossible to overstate the hazard presented by experimentation with high concentrations of hydrogen sulfide. There is a huge discrepancy between the OSHA ceiling concentration limit of 20 ppm and the 10-90% hydrogen sulfide internal refinery process streams. A single inhalation of hydrogen sulfide gas at a concentration of above 0.1% will induce immediate loss of consciousness and death. Despite the inherent danger in working with this reactant, there are many efforts that we take to mitigate these considerable risks.

The first and most important step is to keep the hydrogen sulfide and all experimentation in a continuously ventilated space with adequate volumetric flow. We selected a walk-in fume hood to both store the hydrogen sulfide cylinder and contain the prototype system. A flow velocity minimum of 100 fpm was selected in collaboration with the MIT EHS Industrial Hygiene Officer. This flow velocity is maintained continuously, and is doubled during the testing of new configurations. Further hydrogen sulfide cylinder is kept closed and pressurized only as needed to provide additional gas flow.

Further, reactors hydrogen sulfide are over-designed to ensure complete conversion of the hydrogen sulfide. Qualitative pockets of fluid are also kept down the flow line as a colorimetric test for hydrogen sulfide breakthrough. These crimson dissolved iodine aqueous sections will turn transparent when exposed to hydrogen sulfide. In even further caution, SulfaTreat sour gas absorbents are employed in scrubbers before any gas is vented to the hood to clean any lingering sulfur gases from the system.

Hydrogen sulfide concentrations near the researcher, the gas cylinder, and the venting gases are monitored with Honeywell personal hydrogen sulfide monitors set to alarm at concentrations above 10 ppm. These are coupled with lab-wide hydrogen sulfide sensors integrated into the MIT emergency response system. In the event of hydrogen sulfide concentration above 10 ppm, the building is evacuated and emergency response personnel are automatically summoned.

The final precaution involves working when others are present in the laboratory. This ensures that in the event of an emergency, and immediate collapse there will be others present to help the researcher avoid injury.

4.3 System Inventory

The apparatus consisted of a Vigreux column used as a gas/liquid contactor, leading to a 1 liter boiler. This fed into a tube furnace with a quartz glass tube packed with steam activated carbon. The packed-bed reactor effluent immediately is plunged into a condenser with the water, iodine, and hydroiodic acid accumulating in a flask. The hydrogen gas is collected above the apparatus in a gas sampling bag for analysis. A detailed list of the apparatus components is shown in the table below. In addition to these components, various valves and fittings were used to control flow and connect the component pieces. A labeled schematic is shown in figure below.

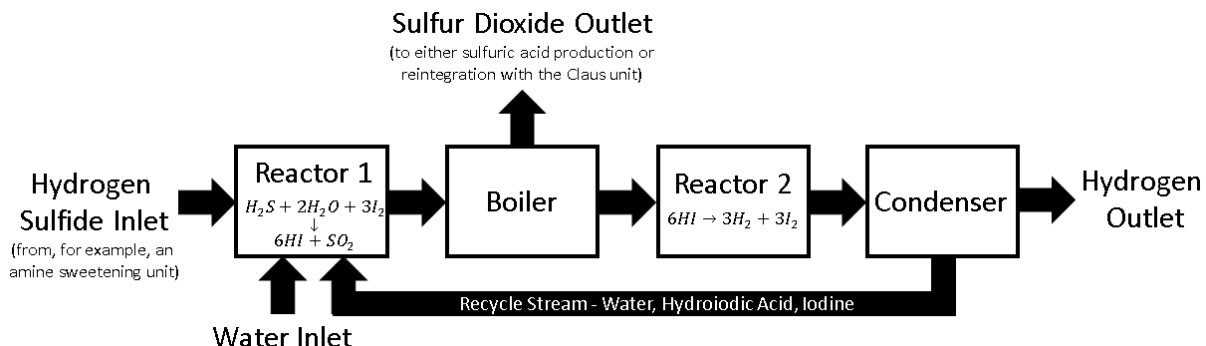


Figure 4-1: Key steps of the process cycle to be tested with the minimum viable experiment.

Table 4.1: Labeled components of the minimum viable experimental system

	Part	Cycle Step	Details	Temperature
1	Gas-Liquid Contact- tor	Reaction 1: $H_2S + 3I_2 + 2H_2O \rightarrow 6HI + SO_2$	Vigreux Column, 2 ft, 24/40 ground glass joints, Ace Glass	23.5 deg C
2	Boiler	Separation 1: SO_2	PID Controlled Heating Mantle, Fisher Scientific	127 deg C

Table 4.1: Labeled components of the minimum viable experimental system

	Part	Cycle Step	Details	Temperature
3	Tube Furnace	Reaction 2: $2\text{HI} \rightarrow \text{H}_2 + \text{I}_2$	120V 1100 C Tube Furnace, Fisher Scientific	350 deg C
4	Condenser	Separation 2: H_2	Coiled PTFE Tubing and a 5 Liter borosilicate glass flask, VWR	23.5 deg C
5	PTFE Tubing	Transfer of material in all sections below 100 deg C	VWR 1/2 and 1/4 inch PTFE Tubing	Up to 100 deg C
6	Metal Tubing	Transfer of material in all sections above 100 deg C	Hastelloy 276C 1/2 inch tubing, TW Metals	127 – 350 deg C
7	Sulfur Gas Scrubber	Effluent Gas is passed through the scrubber before venting	Sulfa-Treat iron pellets, 8 kg	23.5 deg C
8	Hydrogen Sulfide Source	Feed line for Reactor 1	AirGas Hydrogen Sulfide in Nitrogen, 9.86%	23.5 deg C
9	Packed Bed Reactor	Inserted into the tube furnace	1 inch Quartz Glass Tubing, Fisher Scientific	350 deg C
10	Activated Carbon Catalyst	Packed into the quartz glass tubing	Norit Steam activated carbon	350 deg C

Table 4.1: Labeled components of the minimum viable experimental system

	Part	Cycle Step	Details	Temperature
11	Gas Sampling Bag	Collection of product gases for analysis	Multilayer foil 5 L gas sampling bag, VWR	23.5 deg C

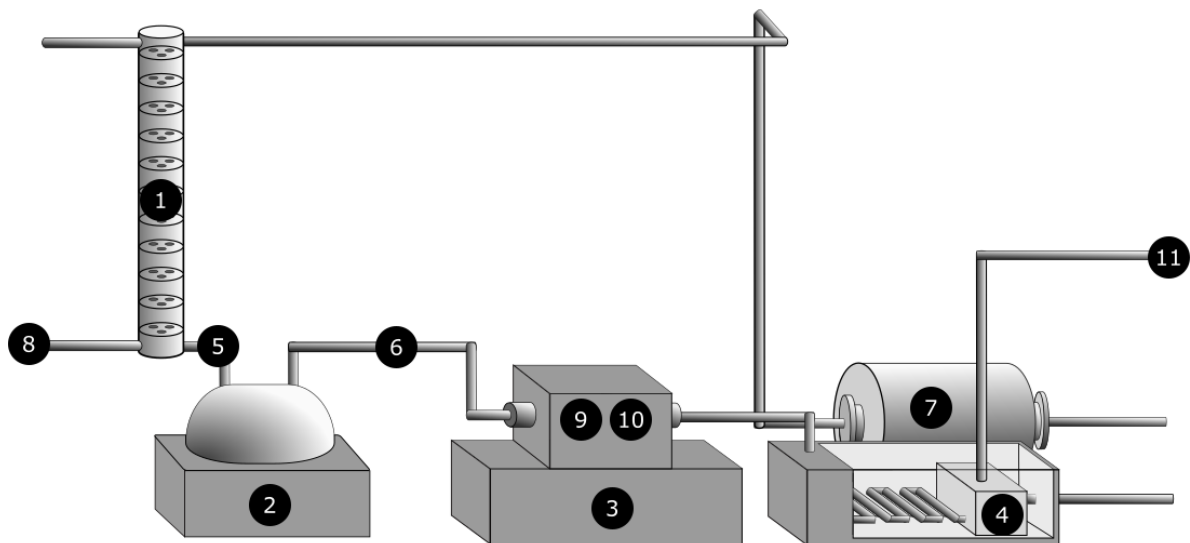


Figure 4-2: Labeled diagram to be used with table

4.3.1 Material Selection

A key concern with this experiment, and any experiment that deals with extremely corrosive substances at elevated temperatures, is the potential for degradation of the experimental apparatus. Hydrogen sulfide, sulfur dioxide and hydroiodic acid are all corrosive reactants posing a danger to normal carbon steels.

In response to this hazard we have designed the prototype experiment to only expose the process stream to glass, polytetrafluoroethylene (PTFE), and Hastelloy 276C, a highly alloyed steel. While the glass is not feasible for a commercial implementation of this process, beyond corrosion resistance, it has the added benefit of

transparency allowing observation of the process stream. This is useful because the process stream changes color based on its composition, ranging from a deep red for iodine rich streams to turbid white/transparent for streams that have been reacted to form primarily hydroiodic acid. Particularly for the initial reactor, this secondary check, allows visual confirmation that the system is behaving as expected.

The remaining low temperature sections of the prototype are composed of polytetrafluoroethylene (PTFE) tubing. Beyond inertness to the acidic process streams, this material is tough, flexible and easily implemented. As the temperature rises near the second reactor, the PTFE is replaced with Hastelloy 276C. This is a high nickel alloy steel that has been shown to have low corrosion rates even at elevated temperatures with high hydroiodic acid concentration process streams.[71]

Vigreux Column details Bubble equations residence time contact area Estimate of gas residence time

4.3.2 Reactor Details

The Gas-Liquid contact reactor is comprised of a borosilicate glass vigreux column 20 inches in length. The reactor is filled with iodine dissolved in water and a hydrogen sulfide containing feed stream is bubbled through the column before the effluent gas is fed to a scrubber before venting to the hood.

The nature of the reaction causes a gradient in color along the length of the column with iodine rich reddish hues near the iodine feed and white/transparent hues near the hydrogen sulfide feed, where the iodine has been completely consumed. This gradient is useful as a visual check to avoid hydrogen sulfide breakthrough.

The design of this reactor is simplistic and the exact bubble size and thus contact area and kinetics of the gas/liquid reaction has not been ascertained. This is a key next step that has been, to this point, avoided, with focus instead on testing the overall process viability through hydrogen production measurements.

The second reactor is a packed quartz glass 1 inch diameter tube held in a tube furnace. The packing pattern first includes a layer of quartz wool followed by a 1 foot length of steam activated carbon pellets before finishing with another layer of quartz

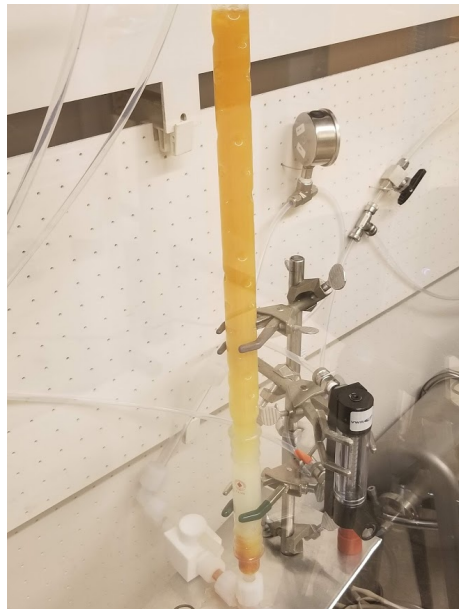


Figure 4-3: Gas-liquid contact reactor for the reaction of hydrogen sulfide with dissolved iodine

wool. The quartz glass is connected to the Hastelloy 276C tubing on either side with cajon type fittings.

Luckily extensive kinetic analysis of hydrogen iodide decomposition in these conditions has been conducted by those interested in a water-splitting variant of this chemical reaction.[47] Given a flow rate and the resulting residence time, this allows the calculation of hydrogen iodide conversion. While useful for process modeling with regards to the prototype tests, the flow rate of gas never exceed 300 cubic centimeters per minute, meaning the reactor residence time never dipped below 30 seconds. This is well above the time required for complete conversion. The degree of conversion is dependent on the temperature of the reactor and is governed by the thermochemistry of the reaction.

This thermochemical prediction was validated[47] and for the tests performed on the constructed prototype at 350 degrees Celsius, 1.8% single-pass conversion is anticipated.

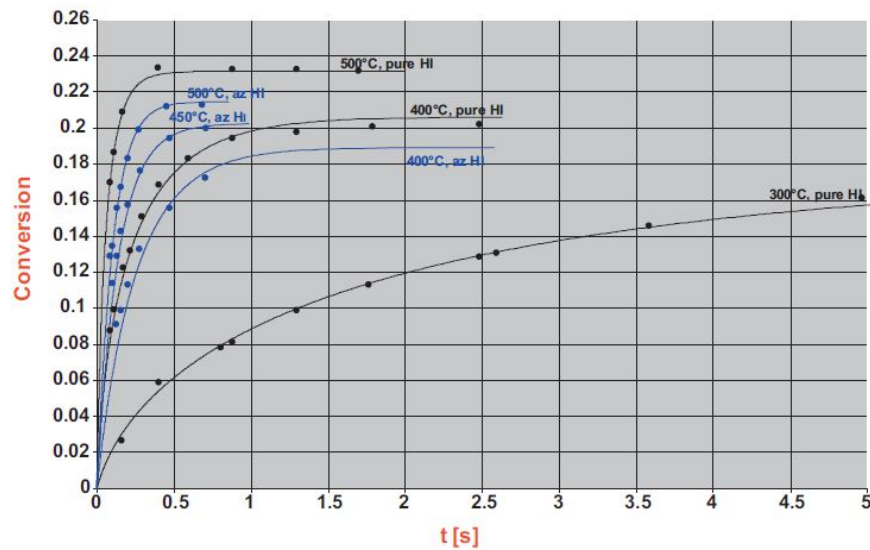


Figure 4-4: Conversion versus contact time plots for HI decomposition reaction using 1 gm of NORIT ROX 0.8 as catalyst at different temperatures and feedings. Dots correspond to experimental values, lines to calculated ones (az HI = HI – H₂O azeotropic solutions; pure HI = pure gaseous HI[47]



Figure 4-5: Hydrogen iodide decomposition reactor

4.4 Analytic Techniques

The principal desired measurement for this experiment was quantity of hydrogen production. Originally this was going to be measured through GC-TCD, but difficulty

with the sensitivity, calibration, and measurement consistency of hydrogen in our chromatographs led to quantitative analysis through the measured mass of the evolved gases with the chromatographs used to list the gases in the evolved product mixture. This combined approach proved favorable as the evolved gases were demonstrated by the chromatographs to be binary (Nitrogen and Hydrogen) in nature, allowing the much more precise mass measurements to quantify hydrogen production.

4.5 Initial Testing Results

We constructed this apparatus according to the specifications and plans described above. The construction took place on a 4'x8' footprint in a continuously vented hood. A photograph of the completed apparatus is shown in the figure below.



Figure 4-6: Photograph of the minimum viable experiment to test for hydrogen generation from hydrogen sulfide

Unfortunately the Covid-19 lockdown occurred shortly after getting this apparatus fully operational. We were however able to complete several experimental runs proving the ability of the device to generate significant amounts of hydrogen gas, as

confirmed by both GC-TCD and mass analysis. However, most of these runs were performed using a recycling feedstock that was necessarily less well characterized. As such, the exact conversion rate was not discernable from those experiments. To get at this information, a single run was performed with a very well characterized feedstock for the second step. In this run, the hydrogen generation was seen to match fairly well with the results provided by Favuzza et. al. While more runs would be desirable (and will occur as circumstances allow), the observed hydrogen generation, and preliminary agreement with literature lends confidence to the ability of this cycle to operate at larger scales. A tabular summary of the runs able to be completed before shutdown are included in Appendix A.

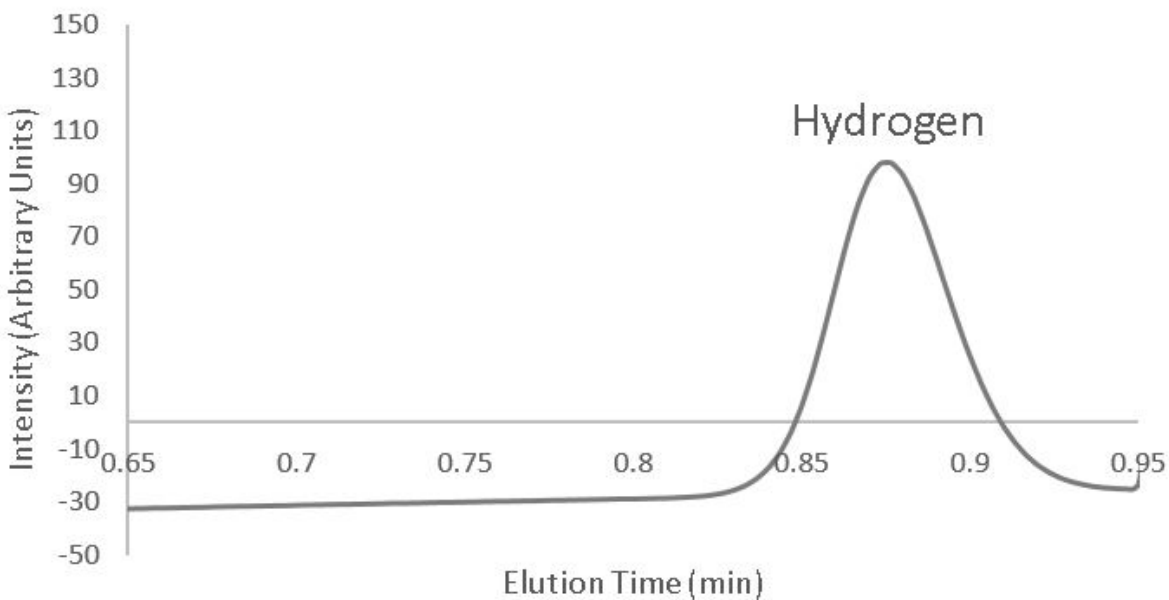


Figure 4-7: TCD detection of hydrogen in the process outlet stream.

4.6 Conclusion and Next Steps

The shutdown presented a choice of whether to wait and complete the originally planned experimental series with the minimum viable experiment, or whether to move beyond this apparatus, upgrading it and allowing more detailed and complete

characterization of the system. We have selected to upgrade the system, using the current waiting time to design the apparatus, assemble the components, and pursue other commercialization activities.

The key restrictions suffered by the minimum viable experiment help to inform the areas for upgrade and scale-up in the version of the apparatus to be constructed when laboratory activities resume.

First, the semi-batch nature of the apparatus was restrictive in that it limited the length of the experimental runs to just a few hours. This forces the system into a perpetual start-up and shut-down and so steady-state is impossible to achieve, and the mass balance during this extended run is similarly difficult. These issues will be corrected by redesigning the apparatus to a truly continuous experiment. The reservoir of $HI/I_2/H_2O$ in the condenser will be kept above the remaining process units allowing gravity to drive flow through the remainder of the system. The gas phase process stream exiting the furnace will be forced by this gravity driven stream up to the condenser where it will continually replenish the reservoir. This upgrade will allow for longer term (12-24 hour) experiments that will provide a better characterization of the full mass balance around the system. These longer experiments will also allow more convincing material property and by-product analyses. The minimum viable experiment was designed to produce H_2 from H_2S , which is a key step in the process. However, the upgrade will include further process stream measurements, including the pH of the liquid process stream exiting the gas/liquid contactor, the SO_2 concentration exiting the boiler, and the temperature, pressure, and flow rates throughout the apparatus. These are key to characterizing the full mass balance around the prototype device and ensuring that we are able to design and prepare for the next stage of scale-up.

The experimental apparatus will largely be comprised of the current minimum viable experiment, reconfigured and with additional probes, sensors, and control systems. A diagram illustrating this control system is shown below.

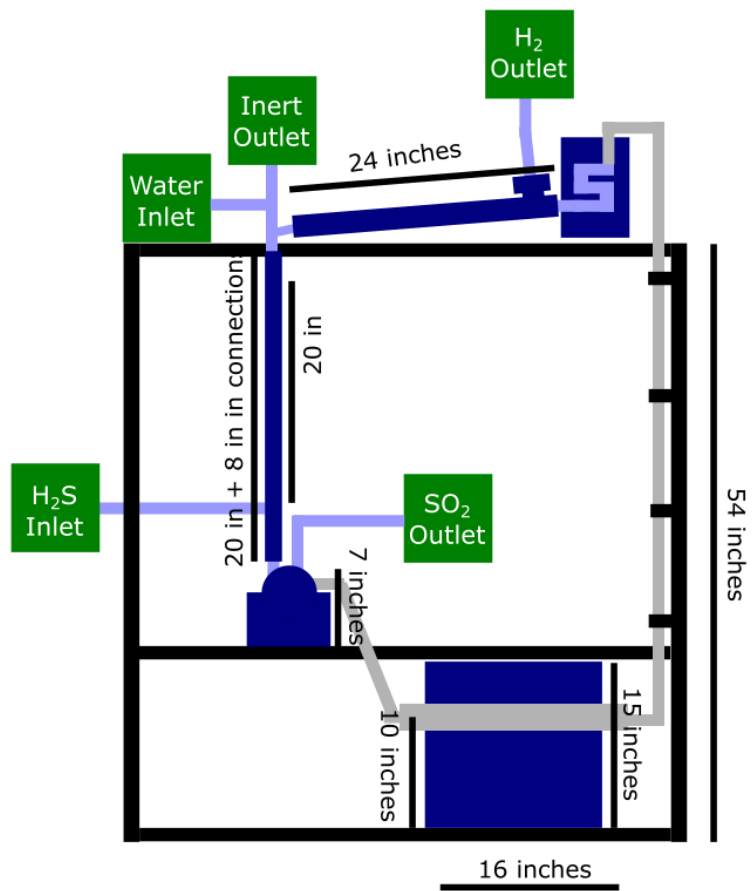


Figure 4-8: Upgraded experimental apparatus

Chapter 5

Techno-economic Modeling and Process Viability Examination

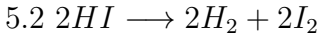
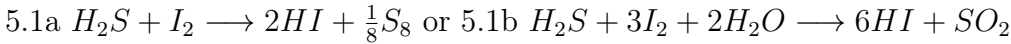
This chapter is, in part, based on my publication in the International Journal of Hydrogen Energy 2020, International Journal of Hydrogen Energy, Volume 43, Issue 29, 19 July 2018, Pages 12939-12947, by Ryan J. Gillis, Khalid Al-Ali and William H. Green, Thermochemical production of hydrogen from hydrogen sulfide with iodine thermochemical cycles.

This chapter will be divided into two sections. Process models related to the production of hydrogen from hydrogen sulfide both through the production of elemental sulfur and sulfur dioxide are discussed. As seen in Chapter 3 there is some ability to toggle between these chemistries based on the concentration and solvation of the hydrogen sulfide and iodine respectively. As will be seen, without the reaction with water the process struggles to produce hydrogen at competitive prices.

5.1 Introduction

We propose a low temperature thermochemical method to accomplish the decomposition of hydrogen sulfide to elemental sulfur and hydrogen gas. The decomposition is accomplished with two reaction and separation steps. The first reaction is performed at low temperatures in a solvent and the second reaction is performed according to

the conditions suggested by Favuzza et. al. in their study of *HI* decomposition.[47]

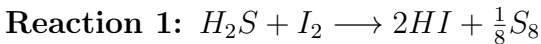


This proposed process is similar to ideas put forth in the 1980s by Kalina[68] [69] and Oosawa[105] but makes use of more recently discovered thermochemical hydrogen iodide decomposition methods and catalysts rather than electrochemical or photoelectrochemical methods. Chakma and Zaman[152] also obliquely mention the potential for this type of process in their review of hydrogen sulfide decomposition methods but they suggest that it should be accomplished by photochemical catalysts. Recent advances in the catalyzed decomposition of *HI*[147] [73] mostly focused toward water splitting schemes, have led us to examine a potential thermochemical *H₂S* splitting scheme.

5.1.1 Thermochemical Cycles

Thermochemical cycles accomplish chemical reactions that are unfavorable in a single step with a series of reaction and separation steps. This series of reaction involves other intermediates that are recycled such that if the stoichiometry of all reaction steps are summed each intermediate cancels out. Thermochemical cycles often also require that each reaction step is performed in distinct conditions. Thermochemical cycles have been studied extensively in the context of splitting water.[104]

As we propose two new thermochemical cycles, we begin by summarizing what is known about each step of the proposed cycle in conditions relevant to the process.



At 25 degrees Celsius without a solvent this reaction is extremely unfavorable with a dGrxn of 35.4 kJ/mol. This is calculated assuming that each species is in their equilibrium form, for example sulfur is an orthorhombic crystal. However, if performed

in water, the solvation of hydroiodic acid drives the reaction to consume the hydrogen sulfide with an overall dGrxn of -71.6 kJ/mol. This implies that in the aqueous phase the thermodynamic limit of the reaction is the almost complete consumption of hydrogen sulfide.

Qualitative descriptions of this reaction in aqueous conditions have been described by various authors[142] [40] but the reaction has little detailed analysis. Mehra and Sharma quantitatively characterize the reaction of hydrogen sulfide and iodine in the context of using iodine as a hydrogen sulfide adsorbent.[99] In this characterization they measure the volumetric rate of adsorption of hydrogen sulfide gas into an iodine solution at ambient conditions. They find that the reactive adsorption happens extremely quickly, observed occurring at rates of 0.1 mol H₂S absorbed per m² gas-liquid interface per second. Kalina and Maas also observed the near complete conversion of hydrogen sulfide (from 25% to less than 1 ppm) at a flow rate of 880 cubic centimeters per min.[69] This was in basic conditions where iodine will be mostly oxidized to the iodate ion as was preferable for their electrochemical process.

The thermochemistry and observations of these authors support a model where hydrogen sulfide bubbled through a concentrated aqueous iodine solution will almost entirely react.

Reaction 2: $2HI \longrightarrow H_2 + I_2$

Hydrogen iodide decomposition is of great importance to many researchers investigating thermochemical cycles for water splitting. The decomposition is the hydrogen generation step for several cycles including the Bunsen cycle. As such, it has been the subject of continuous investigation and characterization.[122] [18] [73] [46] [47] [155] [147] [47] These researchers make use of a variety of catalysts and reaction schemes trying to optimize the production of hydrogen from hydrogen iodide. The reaction is typically performed between 300 and 500 degrees Celsius to achieve high enough kinetic rates while not pushing this entropically unfavored reaction to too high a temperature. Experimentally measured equilibrium constants imply a dGrxn from 21.2-24.4 kJ/mol between 300-500 deg Celsius.[8] [47] This corresponds to equilibrium

conversions ranging from 18-23% in this range.

Sulfur-iodine cycle water splitting attempts run into difficulties at this stage because of the low concentration of HI produced by the Bunsen reaction. The H_2S processing scheme proposed here has the advantage that it is not limited by the low HI and high I_2 concentrations. As such, HI concentrations similar to those tested in experiments can be achieved. Recent studies of the catalysis of this reaction provide detailed information concerning the kinetic behavior of the system. The process model uses the kinetic and catalyst data generated by Favuzza et. al. [47] to describe the decomposition of hydrogen iodide. This decision was made because of the relatively high conversion observed by Favuzza with his activated carbon pellet catalysts and his use of azeotropic mixtures of HI and H_2O . Further this catalyst was tested and found to be stable for at least a week on stream.

5.1.2 Aspen Plus Modeling

Aspen Plus v.10 is a software used to model chemical processes. The software solves the energy and material balances across process units. With user defined inlet streams and realistically designed units complex chemical processing systems can be modeled. There is also extensive functionality related to hazard, economic, and environmental analysis.

Key to realistic unit design is accurate thermodynamic characterization of all important process components. Aspen contains extensive databases defining most common chemicals. When the databases are incomplete group additivity methods fill in the remaining values.

The NRTL property method adapted for electrolytic systems was used for the liquid phase activity coefficients while the Soave-Redlich-Kwong method was used for the vapor phase. The Aspen database and group additivity values defining these methods were accepted, except in the case of the binary interaction parameters between H_2O and HI . This binary mixture is important in many units in the process and so these parameters were fit to experimental data.

5.1.3 Experimental Methods

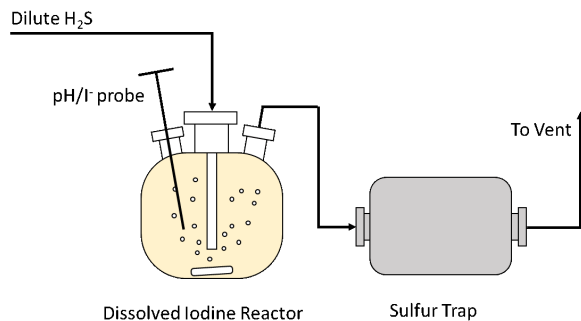


Figure 5-1: Experimental Apparatus

The experiments used pH and I⁻ ion probes to measure the concentration of dissolved HI in a glass reactor that H₂S was bubbled through. The H₂S was supplied at a concentration of 30 ppm with flow controlled by a needle valve and steel ball flow meter. Any unreacted H₂S was adsorbed with Sulfatreat in a large solid phase trap.

The main purpose of the experiment was to determine the viability of using alternative solvents or solvent mixtures in the process. For experiments with low water content, because the pH and I⁻ ion probes only worked in aqueous conditions, continuous ion concentration measurements were not possible. Instead, initial and final reactor samples were diluted with water until the mixture was at least 96% water by mass. Then aqueous probes could be used to measure the concentration and determine the initial and final concentrations of the two ions in the reactor.

5.2 Hydrogen Productions from Hydrogen Sulfide with Elemental Sulfur Byproducts

5.2.1 Water Solvent Process Model

Aspen Plus v.10 was used to create a basic process model that could be used to explore the viability of the process. The process model is scaled to process approximately 50,000 metric tons of sulfur per year. This was chosen to represent a typical amount

of H_2S that a refinery might be required to process. This process model is meant not to represent every detail of every unit, but rather to explore the viability and challenges that implementation of this thermochemical scheme would face. A flow diagram of the process is included below with brief descriptions of the major units.

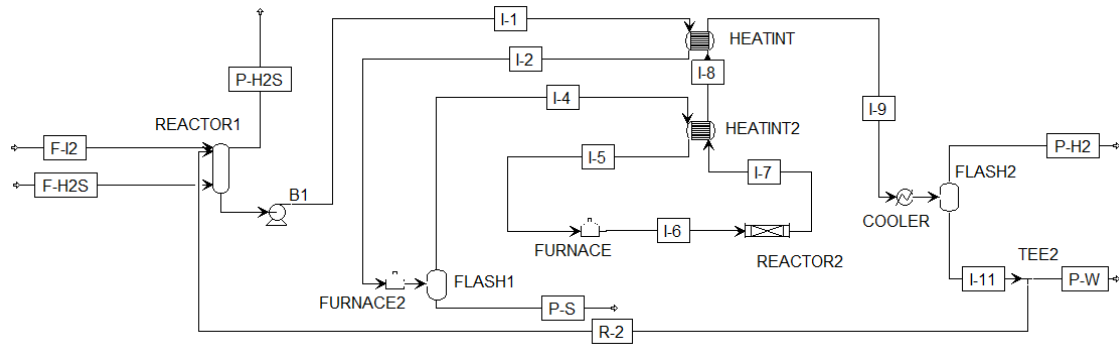


Figure 5-2: Water Solvent Process Flow Diagram

HI Formation Reactor (REACTOR1)

Experimentation suggests that the reaction of hydrogen sulfide with iodine is mass transfer limited and moves quickly to equilibrium.[99] Given this chemistry, the *HI* formation reactor was modeled as an absorption unit with an inlet of hydrogen sulfide in the bottom stage and an inlet of water and iodine in the top stage. The absorption and reaction occurred as the gas and liquid contacted each other in the column and went to equilibrium. The iodine is almost completely consumed during this stage, which is crucial as the later *HI* decomposition reaction is inhibited by iodine.

Pressure Manipulation

The pressure of the process was set to optimize the final separation of hydrogen from the aqueous hydroiodic acid, water, and iodine mixture. Higher pressures allowed more complete separation of hydrogen from the remaining components. To avoid pressurizing a vapor stream with a compressor in the later stages of the process, the liquid stream leaving the *HI* formation reactor was pumped up to a pressure that would allow the desired conditions in the final separation even after significant

pressure losses across the intervening vaporization, heating, and reactive units.

Sulfur Separation (FLASH1)

At this point the elemental sulfur created during the *HI* formation reaction must be removed from the stream. Fortunately, elemental sulfur is much less volatile than the remaining components in the stream. As such, a simple flash separation at 325 degrees Celsius is enough to separate the, then liquid, sulfur from the remaining vapor components. The heat required to vaporize the liquid stream is provided in part by heat integration and in part by a gas furnace.

HI Decomposition Reactor (REACTOR2)

The vapor stream is then heated again with a combination of heat integration and a gas furnace to the temperature of 500 degrees Celsius. The stream flows into a plug flow reactor where it is contacted with an activated carbon catalyst and reacts as described by Favuzza et al.[47] The rate equation and constants corresponding to the process stream conditions are shown below.

$$\frac{d\chi}{dt} = \frac{AP^{0.5}(\chi+E)^{0.5}}{[C+DP^{0.5}(\chi+E)^{0.5}]^3} [(1-\chi) - (\frac{1}{x_e} - 1)\chi^{0.5}(\chi+E)^{0.5}]$$

At the temperatures modeled the parameters fit by Favuzza were $A = 124$, $C = 1.44$, $D = 3.81$, and $E = 2\frac{P_{I_2,feed}}{P}$. Here χ is defined as the reaction conversion in terms of *HI* and P is the total pressure. The unit is modeled as an adiabatic packed multi-tube reactor and achieves a single pass conversion of approximately 20-23% of the inlet *HI*.

Hydrogen Separation (FLASH2)

Finally, the stream is cooled by a combination of heat integration and a cooling water until the hydrogen gas can be flash separated from the remaining liquid or aqueous components. The remaining components are recycled to the liquid inlet of the *HI*

formation reactor. A recycle fraction of 95% was selected to balance model stability with efficiency.

Economic and Environmental Results

The steady state conditions of the model have an inlet flow rate of 180 kmol/hr of H_2S and outlets of 180 kmol/hr of elemental sulfur and 142 kmol/hr of H_2 . The remaining protons are lost as dissolved HI primarily in the purge stream.

Aspen estimates the total capital cost of the project to be \$13.3 million and annual operating cost to be \$15.7 million. The most expensive units in terms of capital cost are the furnaces required to vaporize the aqueous HI streams in preparation for the decomposition of HI in the packed bed reactor. These units are also expected to dominate the utility expenses (over 95%). This points to a key problem with this design. With one reaction step required to be in the aqueous phase and the second required to be in the vapor phase, huge amounts of energy are required to heat and cool these streams. This is compounded by the low single-pass conversion and thus high recycle.

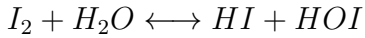
With a few assumptions about the discount rate, tax rate, and depreciation allow the calculation of an H_2 production cost. With a project lifetime of 10 years, 30% tax rate, 15% discount rate, and constant 5 year depreciation rate the hydrogen production cost is \$7.54 per kilogram. This is well above market energy rates. It also excludes costs associated with further purification and pressurization that would be required.

This design also has undesirable environmental properties, as would be expected by the extensive use of natural gas heating. It is estimated that the heating costs, if met by natural gas consumption, would lead to the emission of 19900 kg/hr of CO_2 . With only 285 kg/hr of H_2 created by the process, this process has very little merit in terms of producing H_2 with low carbon emissions. Even extensive integration of other process waste heat or solar heating would likely be unable to make this process favorable.

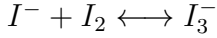
5.2.2 Solvent Substitution Experiments

As shown by the model, one of the largest costs associated with the process is the vaporization of the aqueous phase in which HI is dissolved prior to the catalytic decomposition of hydrogen iodide. If a different, more volatile, solvent or solvent mixture were able to replace water in the system, then the energy costs could be dramatically decreased. Isopropyl alcohol was selected as a potential alternative solvent, because it was already being used as a cosolvent to dissolve the iodine crystals and is significantly more volatile than water. The reaction between H_2S and I_2 was tested in isopropyl alcohol to determine whether HI is formed.

It should be noted that these experiments are prone to a high amount of uncertainty in part because of side reactions. For example, small amounts of HI are formed from I_2 in water.



Similarly I_2 will react with free iodide ions to further cloud the results.



Both of these side reactions are especially problematic in pure isopropyl alcohol experiments because as the reactor volume samples are diluted in large amounts of water to allow pH and iodide concentration measurements even small deviations in the measured concentration of either ion can lead to a significant error.

The experiment involved flowing H_2S through I_2 dissolved in isopropyl alcohol for several hours. Samples were taken from the reactor volume before and after H_2S flow, diluted and then measured. The results are shown below.

Although significant HI has been produced through the side reactions independent of H_2S flow, there is a clearly an increased amount of HI after the H_2S flow. The estimated error of the measurements further supports the conclusion that the

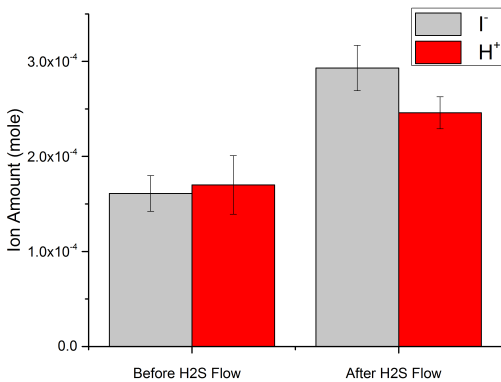


Figure 5-3: Experimental results confirming HI formation in a pure isopropyl alcohol solvent

reaction between H_2S and I_2 occurs quickly in pure isopropyl alcohol. Further, the difference between the measurements before and after H_2S flow suggest that about 2 HI are formed from each H_2S in this non-aqueous solvent, matching the expected stoichiometry.

Others have tested the reaction of H_2S and I_2 in organic solvents. One group dissolved iodine in dimethyl formamide and dispersed 5 vol% H_2S through the mixture regularly measuring the concentration of H_2S in the outlet stream with gas chromatography and visually inspecting the reactor.[140] They observed that the reactor changed from deep red, a color characteristic of dissolved I_2 , to pale yellow with small flakes of yellow solid sulfur. The H_2S concentrations in the outlet stream also matched expectations, with no H_2S observed in the first portion of the experiment due to complete conversion of H_2S to HI and elemental sulfur. In the second portion of the experiment the concentration of the H_2S in the outlet gas quickly rose to the inlet concentration, presumably in response to the depletion of I_2 in the reactor.

These experiments strongly support the idea that HI can be formed even in a variety of non-aqueous solvents.

5.2.3 Isopropyl Alcohol Solvent Process Model

With the goal of improving the economic and environmental properties of the initial process model and guided by experiments suggesting the possibility of replacing water with an organic solvent, an additional process model was created in Aspen Plus v.10 using isopropyl alcohol. A flow diagram of this model is shown below.

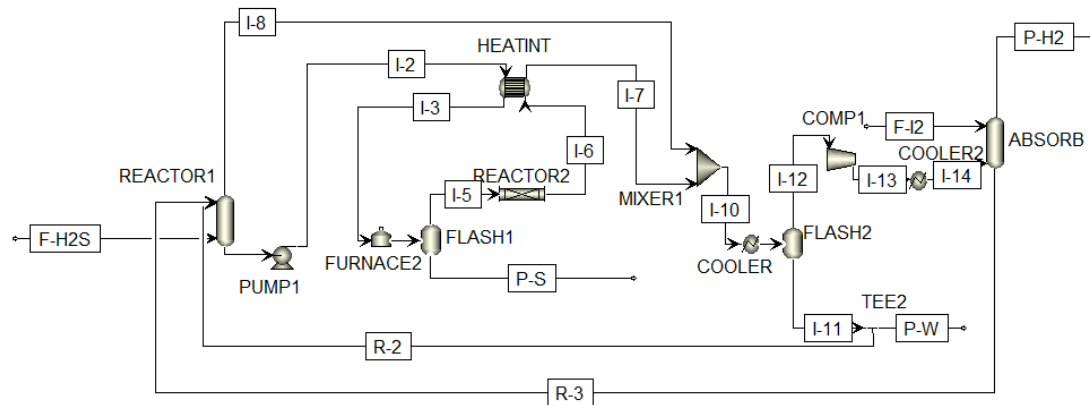


Figure 5-4: Isopropyl Alcohol Solvent Process Flow Diagram

Key Differences

One key difference between the two versions of the process is that *HI* is much less soluble in isopropyl alcohol compared to water. This led to several flow sheet modifications. For example, an absorber was added which uses the inlet isopropyl alcohol/iodine stream to remove *HI* from the product H_2 stream. This required the addition of a compressor and cooler to ensure that the inlet streams were at the appropriate temperature and pressure conditions. Another change involved recycling the gas outlet of the first reactor, which was unnecessary in the water solvent model. The temperature of the *HI* decomposition reaction was also lowered from 500 degrees Celsius to 300 degrees Celsius, sacrificing single pass conversion for lower heat duties in the modeled natural gas furnace, a simplified heat integration design, and lower solvent decomposition potential.

There is very limited VLE data describing the behavior of *HI*/isopropyl alcohol mixtures. While the amount of water solvent was decided as the minimal amount

required to dissociate the *HI* formed in the first reactor, the degree of *HI* solvation in isopropyl alcohol is not well characterized. With no obvious choice, the volumetric flow rate of the solvent at the ambient conditions of the first reactor was held approximately constant. As isopropyl alcohol is less dense than water, mass flow rates of the solvent in this model were less than in the initial water solvent model. There is an admittedly high level of uncertainty around the solubility and vapor liquid equilibrium behavior of the system. However, the trends shown by the model should be valid even if the exact values are not.

In most other respects the process is very similar to the initial water-solvent model.

Isopropyl Alcohol Decomposition

The process model ignores potential isopropyl alcohol reactivity either unimolecularly or with radicals that might be formed at these elevated temperatures. The validity of that assumption was explored using previously published results that examined the pyrolysis of isopropyl alcohol [14] and the reaction of isopropyl alcohol and iodine [144]. To determine the significance of the isopropyl alcohol decomposition in the cycle, the reactor conditions were applied to the fitted rate laws determined by Barnard, Walsh, and Benson.

The rate laws from the relevant sources are shown below along with the rate constant at model reactor conditions.

$$k_{pyrolysis} = 10^{8.4} \exp(-34,000/RT) \text{sec}^{-1} = 2.72 \times 10^{-5} \text{sec}^{-1}$$

$$k_{I_{rad}} = 10^{11.07 - 20,500/RT} \text{Lmol}^{-1} \text{sec}^{-1} = 1.79 \times 10^3 \text{Lmol}^{-1} \text{sec}^{-1}$$

If the concentration of iodine radicals is assumed be in thermodynamic equilibrium with *I*₂ and *HI* respectively then the consumption rates of isopropyl alcohol due to pyrolysis and radical reaction are 0.25 and 26.6 kg/hr respectively. This is less than half a percent of the isopropyl alcohol inlet flow rate and an even lower fraction of the internal flow rates.

It should be noted that the model reactor conditions are outside of or at the

extreme edges of the experimental bounds from which the fitted rate laws were determined. Barnard's study of isopropyl alcohol pyrolysis began taking measurements at 540 deg Celsius while Walsh and Benson's study of iodine and isopropyl alcohol had its highest temperature measurements at 300 degree Celsius. This extrapolation, in addition to the undetermined effect of the catalyst on isopropyl alcohol decomposition introduces significant uncertainty. However, in the absence of experimentation closer to the conditions in question, these results provide the best possible estimates.

Economic and Environmental Results

The H₂S inlet and H₂ and elemental sulfur outlet flow rates were very similar to the water solvent case. The steady state conditions of the model have an inlet flow rate of 180 kmol/hr of H₂S and outlets of 180 kmol/hr of elemental sulfur and 140 kmol/hr of H₂. Also mirroring the initial design, the remaining protons were lost as dissolved *HI* primarily in the purge stream.

Aspen economic tools were again used to estimate the costs associated with installing and operating such a unit. It is estimated that the total capital cost of the project to be \$9.1 million and annual operating cost to be \$3.0 million of which \$1.2 million is spent on utilities. The compressor that prepares the impure *H*₂ stream for further separation is the largest capital cost, with the furnace and heat exchanger used for heat integration also representing significant costs. In terms of utilities the natural gas heating comprises 68% of the total utility costs with electricity for the compressor comprising almost 30% of the total costs.

With the same economic assumptions as the water solvent model, namely a project lifetime of 10 years, 30% tax rate, 15% discount rate, and constant 5 year depreciation rate the hydrogen production cost is \$2.07 per kilogram. The *H*₂ is 98.5% pure and is pressurized to 20 bars. Note that this does not include any costs associated with the solvent or iodine, as both are recycled.

The carbon load associated with this design is much less than those of the water solvent design. It is estimated that the heating costs, if met by natural gas consumption, would lead to the emission of 1308 kg/hr of *CO*₂. Electricity costs, if met

by carbon energy sources, would further contribute 150 kg/hr of CO_2 . This is balanced with the production of 283 kg/hr of H_2 . Even without extensive integration of other process waste heat or solar heating, this process seems to represent a reasonable trade-off between carbon emissions and hydrogen production. If solar heating could be integrated then both the cost and environmental impact of this process could be substantially reduced.

5.2.4 Solvent Selection

The water solvent process model showed that the costs associated with vaporizing the aqueous phase in preparation for HI decomposition makes the process economically uncompetitive. This is unsurprising because water is a solvent that, in many ways, is a poor fit for this thermodynamic cycle. Water has an unusually high latent heat of vaporization. This means that water, much more so than other solvents, requires large amounts of energy to change phases. For the same reason that steam is ideal as a power generation energy vector, water as a solvent in the thermochemical cycle requires much too high an energy cost to be viable. Water also has a boiling point that is higher than many other solvents. A higher boiling point is less favorable because it makes heat integration less effective. Since the majority of the heat transfer must occur at the phase change temperature, the lower the phase change temperature the more heat integration is possible. Other key properties, such as the vapor phase heat capacity, are also not ideal. For many reasons water is not a good choice as a solvent for this cycle.

An ideal solvent has several characteristics. Like water, the solvent should not react with HI or I_2 , even at elevated temperatures. In contrast to water, it should have a low boiling point and smaller latent heat of vaporization. However, it must also provide an environment that solvates dissolved HI enough for the reaction of H_2S and I_2 to favorably produce HI . This implies another balance. The solvent must have strong enough intermolecular interactions to significantly stabilize newly formed HI , while not having intermolecular interactions that are so strong as to drive up the energy requirements of vaporization. The solvation energy of HI in most solvents is

not known, which makes it difficult a priori to select an optimal solvent.

This work used isopropyl alcohol primarily because it was already being used as a minor cosolvent to induce the solvation of I_2 in primarily water solvent experiments. With experimentation suggesting that isopropyl alcohol provided enough solvation to HI for the first reaction step, the implications of a process design with a pure isopropyl alcohol solvent were explored in the second process model. However, this work is not trying to convey that the suggested isopropyl alcohol solvent model at these temperatures is completely optimized. Many other solvents and conditions are likely better suited to the process, but a lack of fundamental data makes prediction without detailed experimental verification difficult.

5.2.5 Process Viability and Comparison

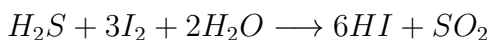
While the isopropyl alcohol model clearly has better properties than the water model, a more natural comparison is to other large-scale commercial H_2 production methods. The table below compares relevant characteristics of H_2 production from the model processes introduced here and natural gas reforming.

	Water Solvent Model	Isopropyl Alcohol Model
Approximate H_2 Production Cost	\$6.53	\$2.07
CO_2/H_2 Production	69.8	5.2

The comparison shows that while natural gas reforming and the proposed isopropyl alcohol solvent process were similarly economically effective methods for H_2 production, steam methane reforming is less ideal with respect to CO_2 emissions. The proposed process using isopropyl alcohol as the solvent could potentially compete economically with natural gas reforming and further improve its CO_2 emission behavior with solar or other alternative heating patterns.

5.3 Hydrogen Productions from Hydrogen Sulfide with Sulfur Dioxide Byproducts

As described in chapter 3, after experimentally testing the reaction of hydrogen sulfide and iodine we found that rather than forming elemental sulfur, in low hydrogen sulfide or high hydroiodic acid concentrations the sulfur dioxide is formed rather than elemental sulfur. This section will shift from the originally anticipated process design to describe a modified process model incorporating and taking advantage of this surprising chemistry.



5.3.1 Flowsheet

In addition to a modified stoichiometry and environment of reactor 1, additional heat integration and purification units have been incorporated to improve the purity of the outlet streams and increase the heat recovery of the system, lowering energy and carbon costs.

The process begins with the inlet of H_2S at a scale comparable to what a mid-sized refinery might experience (about 6 metric tons per hour). We did not consider any impurities in this stream, but anticipate that the majority of impurities that might exist in such a stream (such as carbon dioxide, methane, or other light hydrocarbons) would not have a large effect on the process either because they are chemically inert or largely insoluble in water. The other inlet is principally water, although because of the outlet streams needed to maintain model stability, this stream also includes some iodine.

The inlet streams meet with the recycle streams at a gas-liquid reactor where H_2S , H_2O , and I_2 are consumed to produce HI and SO_2 . The stream is heated and then depressurized to offgas the SO_2 in a first vapor-liquid separator. This principally SO_2 stream is purified in an absorber to recover additional HI , using the primary

water inlet as the absorbing liquid stream. The purified SO_2 is then preferably further oxidized in the Contact process to form H_2SO_4 but this is not included in this model. Returning to the liquid stream comprised of HI and H_2O , this stream is pressurized, vaporized, and then heated to a temperature of 300 degrees Celsius. At this temperature the stream passes through a packed bed reactor where a fraction of the HI catalytically decomposes to H_2 and I_2 . The stream is then cooled and the volatile H_2 is separated from the remaining I_2 , HI , and H_2O in a second vapor liquid separator. The remaining HI and H_2O is recycled back to the first reactor. Note that iodine is not consumed in the process and ideally would be fully recycled such that none would be lost in outlet streams.

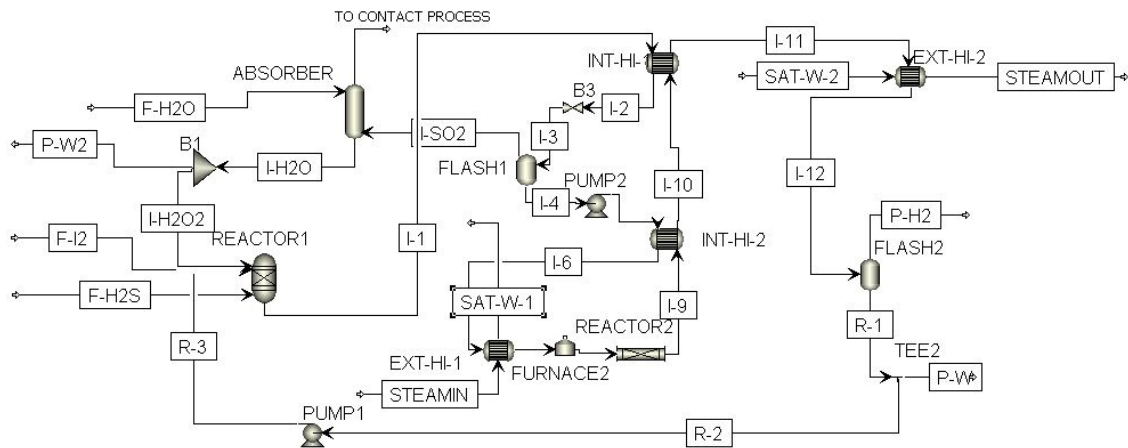


Figure 5-5: Hydrogen sulfide decomposition process flowsheet producing SO_2 as a byproduct

Reactor Modeling

Perhaps the most important components of a process model are the reactors, where the chemistry is principally occurring. There are two reactors in this system, an initial gas-liquid reactor that creates hydroiodic acid from hydrogen sulfide, iodine, and water and a packed-bed reactor that decomposes hydrogen iodide into hydrogen gas and iodine vapor.

The gas liquid contactor is the component of the system that is still the least characterized. While experiments have validated the stoichiometry, for all tested flow

rates the reactant stream was near completely consumed. While frustrating from a characterization standpoint this was actually one of our key safety considerations as breakthrough of the toxic gas present additional hazards to the researcher. This lack of variance in results coupled with unknown bubble characteristics means that the precise kinetics for this reaction between hydrogen sulfide, iodine, and water remain unknown. In the face of these uncertainties we acted conservatively, sizing the reactor to match the ratios we use in our laboratory system. While this almost certainly oversizes the reactor, in the scope of the overall process, this unit is not a major cost and so its sizing is not incredibly sensitive parameter. The next stages of experimentation will certainly look to characterize this less certain component.

The second reactor, the site of hydrogen iodide's decomposition to hydrogen gas and iodine vapor, is modeled, as it appears in our prototype system as a packed bed reactor. Specifically it is a set of parallel 2 cm diameter tubes that are 1 meter in length. These are heated by a natural gas furnace to reach the desired decomposition temperature (300 degrees Celsius in the base case). The kinetics for this reaction are well characterized[47] with a complex Langmuir-Hinshelwood model based on 6 catalytic surface elementary steps. However because the kinetics are relatively fast and the thermodynamic conversion limits are low, this reactor is also oversized, ensuring that thermodynamic limit is reached with minimal impact on the capital cost. The conversion of HI to H_2 along the length of this packed bed reactor is modeled below.

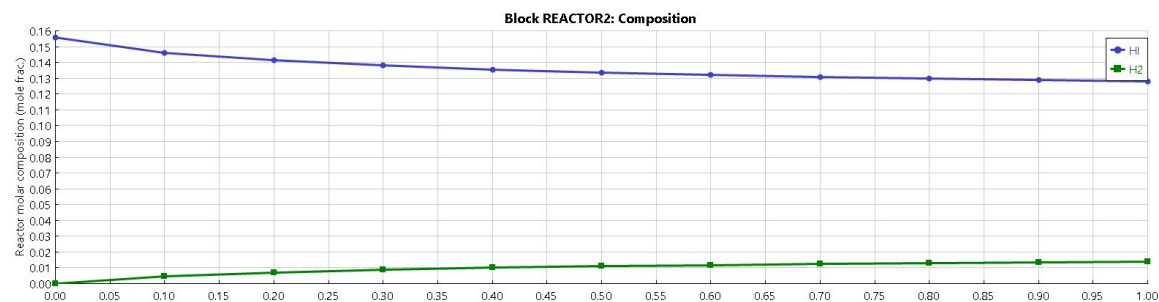


Figure 5-6: Modeled conversion of the HI decomposition reactor

Heat Exchangers

This process requires the alternating vaporization and condensation of the primary reactant stream. The process itself consumes little energy, but requires the use of large amounts of energy to shift the phases of the reactants. Thus recovering the energy through heat integration is a key design challenge, requiring careful design of the associated heat exchangers. In this implementation heat integration within the process, units INT-HI-1 and INT-HI-2, and with other local processes, EXT-HI-1 and EXT-HI-2, are included. Specifically, almost all of the energy needed to vaporize the stream is supplied by high pressure steam in EXT-HI-1. EXT-HI-2 then recovers this and additional energy in the form of lower pressure steam. In the case that there are sufficient local heating needs this generated steam partially compensates for the carbon emissions in the natural gas furnace (FURNACE2). The furnace in the process is essentially replacing another carbon emitting heat source that would have needed to exist anyways. It is readily acknowledged that this design relies on sufficient local heating needs that can be met by the generated steam and would not work in every location. However, heat integration is common within refinery settings and the scale is small enough in comparison to other refinery operations that we do not anticipate this integration being problematic. An approach temperature of five degrees Celsius was selected to balance the need to draw as much energy from one stream to another as possible, while still maintaining reasonable heat exchanger sizes.

Material Factors

An important factor for the capital cost estimation is the materials of construction for each component. In general the system used welded stainless steel for the low temperature sections and Hastelloy 276C for the HI decomposition reactor. Together these increase the capital cost by about 12%, which was calculated using Aspen Plus V.10's economic cost estimator.

5.3.2 Energy and Utilities

Apart from the equipment itself, the process is described by its energy and utility consumption.

Energy and Carbon Costs

The process consumes energy both through electricity, used to drive the pumps pressurizing the recycling liquids, and natural gas, the heating of which is used as the final heating element in the hydrogen iodide decomposition reactor. In addition relatively equivalent amounts of steam are consumed and produced by the process.

Electricity is a minor cost, and was priced at 0.0775 \$/*kWhr*. This price is fairly conservative as the current average U.S. industrial electricity price is 0.064 \$/*kWhr* with an average carbon intensity of approximately .45 kg*CO*₂/*kWhr*.[4] However, as it is a very minor energy input neither of these parameters are very sensitive.

More significant is the natural gas feedstock used as a heating element to raise the process stream's temperature to the degree necessary for efficient decomposition. A price of 0.012 \$/*kWhr* and a carbon intensity of 0.24 kg*CO*₂/*kWhr* was used. In this case the carbon intensity is fairly indisputable, but the cost is again conservatively estimated. The current (July 2020) Henry's Hub price for natural gas is 0.006 \$/*kWhr* which is almost exactly half of the modeled cost. Given the volatility of oil and gas prices, this perhaps overly high price of natural gas was used to ensure that economic analysis will not oversell the technology in a future with higher natural gas prices.

The carbon intensity of this process is also of key concern. Overwhelmingly the carbon intensity comes from the burning of natural gas to prepare for the decomposition reactor. Normalized to the hydrogen gas production rate this equates to approximately 1.3 kg of *CO*₂ per kg of *H*₂ produced. However, due to the decreased Claus unit operation, an additional 1.2 kg of *CO*₂ per kg of *H*₂ is added to account for the additional steam produced with the Claus process. This brings the total carbon cost to approximately 2.5 kg of *CO*₂ per kg of *H*₂.

5.3.3 Results and Viability

From these process models the capital and operational costs are estimated, along with the carbon intensity. From these values the rate of return, production price of hydrogen, net present value and payback period can be projected subject to your estimates of the plant lifetime, tax rates, depreciation timelines, and other economic variables. These calculations largely stem from the calculation of the net present value according to...

$$NPV = \sum \frac{C_{flow}}{(1+i)^t}$$

where C_{flow} is the cash flow associated with time period t and i is the discount rate.

For the base case we assumed hydrogen sulfide processing rates in line with the average U.S. refinery (approximately 50,000 metric tons per year). The table below shows the key economic data used to calculate the profitability of this process.

Table 5.1: Parameters taken from the process model

Key Financial Parameters	
	\$Mil
Equipment Cost	\$13.80
Installed Cost	\$23.20
Total Capital Cost	\$35.20
Annual Operating Cost	\$4.40
Annual Revenue	\$11.80

This together with a 10 year plant lifetime, 21% tax rate, and flat depreciation allow the calculation of process characteristics useful for comparison.

Table 5.2: Calculated values from net present value analysis based on the parameters observed in the process model

Key Results for Comparison	
Hydrogen Production Price	\$1.47 /kg H ₂
Internal Rate of Return (with \$2/kg H ₂ sales price)	15%
Payback Period	2.99 years
CO ₂ /H ₂ Emissions	2.5

Cost Comparisons

The calculated values invite comparison to the current processes that dominate the over \$100 billion hydrogen market.

Table 5.3: Comparison between the proposed process and the current dominant market technologies

	Fossil Fuel Reforming (Merchant)	Electrolysis (Fossil Fuel)	Electrolysis (Renewable)	Reforming (Merchant, Carbon Capture)	Fossil Fuel Proposed
Market Share	96%	3.2%	0.8%	<0.1%	*
Levelized Cost of Hydrogen	\$1.80- \$2.50	\$4 - \$6[138]	\$6 - \$7[138]	\$2.16 \$2.934[45]	-\$1.5
CO ₂ Emissions	$\frac{kg CO_2}{kg H_2}$	10	21[79]	15[79]	3-4[45] 2.5

As can be seen the newly proposed process compares favorably, at least in silico. Further analysis at other operational scales is needed to determine in what situations the process is the most profitable.

5.4 Conclusions

This work does not represent fully optimized technologies ready for immediate implementation. Rather it points to a possible technology that seems to have the capability to extract a large amount of value from a stream that is created and processed on a huge scale.

While there are still many uncertainties, an iodine based thermochemical cycle merits further investigation as a potential replacement for the Claus process which also produces H_2 . Preliminary modeling suggests that this type of process could be comparable in cost and superior in CO_2 emissions to currently used large scale H_2 production methods.

Chapter 6

Summary and Recommendations for Future Work

In this final chapter, I will briefly summarize the work and describe the next steps that researchers should take to build upon this thesis.

6.1 Summary

The thesis is chiefly focused on the practical applications of sulfur chemistry with both computational, experimental, and techno-economic efforts.

First, computational prediction and insight into previously opaque reacting sulfur systems is afforded through the efforts described in chapter 2. These included both thermodynamic, kinetic, and algorithmic changes allowing for an increased range of reaction mechanism generation for sulfur containing systems in the context of the Reaction Mechanism Generator software package. Oxidation was of particular interest due to its importance in the natural and industrial world as well as the previous lack of modeling capability. Overall, the approach was successful with many of the predictions from sample systems matching experimental observations from a variety of authors and works.

Second, experimental efforts focused on the reactions of hydrogen sulfide with dissolved iodine, characterizing and quantifying products using a wide variety of analytic

tools. After some understanding of the reacting system was gained, efforts shifted to understand and test its practical application. The end goal of these experiments was to prepare a system that could convert hydrogen sulfide to hydrogen gas and sulfur dioxide through a reaction with water and several iodo-intermediates. The experimental work culminates in a demonstration of this capability, producing hydrogen gas at the liters scale.

Finally, techno-economic modeling of the novel chemical cycle built upon the observations of the experimental work demonstrate the range of commercial applications for this new technology. Several different models based on varying solvents and flow diagrams were built with their economic and environmental properties compared.

6.2 Recommendations for Future Work

6.2.1 Sulfur Chemistry Expansion

The expansion of reaction mechanism generation into oxidating sulfur systems invites several more valuable studies.

First, and perhaps most obviously, the oxidative pathways to dimethyl sulfone, an observed product without an obvious generation pathway should be solidified. The possibilities of surface and condensed phase kinetics should be examined as well as additional generation pathways beyond those examined to this point.

Second, while this work examined the oxidation of dimethyl sulfide to sulfur dioxide, a more far reaching study would include other organosulfur feedstocks common in nature (organothiols and other more complex species) and expand the model beyond sulfur dioxide at least to sulfuric acid. This would require additional experimental work to verify these reactions again and new capabilities around the interaction of different phases (chiefly gas and condensed liquid droplets).

Third, while some justification for accuracy in thermodynamic property prediction is provided, the sheer breadth of possible reactions makes it difficult to provide a truly comprehensive kinetic prediction capability. However, the expansion of the pre-

dictive capabilities to systems that are anticipated to be of importance (sulfuric acid formation, sulfur polymerization, etc.) should be more fully fleshed out. This would involve finding transition states for several dozen example reactions and calculating the associated kinetic parameters.

6.2.2 Sour Gas Processing

My current work is focused on scaling up the hydrogen production prototype described in chapter 4. A new device, described at the end of chapter 4, is being constructed that represents advances in both scaling and operation time.

Perhaps the most important progress that can be made in advancing this work is in scaling up the demonstrations that have already been performed. The sheer scale of industry (thousands of metric tons of material per day in many applications) makes testing relevant conditions nearly impossible in a laboratory setting. Moving from gram to kilogram to metric ton represent key advances in the commercialization pathway. As such the liters scale demonstrations that have been performed up to this point need to be advanced to tens, hundreds, and eventually thousands of liters before serious commercial implementation can be made. As this scale-up occurs testing various impurities, from water to carbon dioxide to propane, will be crucial to proving the usefulness is real application.

In addition to scaling, more insight into the nature of these branching pathways should be made. While we have found conditions that seem to promote what we currently deem the more desirable pathways at the large scale, the nature of this branching, the specific intermediates along each reaction pathway, and the methods to manipulate these reactions will be key to understanding the fundamental chemistry of this potentially very useful system. This will involve, in part, the kinetic evaluation of the gas liquid contact reaction. While current designs emphasized safety with minimal hydrogen sulfide breakthrough, this kinetic characterization could be easily performed by manipulating reactor residence time, bubble size, and inlet flow rates while monitoring the reactor outlet concentrations.

A final point would return to some early work evaluating the system in a variety

of solvents. Many of the challenges of the current system revolve around its use of water as a solvent. Finding an alternative solvent could greatly reduce the energy requirements of the system.

Finally while several different techno-economic models have been created, they do not begin to represent the breadth of potential application for this technology. Focused mainly on a hypothetical "median refinery" further work evaluating the technology as a desulfurizer at natural gas well-sites or processing facilities deserves serious attention. In fact, given the huge range at which hydrogen sulfide is processed understanding the economics across of the orders of magnitude from relatively small to large refineries is also of great value.

6.3 Final Conclusion

It is the nature of graduate work to meander with the mind of the student (and the funding of the adviser). Despite this sometimes eclectic journey, this thesis was pieced together to include what I believe to be valuable insights and knowledge on a range of subjects from the understanding of the natural world to a potential key piece of greenhouse gas reducing technology. It is my hope that these threads will be picked up by future researchers who will add their own as they weave them into a tapestry of knowledge which will better the human condition.

Appendix A

Tables

Table of Contents 1. Group Additivity Values

- 1.1 Sulfur Centered Groups
- 1.2 Oxygen Centered Groups
- 1.3 Carbon Centered Groups
- 2. Molecule Dataset
 - 2.1 Validation Set Comparison
 - 2.2 Full List with Thermochemistry
 - 2.2.1 Stable Molecules
 - 2.2.2 Radicals
- 3. Kinetics
 - 3.1 High Pressure Rate Constant Expressions
 - 3.1.1 Calculated
 - 3.1.2 Literature
- 4. Experimental Appendix
 - 4.1 Experimental Conditions
 - 4.2 Experimental Index
- 5. Computational Appendix
 - 5.1 Gas Phase Thermochemistries

A.1 Group Additivity Values

The labels for each group describe the nature of the heavy atom and its neighbors. It does this by identifying characteristics such as the valence of the heavy atom (2, 4, or 6 for sulfur), and the types of bonds (s for single, d for double, and t for triple). The characteristics for neighboring atoms follow the same pattern but are separated by a dash. Oxygen and carbon have set valences (2 and 4 respectively) and thus are not explicitly included in the group labels. Some descriptors are more generalized than this, but these exceptions are generally self-explanatory.

Terminal atoms, such as the oxygen in carbonyl, sulfoxide, or sulfone groups are lumped into the groups of the adjacent atoms. For example, the group $S4d-OdCsCs$ represents a sulfur atom double bonded to an oxygen with two neighboring carbon atoms that only have single bonds. As another example, the group $S6dd-OdCdOS$ represents a sulfur atom double bonded to an oxygen atom with neighboring carbon, oxygen, and sulfur atoms double, single, and single bonded respectively. The subgroup $C = O$ represents the entire carbonyl group and the subgroup $C = S2d$ similarly represents the entire thiocarbonyl group.

If the least square problem is formulated as...

$$A x_{GAV} = y_{Enthalpy} \quad (\text{A.1})$$

With A as the matrix of coefficients, x_{GAV} as the vector of GAV enthalpy contributions, and $y_{Enthalpy}$ as the vector of calculated molecule enthalpies minus the known group values, the covariance matrix of the group additivity values is calculated by...

$$Cov_{x_{GAV}} = (A^T A)^{-1} A^T Cov_{y_{Enthalpy}} A (A^T A)^{-1} \quad (\text{A.2})$$

Here we assume that the standard deviation of the enthalpies is, $\sigma_{Enthalpy} = 0.64 \frac{kcal}{mol}$, corresponding to that observed in differences between the experimentally known and calculated enthalpies in the validation set. The uncertainties of known (not fitted as a part of this work) groups are taken from the RMG Database. These

summed variances are assumed to be the components of the diagonal matrix $Cov_{y_{enthalpy}}$.

Tables S1-S3 report the uncertainty corresponding to the diagonal elements of $Cov_{x_{GA}}$ to 2σ .

Table A.1: Sulfur-centered group additivity values. Enthalpies are given in $\frac{kcal}{mol}$. Entropies and heat capacities are given in $\frac{cal}{mol \cdot K}$

Groups	$H(298)$	$2\sigma_H(298)$	$S(298)$	$C_P(300)$	$C_P(400)$	$C_P(500)$	$C_P(600)$	$C_P(800)$	$C_P(1000)$	$C_P(1500)$
S2d-S	4.6	3.6	54.3	9.0	7.5	7.0	6.9	7.5	7.8	8.1
S2s-(C=O)H	-15.6	2.7	23.2	5.4	5.5	6.4	7.0	6.9	6.9	8.8
S2s-(C=S2d)(C=S2d)	-4.2	4.1	3.4	2.0	3.4	5.1	6.0	3.8	2.4	4.8
S2s-(C=S2d)Cmb	-10.7	3.7	0.9	2.4	4.1	5.9	6.6	4.1	2.6	5.5
S2s-(C=S2d)Cs	-13.7	2.9	2.1	2.0	2.6	3.9	4.6	2.3	1.0	3.9
S2s-(C=S2d)H	-4.4	2.2	27.3	4.6	6.0	7.1	7.6	6.6	6.2	8.3
S2s-CbCb	-15.3	5.2	-2.4	2.9	4.8	6.8	7.7	5.4	3.9	7.0
S2s-CbH	-8.3	2.7	24.3	5.1	6.5	7.8	8.5	7.7	7.4	9.8
S2s-CdCb	-13.0	4.1	0.3	3.2	4.4	6.0	6.7	4.4	3.1	6.3
S2s-CdCd	-10.0	3.8	3.6	2.8	3.3	4.5	5.1	2.9	1.8	5.2
S2s-CdCt	-14.9	4.1	-0.5	3.3	4.5	6.2	6.8	4.4	2.9	5.4
S2s-CdH	-6.3	2.0	27.7	4.6	5.2	6.1	6.7	6.2	6.1	8.6
S2s-Cs(C=O)	-23.1	3.5	-5.2	2.6	2.0	3.1	3.9	2.6	1.8	4.6
S2s-CsCb	-14.0	3.4	-0.5	3.4	3.9	5.1	5.5	3.1	1.9	5.1

Table A.1: Sulfur-centered group additivity values. Enthalpies are given in $\frac{kcal}{mol}$. Entropies and heat capacities are given in $\frac{cal}{mol \cdot K}$

Groups	$H(298)$	$2\sigma_H(298)$	$S(298)$	$C_P(300)$	$C_P(400)$	$C_P(500)$	$C_P(600)$	$C_P(800)$	$C_P(1000)$	$C_P(1500)$
S2s-CsCd	-12.9	2.8	1.7	4.4	4.0	4.7	4.9	2.3	1.0	4.0
S2s-CsCs	-12.9	2.5	2.0	4.1	3.2	3.6	3.6	1.1	-0.3	2.5
S2s-CsCt	-17.7	3.4	-0.5	4.3	4.6	5.7	6.1	3.6	2.1	4.8
S2s-CsH	-7.9	1.3	28.8	5.7	5.2	5.6	5.8	5.0	4.9	7.1
S2s-CtCb	-17.0	4.7	-3.8	3.8	5.6	7.4	8.2	5.7	4.1	7.1
S2s-CtCt	1.2	5.0	0.5	5.6	8.4	11.0	12.3	10.4	9.1	12.2
S2s-CtH	-11.2	2.6	23.3	5.8	7.0	8.3	9.0	8.1	7.6	9.5
S2s-OCs	-0.8	1.3	6.4	6.3	5.5	5.6	5.7	4.1	3.3	4.3
S2s-OH	9.7	0.4	30.8	7.2	7.6	7.8	8.1	8.2	8.5	8.7
S2s-OO	6.0	0.8	8.5	7.3	7.7	8.3	8.6	8.3	8.0	7.1
S2s-S _D eH	2.0	0.5	28.5	6.3	6.9	7.0	7.3	7.8	8.1	8.5
S2s-S2O	5.0	0.8	10.6	7.0	6.9	6.9	7.0	6.7	6.5	6.0
S ^a 2s-S ^a 2sCb	-8.3	2.6	4.2	5.2	5.6	6.4	6.8	6.0	5.2	6.4
S ^a 2s-S ^a 2sCd	-2.0	1.9	7.4	3.7	4.3	5.1	5.4	4.2	3.5	4.9

Table A.1: Sulfur-centered group additivity values. Enthalpies are given in $\frac{kcal}{mol}$. Entropies and heat capacities are given in $\frac{cal}{mol \cdot K}$

Groups	$H(298)$	$2\sigma_H(298)$	$S(298)$	$C_P(300)$	$C_P(400)$	$C_P(500)$	$C_P(600)$	$C_P(800)$	$C_P(1000)$	$C_P(1500)$
S2s-S2sCs	-5.1	1.3	6.9	5.0	4.5	4.8	4.9	3.6	3.0	4.3
S2s-S2sCt	-5.0	2.6	4.5	4.8	6.0	7.0	7.4	6.0	5.0	6.0
S2s-S2sH	2.4	0.4	32.5	5.8	6.6	7.1	7.5	8.0	8.4	9.0
S2s-S46C	-6.9	1.3	5.4	5.1	4.5	4.4	4.6	3.3	2.6	4.0
S2s-S4O	6.0	0.9	5.8	6.6	7.2	7.2	7.8	7.9	7.8	7.1
S2s-S6O	4.4	1.3	0.9	6.9	8.8	9.1	9.2	9.1	8.7	6.9
S2s-SsSS	1.8	0.8	9.1	6.3	6.4	6.3	6.5	6.6	6.6	6.0
S4d-CdCC	27.5	3.6	-29.4	3.9	5.7	6.4	6.8	6.7	6.6	7.0
S4d-CdCH	25.8	3.7	-20.1	3.6	5.7	6.7	7.1	5.6	4.8	6.4
S4d-CdHH	42.2	3.6	1.0	1.3	3.4	4.6	5.5	6.5	7.3	8.8
S4d-CdOC	8.8	3.7	-41.4	4.8	6.2	6.7	6.6	3.8	2.2	2.8
S4d-CdOH	22.1	3.6	-18.8	3.5	5.7	6.7	7.3	7.3	7.3	7.7
S4dd-CdCd	21.1	6.4	-51.7	-3.5	-0.7	0.0	0.1	-0.5	-0.9	-0.9
S4dd-CdOd	-24.7	3.6	4.8	2.6	4.7	5.5	5.8	6.0	6.0	6.3

Table A.1: Sulfur-centered group additivity values. Enthalpies are given in $\frac{kcal}{mol}$. Entropies and heat capacities are given in $\frac{cal}{mol \cdot K}$

Groups	$H(298)$	$2\sigma_H(298)$	$S(298)$	$C_P(300)$	$C_P(400)$	$C_P(500)$	$C_P(600)$	$C_P(800)$	$C_P(1000)$	$C_P(1500)$
S4dd-OdS4d	-4.3	3.9	24.9	4.6	7.7	9.3	10.1	10.4	10.9	10.5
S4dd-OdS6d	-14.3	4.0	63.4	13.9	12.3	12.0	12.1	12.9	13.3	14.0
S4dd-S46dCd	0.9	3.5	13.9	8.6	7.4	7.2	7.2	7.2	6.9	6.9
S4d-OdCdCd	-53.3	4.1	17.3	5.8	7.0	9.6	9.6	7.3	6.1	9.3
S4d-OdCdH	-31.3	2.4	37.7	7.5	9.7	11.9	12.3	11.7	11.4	13.5
S4d-OdCS	-33.3	0.9	16.1	9.6	10.1	11.0	11.1	9.8	9.0	10.3
S4d-OdCsCs	-47.9	1.5	9.7	10.7	11.7	12.7	12.8	9.3	7.3	8.6
S4d-OdCsH	-27.2	1.0	31.9	8.8	10.5	12.0	12.9	12.4	12.1	13.6
S4d-OdOH	-25.4	0.7	35.2	10.9	12.2	13.0	13.6	14.1	14.5	14.9
S4d-OdOO	-50.3	1.3	11.0	12.0	13.1	13.6	14.0	13.7	13.4	12.6
S4d-OdOS	-29.9	0.7	17.5	10.9	12.2	13.0	13.2	13.1	12.9	12.0
S4d-OdOsCd	-48.1	2.2	15.9	8.1	9.7	11.4	11.6	10.3	9.6	10.9
S4d-OdOsCs	-46.8	1.0	12.6	11.0	12.1	12.9	13.2	11.2	10.0	10.5
S4d-OdSH	-13.9	0.6	39.7	9.1	10.2	11.6	12.0	13.2	14.0	14.8

Table A.1: Sulfur-centered group additivity values. Enthalpies are given in $\frac{kcal}{mol}$. Entropies and heat capacities are given in $\frac{cal}{mol \cdot K}$

Groups	$H(298)$	$2\sigma_H(298)$	$S(298)$	$C_P(300)$	$C_P(400)$	$C_P(500)$	$C_P(600)$	$C_P(800)$	$C_P(1000)$	$C_P(1500)$
S4d-OdSS	-17.9	1.0	23.3	9.8	10.1	10.6	10.4	10.5	10.7	10.6
S4d-SdCH	-2.0	4.9	24.9	10.7	8.6	8.2	7.4	6.4	5.7	8.6
S4d-SdOC	-0.5	3.9	-38.3	2.7	5.1	6.3	6.7	4.4	2.9	3.0
S4d-SdOH	18.2	3.9	-16.7	4.3	7.3	8.4	8.8	8.3	7.9	7.3
S4d-SdSC	1.8	4.0	-36.5	4.2	5.1	5.0	4.8	1.9	0.3	1.2
S4s-CCCH	29.2	1.7	-10.6	11.5	12.6	13.7	14.0	14.3	14.3	13.4
S4s-SOCH	12.9	3.1	-10.6	14.6	13.5	13.1	13.2	11.8	10.9	11.2
S4t-CtC	-38.3	2.1	45.1	9.5	9.5	9.8	10.1	9.9	9.8	10.8
S4t-CtH	-24.1	2.5	66.6	10.2	10.1	10.6	11.2	13.4	14.7	15.5
S4t-CtO	-40.3	2.4	46.3	12.4	11.7	11.4	11.3	12.2	12.7	12.2
S6dd-CdCdCC	57.8	4.0	-104.3	2.9	1.8	1.6	1.4	-1.3	-2.8	-1.0
S6dd-CdCdCH	69.6	3.5	-73.5	0.1	0.6	1.3	1.8	1.4	1.3	3.2
S6dd-CdCdOC	46.9	3.6	-98.3	1.5	2.6	3.3	3.6	2.2	1.2	1.4

Table A.1: Sulfur-centered group additivity values. Enthalpies are given in $\frac{kcal}{mol}$. Entropies and heat capacities are given in $\frac{cal}{mol \cdot K}$

Groups	$H(298)$	$2\sigma_{H(298)}$	$S(298)$	$C_P(300)$	$C_P(400)$	$C_P(500)$	$C_P(600)$	$C_P(800)$	$C_P(1000)$	$C_P(1500)$
S6ddd-OdOdXd ¹	-46.9	3.3	14.1	4.6	7.8	9.4	10.2	10.6	11.0	11.2
S6ddd-OdXdXd ²	2.3	7.0	-36.8	-3.0	1.8	3.5	4.2	3.8	3.7	3.3
S6dd-OdCdCC	-3.5	2.6	-29.6	8.6	7.9	8.2	8.3	6.9	6.1	7.6
S6dd-OdCdCH	0.8	2.1	-21.9	6.5	7.0	7.8	8.5	8.6	8.9	11.2
S6dd-OdCdOC	-18.8	2.2	-44.2	8.9	9.0	9.5	10.0	8.9	8.1	8.7
S6dd-OdCdOH	-2.0	1.6	-13.9	7.1	9.0	10.5	11.6	12.5	12.9	13.2
S6dd-OdCdOO	-23.6	2.6	-37.3	9.8	11.1	11.8	12.2	11.5	11.1	10.3
S6dd-OdCdOS	-4.9	2.1	-28.9	8.1	8.6	9.1	9.4	9.3	9.2	9.4
S6dd-OdCdSH	12.1	1.6	-5.8	6.1	7.3	8.5	9.3	10.4	11.1	12.0
S6dd-OdOdCdCd	-87.3	3.0	5.4	14.3	14.7	15.1	15.3	13.4	12.5	14.8
S6dd-OdOdCdH	-69.9	1.9	34.7	12.1	13.5	14.6	15.5	15.8	16.3	18.8
S6dd-OdOdCdOs	-94.3	2.0	11.8	13.4	14.3	15.2	15.9	15.4	15.1	16.4
S6dd-OdOdcS	-75.5	1.4	12.8	13.6	14.3	15.3	15.6	15.1	14.9	15.9

¹X here represents either Carbon or Sulfur

²X here represents either Carbon or Sulfur

Table A.1: Sulfur-centered group additivity values. Enthalpies are given in $\frac{kcal}{mol}$. Entropies and heat capacities are given in $\frac{cal}{mol \cdot K}$

Groups	$H(298)$	$2\sigma_H(298)$	$S(298)$	$C_P(300)$	$C_P(400)$	$C_P(500)$	$C_P(600)$	$C_P(800)$	$C_P(1000)$	$C_P(1500)$
S6dd-OdOdCsCs	-90.0	2.3	1.0	14.6	14.5	15.0	15.3	13.4	12.6	14.7
S6dd-OdOdCsH	-74.1	1.2	32.2	12.6	13.9	15.0	16.0	16.1	16.5	18.8
S6dd-OdOdCsOs	-95.5	1.4	9.6	13.6	14.4	15.3	16.0	15.5	15.3	16.4
S6dd-OdOdIH	-55.9	1.3	61.8	11.0	13.1	15.1	16.8	19.3	21.0	23.3
S6dd-OdOdOH	-79.8	1.1	40.9	12.0	13.8	15.4	16.7	18.8	19.7	20.8
S6dd-OdOdOO	-98.0	1.2	15.1	14.6	16.2	17.2	17.8	17.9	18.1	17.8
S6dd-OdOdOS	-77.1	1.0	21.8	14.1	15.3	16.3	16.7	17.1	17.4	17.6
S6dd-OdOdSH	-58.1	1.0	44.4	10.9	12.8	14.6	15.7	17.6	18.8	20.0
S6dd-OdOdSS	-60.0	1.2	24.7	13.7	15.0	16.0	15.8	15.9	16.3	16.7
S6dd-OdSdCH	-16.0	3.7	-20.0	5.1	7.7	9.2	10.1	9.7	9.7	11.2
S6dd-OdSdOC	-36.4	3.7	-43.9	7.4	10.0	11.3	11.7	10.1	9.1	9.1
S6dd-OdSdOH	-19.8	3.7	-11.8	5.4	8.8	10.4	11.4	11.9	12.4	12.9
S6d-OdOCCH	-5.1	2.7	-25.5	12.7	13.0	14.5	15.6	14.8	14.7	17.5
S6s-CCCCCH	76.1	5.7	-111.2	13.5	12.1	12.6	12.7	7.8	5.4	10.6

Table A.1: Sulfur-centered group additivity values. Enthalpies are given in $\frac{kcal}{mol}$. Entropies and heat capacities are given in $\frac{cal}{mol \cdot K}$

Groups	$H(298)$	$2\sigma_H(298)$	$S(298)$	$C_P(300)$	$C_P(400)$	$C_P(500)$	$C_P(600)$	$C_P(800)$	$C_P(1000)$	$C_P(1500)$
S6s-OCCCCH	54.7	4.8	-90.2	14.1	12.4	12.7	12.7	8.7	7.0	11.4
S6s-SOOCCH	40.9	3.5	-66.4	13.7	11.0	11.7	12.2	10.8	10.5	14.2
S6t-CtCCC	11.6	4.3	41.2	19.0	16.0	14.9	14.2	11.6	10.3	12.6
S6t-CtHHH	50.8	2.5	67.3	10.3	10.7	11.9	13.4	17.1	19.6	21.8
S6t-CtOCC	-12.1	3.6	-13.9	16.3	14.4	14.3	14.2	13.2	12.8	14.3
S6t-CtOCH	-0.7	2.9	17.2	14.3	13.7	14.2	14.9	16.1	17.0	18.5
S6td-CtCdC	12.5	2.2	-7.1	7.1	7.8	8.2	8.3	8.2	8.3	8.8
S6td-CtOdc	-55.0	2.8	42.2	13.7	13.2	13.5	13.9	14.8	15.4	16.6
S6td-CtOdh	-44.0	2.5	72.2	13.2	13.8	14.7	15.6	18.3	19.9	21.0

Table A.2: Oxygen-centered group additivity values. Enthalpies are given in $\frac{kcal}{mol}$. Entropies and heat capacities are given in $\frac{cal}{mol \cdot K}$

Groups	$H(298)$	$2\sigma_H(298)$	$S(298)$	$C_P(300)$	$C_P(400)$	$C_P(500)$	$C_P(600)$	$C_P(800)$	$C_P(1000)$	$C_P(1500)$
O2s-Cs(Cds-S2d)	-30.6	1.8	5.7	1.1	1.2	1.8	2.4	3.3	3.9	4.9
O2s-CS2	-22.6	0.7	7.2	2.8	3.5	3.8	4.2	5.0	5.4	5.9
O2s-CS4	-22.2	0.6	10.6	1.7	1.7	1.9	2.3	3.2	3.8	4.4
O2s-CS6	-23.8	0.7	10.7	2.4	2.2	2.3	2.5	3.2	3.6	4.0
O2s-CSH	-47.6	1.8	27.8	2.4	3.2	4.2	5.1	6.2	7.0	8.4
O2s-SdtH	-37.9	0.6	30.0	3.9	4.4	4.7	5.0	5.7	6.3	7.2
O2s-SsH	-36.3	0.5	29.1	3.9	4.9	5.4	5.9	6.7	7.1	7.8
O2s-SsOs	-3.3	0.6	8.7	3.2	3.8	4.1	4.2	4.8	4.9	4.9

Table A.3: Carbon-centered group additivity values. Enthalpies are given in $\frac{kcal}{mol}$. Entropies and heat capacities are given in $\frac{cal}{mol \cdot K}$

Groups	$H(298)$	$2\sigma_{H(298)}$	$S(298)$	$C_P(300)$	$C_P(400)$	$C_P(500)$	$C_P(600)$	$C_P(800)$	$C_P(1000)$	$C_P(1500)$
$C=S2-CsH$	24.1	1.5	36.8	10.1	9.4	9.6	10.1	11.4	12.4	13.9
$C=S2d-HH$	27.7	1.3	56.5	9.1	10.3	11.5	12.5	14.1	15.2	17.1
$C=S2-OsH$	19.1	1.4	34.4	9.1	10.5	11.4	12.2	13.5	14.3	15.0
$C=S4-CsH$	16.5	3.8	38.3	8.6	8.0	8.4	9.2	10.8	11.8	12.9
$C=S4d-HH$	16.5	3.4	57.7	9.8	10.0	10.8	11.8	13.6	14.9	16.6
$C=S4-OsH$	9.6	4.0	32.6	7.7	8.2	9.5	10.9	13.3	15.0	16.4
$C=S6ddd-HH$	11.0	3.6	53.0	10.9	10.5	11.2	12.0	14.0	15.3	17.3
$C=S6dd-HH$	14.2	1.5	54.8	9.8	11.3	12.4	13.2	14.7	15.9	17.4
$C=S6-S2H$	32.3	3.4	64.8	12.7	15.3	16.0	16.8	20.5	22.8	21.0
$C=S-C=SCs$	24.3	1.9	15.9	8.9	8.3	8.4	8.8	9.7	10.2	10.7
$C=S-C=SH$	27.0	0.6	35.6	7.8	9.2	10.4	11.4	12.8	13.6	14.5
$C=S-ChCs$	23.6	2.3	13.6	8.9	8.7	9.0	9.5	10.2	10.5	10.9
$C=S-CdsCs$	23.8	2.6	12.3	9.6	9.4	9.5	9.9	10.5	10.8	11.2
$C=S-CdsH$	24.8	1.4	34.0	7.4	9.2	10.6	11.5	12.8	13.6	14.6

Table A.3: Carbon-centered group additivity values. Enthalpies are given in $\frac{kcal}{mol}$. Entropies and heat capacities are given in $\frac{cal}{mol \cdot K}$

Groups	$H(298)$	$2\sigma_{H(298)}$	$S(298)$	$C_P(300)$	$C_P(400)$	$C_P(500)$	$C_P(600)$	$C_P(800)$	$C_P(1000)$	$C_P(1500)$
C=S-CsCs	20.9	3.7	16.6	10.6	8.2	7.4	7.7	8.7	9.5	10.5
C=S-CsOs	11.7	2.7	12.2	10.5	9.8	9.7	10.1	11.2	11.9	12.2
C=S-CsSs	26.8	2.9	18.8	10.8	9.5	9.0	9.2	11.6	13.0	12.1
C=S-CtCs	26.6	2.0	16.5	9.4	8.3	8.7	8.0	8.8	9.6	10.4
C=S-CtH	30.5	1.4	36.9	8.1	9.0	10.5	10.2	11.4	12.3	13.6
C=S-OsOs	9.7	3.8	11.3	12.2	14.0	14.5	14.7	14.7	14.2	12.4
C=S-OsS	36.9	2.3	16.9	9.4	10.4	10.8	11.4	14.2	15.7	14.3
C=S-S2H	30.1	1.9	39.2	9.9	10.7	11.1	11.7	14.2	15.8	15.3
C=S-S4H	45.4	1.6	42.4	9.0	9.3	9.6	10.2	13.0	14.8	15.2
Cb-S	18.8	2.5	-0.6	3.8	3.8	3.5	3.5	5.2	6.2	4.7
Cdd-CdsS6d	45.7	1.7	34.1	7.2	7.5	7.7	8.0	8.8	9.3	9.8
Cdd-OdSd	-34.8	1.3	55.3	9.8	10.8	11.6	12.2	13.0	13.5	14.1
Cdd-S2S4	60.9	3.8	65.9	11.9	11.1	11.1	11.5	12.3	12.8	13.0
Cdd-S4S4	54.1	6.7	66.2	12.4	10.6	10.5	10.8	11.9	12.8	12.7

Table A.3: Carbon-centered group additivity values. Enthalpies are given in $\frac{kcal}{mol}$. Entropies and heat capacities are given in $\frac{cal}{mol \cdot K}$

Groups	$H(298)$	$2\sigma_{H(298)}$	$S(298)$	$C_P(300)$	$C_P(400)$	$C_P(500)$	$C_P(600)$	$C_P(800)$	$C_P(1000)$	$C_P(1500)$
Cds-CdsC=SCs	9.2	1.9	-11.2	4.2	4.5	4.8	5.0	5.4	5.7	6.0
Cds-CdsC=SH	7.8	1.8	8.3	4.4	5.2	6.1	6.8	8.0	8.8	9.9
Cds-CdsCsS2	20.6	1.9	-8.4	5.3	5.8	5.6	5.6	7.0	7.7	6.1
Cds-CdsCsS4	27.5	2.6	-12.9	5.7	5.6	4.9	5.6	7.7	8.8	7.3
Cds-CdsCsS6	21.4	2.2	-2.6	4.0	5.4	5.8	6.2	7.7	8.4	7.2
Cds-CdsS2H	18.9	1.8	12.2	5.7	6.6	6.8	7.2	9.2	10.4	9.7
Cds-CdsS4H	27.6	1.9	5.1	7.2	7.9	7.5	8.3	10.6	11.9	11.0
Cds-CdsS6H	19.9	1.4	13.6	4.0	5.5	6.4	7.3	9.6	11.0	10.8
CO-CsSs	-19.1	2.8	20.3	7.1	8.6	9.0	9.4	11.0	12.0	11.0
CO-OsSs	-35.6	2.1	16.4	6.9	9.5	10.8	11.6	13.6	14.5	12.9
CO-S2H	-15.2	2.8	41.3	8.3	9.9	10.4	10.8	12.7	14.0	14.1
CO-S4H	-8.5	1.6	39.0	8.5	9.3	9.7	10.3	13.1	14.9	15.2
CO-S6H	-8.0	1.8	48.0	6.1	7.2	8.2	9.2	11.8	13.5	14.3
Cs-(Cds-Cds)CsSsH	10.3	1.6	-9.7	8.0	10.8	11.6	11.8	13.2	13.9	12.8

Table A.3: Carbon-centered group additivity values. Enthalpies are given in $\frac{kcal}{mol}$. Entropies and heat capacities are given in $\frac{cal}{mol \cdot K}$

Groups	$H(298)$	$2\sigma_{H(298)}$	$S(298)$	$C_P(300)$	$C_P(400)$	$C_P(500)$	$C_P(600)$	$C_P(800)$	$C_P(1000)$	$C_P(1500)$
Cs-C=S=SCsCsCs	4.4	2.0	-33.2	2.5	5.5	7.0	7.5	7.8	7.6	7.3
Cs-C=SCsCsSH	2.3	1.9	-10.8	2.4	5.4	7.2	8.2	9.4	9.9	10.6
Cs-C=SCsHHH	-1.7	1.8	10.5	3.0	6.2	8.2	9.4	11.0	12.0	13.7
Cs-C=SCsSSH	12.6	2.6	-10.2	5.8	10.5	12.2	12.7	14.0	14.4	12.8
Cs-C=SHHHH	-7.1	1.8	31.1	4.0	7.2	9.5	11.0	13.1	14.7	17.3
Cs-C=SSsHH	10.0	2.6	11.4	6.7	11.1	12.6	13.3	15.3	16.4	16.0
Cs-CbCsSsH	11.6	1.9	-9.0	6.4	8.9	9.9	10.6	12.5	13.3	12.2
Cs-CbOsSsH	4.6	2.2	-13.4	8.9	11.8	12.6	13.0	14.4	14.8	12.9
Cs-CbSsHH	6.2	1.6	12.9	6.5	8.8	10.0	11.1	13.8	15.4	15.3
Cs-CdsOsSsH	5.4	2.1	-11.8	8.9	11.9	12.9	13.3	14.7	15.0	13.5
Cs-CdsSsHH	7.5	1.6	12.3	9.0	10.9	11.5	12.0	14.2	15.7	15.9
Cs-CsCsCsS2	10.7	1.4	-31.6	5.0	6.9	7.6	8.1	10.1	11.0	9.6
Cs-CsCsCsS4	14.8	1.3	-29.5	4.6	5.5	5.7	6.1	8.5	9.8	8.8
Cs-CsCsOsSs	6.5	1.5	-38.4	7.9	10.9	11.5	11.4	11.9	11.9	9.5

Table A.3: Carbon-centered group additivity values. Enthalpies are given in $\frac{kcal}{mol}$. Entropies and heat capacities are given in $\frac{cal}{mol \cdot K}$

Groups	$H(298)$	$2\sigma_{H(298)}$	$S(298)$	$C_P(300)$	$C_P(400)$	$C_P(500)$	$C_P(600)$	$C_P(800)$	$C_P(1000)$	$C_P(1500)$
Cs-CsCsS2H	11.1	1.4	-7.2	5.4	7.6	8.5	9.2	11.6	12.8	12.1
Cs-CsCsS2S2	24.5	2.7	-26.8	7.8	10.4	10.6	10.8	13.4	14.2	10.8
Cs-CsCsS4H	12.8	0.9	-7.2	4.4	5.1	5.7	6.4	9.6	11.6	12.5
Cs-CsCsS6H	6.0	1.3	-5.7	3.7	5.4	6.4	7.3	9.9	11.4	11.5
Cs-CsCsS6S2	20.3	2.9	-21.8	5.6	8.5	9.5	10.2	13.4	14.4	10.9
Cs-CsOsOsSS	-5.3	1.9	-33.5	6.6	9.0	9.8	10.2	11.9	12.3	10.0
Cs-CsOsS2H	4.2	1.5	-13.3	7.8	10.6	11.6	12.1	13.0	14.2	12.8
Cs-CsOsS4H	5.2	2.2	-20.4	5.7	8.9	10.4	11.9	15.4	17.1	15.2
Cs-CsS2HH	7.0	1.3	14.5	6.0	8.2	9.3	10.4	13.3	15.0	15.4
Cs-CsS2S2H	22.6	2.9	-4.8	8.5	10.8	11.2	11.5	14.7	16.2	13.9
Cs-CsS4HHH	9.1	0.8	12.3	5.1	6.1	6.9	8.0	11.6	14.0	15.1
Cs-CsS4S2H	18.4	2.3	-14.3	8.8	11.5	12.4	13.5	17.9	19.7	16.4
Cs-CsS6HHH	3.8	1.2	19.7	3.9	5.8	7.3	8.6	11.8	13.8	14.8
Cs-CsS6S2H	18.7	3.2	-6.3	4.8	9.8	12.0	13.5	17.5	19.2	16.2

Table A.3: Carbon-centered group additivity values. Enthalpies are given in $\frac{kcal}{mol}$. Entropies and heat capacities are given in $\frac{cal}{mol \cdot K}$

Groups	$H(298)$	$2\sigma_{H(298)}$	$S(298)$	$C_P(300)$	$C_P(400)$	$C_P(500)$	$C_P(600)$	$C_P(800)$	$C_P(1000)$	$C_P(1500)$
Cs-CsSSSSS	37.8	4.0	-23.4	8.8	12.5	12.9	13.0	16.7	17.9	12.8
Cs-CtCsSSH	13.5	1.6	-6.2	5.6	7.8	8.7	9.4	11.7	13.0	11.5
Cs-CtSsHHH	10.2	1.6	15.2	6.0	8.3	9.5	10.5	13.4	15.3	14.8
Cs-OsOsS2H	-3.6	2.3	-10.1	6.3	9.3	10.6	11.6	14.1	15.0	13.7
Cs-OsOsS4H	-3.8	2.0	-12.4	5.7	7.6	8.7	9.9	13.2	15.0	14.5
Cs-OsS2HH	3.3	1.3	11.3	7.6	10.2	11.4	12.3	14.7	16.1	15.9
Cs-OsS4HH	5.6	1.3	8.3	6.0	7.9	9.3	10.7	14.4	16.6	16.9
Cs-OsS4S2H	19.5	2.3	-12.7	5.6	9.0	10.5	11.9	16.6	18.8	16.4
Cs-S2sHHH	2.0	1.3	35.8	6.7	8.9	10.2	11.5	14.9	17.2	18.5
Cs-S4HHH	5.5	0.7	33.8	5.5	6.8	8.1	9.5	13.6	16.5	18.3
Cs-S6HHH	-0.8	1.1	41.3	4.9	7.2	8.8	10.3	13.8	16.2	18.1
Cs-SsSsHH	19.1	2.2	16.5	8.0	11.1	12.1	12.9	16.9	19.0	17.3
Cs-SsSsSSSH	36.1	4.0	-0.6	8.1	12.2	12.8	13.3	17.7	19.7	15.7
Cs-SsSsSSSs	33.2	5.2	-20.5	9.3	15.1	16.6	17.9	24.7	28.0	23.3

Table A.3: Carbon-centered group additivity values. Enthalpies are given in $\frac{kcal}{mol}$. Entropies and heat capacities are given in $\frac{cal}{mol \cdot K}$

Groups	$H(298)$	$2\sigma_{H(298)}$	$S(298)$	$C_P(300)$	$C_P(400)$	$C_P(500)$	$C_P(600)$	$C_P(800)$	$C_P(1000)$	$C_P(1500)$
Ct-CtS2	45.2	2.4	14.6	3.7	3.5	2.9	2.9	4.6	5.7	4.7
Ct-CtS4	56.6	2.0	12.4	2.2	2.0	1.7	1.8	3.7	4.9	4.5
Ct-StH	98.1	2.1	-9.5	-0.3	1.1	1.9	2.3	1.7	1.4	2.2

A.2 Molecule Dataset

A.2.1 Validation Set Comparison

Table A.4: All comparisons are in $\frac{kcal}{mol}$.

	Experiment	CBS-QB3 w/out new BAC	CBS-QB3 w/new BAC	Deviation
CS(=O)C	-35.97[97]	-35.71	-36.69	-0.72
CCS(=O)CC	-49.1[92]	-48.86	-49.84	-0.74
CCCS(=O)CCC	-60.9[92]	-57.88	-58.86	2.04
CS(=O)CC	-43.4[80]	-42.09	-43.07	0.33
CS(=O)(=O)C	-89.1[22]	-88.65	-90.17	-1.07
CS(=O)(=O)C(C)C	-103.6[22]	-102.89	-104.40	-0.80
CS(=O)(=O)CC	-97.6[22]	-95.35	-96.86	0.74
C=CS(=O)(=O)C=C	-36[90]	-33.57	-35.09	0.91
CCS(=O)(=O)CC	-102.6[91]	-101.15	-102.67	-0.07
C=CCS(=O)(=O)C	-73[91]	-69.72	-71.24	1.76
CC(C)S(=O)C(C)C	-64.7[80]	-62.02	-63.01	1.69
CS(=O)C(C)(C)CC	-62.5[80]	-62.46	-63.45	-0.95
CCCS(=O)C(C)C	-62.7[80]	-60.56	-61.54	1.16
CCS(=O)C(C)(C)C	-65.5[92]	-63.48	-64.46	1.04
CCS(=O)(=O)C(C)CC	-115.3[80]	-113.36	-114.88	0.42
CS(=O)(=O)CCC(C)C	-113[80]	-112.33	-113.85	-0.85
CCCS(=O)(=O)CCC	-111.92[91]	-111.31	-112.83	-0.91
CCS(=O)(=O)C(C)C	-110.73[80]	-110.81	-112.32	-1.59
CS(=O)(=O)C(C)CC	-112.6[80]	-109.69	-111.21	1.39
CCS(=O)(=O)C=C	-69.8[80]	-67.49	-69.00	0.80
COS(=O)OC	-115.5[93]	-112.83	-113.51	1.99
COS(=O)OCC	-125.2[93]	-121.93	-122.61	2.59

Table A.4: All comparisons are in $\frac{kcal}{mol}$.

	Experiment	CBS-QB3 w/out new BAC	CBS-QB3 w/new BAC	Deviation
CCOS(=O)OCC	-131.9[93]	-131.05	-131.73	0.17
COS(=O)OC(C)C(C)C	-144[80]	-144.13	-144.81	-0.81
CCCOS(=O)OCCC	-141.8[93]	-141.73	-142.41	-0.61
COS(=O)OCCC	-128.8[80]	-127.57	-128.25	0.55
COS(=O)OC(C)CC	-137.5[80]	-137.49	-138.17	-0.67
COS(=O)(=O)OC	-164.2[93]	-165.16	-166.38	-2.18
COS(=O)(=O)OCC	-172.4[80]	-173.79	-175.00	-2.60
OS(=O)(=O)O	-175.6[24]	-172.58	-173.79	1.81
SO2	-70.9[24]	-70.15	-71.22	-0.32
SO3	-94.6[24]	-93.33	-94.93	-0.33
SO	1.2[24]	0.80	0.26	-0.94
O=C=S	-33.1[24]	-34.79	-34.79	-1.69
HSOH	-27[80]	-28.08	-27.46	-0.46
H2S	-4.9[24]	-5.62	-4.24	0.66
CSC	-8.96[143]	-9.30	-9.75	-0.79
CSCC	-14.42[63]	-15.14	-15.59	-1.17
CSC(C)C	-21.43[64]	-22.40	-22.85	-1.42
SCC	-11.03[98]	-11.80	-11.33	-0.30
SC	-5.46[59]	-5.87	-5.40	0.06
SC(C)C	-18.39[63]	-19.47	-19.00	-0.61
[S][S]	30.74[29]	30.05	31.51	0.77
CSSC	-5.76[143]	-6.42	-5.41	0.35
CSSCC	-11.8[61]	-12.79	-11.78	0.02
CCSSCC	-17.8[143]	-19.40	-18.39	-0.59
CSSC(C)C	-18.9[61]	-20.46	-19.45	-0.55

A.2.2 Full Molecule List with Thermochemistry

Table A.5: A list of the molecules used in the study and their thermodynamic properties. Enthalpies are given in $\frac{kcal}{mol}$. Entropies and heat capacities are given in $\frac{cal}{mol \cdot K}$.

	$H_f(298)$	$S_f(298)$	Cp(300)	Cp(400)	Cp(500)	Cp(600)	Cp(800)	Cp(1000)	Cp(1500)	Source
CS(=O)C	-36.7	78.6	21.9	25.7	29.0	31.9	36.6	40.1	45.6	CBS-QB3
C=CS(=O)C=C	14.3	82.7	30.5	35.5	39.7	43.2	48.6	52.4	57.6	CBS-QB3
CCS(=O)CC	-49.8	95.8	32.6	39.3	45.1	50.2	58.5	64.7	74.0	CBS-QB3
CCCS(=O)CCC	-58.9	116.6	44.6	53.1	61.4	68.7	80.5	89.4	102.7	CBS-QB3
CS(=O)CC	-43.1	88.8	26.9	32.3	36.9	41.0	47.5	52.4	59.7	CBS-QB3
CS(=O)(=O)C	-90.2	82.4	24.3	28.7	32.5	35.9	41.2	45.2	51.0	CBS-QB3
CS(=O)(=O)C(C)C	-104.4	100.9	35.0	42.4	48.9	54.4	63.3	69.8	79.3	CBS-QB3
CS(=O)(=O)CC	-96.9	91.1	29.3	35.3	40.4	44.9	52.1	57.4	65.1	CBS-QB3
C=CS(=O)(=O)C=C	-35.1	87.3	33.1	39.2	43.6	47.3	53.1	57.1	62.7	CBS-QB3
CCS(=O)(=O)CC	-102.7	101.4	34.7	41.8	48.3	53.9	63.0	69.7	79.5	CBS-QB3
C=CCS(=O)(=O)C	-71.2	93.8	35.7	42.1	47.1	51.4	58.3	63.4	71.0	CBS-QB3
CC(C)S(=O)C(C)C	-63.0	115.9	45.3	54.0	62.1	69.2	80.9	89.5	102.6	CBS-QB3
CS(=O)C(C)C(CC)	-63.4	115.0	44.2	53.9	62.4	69.8	81.5	90.0	102.6	CBS-QB3
CCCS(=O)C(C)C(C)	-61.5	117.1	43.7	52.7	61.2	68.5	80.5	89.4	102.6	CBS-QB3
CCS(=O)C(C)(C)C	-64.5	113.9	45.7	55.2	63.4	70.4	81.7	90.2	103.0	CBS-QB3
CCS(=O)(=O)C(C)CC	-114.9	119.2	46.9	56.4	65.2	72.9	85.2	94.4	108.0	CBS-QB3
CS(=O)(=O)CCC(C)C	-113.8	121.6	45.8	55.8	64.9	72.7	85.4	94.7	108.2	CBS-QB3
CCCS(=O)(=O)CCC	-112.8	120.3	46.0	55.5	64.4	72.2	84.9	94.2	108.0	CBS-QB3
CCS(=O)(=O)C(C)C	-112.3	102.0	41.7	50.0	57.3	63.7	74.2	82.0	93.8	CBS-QB3
CS(=O)(=O)C=CCC	-78.5	100.4	38.9	46.7	53.6	59.4	68.8	75.6	85.3	CBS-QB3

Table A.5: A list of the molecules used in the study and their thermodynamic properties. Enthalpies are given in $\frac{kcal}{mol}$. Entropies and heat capacities are given in $\frac{cal}{mol \cdot K}$.

	$H_f(298)$	$S_f(298)$	Cp(300)	Cp(400)	Cp(500)	Cp(600)	Cp(800)	Cp(1000)	Cp(1500)	Source
CS(=O)(=O)C(C)CC	-111.2	101.3	40.8	49.3	56.8	63.4	74.0	81.9	93.8	CBS-QB3
CCS(=O)(=O)C=C	-69.0	94.7	33.5	40.0	45.7	50.5	58.1	63.5	71.1	CBS-QB3
COS(=O)OC	-113.5	95.9	26.2	30.5	34.7	38.4	44.4	48.8	55.2	CBS-QB3
COS(=O)OCC	-122.6	102.1	33.8	40.3	46.0	50.9	58.5	63.8	71.0	CBS-QB3
CCOS(=O)OCC	-131.7	107.9	37.6	45.5	52.6	58.8	68.7	75.9	86.2	CBS-QB3
COS(=O)OC(C)C(C)C	-144.8	126.1	52.0	62.6	71.8	79.8	92.3	101.3	113.6	CBS-QB3
CCCO(=O)OCCC	-142.4	131.6	47.9	58.4	68.1	76.5	89.8	99.5	113.0	CBS-QB3
COS(=O)OCCCC	-128.3	107.5	39.0	46.8	53.9	60.1	70.0	77.3	87.8	CBS-QB3
COS(=O)OC(C)CC	-138.2	119.7	47.0	56.2	64.1	70.9	81.5	89.0	99.2	CBS-QB3
COS(=O)(=O)OC	-166.4	95.8	32.9	37.6	41.7	45.2	50.8	54.8	60.6	CBS-QB3
COS(=O)(=O)OCC	-175.0	106.4	36.4	42.8	48.4	53.3	61.2	66.9	75.1	CBS-QB3
OS(=O)(=O)O	-173.8	75.8	22.3	24.9	26.4	27.5	29.3	30.6	32.4	CBS-QB3
C ₂ SO	-35.2	71.4	16.2	19.1	21.3	23.1	25.9	27.9	30.9	CBS-QB3
O=S=O	-71.2	60.7	9.6	10.4	11.2	11.7	12.4	12.9	13.4	CBS-QB3
O=S(=O)=O	-94.9	61.5	12.2	13.9	15.2	16.2	17.5	18.3	19.1	CBS-QB3
S=O	0.3	50.9	7.3	7.6	7.8	8.1	8.4	8.6	8.8	CBS-QB3
O=C=S	-34.8	55.3	9.8	10.8	11.6	12.2	13.0	13.5	14.1	CBS-QB3
SO	-27.5	59.7	10.7	12.2	13.4	14.2	15.3	16.1	17.1	CBS-QB3
O=S(C)OO	-59.7	82.1	25.5	29.4	31.9	33.9	37.0	39.1	41.9	CBS-QB3
O=S(SC)CC	-38.9	101.0	32.7	37.5	42.2	46.3	53.0	57.9	65.3	CBS-QB3

Table A.5: A list of the molecules used in the study and their thermodynamic properties. Enthalpies are given in $\frac{kcal}{mol}$. Entropies and heat capacities are given in $\frac{cal}{mol \cdot K}$.

	$H_f(298)$	$S_f(298)$	Cp(300)	Cp(400)	Cp(500)	Cp(600)	Cp(800)	Cp(1000)	Cp(1500)	Source
O=S(S)C(O)=S	-42.0	89.3	27.7	30.6	33.0	35.0	37.9	39.7	41.5	CBS-QB3
O=S(C)S(=O)SO	-75.6	106.2	35.4	39.2	42.2	44.7	48.4	50.7	53.4	CBS-QB3
O=S(SC)OC=O	-100.0	100.6	32.7	36.8	40.2	43.0	47.2	50.0	53.2	CBS-QB3
O=S(C)OC	-74.3	87.1	24.7	28.8	32.5	35.8	41.1	45.0	50.7	CBS-QB3
O=S(OC)S(C)=S	-50.3	110.1	37.3	41.0	44.2	47.2	52.1	55.8	61.3	CBS-QB3
O=S(C)S(OS)=O	-68.0	106.9	36.0	39.4	42.2	44.6	48.2	50.7	53.7	CBS-QB3
O=S(SC)O	-74.5	86.8	26.1	29.8	32.3	34.3	37.4	39.5	42.0	CBS-QB3
O=S(O)(SC)=O	-121.7	90.7	30.6	33.6	35.9	37.9	41.0	43.3	46.9	CBS-QB3
O=S(=S)=S=O	-7.4	80.8	20.0	21.6	22.5	23.2	24.1	24.8	25.4	CBS-QB3
O=S(C)SC	-32.5	92.7	26.3	30.1	33.6	36.6	41.6	45.3	50.9	CBS-QB3
O=S(O)C(S)CS	-75.2	100.3	41.1	46.7	50.5	53.6	58.1	60.8	63.6	CBS-QB3
O=S(S)CS	-19.0	87.8	29.3	33.1	35.2	37.0	39.6	41.2	43.2	CBS-QB3
O=S(C)SSC=C	-5.1	105.2	36.0	40.6	44.5	47.9	53.2	57.1	62.5	CBS-QB3
O=S(S)SCC	-26.8	101.1	34.4	38.6	41.6	44.0	48.1	51.5	56.5	CBS-QB3
O=S(C)OS	-52.9	87.7	26.1	29.4	31.9	34.1	37.3	39.5	42.3	CBS-QB3
O=S(C)SCC	-37.7	102.0	31.6	36.7	41.6	45.8	52.7	57.8	65.2	CBS-QB3
O=S([H])C(CC)=C	12.5	104.7	37.5	42.9	47.6	51.9	58.8	63.9	71.5	CBS-QB3
O=S(C)(S)=O	-74.1	83.5	24.7	28.3	30.9	33.1	36.6	39.0	42.5	CBS-QB3
O=S(CC=C)(C)=O	-71.2	93.8	35.8	42.2	47.1	51.4	58.4	63.4	71.0	CBS-QB3
O=S(C)(SSC)=O	-77.7	102.6	36.9	42.3	46.4	49.9	55.2	58.7	63.1	CBS-QB3

Table A.5: A list of the molecules used in the study and their thermodynamic properties. Enthalpies are given in $\frac{kcal}{mol}$. Entropies and heat capacities are given in $\frac{cal}{mol \cdot K}$.

	$H_f(298)$	$S_f(298)$	Cp(300)	Cp(400)	Cp(500)	Cp(600)	Cp(800)	Cp(1000)	Cp(1500)	Source
O=S(CO)(O)=O	-168.5	84.5	29.7	33.5	36.1	38.2	41.6	43.9	47.1	CBS-QB3
O=S(O)(OSC)=O	-153.4	98.0	34.9	38.3	41.1	43.3	46.8	49.2	52.4	CBS-QB3
O=S(S)(OCS)=O	-101.1	100.3	34.5	38.4	41.5	44.1	47.9	50.3	53.1	CBS-QB3
O=S(CSS)([H])=O	-58.2	90.2	33.0	37.3	39.7	41.7	44.6	46.5	49.1	CBS-QB3
O=S(OC(S)C)([H])=O	-117.1	98.8	34.5	39.8	44.2	47.8	53.5	57.3	62.3	CBS-QB3
O=S(C)(OS)=O	-105.3	90.6	29.7	33.0	35.8	38.2	41.8	44.3	47.6	CBS-QB3
O=S(CC)([H])=O	-80.0	80.0	22.6	27.5	31.7	35.3	41.0	45.2	51.3	CBS-QB3
O=S(=C(SC)C)=O	-41.2	101.1	32.3	37.3	41.6	45.3	51.3	55.6	61.8	CBS-QB3
O=S(SC)(SC)=O	-72.0	104.7	37.9	42.8	46.3	48.9	53.0	56.4	61.7	CBS-QB3
O=S(S(=O)C=C)([H])=O	-57.6	93.2	32.8	37.2	40.7	43.6	48.0	50.9	54.4	CBS-QB3
O=S(C)(C(C)C)=O	-104.4	100.4	35.3	42.6	49.0	54.5	63.3	69.8	79.4	CBS-QB3
O=S(CS)([H])=O	-64.4	80.9	25.0	29.4	32.2	34.4	37.8	40.1	43.1	CBS-QB3
O=S(SC)([H])=O	-63.7	85.2	22.3	25.8	28.9	31.5	35.6	38.5	42.4	CBS-QB3
O=S(=S)=O	-42.3	68.3	13.6	15.3	16.4	17.1	18.1	18.7	19.3	CBS-QB3
O=S(C)(O)=O	-134.5	79.8	21.9	25.8	28.8	31.2	35.2	38.0	41.9	CBS-QB3
O=S(C=O)(S)=O	-81.6	89.3	26.0	28.4	30.5	32.2	34.7	36.5	38.6	CBS-QB3
O=S([H])C=O	-35.8	70.9	17.3	19.8	21.7	23.2	25.5	27.0	28.8	CBS-QB3
O=S(=C)(CC=O)S	-7.9	99.3	36.2	40.9	45.0	48.5	53.8	57.5	62.6	CBS-QB3
O=S([H])C(C=O)=S=C	7.7	91.5	32.1	36.8	40.5	43.6	48.2	51.4	55.2	CBS-QB3
O=S(CC)S([H])=O	-47.2	97.5	31.2	35.2	39.0	42.3	47.6	51.4	57.0	CBS-QB3

Table A.5: A list of the molecules used in the study and their thermodynamic properties. Enthalpies are given in $\frac{kcal}{mol}$. Entropies and heat capacities are given in $\frac{cal}{mol \cdot K}$.

	$H_f(298)$	$S_f(298)$	Cp(300)	Cp(400)	Cp(500)	Cp(600)	Cp(800)	Cp(1000)	Cp(1500)	Source
O=S(S)C(O)CO	-113.2	93.1	36.6	43.0	47.4	51.0	56.3	59.7	63.5	CBS-QB3
O=S(SC)C(C)C	-46.0	111.2	36.8	43.4	49.6	54.9	63.6	70.0	84.0	CBS-QB3
O=S([H])OCSOC	-78.3	100.7	35.3	40.1	44.1	47.6	52.9	56.6	61.6	CBS-QB3
O=S([H])CS	-15.4	75.9	21.5	26.0	29.2	31.3	34.2	36.0	38.1	CBS-QB3
O=S([H])S(C)=O	-40.8	87.5	24.1	27.3	32.2	32.7	36.5	39.3	42.9	CBS-QB3
O=S(=C)([H])C(S)CO	-21.9	94.3	37.4	45.6	51.7	56.3	63.4	68.1	73.8	CBS-QB3
O=S([H])SOC(C)O	-102.0	95.2	33.2	39.5	44.9	49.7	57.1	62.4	68.9	CBS-QB3
O=S([H])(O)=C	-29.4	69.7	19.8	24.3	27.8	30.2	33.6	35.7	38.1	CBS-QB3
O=S([H])SC	-18.8	81.4	20.3	23.0	25.5	27.7	31.1	33.6	37.1	CBS-QB3
O=S(=S=C)([H])OOC	-21.3	107.4	37.1	42.0	46.3	49.9	55.5	59.4	64.3	CBS-QB3
O=S([H])SO	-42.8	75.7	20.6	23.5	25.1	26.2	27.7	28.5	28.9	CBS-QB3
O=S([H])(=CS)CC	13.8	95.0	33.4	39.1	44.0	48.3	55.0	60.0	67.1	CBS-QB3
O=S=CO	-54.6	67.3	14.9	17.6	20.0	22.0	25.2	27.5	30.3	CBS-QB3
O=S=CC	-18.4	73.5	17.4	20.5	23.3	25.8	29.8	32.6	36.9	CBS-QB3
O=S([H])(C)=S	-12.3	75.6	19.0	22.4	25.1	27.4	31.0	33.6	37.4	CBS-QB3
O=S([H])(=C)C(C)=C	32.5	88.3	31.6	37.8	42.9	47.2	54.2	59.2	66.6	CBS-QB3
O=S([H])OS	-37.0	75.0	21.5	24.4	25.8	26.5	27.5	28.0	28.5	CBS-QB3
O=S([H])C(CC)C=S	-4.5	99.0	36.4	42.6	48.0	52.6	59.8	64.8	71.6	CBS-QB3
O=S(CC)(OO)=S	-57.9	96.8	35.1	41.2	46.0	49.6	54.8	58.4	63.1	CBS-QB3
O=S([H])(=C)C(C)(S)C	6.9	100.7	40.0	47.6	53.9	59.4	67.8	73.6	81.7	CBS-QB3

Table A.5: A list of the molecules used in the study and their thermodynamic properties. Enthalpies are given in $\frac{kcal}{mol}$. Entropies and heat capacities are given in $\frac{cal}{mol \cdot K}$.

	$H_f(298)$	$S_f(298)$	Cp(300)	Cp(400)	Cp(500)	Cp(600)	Cp(800)	Cp(1000)	Cp(1500)	Source
O=S(OC)(OC)=C	-77.4	99.6	36.5	42.2	47.1	51.4	58.2	63.1	70.4	CBS-QB3
O=S(O)C(C)=C	-62.4	91.1	29.1	33.9	37.9	41.4	46.9	50.8	56.2	CBS-QB3
O=S([H])C(O)OCC	-112.5	98.0	34.7	41.5	47.3	52.3	60.0	65.4	72.5	CBS-QB3
O=S=S=C(OC)C	-33.1	96.9	33.0	38.9	43.7	47.7	53.6	57.7	63.4	CBS-QB3
O=S([H])(SO)=CC	-8.5	93.8	32.8	37.8	41.7	45.1	50.1	53.5	57.9	CBS-QB3
O=S([H])OO	-43.4	72.9	19.3	21.6	23.0	24.2	25.9	27.0	28.2	CBS-QB3
O=S([H])(=S)C	-12.2	75.5	19.1	22.3	25.1	27.4	31.1	33.7	37.4	CBS-QB3
O=S(S)(CC)=O	-81.0	93.1	29.8	34.5	38.6	42.1	47.5	51.4	56.7	CBS-QB3
O=S=C=S	36.2	70.7	14.5	15.8	16.6	17.3	18.2	18.8	19.3	CBS-QB3
O=S([H])(=C)OC	-22.8	83.7	25.8	30.2	33.9	37.1	42.3	46.0	51.5	CBS-QB3
O=S(OS)C=C	-24.3	89.9	30.9	34.5	37.3	39.6	43.1	45.4	48.2	CBS-QB3
O=S([H])(O)=CO	-56.0	79.4	25.1	29.4	32.3	34.7	38.2	40.5	43.3	CBS-QB3
O=S([H])CS	-15.4	75.3	22.2	26.8	29.9	31.9	34.5	36.1	38.0	CBS-QB3
O=S([H])(=C)SC	23.1	88.7	27.5	31.7	35.3	38.4	43.3	46.9	51.9	CBS-QB3
O=S([H])OC	-59.7	75.9	19.5	22.4	24.8	27.0	30.5	33.0	36.8	CBS-QB3
O=S([H])OC=C	-36.5	80.6	23.1	26.3	29.2	31.7	35.6	38.4	42.4	CBS-QB3
O=S(C)#S	-26.7	79.2	21.6	24.5	26.8	28.8	31.9	34.2	37.6	CBS-QB3
O=S([H])(=S)OC	-48.9	83.6	23.3	26.5	29.1	31.3	35.1	38.0	42.2	CBS-QB3
O=S(O)(S)=C	-27.8	81.8	27.1	30.4	32.7	34.6	37.6	39.7	42.7	CBS-QB3
O=S([H])CO	-61.1	72.5	19.2	23.3	26.6	29.1	32.9	35.4	38.2	CBS-QB3

Table A.5: A list of the molecules used in the study and their thermodynamic properties. Enthalpies are given in $\frac{kcal}{mol}$. Entropies and heat capacities are given in $\frac{cal}{mol \cdot K}$.

	$H_f(298)$	$S_f(298)$	Cp(300)	Cp(400)	Cp(500)	Cp(600)	Cp(800)	Cp(1000)	Cp(1500)	Source
O=S(=S)(C)O	-70.5	81.8	25.0	28.5	31.0	33.2	36.6	39.0	42.4	CBS-QB3
O=S([H])(=C)S	29.5	77.1	22.7	25.8	28.1	30.0	33.0	35.1	38.1	CBS-QB3
O=S([H])SOO	-25.1	87.2	23.2	25.7	27.6	29.2	31.4	32.7	33.6	CBS-QB3
O=S(O)(SO)=C	-59.3	88.4	33.6	38.7	41.2	42.9	45.4	46.9	48.6	CBS-QB3
O=S([H])SO	-42.8	75.7	20.6	23.5	25.1	26.2	27.7	28.5	28.9	CBS-QB3
O=S(OC)S	-65.0	81.7	24.7	28.5	31.5	34.1	37.8	40.2	42.7	CBS-QB3
O=S(C)(=C)SO	-20.6	91.5	33.6	39.7	43.7	46.9	51.6	54.7	58.2	CBS-QB3
O=S([H])SC	-18.9	81.4	20.3	23.0	25.5	27.7	31.1	33.6	37.1	CBS-QB3
O=S(C#C)COC	7.4	94.7	33.7	38.5	42.7	46.2	51.7	55.6	61.1	CBS-QB3
O=S([H])(O)=C=C	12.4	78.2	23.2	27.1	30.2	32.8	36.8	39.6	43.3	CBS-QB3
O=S(SOC)O	-94.1	91.1	30.3	35.4	38.6	41.1	44.6	46.7	48.7	CBS-QB3
O=S(SC)CCC	-44.2	111.0	37.9	44.0	50.0	55.3	63.8	70.1	79.5	CBS-QB3
O=S([H])C=S	18.1	74.3	17.8	19.8	21.6	23.1	25.4	26.9	28.7	CBS-QB3
O=S([H])(=S)O	-53.4	72.3	17.9	20.4	22.0	23.3	25.3	26.6	28.3	CBS-QB3
O=S(CCC)CO	-89.1	95.7	38.2	45.6	52.0	57.4	66.0	72.2	80.8	CBS-QB3
O=S(C)(SC)=O	-80.5	94.9	29.6	34.1	37.9	41.3	46.6	50.5	56.3	CBS-QB3
O=S=C=S=CC	56.9	88.0	26.3	30.3	33.8	36.7	41.3	44.4	48.6	CBS-QB3
O=S([H])(S)=C=C	65.6	84.1	24.7	28.1	31.0	33.4	37.3	40.0	43.6	CBS-QB3
O=S(C)C(S)OC	-64.7	99.2	37.0	43.6	49.3	54.0	61.3	66.2	72.5	CBS-QB3
O=S(=C)(C)OOOC	-24.6	98.1	37.7	44.1	49.3	53.8	60.8	65.6	72.1	CBS-QB3

Table A.5: A list of the molecules used in the study and their thermodynamic properties. Enthalpies are given in $\frac{kcal}{mol}$. Entropies and heat capacities are given in $\frac{cal}{mol \cdot K}$.

	$H_f(298)$	$S_f(298)$	$Cp(300)$	$Cp(400)$	$Cp(500)$	$Cp(600)$	$Cp(800)$	$Cp(1000)$	$Cp(1500)$	Source
O=S([H])(C)=CS([H])=O	1.1	89.2	30.0	35.1	39.4	43.1	48.8	52.8	58.2	CBS-QB3
O=S(=O)(C=C)SC	-54.4	96.5	35.1	39.9	44.0	47.5	53.0	56.8	62.2	CBS-QB3
O=S([H])(=C)OC	-17.9	92.6	30.9	36.4	40.9	44.7	50.3	54.1	59.5	CBS-QB3
O(CS)SO	-57.2	85.7	26.5	30.7	33.7	35.9	39.1	41.3	43.6	CBS-QB3
O(S#C)SCC=O	13.9	103.3	35.3	38.6	41.5	43.9	47.4	49.8	52.8	CBS-QB3
OSOC	-63.4	75.8	20.3	23.6	26.5	28.8	32.4	34.8	37.7	CBS-QB3
O(S)SOO	-24.7	88.1	26.5	28.2	29.5	30.6	32.1	33.0	33.7	CBS-QB3
O(CS)S	-16.8	78.7	24.8	28.0	29.7	31.1	33.3	34.9	37.1	CBS-QB3
O(S)SC	-7.7	82.7	24.2	26.5	28.2	29.7	32.0	33.7	36.3	CBS-QB3
O(C)S([H])=S	-9.6	78.5	21.0	24.1	26.5	28.5	31.7	34.0	37.1	CBS-QB3
OSCS	-27.1	80.5	24.2	26.9	28.9	30.6	33.1	34.8	36.9	CBS-QB3
O(C)SSC	-30.1	90.6	27.7	31.9	35.5	38.6	43.5	47.0	51.8	CBS-QB3
OS(=C)S	7.6	80.9	25.3	27.7	29.3	30.7	33.0	34.6	37.1	CBS-QB3
O(C(=O)SOC)S	-81.8	101.7	30.9	35.4	39.2	42.3	47.0	50.1	53.5	CBS-QB3
O(SO)SOC	-75.7	92.9	30.8	35.8	39.7	42.6	46.1	47.9	49.8	CBS-QB3
O(S)SO	-39.7	77.9	22.0	23.9	25.2	26.2	27.6	28.4	28.9	CBS-QB3
OS(=S)C	-28.3	79.8	21.1	23.8	26.1	28.1	31.2	33.4	36.7	CBS-QB3
OS(SC)OC	-45.6	103.5	35.4	40.6	45.1	48.9	55.0	59.3	65.3	CBS-QB3
O(C)S(O)=O	-120.0	83.9	26.0	28.5	30.5	32.2	35.1	37.4	40.9	CBS-QB3
OSCO	-72.9	77.5	22.1	24.8	26.9	28.6	31.4	33.3	36.0	CBS-QB3

Table A.5: A list of the molecules used in the study and their thermodynamic properties. Enthalpies are given in $\frac{kcal}{mol}$. Entropies and heat capacities are given in $\frac{cal}{mol \cdot K}$.

	$H_f(298)$	$S_f(298)$	Cp(300)	Cp(400)	Cp(500)	Cp(600)	Cp(800)	Cp(1000)	Cp(1500)	Source
O(C)S(=C)COC	-34.0	107.2	37.8	43.9	49.7	55.0	63.5	69.8	79.4	CBS-QB3
O(CC)SC=C	-14.9	94.0	32.1	37.7	42.5	46.7	53.3	58.1	65.1	CBS-QB3
O(C=S)S([H])=C	31.1	85.0	23.7	27.2	30.3	32.9	36.9	39.7	43.5	CBS-QB3
OS(C)(C)(O)([H])SO	-65.4	104.4	42.1	48.9	54.7	59.7	67.5	73.0	80.8	CBS-QB3
O(C)S([H])=C	8.1	80.3	21.1	25.0	28.6	31.7	36.8	40.5	45.9	CBS-QB3
O(C=C)S	-1.0	74.9	18.9	22.2	25.0	27.4	31.0	33.6	37.0	CBS-QB3
OSSOC	-59.3	88.3	26.6	29.5	32.0	34.1	37.3	39.5	42.5	CBS-QB3
O(OC)S	-10.1	79.0	19.4	22.6	25.4	27.7	31.4	34.0	37.2	CBS-QB3
O(O)SS	-12.9	78.8	21.1	23.1	24.5	25.5	27.2	28.3	29.3	CBS-QB3
O(CO)S(S)([H])CC	-63.6	109.4	44.5	50.9	56.3	60.9	68.1	73.1	80.0	CBS-QB3
CS(=O)C	-36.7	78.6	21.9	25.7	29.0	31.9	36.6	40.1	45.5	CBS-QB3
CS(=O)(=O)C	-90.2	82.5	24.3	28.7	32.5	35.9	41.2	45.1	51.0	CBS-QB3
SS(=O)S	-13.4	83.1	21.3	22.6	23.7	24.6	25.9	26.8	28.0	CBS-QB3
SS(=O)(=O)S	-53.9	84.1	25.7	27.7	28.8	29.5	30.7	32.0	33.8	CBS-QB3
CS(=O)O	-79.3	76.5	19.7	23.1	25.5	27.5	30.7	33.0	36.4	CBS-QB3
CS(=O)(=O)O	-134.5	79.6	22.2	26.0	28.9	31.4	35.3	38.0	41.9	CBS-QB3
CS(=O)S	-26.5	80.3	22.6	25.1	27.1	28.8	31.6	33.7	36.9	CBS-QB3
Cl[SH](=O)(=O)	-73.8	72.4	17.4	20.7	23.7	26.2	30.1	33.0	37.1	CBS-QB3
CS([H])=O	-23.2	68.5	15.1	17.9	20.3	22.4	25.7	28.2	31.7	CBS-QB3
O=[SH2]=O	-55.9	61.8	11.0	13.1	15.1	16.8	19.3	21.0	23.3	CBS-QB3

Table A.5: A list of the molecules used in the study and their thermodynamic properties. Enthalpies are given in $\frac{kcal}{mol}$. Entropies and heat capacities are given in $\frac{cal}{mol \cdot K}$.

	$H_f(298)$	$S_f(298)$	Cp(300)	Cp(400)	Cp(500)	Cp(600)	Cp(800)	Cp(1000)	Cp(1500)	Source
SS([H])=O	-12.8	69.1	15.8	17.8	19.0	19.9	21.3	22.2	23.3	CBS-QB3
SS([H])(=O)=O	-55.4	73.4	17.5	20.1	21.9	23.3	25.5	26.9	28.7	CBS-QB3
O=S=C	-8.2	62.5	12.5	14.6	16.3	17.6	19.6	21.0	22.9	CBS-QB3
C=CS([H])=O	2.5	70.3	19.9	23.9	26.9	29.1	32.4	34.6	37.7	CBS-QB3
C=CS(=O)O	-52.1	78.1	24.6	28.9	31.7	33.9	37.3	39.5	42.6	CBS-QB3
CCS(=O)C	-42.9	88.6	27.3	32.5	37.1	41.1	47.6	52.4	59.8	CBS-QB3
CCS(=O)CC	-51.5	88.6	33.0	39.5	45.2	50.2	58.4	64.7	74.2	CBS-QB3
CCS([H])=O	-29.0	75.9	20.4	24.6	28.3	31.5	36.6	40.4	45.9	CBS-QB3
CCS(=O)O	-85.6	86.3	25.3	29.7	33.4	36.6	41.6	45.2	50.7	CBS-QB3
CCS(=O)S	-33.1	89.4	28.5	32.5	35.6	38.2	42.6	46.0	51.1	CBS-QB3
OS(=O)O	-124.4	74.3	19.7	21.1	22.1	23.0	24.3	25.3	26.8	CBS-QB3
OS(=O)S	-67.4	76.7	21.3	23.9	25.0	25.6	26.4	27.0	27.7	CBS-QB3
C=CS(=O)(=O)C=C	-35.1	88.3	32.1	37.8	42.5	46.4	52.6	56.9	62.8	CBS-QB3
C=C[SH](=O)=O	-43.8	75.9	21.2	25.3	28.5	31.2	35.5	38.5	42.8	CBS-QB3
C=CS(=O)(=O)O	-106.1	83.0	26.4	30.6	33.9	36.6	40.8	43.7	47.6	CBS-QB3
CCS(=O)(=O)C	-96.4	92.2	29.3	35.3	40.5	44.9	52.0	57.2	65.2	CBS-QB3
CCS(=O)(=O)CC	-102.7	101.5	34.7	41.9	48.3	53.9	63.0	69.6	79.4	CBS-QB3
CC[SH](=O)=O	-79.9	80.0	22.9	27.5	31.6	35.3	41.1	45.2	51.3	CBS-QB3
CCS(=O)(=O)O	-141.1	89.4	27.5	32.5	36.8	40.4	46.1	50.2	56.2	CBS-QB3
O[SH](=O)=O	-118.2	69.5	15.4	18.1	20.1	21.7	24.2	25.9	28.0	CBS-QB3

Table A.5: A list of the molecules used in the study and their thermodynamic properties. Enthalpies are given in $\frac{kcal}{mol}$. Entropies and heat capacities are given in $\frac{cal}{mol \cdot K}$.

	$H_f(298)$	$S_f(298)$	Cp(300)	Cp(400)	Cp(500)	Cp(600)	Cp(800)	Cp(1000)	Cp(1500)	Source
OS(=O)(=O)S	-113.7	83.3	25.2	27.5	28.8	29.6	30.6	31.8	33.6	CBS-QB3
C[SH](C)C	46.9	88.1	27.5	32.7	37.7	42.2	55.3	63.9	68.4	CBS-QB3
C[SH](C)(C)(C)C	71.9	95.3	38.1	48.0	56.7	64.4	76.9	86.4	101.0	CBS-QB3
O[SH](C)(C)(C)C	15.0	104.1	37.7	46.0	53.4	59.9	70.7	79.0	91.6	CBS-QB3
O[SH](=O)(C)C	-44.7	87.1	26.5	31.8	36.8	41.2	48.2	53.4	60.9	CBS-QB3
C[SH]=C	47.8	71.5	18.9	22.5	25.6	28.4	32.8	36.1	41.2	CBS-QB3
[SH2]=C	58.6	58.7	11.1	13.4	15.4	17.2	20.1	22.2	25.4	CBS-QB3
OS(=C)C	-8.4	78.1	24.2	28.0	31.0	33.6	37.8	40.9	45.8	CBS-QB3
O[SH]=C	3.0	67.4	17.7	20.8	23.0	24.6	27.2	29.1	31.9	CBS-QB3
C#SC	65.4	69.4	14.7	17.5	19.9	21.9	25.2	27.7	31.3	CBS-QB3
C#[SH]	74.0	57.1	9.9	11.3	12.5	13.5	15.1	16.2	17.8	CBS-QB3
C#SO	22.5	65.0	14.7	16.6	17.9	18.7	19.9	20.8	22.1	CBS-QB3
CS(=C)(=C)C	84.5	87.8	32.3	38.8	44.0	48.5	55.9	61.4	70.0	CBS-QB3
C[SH](=C)(=C)	97.2	77.3	24.6	30.3	34.8	38.6	44.7	49.3	56.1	CBS-QB3
CS(=C)(=C)O	36.5	82.5	29.9	36.7	41.6	45.4	51.3	55.5	61.5	CBS-QB3
CS(=O)(=C)C	5.6	116.2	29.7	34.7	38.9	42.7	48.8	53.5	60.7	CBS-QB3
C[SH](=O)(=C)	15.8	75.4	21.4	25.7	29.3	32.4	37.4	41.1	46.6	CBS-QB3
CS(=O)(=C)O	-43.3	83.3	26.7	31.0	34.6	37.8	42.8	46.4	51.5	CBS-QB3
C#S(C)(C)C	107.2	155.6	33.5	38.7	43.3	47.6	54.8	60.3	69.1	CBS-QB3
C#[SH3]	148.9	57.8	10.0	11.9	13.9	15.8	18.9	21.0	24.1	CBS-QB3

Table A.5: A list of the molecules used in the study and their thermodynamic properties. Enthalpies are given in $\frac{kcal}{mol}$. Entropies and heat capacities are given in $\frac{cal}{mol \cdot K}$.

	$H_f(298)$	$S_f(298)$	Cp(300)	Cp(400)	Cp(500)	Cp(600)	Cp(800)	Cp(1000)	Cp(1500)	Source
C#SO(O)(C)C	48.0	88.2	29.7	34.8	39.3	43.1	49.3	53.8	60.5	CBS-QB3
C#[SH](O)C	60.3	78.0	22.8	26.9	30.4	33.5	38.3	41.7	46.6	CBS-QB3
C#S(=C)C	120.7	77.6	22.6	26.6	30.1	33.0	37.8	41.2	46.4	CBS-QB3
C#S(=O)C	42.4	74.0	18.4	21.5	24.3	26.6	30.3	33.0	36.9	CBS-QB3
C#[SH](=O)	54.2	62.7	12.9	15.0	16.6	18.0	20.0	21.4	23.2	CBS-QB3
OSO	-68.1	64.9	15.0	17.4	19.2	20.4	22.0	22.9	23.7	CBS-QB3
C\$OO	-20.2	77.3	21.3	23.9	26.2	28.2	31.4	33.7	36.9	CBS-QB3
C\$C=O	-37.1	72.6	17.9	21.1	23.9	26.4	30.2	32.9	36.9	CBS-QB3
COOS(=O)C	-60.6	93.5	31.6	35.8	39.4	42.6	47.5	51.1	56.2	CBS-QB3
C\$COO	-32.6	87.2	27.4	31.3	34.6	37.5	42.1	45.5	50.4	CBS-QB3
C=S=C	54.1	63.8	16.1	19.2	21.7	23.6	26.7	28.9	32.2	CBS-QB3
CSOC	-30.1	82.5	21.6	25.2	28.4	31.2	35.8	39.3	44.8	CBS-QB3
CS(=O)OO	-59.6	83.0	24.7	28.1	30.8	33.1	36.6	38.9	42.0	CBS-QB3
C=S(=O)(=O)	-35.9	67.0	15.5	18.3	20.5	22.2	24.6	26.3	28.5	CBS-QB3
C\$OOC	-19.7	85.7	24.9	29.5	33.5	36.9	42.3	46.0	51.1	CBS-QB3
c1ccccc1SSc1cccc1	51.8	122.9	50.9	63.3	74.2	83.6	97.9	107.1	119.7	CBS-QB3
CC(C)(C)SSC(C)(C)C	-51.2	129.4	56.4	69.2	80.4	90.1	105.6	117.1	134.3	CBS-QB3
e1ccccc1CS	18.2	91.5	31.1	39.1	46.2	52.3	61.4	67.7	77.1	CBS-QB3
O=SO	-63.6	64.5	13.6	15.8	17.7	19.0	20.8	22.0	23.5	CBS-QB3
O=S(=S)=C	17.6	70.4	16.9	19.7	21.7	23.1	25.3	26.8	28.7	CBS-QB3

Table A.5: A list of the molecules used in the study and their thermodynamic properties. Enthalpies are given in $\frac{kcal}{mol}$. Entropies and heat capacities are given in $\frac{cal}{mol \cdot K}$.

	$H_f(298)$	$S_f(298)$	Cp(300)	Cp(400)	Cp(500)	Cp(600)	Cp(800)	Cp(1000)	Cp(1500)	Source
S	-5.4	50.5	8.2	8.5	8.8	9.2	10.1	10.8	12.1	[141]
SC	-5.5	63.3	12.1	14.1	15.9	17.5	20.2	22.3	25.8	[141]
SCC	-11.1	73.0	17.6	21.0	24.2	26.9	31.3	34.6	40.0	[141]
SC(C)C	-18.3	82.5	23.3	28.3	32.8	36.6	42.6	47.1	54.3	[141]
SC(C)(C)C	-26.4	90.3	29.5	36.2	42.0	46.9	54.4	60.0	68.9	[141]
SCC=C	14.9	76.2	23.6	27.1	30.0	32.6	36.9	40.2	45.7	[141]
SC(C)C=C	7.7	85.1	29.0	34.7	39.2	42.8	48.5	52.9	60.1	[141]
SCC#C	57.4	74.3	19.7	22.8	25.3	27.4	30.6	33.1	37.0	[141]
SC(C)C#C	50.5	83.4	25.4	30.1	33.9	37.0	41.9	45.5	51.3	[141]
SC=C	19.3	67.4	15.6	18.4	20.7	22.7	25.6	27.9	31.5	[141]
SC(C)=C	10.3	77.9	20.9	25.1	28.6	31.6	36.3	39.9	45.6	[141]
SC#C	62.3	63.0	14.4	16.1	17.4	18.4	19.9	21.1	23.0	[141]
c1ccccc1S	27.1	82.1	25.2	32.5	38.5	43.4	50.6	55.6	62.9	[141]
CSC	-8.9	74.6	17.8	20.9	23.9	26.5	30.8	34.2	39.7	[141]
CSCC	-14.1	84.7	22.8	27.5	31.8	35.6	41.7	46.4	53.8	[141]
CSC(C)C	-21.2	93.2	28.8	35.1	40.7	45.5	53.1	58.9	68.2	[141]
CSC(C)(C)C	-29.0	101.4	34.8	42.9	49.8	55.6	64.8	71.7	82.6	[141]
CSCC=C	10.9	86.2	29.4	34.7	38.9	42.4	48.0	52.4	59.7	[141]
CSC(C)C=C	3.4	94.1	34.3	42.6	48.8	53.4	60.3	65.6	74.3	[141]
CSCC#C	53.1	84.8	25.5	30.0	33.6	36.6	41.3	45.0	50.9	[141]

Table A.5: A list of the molecules used in the study and their thermodynamic properties. Enthalpies are given in $\frac{kcal}{mol}$. Entropies and heat capacities are given in $\frac{cal}{mol \cdot K}$.

	$H_f(298)$	$S_f(298)$	Cp(300)	Cp(400)	Cp(500)	Cp(600)	Cp(800)	Cp(1000)	Cp(1500)	Source
CSC(C)C#C	46.3	93.8	31.6	37.4	42.3	46.3	52.7	57.5	65.2	[141]
CSC=C	14.6	77.0	22.0	25.9	29.3	32.1	36.5	40.0	45.5	[141]
CSC(C)=C	5.9	86.5	28.0	33.3	37.6	41.3	47.3	51.9	59.5	[141]
CSC#C	57.8	75.1	19.6	22.6	25.0	27.0	30.2	32.7	36.7	[141]
c1ccccc1SC	23.4	93.1	30.1	38.7	46.0	52.0	60.9	67.2	76.6	[141]
C=CSC=C	40.3	83.5	24.5	29.3	33.3	36.5	41.5	45.2	51.1	[141]
C=CSC#C	82.9	78.6	23.0	26.9	29.9	32.3	35.8	38.4	42.5	[141]
c1cccc1SC=C	47.9	97.2	34.0	43.4	51.2	57.4	66.6	72.9	82.3	[141]
C#CSC#C	145.5	79.0	23.6	27.3	29.8	31.7	34.5	36.4	39.4	[141]
c1cccc1SC#C	90.9	92.6	32.8	41.1	47.7	53.0	60.6	65.9	73.8	[141]
c1cccc1Sc1cccc1	55.2	111.7	42.8	56.7	68.4	77.7	91.1	100.3	113.6	[141]
SS	3.9	63.2	11.9	13.2	14.2	15.0	16.1	16.8	17.9	[141]
SSC	-1.0	74.8	17.3	19.8	21.9	23.7	26.5	28.5	31.6	[141]
CSSC	-5.8	86.6	22.5	26.1	29.4	32.2	36.7	40.1	45.4	[141]
SSC=C	24.4	79.6	20.5	23.9	26.6	28.7	31.8	34.0	37.3	[141]
SSC#C	68.6	75.3	19.5	21.8	23.4	24.5	26.0	27.0	28.6	[141]
c1cccc1SS	32.2	93.4	30.1	37.9	44.3	49.4	56.6	61.4	68.3	[141]
SSS	7.4	74.8	17.3	19.0	20.2	21.2	22.4	23.2	23.9	[141]
SSSC	1.8	86.3	23.3	25.9	28.1	29.9	32.8	34.8	37.6	[141]
CSSSC	-4.0	96.6	29.8	33.5	36.7	39.4	43.6	46.8	51.4	[141]

Table A.5: A list of the molecules used in the study and their thermodynamic properties. Enthalpies are given in $\frac{kcal}{mol}$. Entropies and heat capacities are given in $\frac{cal}{mol \cdot K}$.

	$H_f(298)$	$S_f(298)$	Cp(300)	Cp(400)	Cp(500)	Cp(600)	Cp(800)	Cp(1000)	Cp(1500)	Source
SC=S	25.8	66.2	14.3	16.5	18.0	19.2	20.9	22.0	23.7	[141]
CSC=S	18.4	77.1	18.7	22.3	25.5	28.0	31.5	34.1	37.8	[141]
C=CSC=S	45.2	80.2	22.8	27.6	31.2	33.9	37.5	39.9	43.6	[141]
C#CSC=S	91.5	79.4	21.2	24.3	26.5	28.1	30.4	32.1	34.4	[141]
c1ccccc1SC=S	54.6	97.2	32.2	40.8	47.8	53.3	61.3	66.6	74.2	[141]
S=CSC=S	56.0	81.8	21.7	24.8	27.3	29.3	32.2	33.9	35.5	[141]
SSC=S	31.3	79.4	19.3	21.7	23.5	24.8	26.6	27.8	29.2	[141]
SCS	3.9	73.5	20.7	22.1	23.3	24.5	26.5	28.3	31.3	[141]
SC(C)S	-3.5	83.2	26.1	29.1	31.7	33.9	37.7	40.7	45.6	[141]
S=CCS	26.2	77.0	22.5	25.7	27.7	29.2	31.7	33.6	36.9	[141]
S=CC(C)S	18.6	85.8	27.8	32.9	36.7	39.4	43.4	46.4	51.3	[141]
c1ccccc1CS	22.3	91.6	31.2	39.7	46.9	52.7	61.5	67.7	77.0	[141]
c1ccccc1C(C)S	15.5	100.1	37.2	47.3	55.9	62.8	73.2	80.5	91.4	[141]
C=S	27.7	56.5	9.1	10.3	11.5	12.5	14.1	15.2	17.1	[141]
CC=S	17.1	67.8	13.9	16.5	19.0	21.2	24.6	27.1	31.1	[141]
CCC=S	12.1	77.5	19.1	23.3	27.0	30.3	35.4	39.3	45.3	[141]
CC(C)C=S	6.0	87.3	25.2	30.8	35.8	40.0	46.7	51.6	59.5	[141]
CC(C)C=C=S	-2.1	94.9	31.1	38.5	44.8	50.0	58.2	64.3	73.9	[141]
C=CC=S	39.4	69.2	17.2	21.3	24.7	27.4	31.3	33.9	37.8	[141]
C#CC=S	85.7	68.1	15.9	18.5	20.5	22.0	24.2	25.8	28.3	[141]

Table A.5: A list of the molecules used in the study and their thermodynamic properties. Enthalpies are given in $\frac{kcal}{mol}$. Entropies and heat capacities are given in $\frac{cal}{mol \cdot K}$.

	$H_f(298)$	$S_f(298)$	Cp(300)	Cp(400)	Cp(500)	Cp(600)	Cp(800)	Cp(1000)	Cp(1500)	Source
c1ccccc1C=S	47.0	83.8	27.2	35.3	42.2	47.8	55.8	61.2	69.0	[141]
S=CC=S	54.2	71.5	15.6	18.3	20.7	22.7	25.5	27.2	29.0	[141]
CC(C)=S	6.7	78.8	18.6	22.6	26.4	29.7	35.0	38.9	45.1	[141]
CC(=S)C=C	30.3	80.4	23.2	27.9	32.1	35.7	41.2	45.2	51.3	[141]
CC(=S)C#C	74.9	78.8	21.2	25.0	28.2	30.8	34.8	37.7	42.2	[141]
c1ccccc1C(=S)C	38.7	94.6	32.7	42.1	50.2	56.7	66.3	72.9	82.6	[141]
CC(=S)C=S	43.7	82.3	20.7	24.9	28.5	31.5	35.9	38.7	42.6	[141]
CC(=S)S	15.0	77.3	19.4	22.8	25.5	27.7	31.2	33.8	37.5	[141]
C=CSCC	9.7	87.1	27.1	32.5	37.2	41.2	47.5	52.3	59.8	[141]
C=CSC(C)C	2.5	95.3	32.7	40.2	46.5	51.6	59.3	65.0	74.0	[141]
C=C(C)SC(C)C	-5.8	105.4	38.7	47.3	54.6	60.6	70.1	77.1	88.0	[141]
C=CSC#CC	72.3	90.6	27.4	32.4	36.7	40.2	45.8	50.0	56.4	[141]
CSC#CS	62.1	87.3	24.5	27.8	30.5	32.6	36.0	38.5	42.3	[141]
CC(=C)SC(=C)C	23.3	102.7	36.0	43.3	49.5	54.7	63.0	69.2	78.9	[141]
S=CSC=CSC	45.6	101.8	35.0	41.1	45.8	49.3	54.2	57.7	63.0	[141]
S=CSCC	13.0	86.5	24.1	29.4	33.8	37.3	42.6	46.4	52.1	[141]
CC(=S)SCC	2.8	96.6	28.8	35.2	41.0	45.8	53.3	58.6	66.4	[141]
SC(=S)CC	10.7	87.3	24.7	29.8	33.9	37.2	42.3	46.1	51.7	[141]
C=CC(=S)C(C)C	19.8	97.9	33.4	41.8	49.0	55.0	64.1	70.5	80.1	[141]
CC(=C)C(=S)C	22.5	89.6	29.4	35.9	41.3	45.7	52.5	57.4	65.3	[141]

Table A.5: A list of the molecules used in the study and their thermodynamic properties. Enthalpies are given in $\frac{kcal}{mol}$. Entropies and heat capacities are given in $\frac{cal}{mol \cdot K}$.

	$H_f(298)$	$S_f(298)$	Cp(300)	Cp(400)	Cp(500)	Cp(600)	Cp(800)	Cp(1000)	Cp(1500)	Source
CC(=C)C=S	29.7	81.4	22.6	27.3	31.6	35.3	40.9	45.0	51.3	[141]
CCC(=S)C#C	69.6	88.6	26.6	31.9	36.4	40.0	45.7	49.9	56.4	[141]
c1ccccc1SSC=C	51.9	108.6	39.1	48.7	56.6	63.0	72.1	78.2	87.0	[141]
C#CSSSC=S	96.3	91.5	27.4	30.7	32.9	34.5	36.6	38.0	39.9	[141]
CC(=S)C(=S)C	34.7	94.1	25.8	31.0	35.7	39.6	45.6	49.8	55.9	[141]
SSC(C)(C)C	-23.2	100.7	34.8	42.3	48.4	53.3	60.9	66.4	74.9	[141]
c1cc(SC#C)ccc1SC=C	117.6	120.4	47.2	57.6	65.9	72.5	82.0	88.6	98.3	[141]
c1c(SC)cc(S)cc1SS	39.8	128.4	47.0	56.0	63.4	69.3	77.9	83.8	92.2	[141]
SC(S)S	12.4	85.6	25.3	27.8	29.4	30.7	32.7	34.3	36.9	[141]
SC(S)(S)C	3.8	93.3	32.1	36.0	38.9	41.2	44.6	47.3	51.5	[141]
SC(C)(C)S	-11.8	91.4	32.0	36.8	40.8	44.1	49.5	53.6	60.1	[141]
CC(S)(S)CC	-16.6	101.1	36.9	43.2	48.6	53.1	60.3	65.8	74.4	[141]
SC(S)(S)SC	-1.5	103.6	37.3	42.8	47.1	50.5	55.6	59.4	65.5	[141]
CCCS	-17.9	81.5	23.3	27.8	32.0	35.9	42.2	47.0	54.2	[141]
CC=CS	10.6	77.8	20.8	24.5	27.9	31.0	36.0	39.7	45.5	[141]
OCS	-44.4	70.0	18.4	21.1	22.9	24.4	26.4	28.0	30.9	[27]
CC(S)O	-54.0	77.2	24.6	28.7	31.7	34.1	34.6	40.3	45.1	[27]
CCC(S)O	-59.2	86.3	31.0	36.0	40.0	43.2	48.5	52.5	59.3	[27]
CC(S)(O)C	-64.5	83.8	31.0	36.5	40.7	44.0	49.0	52.8	59.4	[27]
C=CC(S)O	-27.2	82.5	28.4	33.3	36.8	39.4	43.2	46.1	50.9	[27]

Table A.5: A list of the molecules used in the study and their thermodynamic properties. Enthalpies are given in $\frac{kcal}{mol}$. Entropies and heat capacities are given in $\frac{cal}{mol \cdot K}$.

	$H_f(298)$	$S_f(298)$	Cp(300)	Cp(400)	Cp(500)	Cp(600)	Cp(800)	Cp(1000)	Cp(1500)	Source
c1ccccc1C(O)S	-20.8	95.3	38.1	47.0	54.1	59.7	67.9	73.6	82.2	[27]
OC(S)O	-90.5	78.6	21.1	23.9	26.2	28.0	30.8	32.8	35.9	[27]
CC(S)(O)O	-101.9	86.4	27.8	31.6	34.8	37.4	41.6	44.7	49.7	[27]
CCC(S)(O)O	-107.7	94.1	32.9	38.3	42.8	46.7	52.8	57.3	64.1	[27]
O=CS	-31.8	64.5	13.5	15.2	16.7	18.0	19.9	21.3	23.2	[27]
S=CO	-29.7	62.3	11.7	13.9	15.8	17.5	20.0	21.6	23.7	[27]
CC(=O)S	-44.3	74.7	18.7	22.0	24.8	27.1	30.7	33.2	37.1	[27]
CC(=S)O	-41.9	71.0	16.7	20.1	23.3	26.1	30.4	33.5	37.8	[27]
CCC(=O)S	-49.7	82.7	25.1	29.3	33.0	36.2	41.5	45.3	51.1	[27]
CCC(=S)O	-47.6	81.0	22.1	26.9	31.3	35.2	41.3	45.6	51.7	[27]
SC(=O)O	-90.7	69.5	16.8	19.7	22.1	23.9	26.4	27.8	29.2	[27]
OC(=S)O	-85.5	66.8	17.0	20.3	22.9	24.8	27.2	28.3	29.2	[27]
CSCO	-47.8	77.4	24.0	28.6	31.9	34.5	38.0	40.5	44.8	[27]
COCS	-39.8	78.3	23.6	27.2	30.2	32.7	36.8	40.0	45.2	[27]
CSCOC	-44.3	84.6	27.5	32.6	37.1	41.1	47.5	52.2	59.7	[27]
O=CSC	-34.6	71.2	17.3	20.5	23.3	25.8	29.8	32.8	37.1	[27]
S=COC	-20.6	70.5	16.0	19.2	22.3	25.0	29.3	32.4	36.9	[27]
CC(=O)SC	-50.5	80.2	22.2	27.2	31.7	35.6	41.6	45.7	51.5	[27]
CC(=S)OC	-37.4	79.5	21.9	26.1	30.4	34.3	40.7	45.3	51.9	[27]
CC(=O)SCC	-56.5	91.5	28.0	34.1	39.9	44.9	52.8	58.3	66.1	[27]

Table A.5: A list of the molecules used in the study and their thermodynamic properties. Enthalpies are given in $\frac{kcal}{mol}$. Entropies and heat capacities are given in $\frac{cal}{mol \cdot K}$.

	$H_f(298)$	$S_f(298)$	$Cp(300)$	$Cp(400)$	$Cp(500)$	$Cp(600)$	$Cp(800)$	$Cp(1000)$	$Cp(1500)$	Source
CCSCO	-50.2	87.4	28.3	34.7	39.4	43.0	48.3	52.3	59.0	[27]
CCCSCO	-55.3	98.3	33.2	40.8	46.8	51.5	58.8	64.2	73.1	[27]
CSC(O)C	-56.2	83.2	28.7	35.1	40.0	43.5	48.6	52.4	59.0	[27]
CCSC(O)C	-61.2	93.3	33.8	41.8	48.0	52.8	59.6	64.7	73.2	[27]
CSC(O)CC	-61.1	92.9	34.3	42.0	48.0	52.7	59.5	64.6	73.2	[27]
CSC(O)(C)C	-64.5	87.8	35.6	43.5	49.3	53.5	59.9	64.8	73.2	[27]
CCSC(O)(C)C	-68.2	97.5	41.0	50.5	57.7	63.1	71.1	77.3	87.6	[27]
CSC(O)(C)CC	-67.0	101.3	41.0	50.1	57.1	62.5	70.7	77.0	87.4	[27]

Table A.6: A list of the radical species used in the study, their thermodynamic properties, and the source of the data. Enthalpies are given in $\frac{kcal}{mol \cdot K}$. Entropies and heat capacities are given in $\frac{cal}{mol \cdot K}$.

	Hf(298)	Sf(298)	Cp(300)	Cp(400)	Cp(500)	Cp(600)	Cp(800)	Cp(1000)	Cp(1500)	Source
[SH]=O	-5.40	57.80	9.02	9.93	10.73	11.36	12.22	12.73	13.34	CBS-QB3
O[S]=O	-58.79	66.84	12.72	14.09	14.96	15.52	16.32	16.84	17.48	CBS-QB3
O=[SH]=O	-33.80	63.68	11.94	13.68	14.99	15.97	17.28	18.05	18.98	CBS-QB3
OS(=O)[O]	-89.67	71.04	15.73	17.82	19.11	20.00	21.29	22.12	23.09	CBS-QB3
Cl[S](O)C	-9.50	88.73	25.63	29.41	32.59	35.40	40.18	43.85	49.65	CBS-QB3
CSO[O]	21.39	79.36	19.60	21.74	23.39	24.75	27.03	28.81	31.61	CBS-QB3
CS[Cl]=O	0.69	77.04	16.46	18.73	20.82	22.65	25.61	27.82	31.10	CBS-QB3
S=[CH]	75.63	52.39	7.86	8.49	9.03	9.47	10.16	10.69	11.50	CBS-QB3
CS(=O)[O]	-51.98	74.40	17.30	19.92	22.11	24.01	27.01	29.18	32.28	CBS-QB3
CS[O]	-17.80	67.70	14.26	16.42	18.37	20.05	22.69	24.66	27.61	CBS-QB3
COOS[O]	-37.83	82.60	22.83	25.49	27.74	29.64	32.59	34.63	37.40	CBS-QB3
C[SH]([O])C	19.79	82.65	23.65	28.29	32.31	35.77	41.27	45.26	51.04	CBS-QB3
CSC[O]	5.13	78.80	20.92	24.38	27.37	29.94	34.03	36.99	41.27	CBS-QB3
C[S]	29.51	60.67	10.83	12.54	14.07	15.41	17.61	19.29	21.90	CBS-QB3
c1ccccc1C[S]	54.56	87.52	29.02	37.09	43.75	49.34	58.10	64.32	72.85	CBS-QB3
[SH]	33.37	45.90	6.94	6.96	7.01	7.11	7.36	7.62	8.15	[27]
Cl[CH]S	29.30	73.07	17.02	19.75	22.33	24.65	28.44	31.26	35.56	[27]
Cl[CH]C=S	36.76	73.29	18.52	22.07	25.33	28.22	32.87	36.29	41.44	[27]
CC[C]=S	49.83	77.54	18.41	21.51	24.62	27.48	32.14	35.55	40.62	[27]
OC[S]	-9.18	67.86	13.86	16.21	18.23	19.92	22.44	24.14	26.67	[27]

Table A.6: A list of the radical species used in the study, their thermodynamic properties, and the source of the data. Enthalpies are given in $\frac{kcal}{mol \cdot K}$. Entropies and heat capacities are given in $\frac{cal}{mol \cdot K}$.

	Hf(298)	Sf(298)	Cp(300)	Cp(400)	Cp(500)	Cp(600)	Cp(800)	Cp(1000)	Cp(1500)	Source
CC(O)[S]	-18.27	75.12	20.01	23.77	26.92	29.55	33.62	36.54	40.98	[27]
C[C](O)S	-14.01	79.80	22.83	26.13	28.86	31.14	34.73	37.31	41.18	[27]
CCC(O)[S]	-23.71	85.29	25.77	30.82	35.22	38.97	44.84	49.07	55.37	[27]
CC[C](O)S	-19.57	88.10	28.32	33.46	37.50	40.77	45.71	49.25	54.78	[27]
C[CH]C(O)S	-12.43	88.20	29.46	34.13	37.83	40.89	45.67	49.22	54.85	[27]
O=C[S]	6.87	64.18	11.24	12.44	13.48	14.38	15.76	16.74	18.12	[27]
CC(=O)[S]	-7.56	72.83	15.95	18.64	21.03	23.10	26.34	28.66	32.08	[27]
CCC(=O)[S]	-12.43	82.55	22.01	25.56	28.93	31.98	36.95	40.60	46.08	[27]
C=C[S]	47.30	64.51	13.15	15.75	17.97	19.74	22.44	24.38	27.44	[141]
C#C[S]	86.57	57.91	13.48	14.39	15.03	15.56	16.40	17.04	18.14	[141]
c1ccccc1[S]	56.09	78.01	23.47	30.47	36.33	40.97	47.68	52.22	58.82	[141]
S=C[S]	53.73	65.94	11.45	13.03	14.22	15.13	16.35	17.16	18.33	[141]
s[S]	25.81	60.92	9.56	10.28	10.78	11.19	11.81	12.28	13.00	[141]
CS[S]	17.66	70.87	14.34	16.37	18.16	19.67	22.01	23.80	26.67	[141]
SS[S]	27.99	74.90	14.65	15.42	15.92	16.28	16.83	17.28	17.95	[141]
[CH2]S	37.83	62.72	12.93	14.46	15.70	16.73	18.33	19.60	21.70	[141]
C[CH]S	30.90	72.80	16.92	19.86	22.51	24.78	28.39	31.17	35.54	[141]
C=C[CH]S	44.65	76.63	20.46	24.55	27.89	30.57	34.61	37.57	42.21	[141]
C#C[CH]S	88.58	74.19	20.08	22.80	24.81	26.34	28.59	30.26	32.89	[141]
c1ccccc1[CH]S	55.11	89.27	30.88	39.29	46.22	51.74	59.78	65.32	73.40	[141]

Table A.6: A list of the radical species used in the study, their thermodynamic properties, and the source of the data. Enthalpies are given in $\frac{kcal}{mol \cdot K}$. Entropies and heat capacities are given in $\frac{cal}{mol \cdot K}$.

	Hf(298)	Sf(298)	Cp(300)	Cp(400)	Cp(500)	Cp(600)	Cp(800)	Cp(1000)	Cp(1500)	Source
S=C[CH]S	45.65	73.16	18.76	22.75	25.62	27.70	30.47	32.34	34.89	[141]
S[CH]S	41.95	74.81	16.18	18.14	19.67	20.91	22.85	24.31	26.60	[141]
CCS	22.80	82.05	22.51	26.39	30.09	33.41	38.81	42.97	49.52	[141]
C=CCS	35.47	84.70	24.88	30.33	34.99	38.84	44.81	49.26	56.09	[141]
C#CCS	80.19	84.80	24.78	28.68	31.93	34.58	38.72	41.83	46.73	[141]
c1ccccc1CS	47.47	97.51	35.25	45.03	53.32	60.06	70.05	76.98	87.02	[141]
S=CCS	35.68	81.62	23.92	29.09	33.25	36.47	41.13	44.34	48.95	[141]
C[C](S)S	34.44	86.47	22.75	25.10	27.51	29.71	33.37	36.19	40.61	[141]
C=C[S]	79.18	68.28	16.73	18.64	20.10	21.27	23.18	24.69	27.15	[141]
S=[CH]	68.00	56.38	8.77	9.46	10.04	10.52	11.21	11.76	12.62	[141]
C=C=S	56.91	66.09	12.69	14.77	16.75	18.50	21.25	23.30	26.46	[141]
[S]	66.92	38.50	4.97	4.97	4.97	4.97	4.97	4.97	4.97	[141]
CC[S]	23.90	68.04	15.89	19.12	21.99	24.43	28.32	31.29	36.02	[141]
CC(C)[S]	17.69	74.74	21.15	26.05	30.33	33.91	39.51	43.69	50.26	[141]
CC(C)(C)[S]	9.73	80.98	27.39	33.82	39.39	44.02	51.15	56.41	64.72	[141]
CSC[S]	33.44	80.38	20.67	24.59	27.80	30.28	33.99	36.74	41.16	[141]
C=CC[S]	50.00	74.14	18.67	22.73	26.15	28.97	33.32	36.52	41.54	[141]
C=CC=C[S]	56.96	77.87	21.77	27.06	31.45	34.92	39.91	43.36	48.40	[141]
C=C(C)[S]	38.65	73.35	18.62	22.47	25.86	28.68	33.10	36.35	41.47	[141]
CC=C[S]	38.19	74.76	18.59	22.30	25.69	28.56	33.05	36.35	41.47	[141]

Table A.6: A list of the radical species used in the study, their thermodynamic properties, and the source of the data. Enthalpies are given in $\frac{kcal}{mol \cdot K}$. Entropies and heat capacities are given in $\frac{cal}{mol \cdot K}$.

	Hf(298)	Sf(298)	Cp(300)	Cp(400)	Cp(500)	Cp(600)	Cp(800)	Cp(1000)	Cp(1500)	Source
CC=C[S]	37.60	74.33	18.50	22.25	25.67	28.56	33.08	36.40	41.56	[141]
CSS[S]	22.01	84.66	19.24	21.37	23.16	24.67	27.01	28.80	31.64	[141]
Cc1c([S])cccc1	47.75	86.71	28.68	36.88	43.91	49.64	58.15	64.08	72.80	[141]
Cc1cc([S])ccc1	47.20	86.81	28.61	36.83	43.88	49.62	58.15	64.08	72.80	[141]
CS[CH2]	33.10	73.23	17.69	20.55	23.06	25.22	28.61	31.21	35.47	[141]
CSS[CH2]	38.48	84.13	23.14	26.41	29.06	31.19	34.39	36.81	40.73	[141]
SCS[CH2]	42.71	86.11	25.22	27.99	30.16	31.98	34.89	37.19	41.01	[141]
CS[CH]C	26.72	82.86	22.01	26.05	29.88	33.20	38.58	42.69	49.24	[141]
CCS[CH]C	21.51	91.92	28.35	33.77	38.77	43.04	49.93	55.19	63.55	[141]
CCS[Cl](C)C	13.93	100.31	32.96	39.48	45.72	51.20	60.06	66.78	77.29	[141]
CSCC#CC	64.94	101.84	34.27	40.85	46.58	51.43	59.18	65.06	74.35	[141]
S=[C]CC	52.01	76.60	18.31	21.73	24.93	27.72	32.15	35.44	40.58	[141]

A.3 Kinetics

A.3.1 High Pressure Rate Constant Expressions

Up to this point the thermochemistries of the relevant species have been discussed at length, but very little attention has gone toward the kinetics. In general RMG estimates reaction kinetics using best fits of the reacting sites to trees of kinetic values which themselves correspond to specific reaction types.[54] Rate constants experimentally measured, calculated in literature, or calculated by the authors were made available through the input file. These were implemented both as a kinetic library and as training reactions for automatic kinetic estimation within RMG.

Table A.7: Rate expressions determined with transition state theory by the author. Prefactors (A) are provided in units of s^{-1} for unimolecular reactions and $\frac{cm^3}{mol \cdot s}$. Temperatures are provided in K.

Index	Reaction	A	n	Ea ($\frac{kJ}{mol}$)	T_0	T_{min}	T_{max}	Method
1	$CSC + H \rightarrow CSCrad + H_2$	1.53E+03	2.79	16.81	1	250	2500	CBS-QB3
2	$CSC + CH_3 \rightarrow CSCrad + CH_4$	1.16E-04	4.96	19.92	1	250	2500	CBS-QB3
3	$CS(=O)C + H \rightarrow CS(=O)Crad + H_2$	4.97E+02	2.95	28.40	1	250	2500	CBS-QB3
4	$CS(=O)C + OH \rightarrow CS(=O)Crad + H_2O$	1.30E+00	3.18	-17.59	1	250	2500	CBS-QB3
5	$CS(=O)C + CH_3 \rightarrow CS(=O)Crad + CH_4$	1.25E-06	5.04	23.59	1	250	2500	CBS-QB3
6	$DMSO_2 + H \rightarrow DMSO_2rad + H_2$	6.08E+02	2.96	39.28	1	250	2500	CBS-QB3
7	$DMSO_2 + OH \rightarrow DMSO_2rad + H_2O$	2.47E-01	3.68	4.48	1	250	2500	CBS-QB3
8	$DMSO_2 + CH_3 \rightarrow DMSO_2rad + CH_4$	1.13E-06	5.14	29.70	1	250	2500	CBS-QB3
9	$DMS + OOH \rightarrow DMSO + OH$	5.08E-04	4.13	51.58	1	250	2500	CBS-QB3
10	$DMSO + OOH \rightarrow DMSO_2 + OH$	8.03E-01	3.12	36.24	1	250	2500	CBS-QB3
11	$DMSO + H_2O_2 \rightarrow DMSO_2 + H_2O$	2.85E-03	3.85	99.84	1	250	2500	CBS-QB3
12	$DMSO + O_2 \rightarrow DMSO_2 + Otrip$	4.12E-02	3.61	233.99	1	250	2500	CBS-QB3
13	$CS(O)(O[O])C \rightarrow CS(O)([O])(=O)C$	2.09E+12	0.43	180.55	1	250	2500	CBS-QB3

Table A.7: Rate expressions determined with transition state theory by the author. Prefactors (A) are provided in units of s^{-1} for unimolecular reactions and $\frac{cm^3}{mol \cdot s}$. Temperatures are provided in K.

Index	Reaction	A	n	Ea ($\frac{kJ}{mol}$)	T_0	T_{min}	T_{max}	Method
14	$CS(O)(OO)C \rightarrow CS(O)(O)(=O)C$	2.23E+11	0.45	148.89	1	250	2500	CBS-QB3
15	$CSOOrad \rightarrow CS(=O)O$	1.16E+09	1.04	64.05	1	250	2500	CBS-QB3
16	$CSCOOrad + OOH \rightarrow CSCOOH + O_2$	1.54E+00	3.14	-19.36	1	250	2500	CBS-QB3
17	$CS(=O)(O)C + O_2 \rightarrow CS(=O)(=O) + OOH$	6.80E+02	2.54	9.81	1	250	2500	CBS-QB3
18	$CSC(=O)(O)C \rightarrow CS(=O)O + CH_3$	3.87E+02	2.44	25.30	1	250	2500	CBS-QB3
19	$CS(=O)(O)(O)C \rightarrow CS(=O)(=O)C + H_2O$	7.17E+11	0.35	5.07	1	250	2500	CBS-QB3
20	$DMSO_4H \rightarrow DMSO_2 + OOH$	1.43E+12	0.21	46.33	1	250	2500	CBS-QB3
21	$CS(O)(O[O])C \rightarrow DMSSO_2 + OH$	1.37E-32	12.45	63.73	1	250	2500	m06-2x/CBSB7

The transition state calculations were performed with the Arkane (formerly Cantherm) software[54] with the structures, frequencies, and energies of the reactants, transition states, and products calculated in Gaussian using CBS-QB3. The structure of the transition states are included in the list of molecules.

Table A.8: Rate expressions used in model generation that were taken from literature experiments or calculations. Prefactors (A) are provided in units of s^{-1} for unimolecular reactions and $\frac{cm^3}{mol \cdot s}$. Temperatures are provided in K.

Index	Reaction	A	n	Ea ($\frac{kJ}{mol}$)	Source
1	$O_2 + DMSOH \rightarrow DMSO + OOH$	3.01E+12	0	0	[137]
2	$OH + DMS \rightarrow DMSOH$	1.82E+57	-17.2	14.7	[13]
3	$OH + DMS \rightarrow DMSrad + H_2O$	6.80E+12	0	2.11	[13]
4	$OH + DMSO \rightarrow DMSO_2H$	7.23E+12	0	3	[52] Analogy to OH reaction with the S in SO ₂
5	$O_2 + DMSO_2H \rightarrow DMSO_4H$	1.14E+12	0	0	[77] Analogy to O ₂ reaction with the S radical in Csrad
6	$DMSO_2 \rightarrow CS(=O)Orad + CH_3$	2.14E+14	0	253	[23]
7	$CSCOOOrad + CSCOOOrad \rightarrow CSCOrad + CSCOrad + O_2$	3.31E+12	0	0	[13] Analogy to HOOCOOOrad reactions
8	$CSCOOOrad + CSCOOOrad \rightarrow CSCOOH + MTF + O_2$	3.43E+10	0	-6.236	[13] Analogy to HOOCOOOrad reactions
9	$MTF + CH_3 \rightarrow MTFrad + CH_4$	7.95E+10	0	37.66	[131] Analogy to COC=O

Table A.8: Rate expressions used in model generation that were taken from literature experiments or calculations. Prefactors (A) are provided in units of s^{-1} for unimolecular reactions and $\frac{cm^3}{mol \cdot s}$. Temperatures are provided in K.

Index	Reaction	A	n	Ea ($\frac{kJ}{mol}$)	Source
10	$MTF + OH \rightarrow MTFrad + H_2O$	9.69E+10	0	0	[58] analogy to COC=O
11	$CSrad + O_2 \rightarrow CSOOrad$	1.39E+43	-11.3	24.69	[157]
12	$CSrad + O_2 \rightarrow C = S + OOH$	5.25E+24	-4.7	34.73	[157]
13	$CSrad + O_2 \rightarrow CSOrad + Otrip$	5.19E+13	-1.5	70.71	[157]
14	$CSrad + O_2 \rightarrow CH_3 + SO_2$	9.77E+25	-3.8	51.5	[157]
15	$SO_2 + CH_3 \rightarrow CS(=O)[O]$	1.55E+12	0	5.4	[48]
16	$HOOC = O \rightarrow H_2O + CO_2$	2.13E+11	0	118.9	[38]

A.4 Experimental Appendix

A.4.1 Experimental Conditions

Table A.9:

Sample of Typical Experiment Parameters

Total Volume of the Reactor	500 cc
Water Volume	460 cc
Isopropyl Alcohol Volume	10 cc
Iodine Mass Dissolved in Liquid Reactor	0.01 g
Reactive Gas Stream Composition	30 ppm H_2S
	Balance N_2
Reactive Gas Stream Flow Rate	100 cc/min
Total Experimental Time	300 min
Purge Reactor with Pure N_2	60 min
Add I_2 and wait for equilibrium	30 min
Flow H_2S through the reactor	150 min
Purge reactor with pure N_2	60 min

A.4.2 Experimental Index

-4cm

Table A.10: An index of experiments concerning the reaction of H_2S and I_2 .

Date	H_2S Flow Rate (ccm)	Total Flow Rate	H_2S Concen- tration (ppm)	Mixing	H per H ₂ S	I per H ₂ S	Other Notes
10/29/2018	10	100	8980	Stir Bar	5.78		4 Molar KI
10/25/2018	10	100	8980	Stir Bar	5.82		4 Molar KI
10/23/2018	5	200	2245	Stir Bar	2.04		
10/23/2018	5	200	2245	Stir Bar	2.1		
10/22/2018	5	100	4490	Stir Bar	1.93		
10/22/2018	10	200	4490	Stir Bar	1.91		
10/19/2018	10	30	29933	Stir Bar	1.59		
10/18/2018	10	30	29933	Stir Bar	1.6		
6/21/2018	10	10	89800	Rotor	1.81		
6/13/2018	5	5	89800	Stir Bar	1.93		
6/11/2018	5	100	4490	Stir Bar	2.38		
5/15/2018	25	25	89800	Stir Bar	1.42		Very short run (<1 hr of data points)
5/15/2018	15	15	89800	Stir Bar	1.63		Very short run (<1 hr of data points)
5/9/2018	25	25	89800	Rotor	5.64		4 Molar KI
5/8/2018	25	25	89800	Rotor	1.33		
2/16/2018	100	0	30.16	Stir Bar		6.18	1 Molar HCl, pH = 0
2/12/2018	100	0	30.16	Stir Bar		6.54	1 Molar HCl, pH = 0
2/9/2018	100	0	30.16	Stir Bar	6.25		4 Molar KI

2/8/2018	100	0	30.16	Stir Bar	6.56		4 Molar KI
7/20/2017	100	0	30.16	Stir Bar	5.59	4.16	w/I3 corrections the [I-] goes to 5.47
7/13/2017	100	0	30.16	Stir Bar	5.62	4.39	w/I3 corrections the [I-] goes to 5.38
6/22/2017	100	0	30.16	Stir Bar	5.53	4.85	Adds ZnCl to trap any sulfide ion, w/I3 corrections the [I-] goes to 4.94
6/21/2017	100	0	30.16	Stir Bar	6.32	5.3	
6/20/2017	100	0	30.16	Stir Bar	5.73	5.23	Starts at pH = 3.5
6/14/2017	100	0	30.16	Stir Bar	6.94	6.31	Starts at pH = 3.5, strange beginning to the experiment, unexplained drop in pH prior to readings
5/11/2017	100	0	30.16	Stir Bar	6.25	5.46	

A.5 Computational Appendix

A.5.1 Gas Phase Thermochemistries

Table A.11: Computed BP86, CCSD(T), and MRCI geometries of H_2S , I_2 , HSI , HI , H_2O , $HSOH$, $HOSI$, $HOSOH$, $HOS(O)I$ and SO_2 . Experimental numbers are provided wherever available from the NIST molecular database

Molecule	Geometry*
----------	-----------

		BP86	CCSD(T)	MRCI	Experimental
H2S	rSH	1.351	1.339	1.337	1.336
	aHSH	91.78	92.253	92.646	92.11
I2	rII	2.692	2.705	2.716	2.665
HSI	rSH	1.354	1.341	1.339	
	rSI	2.412	2.413	2.416	
	aHSI	95.1	94.693	95.487	
HI	rHI	1.624	1.62	1.615	1.609
H2O	rOH	0.969	0.962	0.962	0.958
	aHOH	104.01	104.179	102.75	104.478
HSOH	rSH	1.362	1.345	1.334	
	rSO	1.688	1.675	1.682	
	rOH	0.973	0.964	0.964	
	aHSO	98.62	98.217	98.603	
	aHOS	106.37	106.91	104.298	
	daHSOH	91.72	91.504	90.796	
HOSI	rOH	0.976	0.967	0.969	
	rOS	1.663	1.653	1.663	
	rSI	2.433	2.421	2.396	

	aHOS	107.54	107.695	106.599	
	aISO	105.76	103.874	103.693	
	daHOSI	274.02	273.853	277.513	
HOSOH	rOH	0.975	0.966	0.964	
	rOS	1.667	1.649	1.649	
	aHOS	107.59	108.043	107.079	
	aOSO	104.335	102.965	103.246	
	daHOSO	84.42	84.328	83.26	
HOS(O)I	rOH	0.981	0.972	0.947	
	rOS	1.642	1.618	1.579	
	rS(O)	1.465	1.455	1.445	
	rSI	2.581	2.54	2.608	
	aHOS	109.85	110.019	113.909	
	aOS(O)	109.04	108.703	108.723	
	aOSI	99.81	98.405	97.801	
	daHOS(O)	321.53	317.101	318.9	
	daHOSI	73.09	67.651	68.3	
SO2	rSO	1.457	1.443	1.435	1.432
	aOSO	118.98	119.26	119.36	119.5

*All the bond lengths (rX) are in Angstrom units. All the bond angles (aX) and dihedral angles (daX) are in degrees

Table A.12: Computed BP86, CCSD(T), Davidson corrected MRCI energies; and T1 diagnostics of H_2S , I_2 , HSI , HI , H_2O , $HSOH$, $HOSI$, $HOSOH$, $HOS(O)I$ and SO_2 .

Molecule	Energy (a.u.)			T1 Diag
	BP86	CCSD(T)	MRCI	
H_2S	-399.457	-398.944	-398.941	0.010084
I_2	-595.739	-589.666	-589.653	0.009206
HSI	-696.721	-693.172	-693.16	0.010747
HI	-298.461	-295.424	-295.417	0.007957
H_2O	-76.471	-76.3423	-76.3392	0.010064
$HSOH$	-474.695	-474.052	-474.04	0.013137
$HOSI$	-771.974	-768.291	-768.211	0.015361
$HOSOH$	-549.962	-549.188	-549.165	0.01579
$HOS(O)I$	-847.251	-843.433	-843.103	0.019347
SO_2	-548.779	-548.006	-547.978	0.021378

Table A.13: Computed and available experimental frequencies of H_2S , I_2 , HSI , HI , H_2O , $HSOH$, $HOSI$, $HOSOH$, $HOS(O)I$ and SO_2 .

Molecule	Frequencies (cm-1)			
	BP86	CCSD(T)	MRCI	Experimental
H ₂ S	1171.18	1211.43	1194.32	1183
	2627.75	2715.71	2710.1	2615
	2641.45	2731.16	2729.31	2626
I ₂	209.32	212.88	207.15	214.5
HSI	353.51	362.49	353.29	
	772.71	804.82	820.93	
	2604.35	2702	2685.29	
HI	2245.26	2311.88	2299.47	2309
H ₂ O	1600.64	1645.65	1701.54	1595
	3702.77	3810.39	3843.12	3657
	3808.18	3919.53	3869.19	3756
HSOH	478.89	478.54	493.65	
	734.31	769.88	770.16	
	980.39	1024.32	1045.15	
	1164.34	1207.61	1277.27	
	2520.31	2650.62	2741.48	
	3674.33	3801.61	3825.63	

HOSI	193.19	201.28	210.02	
	345.15	361.75	371.65	
	488.28	469.45	468.86	
	750.33	783.48	815.32	
	1149.4	1201	1307.22	
	3628.57	3761.25	3872.36	
HOSOH	328.75	350.07	355.07	
	509.08	502.6	521.64	
	530.98	518.03	555.44	
	739.74	793.96	801.3	
	752.19	802.28	810.2	
	1144.55	1197.88	1230.92	
	1144.56	1198.67	1232.46	
	3630.95	3768.36	3792.76	
	3634.66	3771.2	3793.11	
HOS(O)I	158.84	174.79	176.72	
	193.42	207.13	205.91	
	270.09	279.3	306.02	
	377.27	399.7	414.32	
	430.55	459.04	501.56	
	721.3	782.82	898.76	
	1053.4	1113.62	1176.45	
	1193.68	1233.92	1280.71	
	3589.89	3709.58	4074.12	

SO2	492.69	511.75	535.92	517.7
	1111.78	1156.14	1179.43	1151.4
	1305.5	1365.85	1367.08	1361.8

*All experimental values are taken from the NIST database

Table A.14: Energies, geometrical parameters, frequencies and zero point energies (ZPE) of $HSSH$, $HSSI$, $HSSH$, $HSSI$, HS_4H , HS_4I , HS_5H , HS_5I , HS_6H , HS_6I , HS_7H , HS_7I , HS_8H , HS_8I , and S_8 computed at BP86/def2-TZVPD is listed below. The following convention is used for the larger molecules: In $HSSI$, $rS(2)S(3)$ would refer to the distance between the second atom and the third atom(first sulfur and the second sulfur atom).

Species	Energy (a.u.)	Geometry	Frequencies (cm ⁻¹)	ZPE (a.u.)
HSSH	-797.715	$rSH = 1.358$	450.58	0.017733
		$rSS = 2.072$	495.83	
		$aHSS = 98.63$	866.6	
		$daHSSH = 90.7$	868.26	
			2549.68	
			2552.79	
HSSI	-1094.99	$rSH = 1.362$	137.2	0.010731
		$rSS = 2.027$	308.49	
		$rSI = 2.467$	390.23	
		$aHSS = 99.86$	499.42	
		$aISS = 109.12$	863.17	
		$daHSSI = 87.38$	2512.03	
HSSH	-1195.98	$rSH = 1.358$	196.94	0.019535
		$rSS = 2.075$	342.31	

		aHSS = 98.39	352.56	
		aSSS = 109.03	442.08	
		daHSSS = 269.79	471.17	
			829.48	
			844.15	
			2547.19	
			2549.03	
HSSI	-1493.26	rSH = 1.357	61.18	0.012055
		rS(2)S(3) = 2.097	140.3	
		rS(3)S(4) = 2.012	207.71	
		rSI = 2.469	273.36	
		aHSS = 96.36	316.71	
		aSSS = 109.82	429.2	
		aISS = 109.85	481.13	
		daHSSS = 262.21	809.9	
		daISSS = 88.49	2572.13	
HS4H	-1594.25	rSH = 1.357	70.6	0.020981
		rS(2)S(3) = 2.081	168.86	
		rS(3)S(4) = 2.069	204.77	
		rS(4)S(5) = 2.081	323.06	
		aHSH = 97.47	332.48	
		aSSS = 108.78	405.59	
		daHSSS = 93.57	463.73	
		daSSSS = 271.52	465.26	
			814.33	
			842.41	

			2558.91	
			2559.65	
HS4I	-1891.53	rSH = 1.358	27.79	0.013664
		rS(2)S(3) = 2.062	58.23	
		rS(3)S(4) = 2.112	100.93	
		rS(4)S(5) = 2.012	192.41	
		rSI = 2.469	240.93	
		aHSS = 97.66	302.11	
		aS(2)S(3)S(4) = 108.02	338	
		aS(3)S(4)S(5) = 110.02	373.69	
		aS(4)S(5)I = 110.75	469.85	
		daHSSS = 90.99	487.99	
		daSSSS = 288.64	848.87	
		daISSS = 276.82	2557.03	
HS5H	-1992.52	rSH = 1.357	51.06	0.022487
		rS(2)S(3) = 2.077	55.29	
		rS(3)S(4) = 2.08	166.73	
		rS(4)S(5) = 2.08	169.77	
		rS(5)S(6) = 2.077	227.18	
		aHSS = 98.06	315.33	
		aS(2)S(3)S(4) = 109.19	351.92	
		aS(3)S(4)S(5) = 108.79	377.45	
		aS(4)S(5)S(6) = 109.19	443.52	
		daHSSS = 91.54	464.44	
		daS(2)S(3)S(4)S(5) = 264.15	468.56	
		daS(3)S(4)S(5)S(6) = 93.74	827.97	

			831.44	
			2559.16	
			2560.75	
HS5I	-2289.79	rSH = 1.357	26.91	0.015078
		rS(2)S(3) = 2.076	33.02	
		rS(3)S(4) = 2.066	69.26	
		rS(4)S(5) = 2.122	119.21	
		rS(5)S(6) = 2.01	176.49	
		rSI = 2.469	194.32	
		aHSS = 97.75	218.51	
		aS(2)S(3)S(4) = 109.67	305.69	
		aS(3)S(4)S(5) = 107.58	325.07	
		aS(4)S(5)S(6) = 109.42	361.36	
		aISS = 110.9	441.23	
		daHSSS = 275.7	466.14	
		daS(2)S(3)S(4)S(5) = 270.19	492.61	
		daS(3)S(4)S(5)S(6) = 111.65	827.51	
		daISSS = 268.87	2561	
HS6H	-2390.78	rSH = 1.357	27.22	0.023983
		rS(2)S(3) = 2.075	51.37	
		rS(3)S(4) = 2.078	62.31	
		rS(4)S(5) = 2.085	135.96	
		rS(5)S(6) = 2.078	168.11	
		rS(6)S(7) = 2.075	220.59	
		aHSS = 97.87	238.15	
		aS(2)S(3)S(4) = 109.24	329.24	

		aS(3)S(4)S(5) = 109.05	344.74	
		aS(4)S(5)S(6) = 109.05	364.62	
		aS(5)S(6)S(7) = 109.24	421.38	
		daHSSS = 92.43	448.5	
		daS(2)S(3)S(4)S(5) = 274.03	464.71	
		daS(3)S(4)S(5)S(6) = 269.62	467.08	
			831.98	
			833.68	
			2558.68	
			2558.98	
HS6I	-2688.06	rSH = 1.358	18.17	0.016533
		rS(2)S(3) = 2.074	27.99	
		rS(3)S(4) = 2.078	43.29	
		rS(4)S(5) = 2.074	58.28	
		rS(5)S(6) = 2.114	101.46	
		rS(6)S(7) = 2.014	158.14	
		rSI = 2.466	189.25	
		aHSS = 97.78	221.23	
		aS(2)S(3)S(4) = 109.10	252.54	
		aS(3)S(4)S(5) = 108.61	307.42	
		aS(4)S(5)S(6) = 108.59	338.25	
		aS(5)S(6)S(7) = 110.64	350.96	
		aISS = 110.33	405.35	
		daHSSS = 92.74	450.09	
		daS(2)S(3)S(4)S(5) = 265.41	468.69	
		daS(3)S(4)S(5)S(6) = 93.28	478.89	
		daS(4)S(5)S(6)S(7) = 75.36	828.53	

		$\text{daISSS} = 84.61$	2558.56	
HS7H	-2789.05	$\text{rSH} = 1.357$	21.95	0.025421
		$\text{rS}(2)\text{S}(3) = 2.075$	26.92	
		$\text{rS}(3)\text{S}(4) = 2.078$	56.43	
		$\text{rS}(4)\text{S}(5) = 2.083$	64.02	
		$\text{rS}(5)\text{S}(6) = 2.083$	121.2	
		$\text{rS}(6)\text{S}(7) = 2.078$	151.46	
		$\text{rS}(7)\text{S}(8) = 2.075$	205.72	
		$\text{aHSS} = 97.72$	231.66	
		$\text{aS}(2)\text{S}(3)\text{S}(4) = 108.77$	248.48	
		$\text{aS}(3)\text{S}(4)\text{S}(5) = 109.34$	331.59	
		$\text{aS}(4)\text{S}(5)\text{S}(6) = 108.67$	337.63	
		$\text{aS}(5)\text{S}(6)\text{S}(7) = 109.33$	356.32	
		$\text{aS}(6)\text{S}(7)\text{S}(8) = 108.76$	402.3	
		$\text{daHSSS} = 267.70$	441.85	
		$\text{daS}(2)\text{S}(3)\text{S}(4)\text{S}(5) = 86.48$	446.31	
		$\text{daS}(3)\text{S}(4)\text{S}(5)\text{S}(6) = 89.09$	466.26	
		$\text{daS}(4)\text{S}(5)\text{S}(6)\text{S}(7) = 269.38$	467.37	
			830.42	
			833.51	
			2558.05	
			2559.05	
HS7I	-3086.33	$\text{rSH} = 1.358$	19.27	0.018019
		$\text{rS}(2)\text{S}(3) = 2.074$	21.36	
		$\text{rS}(3)\text{S}(4) = 2.076$	28.72	
		$\text{rS}(4)\text{S}(5) = 2.086$	48.31	

		rS(5)S(6) = 2.067	62.77	
		rS(6)S(7) = 2.115	89	
		rS(7)S(8) = 2.012	131.23	
		rSI = 2.466	183.62	
		aHSS = 97.91	214.39	
		aS(2)S(3)S(4) = 109.29	245.97	
		aS(3)S(4)S(5) = 109.43	267.49	
		aS(4)S(5)S(6) = 109.16	306.31	
		aS(5)S(6)S(7) = 108.80	337.04	
		aS(6)S(7)S(8) = 110.70	347.14	
		aISS = 110.31	389.1	
		daHSSS = 84.44	436.06	
		daS(2)S(3)S(4)S(5) = 82.98	443.53	
		daS(3)S(4)S(5)S(6) = 78.44	466.6	
		daS(4)S(5)S(6)S(7) = 80.00	481.19	
		daS(5)S(6)S(7)S(8) = 71.75	829.99	
		daISSS = 84.57	2560.22	
HS8H	-3187.32	rSH = 1.357	17.18	0.02689
		rS(2)S(3) = 2.077	23.03	
		rS(3)S(4) = 2.076	45.28	
		rS(4)S(5) = 2.081	49.56	
		rS(5)S(6) = 2.081	70.56	
		rS(6)S(7) = 2.081	118.13	
		rS(7)S(8) = 2.077	159.52	
		rS(8)S(9) = 2.077	177.64	
		aHSS = 97.69	207.54	
		aS(2)S(3)S(4) = 109.35	240.16	

		aS(3)S(4)S(5) = 109.35	246.36	
		aS(4)S(5)S(6) = 109.03	332.44	
		aS(5)S(6)S(7) = 109.35	333.56	
		aS(6)S(7)S(8) = 109.33	352.31	
		aS(7)S(8)S(9) = 109.33	388.85	
		daHSSS = 274.77	428.47	
		daS(2)S(3)S(4)S(5) = 267.52	446.74	
		daS(3)S(4)S(5)S(6) = 93.85	449.94	
		daS(4)S(5)S(6)S(7) = 93.32	464.75	
		daS(5)S(6)S(7)S(8) = 268.71	467.78	
			831.44	
			833.31	
			2559.14	
			2559.68	
HS8I	-3484.59	rSH = 1.357	12.04	0.019453
		rS(2)S(3) = 2.074	12.99	
		rS(3)S(4) = 2.078	26.62	
		rS(4)S(5) = 2.082	42.04	
		rS(5)S(6) = 2.082	57.1	
		rS(6)S(7) = 2.07	66.01	
		rS(7)S(8) = 2.114	90.72	
		rS(8)S(9) = 2.012	138.29	
		rSI = 2.466	160.68	
		aHSS = 97.91	194.28	
		aS(2)S(3)S(4) = 109.29	221.34	
		aS(3)S(4)S(5) = 109.43	237.93	
		aS(4)S(5)S(6) = 109.16	257.66	

		aS(5)S(6)S(7) = 108.78	301.62	
		aS(6)S(7)S(8) = 110.71	338.72	
		aS(7)S(8)S(9) = 111.03	349.14	
		aISS = 110.65	375.37	
		daHSSS = 275.82	420.3	
		daS(2)S(3)S(4)S(5) = 276.42	444.1	
		daS(3)S(4)S(5)S(6) = 271.29	451.59	
		daS(4)S(5)S(6)S(7) = 95.87	467.2	
		daS(5)S(6)S(7)S(8) = 96.04	481.77	
		daS(6)S(7)S(8)S(9) = 284.41	831.56	
		daISSS = 275.72	2559.58	
S8	-3186.14	rSS = 2.079	71.85	0.011513
		aSSS = 109.19	71.85	
		daSSSS = 262.68	135.12	
			135.12	
			183.15	
			183.15	
			208.44	
			227.69	
			242.87	
			242.87	
			340.9	
			377.32	
			377.32	
			442.31	
			442.31	
			453.55	

			453.55	
			464.31	

Molecule	Rotational Constants (GHz)		
	BP86	CCSD(T)	Experimental[30]
HOSOH	25.93039	25.77582	26.16431
	8.18620	8.52275	8.59053
	6.47596	6.66761	6.71316

Table A.15: Computed and experimental rotational constants (GHz) of *HOSOH*.

Appendix B

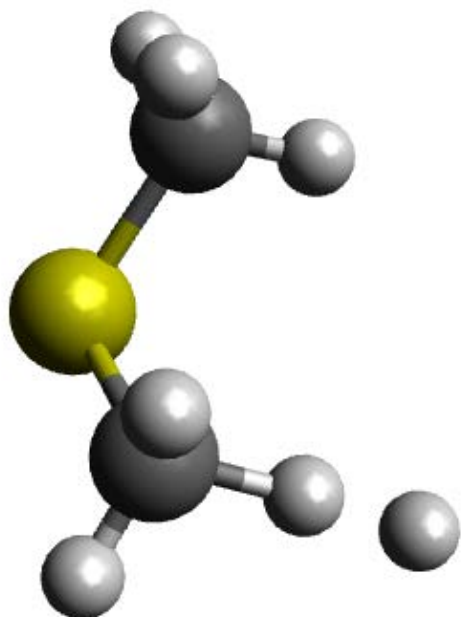
Figures

B.1 Table of Contents

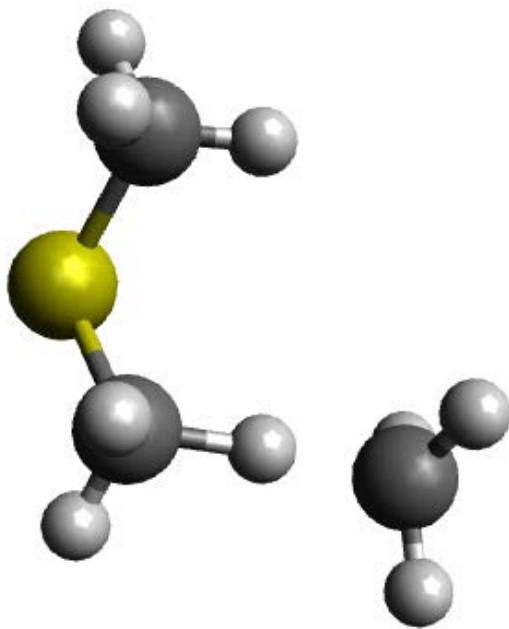
1. Sulfur Species Reaction Mechanism Information
 - 1.1 Transition States
 - 1.2 Additional Sensitivity Plots
2. Experimental Details
 - 2.1 Side Reactions
 - 2.2 I_2 Kinetic Dependence
 - 2.3 Sulfur Product Analysis
3. Computational Figures
 - 3.1 Thermochemistries
 - 3.2 Branching Points

B.1.1 Transition States

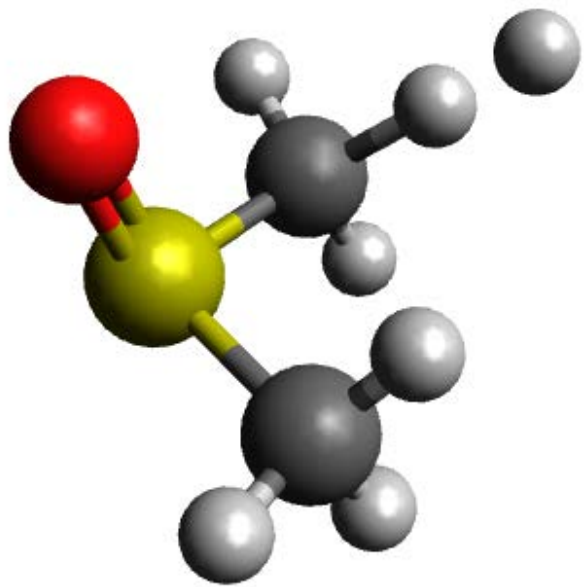
The transition state geometries (coordinates in angstroms) for the 21 calculated reactions are provided below. Each rate was calculated using transition state theory implemented in Arkane (formerly referred to as Cantherm)[54]. CBS-QB3 was generally used, with one exception as noted in table S7.



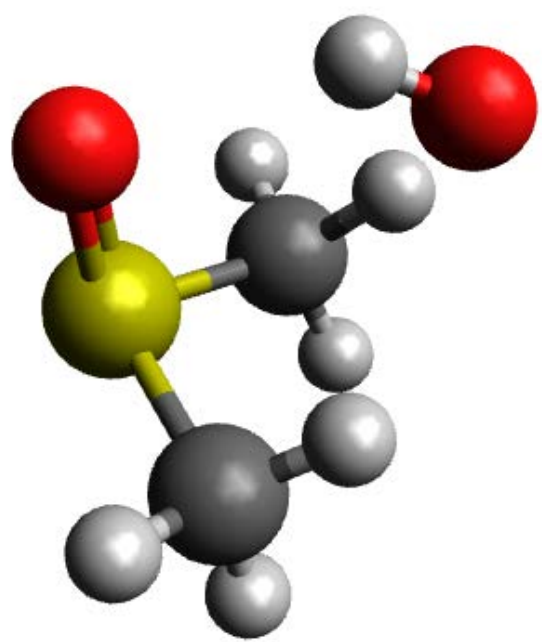
S 0.3087782000 -1.2858945000 0.1336232000
C 1.5737182000 0.0081715000 -0.0662278000
C -1.1541278000 -0.3667865000 -0.2640668000
H 1.5736842000 0.3963275000 -1.0860888000
H 2.5380332000 -0.4571595000 0.1392602000
H 1.4082392000 0.8188145000 0.6446742000
H -2.0167858000 -1.0316945000 -0.2775788000
H -1.0784608000 0.2209665000 -1.1799668000
H -1.4345218000 0.4940155000 0.6410002000
H -1.7185568000 1.2032395000 1.3153712000



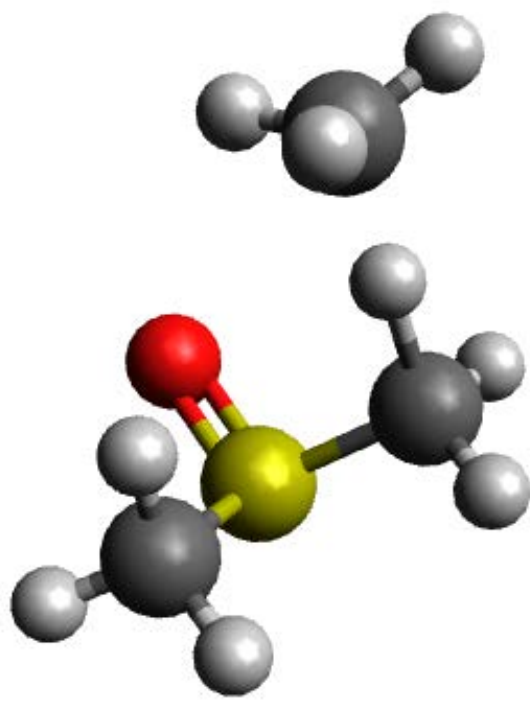
S -1.6058026923 -0.7824020769 -0.5752220769
C -1.9265306923 0.9009189231 0.0400239231
C -0.1481276923 -1.1963950769 0.3600519231
H -2.0952746923 0.8935339231 1.1184029231
H -2.8294046923 1.2544149231 -0.4588740769
H -1.0992316923 1.5685859231 -0.2045030769
H 0.1176033077 -2.2350070769 0.1635749231
H -0.2490806923 -1.0077970769 1.4306139231
H 0.8838193077 -0.5158760769 -0.0177370769
C 2.0723613077 0.1825929231 -0.4060030769
H 2.0627973077 1.1008769231 0.1760699231
H 2.8859393077 -0.4924030769 -0.1525270769
H 1.9309323077 0.3289569231 -1.4738710769



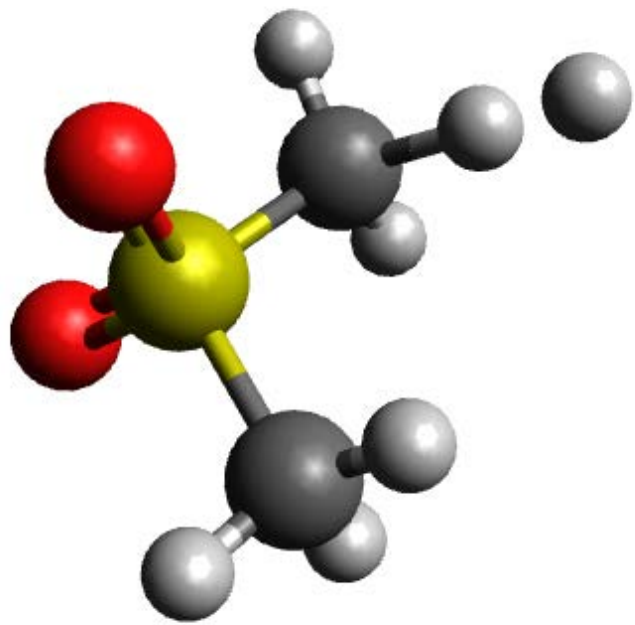
S -0.4766664545 0.8777354545 -0.7235619091
O -0.7780324545 1.9922704545 0.2193480909
C -1.3627774545 -0.6084555455 -0.1278039091
C 1.1845515455 0.2906974545 -0.4176799091
H -1.0515084545 -1.4787335455 -0.7082359091
H -2.4249854545 -0.4168795455 -0.2775579091
H -1.1466704545 -0.7367825455 0.9333750909
H 1.8964585455 1.1078614545 -0.5231649091
H 1.4385045455 -0.5852815455 -1.0156389091
H 1.2915185455 -0.0765275455 0.8776000909
H 1.4296075455 -0.3659045455 1.7633200909



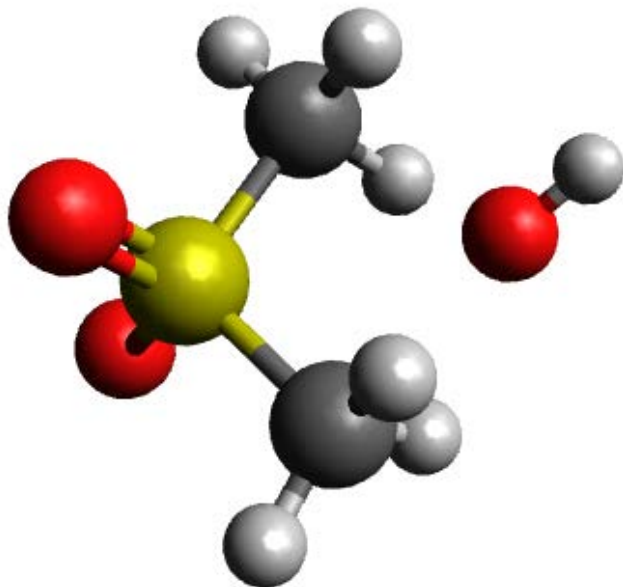
S 0.9521740000 -0.7626724167 -0.2198437500
O 0.3532800000 -1.7358004167 0.7565742500
C 1.1884840000 0.8030635833 0.6852132500
C -0.3998050000 -0.2194404167 -1.2682957500
H 1.5644000000 1.5666845833 0.0018312500
H 1.9218840000 0.6011495833 1.4652372500
H 0.2255280000 1.0800435833 1.1151292500
H -0.7115250000 -1.0347744167 -1.9198157500
H -0.1803500000 0.7005895833 -1.8110557500
H -1.3266350000 -0.0358864167 -0.4574257500
O -2.0269530000 -0.1043824167 0.6190792500
H -1.5604820000 -0.8585744167 1.0333722500



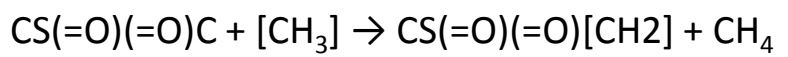
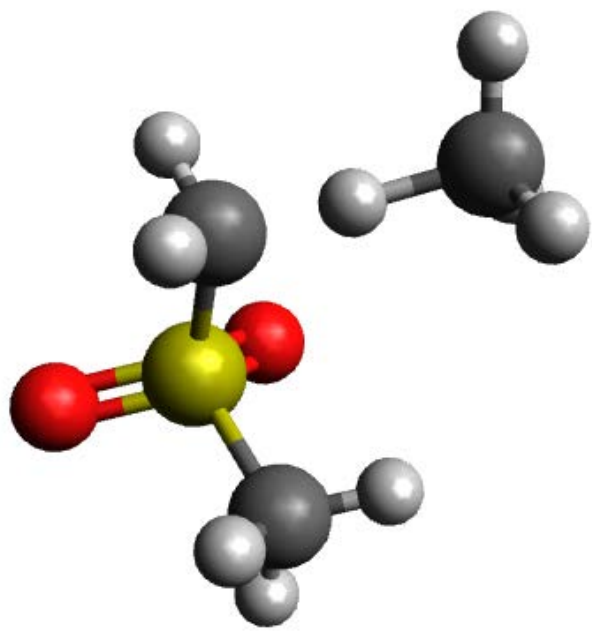
S 1.5570413571 -0.6985326429 -0.2103967857
O 1.2001903571 -1.5848686429 0.9413892143
C 1.6289073571 1.0166113571 0.4252782143
C 0.0887013571 -0.5022056429 -1.2245747857
H 1.7903753571 1.7072503571 -0.4045867857
H 2.4745083571 1.0538483571 1.1118502143
H 0.7042053571 1.2419913571 0.9572952143
H -0.1326396429 -1.4430986429 -1.7270407857
H 0.1594463571 0.3380933571 -1.9162237857
H -0.9337806429 -0.3079086429 -0.3958147857
C -1.9843986429 -0.2131666429 0.4818462143
H -2.1595806429 0.8513293571 0.6197932143
H -2.7998976429 -0.7332036429 -0.0145327857
H -1.5930786429 -0.7261396429 1.3557182143



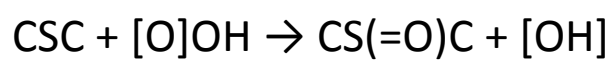
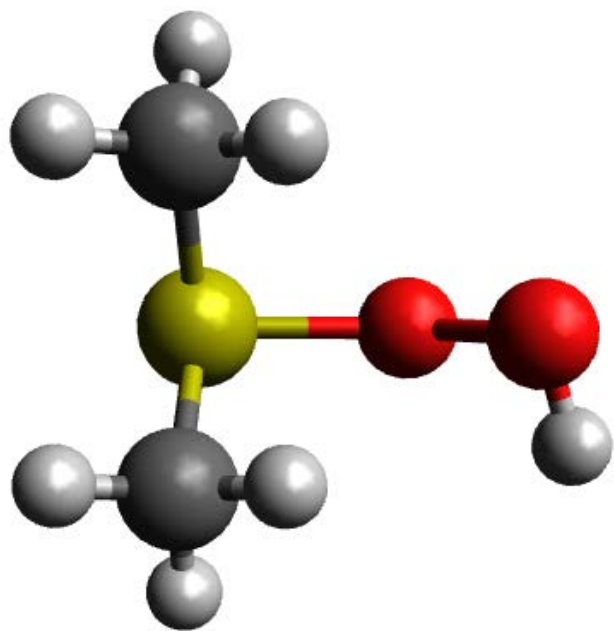
S -0.6487185833 -0.6906674167 -0.2282764167
O -0.6311705833 -0.9024024167 -1.6597354167
O -1.4306615833 -1.5537194167 0.6379175833
C 1.0276224167 -0.7395084167 0.3525305833
C -1.1551265833 1.0021235833 0.0824005833
H 1.1343164167 -0.4948104167 1.4066375833
H 1.7469424167 0.2340735833 -0.3215964167
H 1.5005144167 -1.6700824167 0.0474885833
H -2.1923415833 1.0652695833 -0.2482144167
H -0.5299085833 1.6770565833 -0.5007394167
H -1.0884655833 1.2096615833 1.1498695833
H 2.2669974167 0.8630055833 -0.7182824167



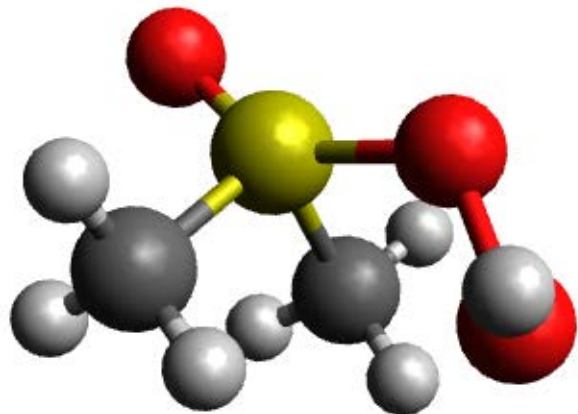
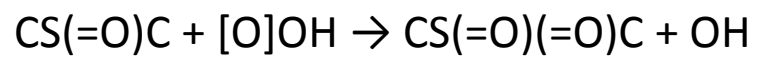
S 1.1359843077 0.2184691538 0.3599087692
O 1.1503393077 0.2963081538 1.8038337692
O 2.3011103077 0.6072981538 -0.4149732308
C 0.6602353077 -1.4450278462 -0.1101082308
C -0.2217986923 1.2194101538 -0.2356032308
H 0.7036703077 -1.5343278462 -1.1950672308
H -0.3427806923 -1.6333148462 0.2708447692
H 1.3880503077 -2.1088198462 0.3569547692
H -0.1307286923 2.2223881538 0.1803217692
H -1.2377246923 0.7151921538 0.2376197692
H -0.2806736923 1.2077261538 -1.3223552308
O -2.3276506923 0.0535611538 0.4544607692
H -2.7980326923 0.1811371538 -0.3858372308



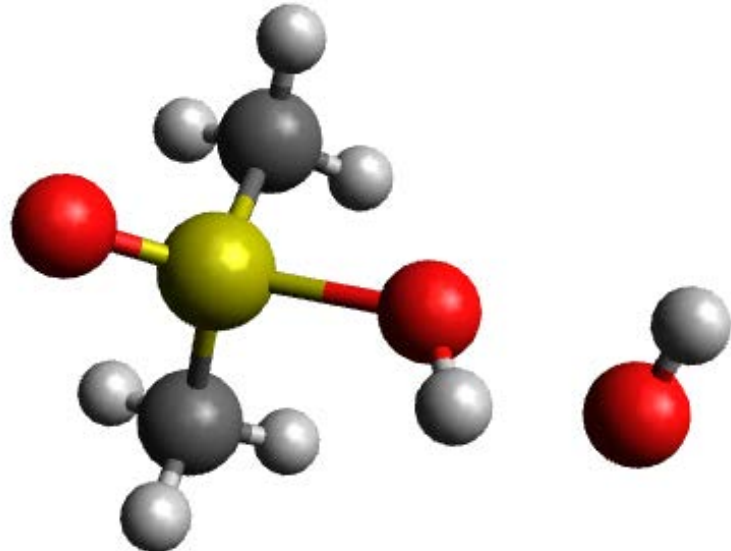
S 1.4232458000 -0.3345781333 -0.3393568000
O 1.1128678000 -0.4162731333 -1.7533088000
O 2.6766668000 -0.8645121333 0.1668132000
C 1.3335528000 1.3921198667 0.1480572000
C 0.0937478000 -1.0922421333 0.5560942000
H 1.4855108000 1.4726538667 1.2238672000
H 0.3730358000 1.8062828667 -0.1556758000
H 2.1447368000 1.8904578667 -0.3835368000
H 0.0473228000 -2.1456121333 0.2851782000
H -1.0712412000 -0.5683561333 0.1246712000
H 0.1613038000 -0.9232811333 1.6291922000
C -2.2659662000 -0.1200011333 -0.3072888000
H -2.9626712000 -0.9209901333 -0.0731278000
H -2.1025522000 0.0284348667 -1.3714738000
H -2.4495602000 0.7958968667 0.2498952000



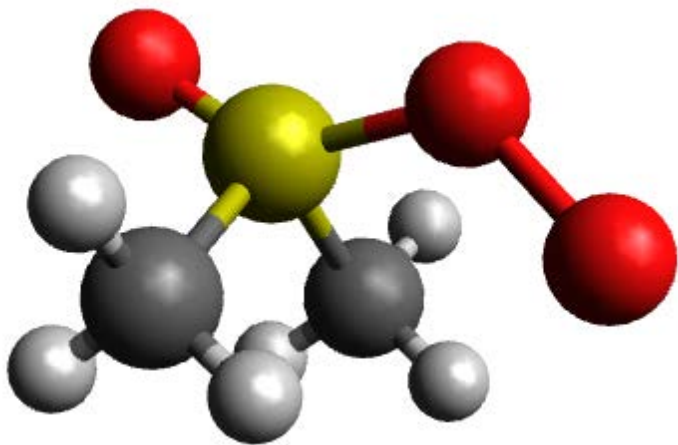
S 0.6490676667 -0.0587620833 -1.0197598333
O -1.2006473333 -0.2917010833 -1.2111968333
C 0.8384996667 -1.3872350833 0.1932891667
C 0.5293926667 1.3697949167 0.0822691667
H 1.7449446667 -1.2385150833 0.7818631667
H 0.9056636667 -2.3180970833 -0.3685258333
H -0.0565493333 -1.3936890833 0.8164501667
H 0.4347626667 2.2539249167 -0.5476248333
H 1.4237916667 1.4482549167 0.7012221667
H -0.3686003333 1.2350439167 0.6887211667
O -2.2634733333 -0.2420090833 0.0489661667
H -2.6368523333 0.6229899167 -0.1656738333



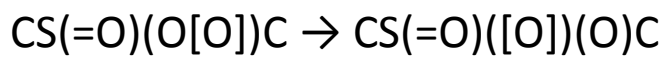
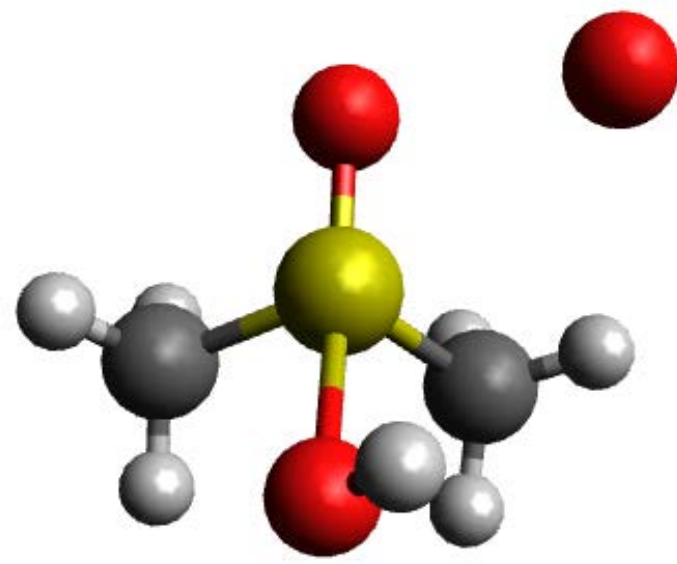
S -0.6537637692 -0.0356629231 -0.7136556923
O 1.0405572308 -0.1932249231 -1.3464336923
C -0.3309107692 1.3543020769 0.3906573077
C -0.5358847692 -1.4547019231 0.3919383077
H -1.1070737692 1.3622640769 1.1551953077
H -0.3996397692 2.2538880769 -0.2205456923
H 0.6660972308 1.2408350769 0.8101723077
H -0.6627007692 -2.3397689231 -0.2303726923
H -1.3402377692 -1.3872829231 1.1242513077
H 0.4513842308 -1.4530109231 0.8500383077
O 2.2869612308 -0.1185209231 -0.3700466923
H 2.6768352308 0.6898440769 -0.7297456923
O -2.0916237692 0.0810400769 -1.1114526923



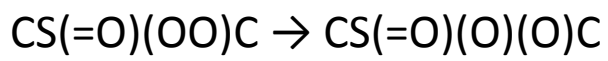
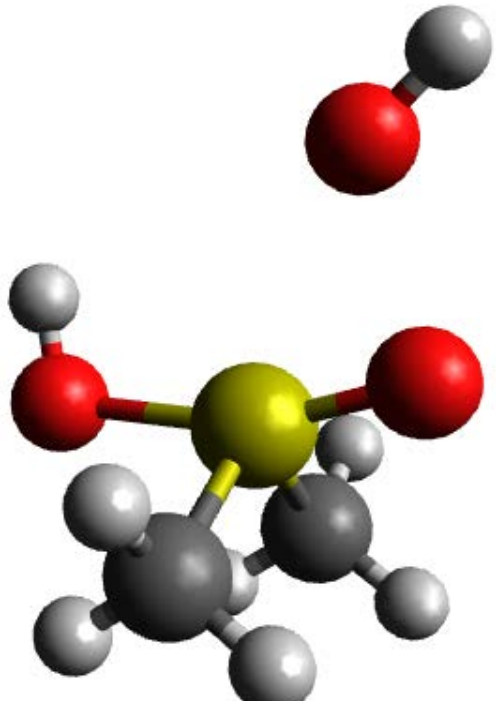
S 0.6810943571 0.0019027143 0.6336326429
O -1.2747206429 -0.1969472857 0.6144426429
C 0.8353603571 1.4222427143 -0.4796123571
C 0.9190903571 -1.3757692857 -0.5082643571
H 1.8388193571 1.4217447143 -0.9069203571
H 0.6912373571 2.3121967143 0.1331476429
H 0.0590603571 1.3557487143 -1.2394693571
H 0.8294843571 -2.2839652857 0.0869466429
H 1.9196973571 -1.2985242857 -0.9342843571
H 0.1386863571 -1.3419122857 -1.2653403571
O -3.2067196429 0.1269317143 0.3923786429
H -3.4494786429 -0.6996182857 0.8290916429
O 1.8108283571 0.0337437143 1.5904216429
H -1.7924396429 0.5222257143 1.0538296429



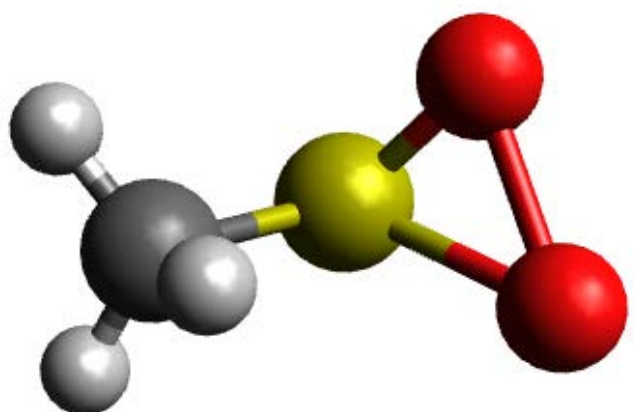
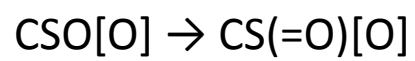
S -0.4048008333 -0.0000940833 -0.7534073333
O 1.2172671667 0.0001589167 -1.3866253333
C -0.2169708333 1.4130279167 0.3467206667
C -0.2161368333 -1.4129880833 0.3468966667
H -1.0387238333 1.3996319167 1.0620136667
H -0.2766998333 2.3012209167 -0.2816513333
H 0.7580531667 1.3471809167 0.8256576667
H -0.2753698333 -2.3012340833 -0.2814413333
H -1.0378288333 -1.4000520833 1.0622726667
H 0.7589001667 -1.3465100833 0.8257226667
O 2.5350851667 0.0001239167 -0.5169163333
O -1.8027748333 -0.0004660833 -1.2492423333



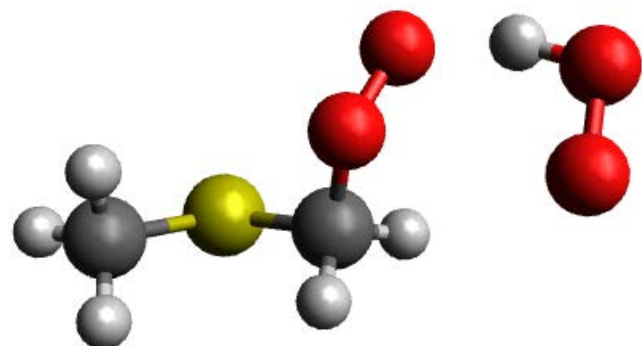
C -1.3339109231 -0.9168923077 -0.4949036923
H -1.2675439231 -1.8229733077 0.1068293077
H -1.5389839231 -1.1691613077 -1.5343366923
H -2.0761619231 -0.2155093077 -0.1233836923
S 0.2936830769 -0.1318073077 -0.4736796923
C 0.4845240769 0.2882116923 1.2780133077
H 1.4511960769 0.7837336923 1.3545783077
H -0.3205509231 0.9549736923 1.5737403077
H 0.4950860769 -0.6431573077 1.8448673077
O -0.6523949231 1.6296716923 -0.8963256923
H 0.0516080769 2.1755376923 -1.2728106923
O 1.2623730769 -1.2686023077 -0.7213356923
O 3.1510760769 0.3359746923 -0.6412526923



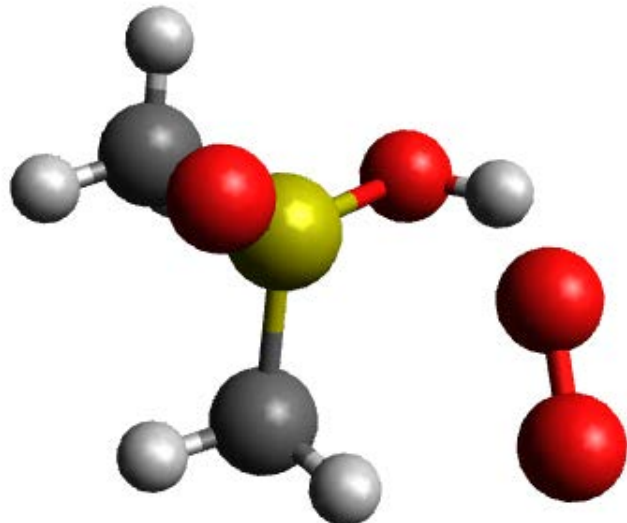
C 0.7313203571 -0.4987743571 1.4439273571
H 0.6979843571 -1.5867123571 1.4663173571
H 0.2204863571 -0.0816533571 2.3106493571
H 1.7426993571 -0.1060573571 1.3840813571
S -0.1769276429 0.0830166429 0.0002063571
C 0.7303973571 -0.5029983571 -1.4424886429
H 0.2194173571 -0.0878663571 -2.3100846429
H 1.7420073571 -0.1106713571 -1.3840726429
H 0.6964793571 -1.5909753571 -1.4621056429
O 0.8588233571 1.7246926429 -0.0015226429
H 0.1808243571 2.4119256429 -0.0064166429
O -1.3744846429 -0.8742223571 0.0018933571
O -2.6560116429 0.6974396429 -0.0003116429
H -3.6130156429 0.5228566429 -0.0000726429



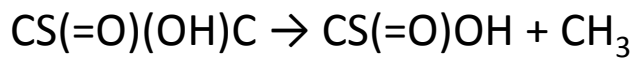
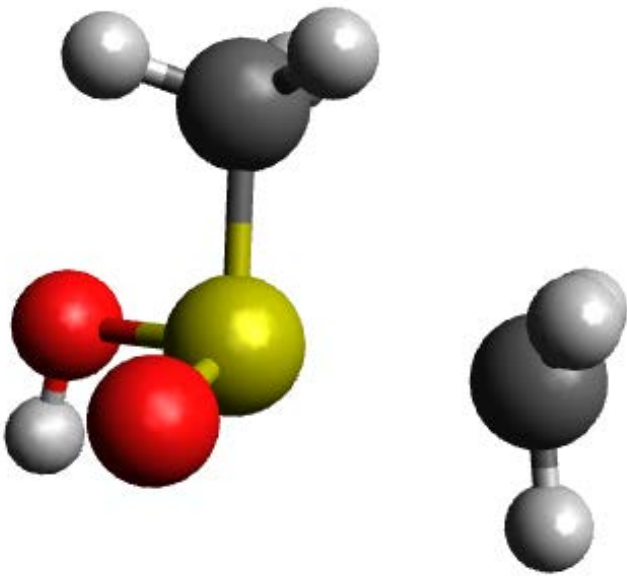
C 0.8377294286 0.1281574286 0.0484228571
H 1.4488824286 0.4861124286 -0.7826691429
H 1.4291574286 -0.5099735714 0.7061488571
H 0.4001004286 0.9638454286 0.5917868571
S -0.5432005714 -0.8136485714 -0.6433401429
O -1.5886805714 -0.8496995714 0.4966378571
O -1.9839885714 0.5952064286 -0.4169871429



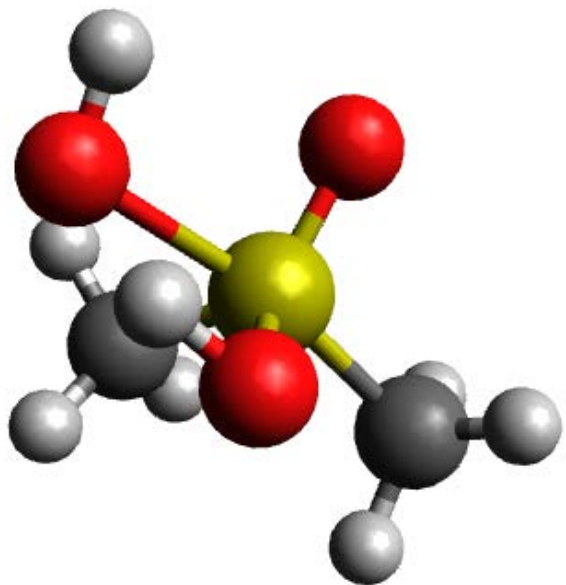
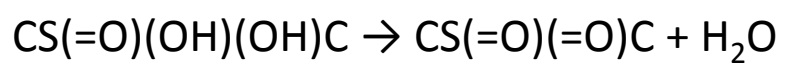
C 0.0445510000 0.2063416154 -0.6813938462
C 2.4939360000 0.2657566154 0.6359541538
S 1.6717500000 -0.5534493846 -0.7721918462
O -0.7591550000 -0.2663203846 0.4426911538
O -1.3475330000 -1.4308953846 0.1777211538
H 0.1065330000 1.2815416154 -0.5161118462
H -0.4937830000 -0.0254433846 -1.5981688462
H 1.9965400000 0.0163646154 1.5722931538
H 3.5130890000 -0.1206803846 0.6607011538
H 2.5264330000 1.3469806154 0.4944721538
H -2.8067920000 -1.0072053846 0.0542401538
O -3.6597230000 -0.4742053846 -0.1491018462
O -3.2858460000 0.7612146154 -0.3211048462



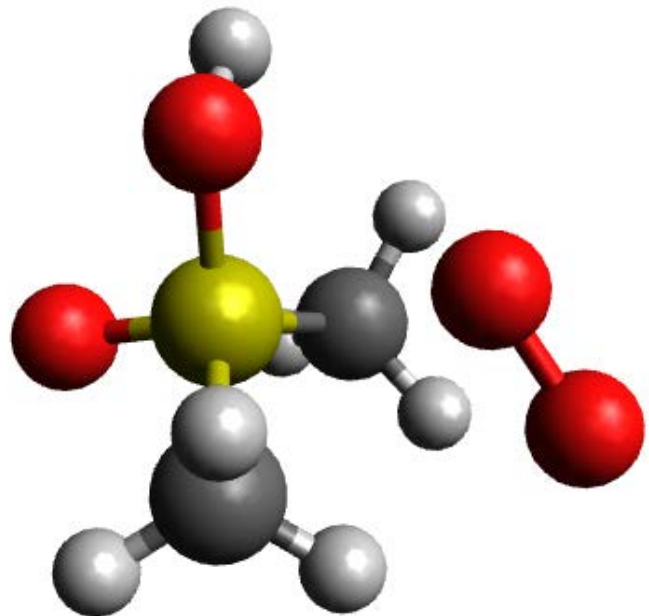
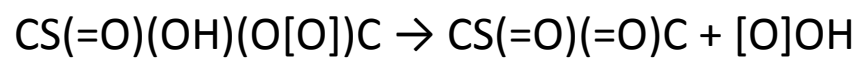
S -0.0640985714 0.0917377857 -0.5334024286
C -1.8521015714 -0.1065422143 -0.3578054286
H -2.2716645714 0.8903687857 -0.2326824286
H -2.2051585714 -0.5492382143 -1.2876084286
H -2.0774295714 -0.7620432143 0.4796825714
C 0.3970284286 0.6933747857 1.1093445714
H 0.1078074286 -0.0566212143 1.8419475714
H 1.4775284286 0.8456357857 1.1120655714
H -0.1202835714 1.6403557857 1.2626675714
O 0.0397574286 1.1851687857 -1.5325944286
O 0.0422214286 -1.7272432143 -0.2969854286
H 0.9695324286 -1.9320922143 -0.4828964286
O 3.1619554286 0.1864997857 -0.1507154286
O 2.3949054286 -0.3993612143 -0.9310174286



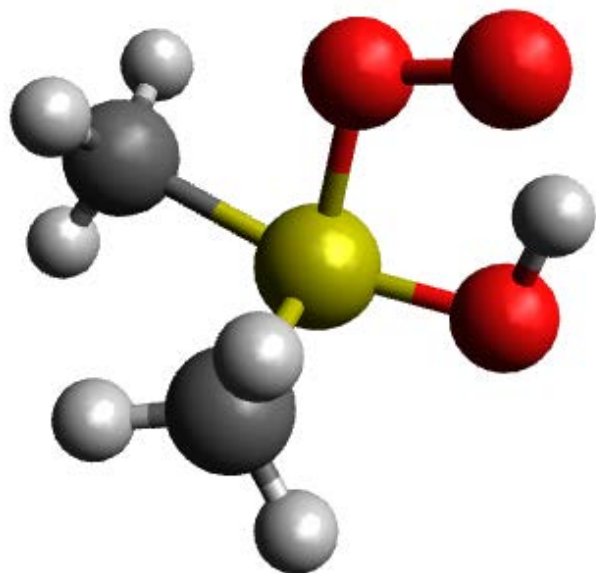
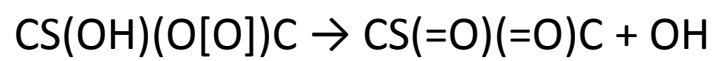
S -0.4608969167 -0.5734176667 -0.0585244167
C 1.8022240833 -0.4072706667 -0.4420734167
H 2.0088330833 -1.4020346667 -0.8193144167
H 1.9082790833 0.3952023333 -1.1652794167
H 2.1784790833 -0.2069186667 0.5555495833
C -0.6136989167 1.1334823333 0.5376585833
H -0.6290479167 1.8067103333 -0.3197004167
H -1.5498359167 1.1904803333 1.0904115833
H 0.2384710833 1.3378963333 1.1826515833
O -0.4404709167 -1.4664796667 1.1121885833
O -2.1389209167 -0.4818846667 -0.6152184167
H -2.3034149167 -1.3257656667 -1.0583494167



C -0.3215909286 1.4080910714 -0.1040475000
H 0.6128240714 1.9383980714 0.0789585000
H -1.1303539286 1.7356630714 0.5389415000
H -0.6232209286 1.4815470714 -1.1469235000
S -0.0562889286 -0.3484239286 0.2504965000
C 1.7372620714 -0.4100929286 -0.0362935000
H 1.9709170714 -0.0438109286 -1.0361245000
H 2.2225950714 0.1906540714 0.7314795000
H 2.0371700714 -1.4517029286 0.0613705000
O -0.3440689286 -1.2920609286 -1.0045785000
H -1.3775829286 -1.2467029286 -0.9030825000
O -0.1405259286 -0.7781949286 1.6406805000
O -2.1380149286 -0.3719119286 0.0654055000
H -2.4491209286 -0.8114519286 0.8637175000



C 0.0179220000 -1.5136590000 -0.7629990000
H -0.7576470000 -1.8903990000 -1.4259850000
H 0.2167930000 -2.1701980000 0.0815730000
H 0.9529590000 -1.2623870000 -1.2651590000
S -0.6339190000 0.0060120000 -0.0588080000
C 0.0614890000 1.6204330000 -0.5217080000
H 0.9561750000 1.4156310000 -1.1110690000
H -0.7269040000 2.1339950000 -1.0660150000
H 0.3575470000 2.1249170000 0.3961030000
O 1.5545640000 -0.0436160000 0.6757440000
O -2.0125660000 0.0982860000 -0.5364150000
O -0.7568540000 -0.2749520000 1.5480000000
H -0.8854460000 0.5640540000 2.0126950000
O 2.4089510000 0.0137270000 -0.3089500000



S -0.3425020000 0.2430460000 0.4663960000
O 1.0551890000 1.0207020000 0.7491210000
C -0.8285350000 1.3042880000 -0.8978400000
C -1.7684830000 -1.0693400000 0.1548600000
H -0.1823250000 1.0158390000 -1.7308630000
H -1.8753890000 1.1483550000 -1.1461350000
H -0.6231130000 2.3321650000 -0.6128710000
H -2.6594320000 -0.5565560000 0.5155700000
H -1.5169970000 -1.9235350000 0.7775910000
H -1.8256970000 -1.3367780000 -0.8977760000
H 1.7617110000 0.3607220000 0.1947480000
O 0.5922430000 -1.0938560000 -0.2401540000
O 1.8504910000 -0.7191770000 -0.5220570000

B.1.2 Additional Sensitivity Plots

The sensitivity plot for the most sensitive rates and kinetics for methylthiol formate is included below.

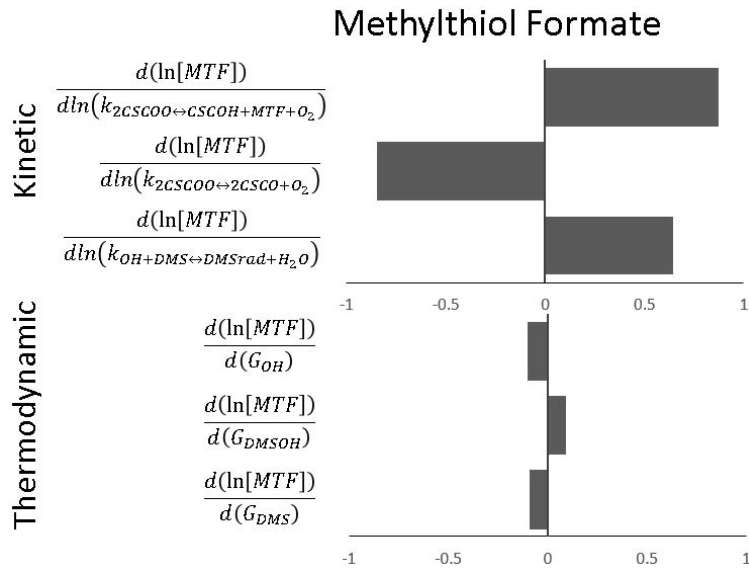
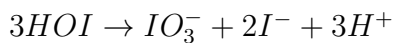
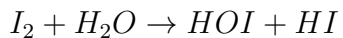


Figure B-1: Top three most sensitive kinetic and thermodynamic parameters for methylthiol formate formation. Thermodynamic sensitivities are reported in units of $\frac{\text{mol}}{\text{kcal}}$.

B.2 Experimental Details

B.2.1 Side reactions

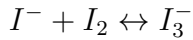
There are several side reactions that must be considered. These side reactions produce and consume iodide ions potentially clouding the true rates of formation of HI from the reaction of H_2S and I_2 . The first reactions to consider are the reactions of I_2 with H_2O . The two important reactions of this type involve the creation and depletion of HOI .



Yoneda studied these reactions in basic aqueous solutions in detail finding that a wide variety of species, including I^- , I_3^- , HOI , and IO_3^- , form upon the introduction of I_2 to aqueous solutions.[148, 100] In general, the HOI formation reaction proceeded quickly in comparison to the slower IO_3^- producing reaction. Yoneda generally worked with much lower I_2 concentrations and at a different pH, but the ratio of I_2 and I^- observed by Yoneda roughly matched the equilibrium observed in several experiments performed here that had I_2 concentrations most similar to the earlier Yoneda work. As I_2 concentration was increased the amount of I^- also was observed to rise but at a lower rate than the increasing I_2 concentration. This was also consistent with Yoneda's observations.

The HI formation resulting from these side reactions can be seen in the quick rise of both proton and iodide concentrations observed after the addition of I_2 to the aqueous reactor. The IO_3^- formation reaction is expected to equilibrate at a concentration at least an order of magnitude lower than the I^- and thus not have a large effect on the observed ion concentrations. Fortunately, this small rise can be isolated from the increases in proton and iodide concentrations observed during H_2S flow.

Another side reaction reduces the amount of dissolved I^- by converting some to I_3^- .



This is more difficult to isolate as I^- is one of the primary products. Qualitatively this is observed as the proton concentrations measured during most experiments were slightly higher than measured iodide ions. During experiments with large excesses of I_2 this discrepancy between I^- and H^+ is more pronounced, as would be expected given this side channel depletion of I^- .

Quantitative description of this behavior is difficult because the exact thermochemistry of I_2 , I^- , and I_3^- in the water/isopropyl alcohol mixture is unknown. However, the equilibrium constant in water is was observed by several sources[148, 113]

with approximations at 25 degrees Celsius ranging from 550 to 720 (M^{-1}). Applied to the experiments performed here, these equilibrium constants predict that a large proportion of the I^- would be converted to I_3^- , up to about 50%. This is inconsistent with our observations which suggested that approximately 10% of the I^- could be equilibrated to I_3^- . However, it is unsurprising that observations in pure water predict greater formation of I_3^- than was observed in the water/isopropyl alcohol mixture used in the experiment as the alcohol is expected to greatly stabilize the I_2 . The degree of I_2 stabilization was estimated based on another work that observed the changing solubility of iodine in water/alcohol mixtures.[101] This work suggested that small amounts of ethanol in water lowered the solvation energy of I_2 by about 0.3 kcal/mol. If we assume that the I_2 is stabilized by this amount than the equilibrium constant falls to about 300-450 (M^{-1}). This is a much closer match to our observations in iodine-rich experiments, although it still over-predicts I_3^- formation. This can be attributed to the fact that isopropyl alcohol would be expected to stabilize I_2 more than ethanol. Demonstration of the estimated effect of I_3^- on the observed I^- concentrations is shown below.

However, eventually when the I_2 is completely consumed by H_2S the discrepancies in ion concentrations that may have been present earlier in the experiment disappear.

Low I_2 experiments should not have significant I_3^- formation, but a discrepancy between iodide and proton concentrations is seen in almost every experiment. The cause of this minor difference in ion concentrations is uncertain.

B.2.2 Kinetic Inference on the Iodine Concentration Dependence

The presence of I_2 inhibits the decomposition of HI [47]. Additionally, the separation of HI from $HI/H_2O/I_2$ mixtures is difficult because of the presence of azeotropes in this mixture. This is compounded because increasing of I_2 concentration lowers the azeotrope HI composition. For these reasons the complete or near-complete consumption of I_2 is important for the viability of the H_2S decomposition scheme.

However due to the multiple reacting phases and aqueous intermediates, it is difficult to predict a priori the kinetic dependence of the formation of HI on I_2 concentration. However, examining the reaction rate as a function of I_2 concentration can give some clue about this dependence.

After experimentation it is clear that the dependence is near zero order. This can be inferred because with constant feed rates of H_2S the rate of HI formation is only marginally affected by the decreasing amount of I_2 dissolved in the reactor. Even as the I_2 is almost completely depleted the $\frac{d[H^+]}{dt}$ has dropped by less than 50% only quickly dropping to zero the moment that the I_2 is completely consumed.

B.2.3 Sulfur Product Analysis

During experiments at high H_2S concentrations a yellow clumped solid was observed to form. This was determined to be elemental sulfur as confirmed by PXRD. The spectra is shown below.

One uncertain aspect of the experimental work was the nature of the products formed during experiments which used the isopropyl alcohol cosolvent. A white solid was observed to form which chromatography suggested was composed of a mixture of species. A chromatogram and spectra for several of the peaks are included to demonstrate the variety and types of observed species.

There are far more peaks but these provide a representative sample. Note that because of the overlap between peaks and the polysiloxane column signal all spectra were processed to remove the background.

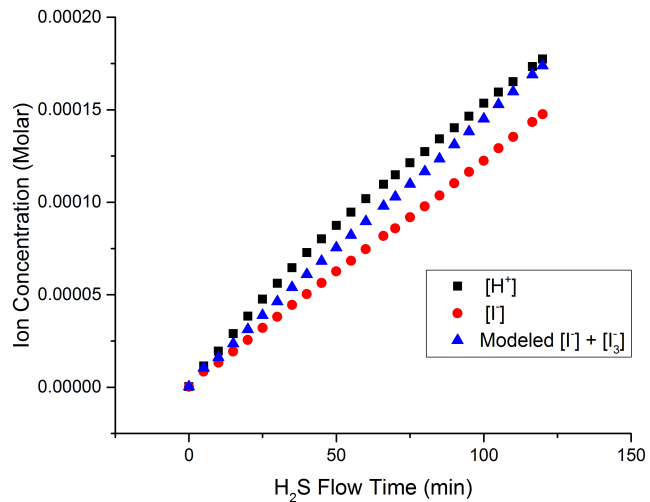


Figure B-2: The discrepancy between I^- and H^+ in excess I_2 experiments can be partially explained by the formation of I_3^- .

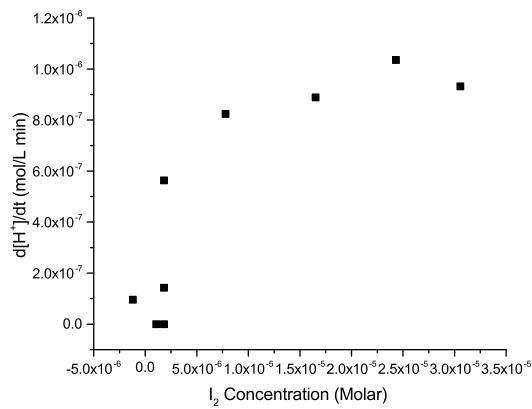


Figure B-3: Reaction rate as a function of I_2 concentration. The reaction rate drops less than a factor of 2 as the concentration of I_2 drops a factor of 20, then falls to near 0 as the I_2 concentration falls near zero.

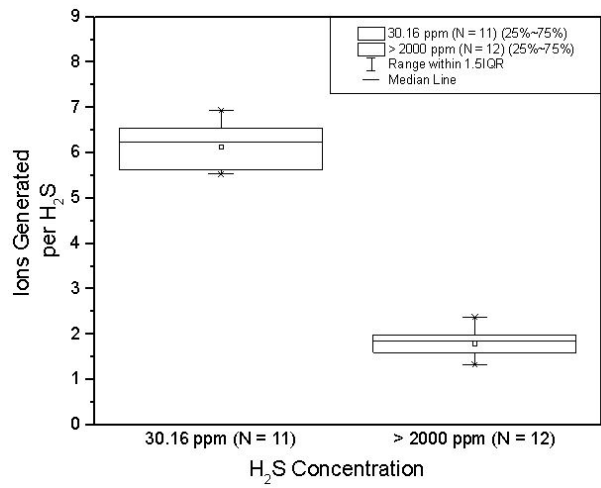


Figure B-4: Comparison between experiments performed at high and low concentrations, using the alcohol cosolvent

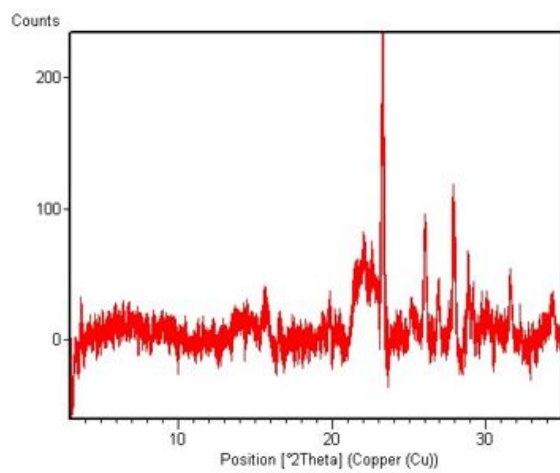


Figure B-5: Sample PXRD spectra, consistent with orthorhombic S_8

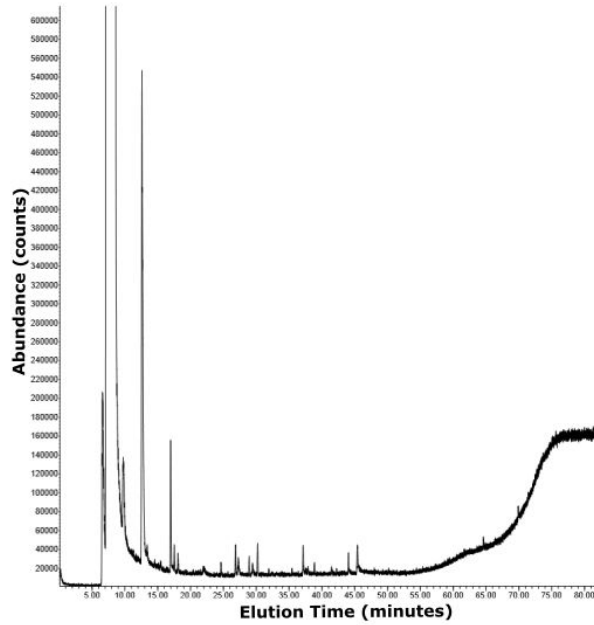


Figure B-6: Chromatogram for a mixture of species formed during the reaction of H_2S and I_2 in isopropyl alcohol

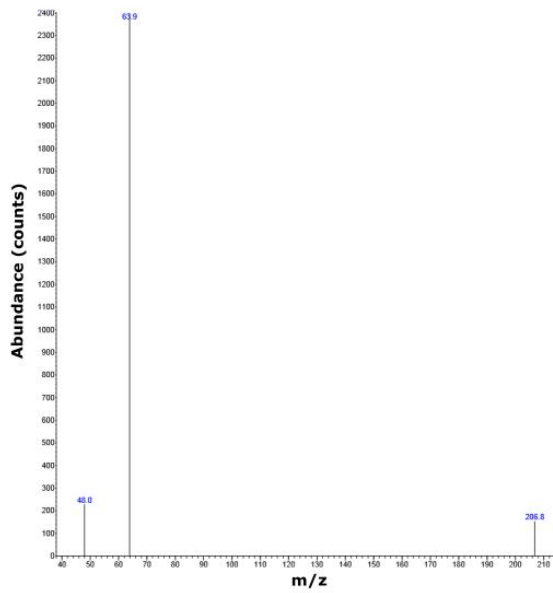


Figure B-7: Mass spectra at 6.7 minutes, identified as SO_2

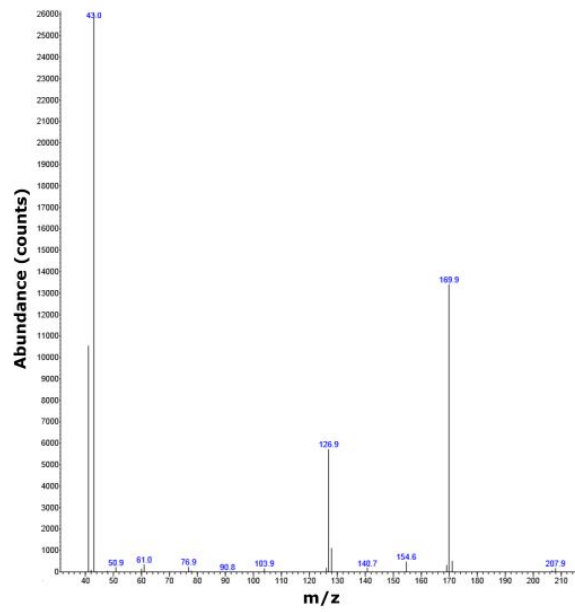


Figure B-8: Mass spectra at 9.8 minutes, hypothesized to be isopropyl iodide

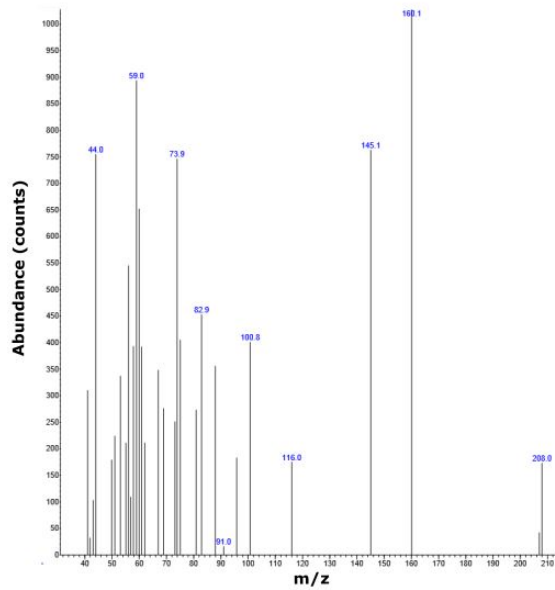


Figure B-9: Mass spectra at 24.7 minutes, hypothesized to have the formula $C_6H_8O_3S$

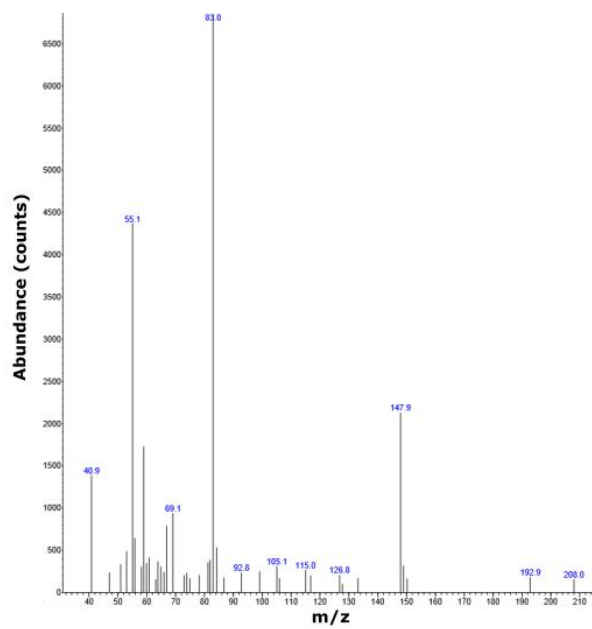


Figure B-10: Mass spectra at 26.9 minutes, hypothesized to have the formula $C_6H_{12}O_2S$

B.3 Computational Details

B.3.1 Thermochemistries

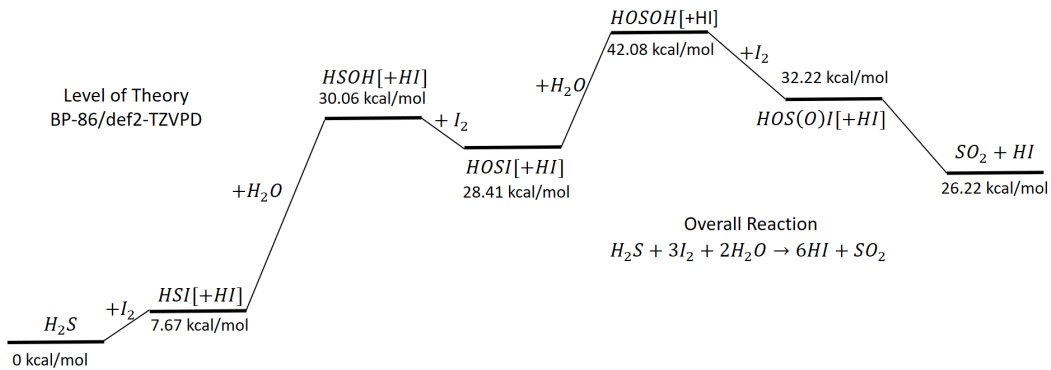


Figure B-11: Free energy change of the overall reaction $H_2S + 3I_2 + 2H_2O \rightarrow 6HI + SO_2$ in gas phase using BP86/def2-TZVPD level of theory. One mole of HI is formed in each intermediate step and is not considered to react in the subsequent step. All the energies are zeroed with respect to H_2S and calculated at 298.15 K.

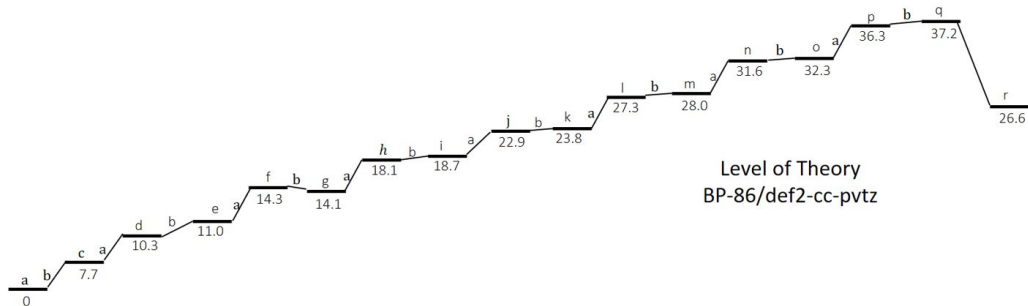


Figure B-12: The alternative pathway in gaseous phase is represented in the above figure. One mole of HI is formed in each intermediate step and is not considered to react in the subsequent step. a. H_2S , b. I_2 , c. HSI , d. $HSSH$, e. $HSSI$, f. $HSSSH$, g. $HSSSI$, h. HS_4H , i. HS_4I , j. HS_5H , k. HS_5I , l. HS_6H , m. HS_6I , n. HS_7H , o. HS_7I , p. HS_8H , q. HS_8I , r. S_8 . All the energies are zeroed with respect to H_2S , calculated at 298.15 K and the units used are kcal/mol. It can be seen that the free energy change for the overall alternative reactive, $:8H_2S + 8I_2 \rightarrow 16HI + S_8$ is 26.6 kcal/mol (or) 3.32 kcal/mol for the reaction, $H_2S + I_2 \rightarrow 2HI + 1/8S_8$.

It must be pointed out that since the T1 diagnostic values are 0.02 (with the exception of SO_2 with a T1 value of 0.021) and below, it is acceptable to use a single reference method like CCSD(T)[84] to get an insight of how the energy changes in

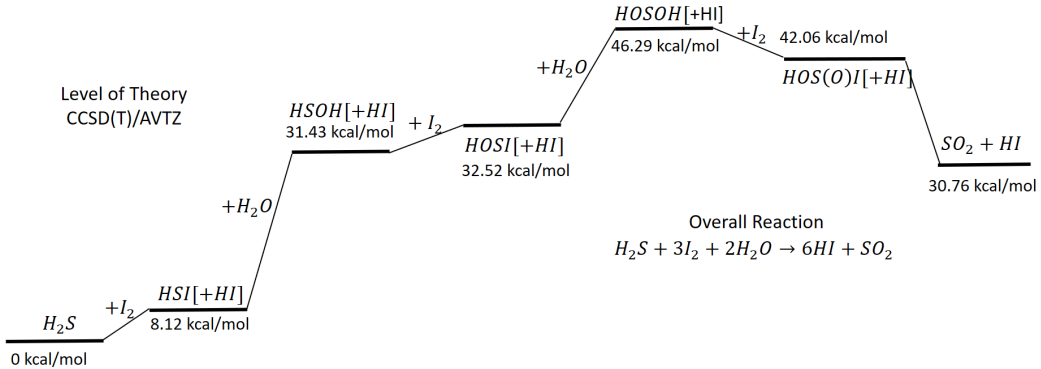


Figure B-13: Free energy change of the overall reaction $H_2S + 3I_2 + 2H_2O \rightarrow 6HI + SO_2$ in gas phase using CCSD(T)/AVTZ level of theory. One mole of HI is formed in each intermediate step and is not considered to react in the subsequent step. All the energies are zeroed with respect to H_2S and calculated at 298.15 K.

the family of reactions. However, if one needs to study each of these species and their corresponding kinetics, it is recommended that a suitable multi-reference[123, 37] method is used as there are a few species that have a higher T1 diagnostic (greater than 0.015). While doing an all-electron multi-reference energy surface is beyond the current computational capabilities, it was possible to identify several compounds where such methods might be needed for future studies. MRCI calculations were performed with default active spaces except for HOSOI where 20 orbitals were closed in the CASSCF calculation, leading to 20 orbitals included in the core of the MRCI calculation. It is worth noting that default active space is not necessarily the best option for each species but it had to be adopted for computational purposes. Davidson corrected energies (important to account for higher order correlations), optimized geometries, frequencies of all the above species have been calculated using MRCI/AVTZ level of theory and reported in the table below. Peterson's pseudopotential basis was employed to describe Iodine containing species.

B.3.2 Branching Points

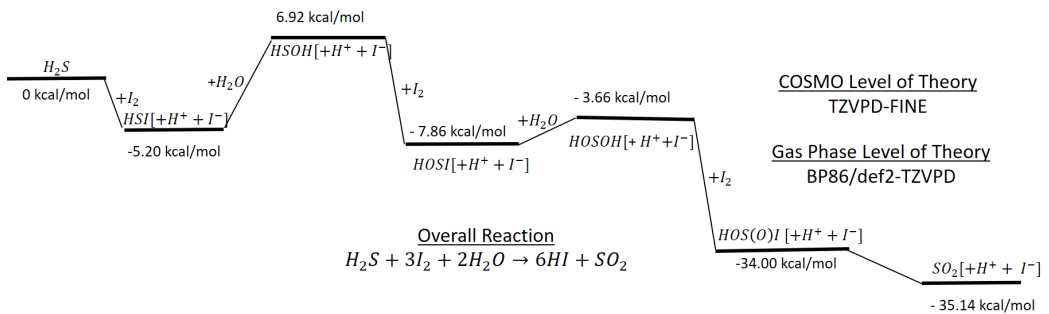


Figure B-14: Free energy change of the overall reaction $H_2S + 3I_2 + 2H_2O \rightarrow 6HI + SO_2$ in gas phase using BP86/def2-TZVPD level of theory. One mole of HI is formed in each intermediate step and is not considered to react in the subsequent step. All the energies are zeroed with respect to H_2S and calculated at 298.15 K.

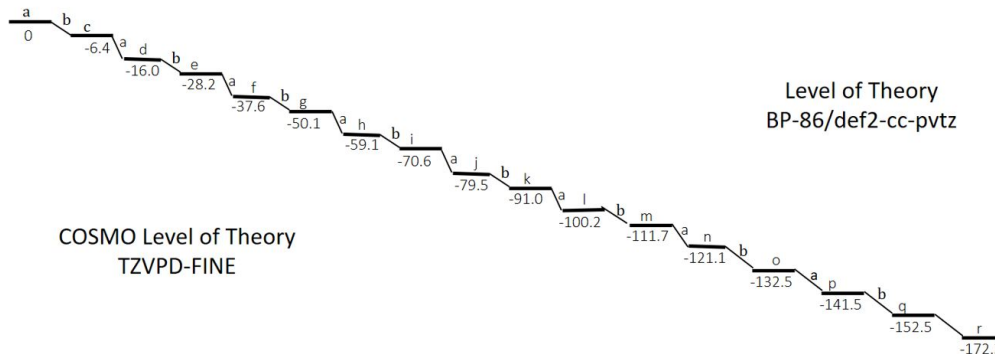


Figure B-15: The alternative pathway in gaseous phase is represented in the above figure. One mole of HI is formed in each intermediate step and is not considered to react in the subsequent step. a. H_2S , b. I_2 , c. HSI , d. $HSSH$, e. $HSSI$, f. $HSSSH$, g. $HSSSI$, h. HS_4H , i. HS_4I , j. HS_5H , k. HS_5I , l. HS_6H , m. HS_6I , n. HS_7H , o. HS_7I , p. HS_8H , q. HS_8I , r. S_8 . All the energies are zeroed with respect to H_2S , calculated at 298.15 K and the units used are kcal/mol. It can be seen that the free energy change for the overall alternative reactive, $:8H_2S + 8I_2 \rightarrow 16HI + S_8$ is -172.3 kcal/mol (or) -21.5 kcal/mol for the reaction, $H_2S + I_2 \rightarrow 2HI + 1/8S_8$

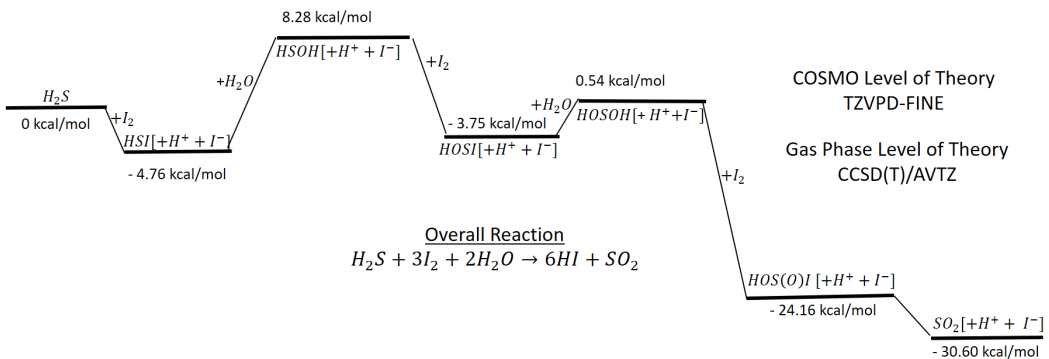


Figure B-16: Free energy change of the overall reaction $H_2S + 3I_2 + 2H_2O \rightarrow 6HI + SO_2$ in gas phase using CCSD(T)/AVTZ level of theory. One mole of HI is formed in each intermediate step and is not considered to react in the subsequent step. All the energies are zeroed with respect to H_2S and calculated at 298.15 K.

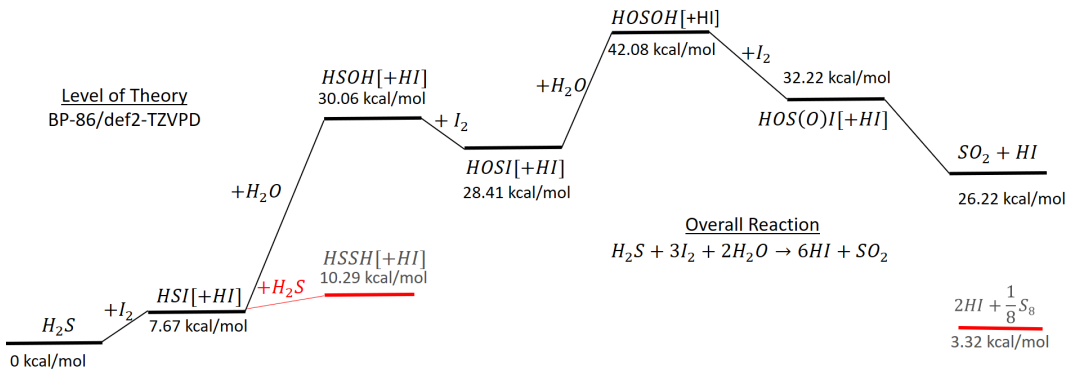


Figure B-17: The first and the last steps of the alternative pathway in gaseous phase is represented in the above figure, after the formation of the first intermediate, HSI using BP86/def2-TZVPD level of theory. One mole of HI is formed in each intermediate step and is not considered to react in the subsequent step. All the energies are zeroed with respect to H_2S and calculated at 298.15 K. A complete energy diagram at this level of theory can be seen in the supporting information.

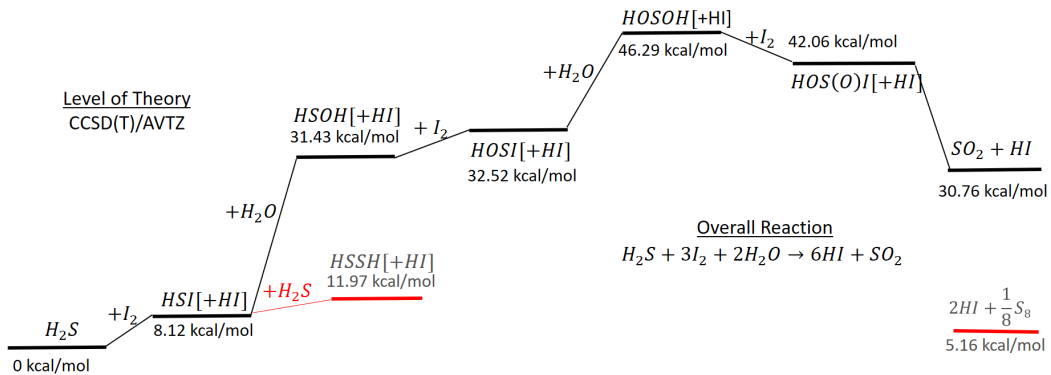


Figure B-18: The first and the last steps of the alternative pathway in gaseous phase is represented in the above figure, after the formation of the first intermediate, HSI using CCSD(T)/AVTZ level of theory. One mole of HI is formed in each intermediate step and is not considered to react in the subsequent step. All the energies are zeroed with respect to H_2S and calculated at 298.15 K.

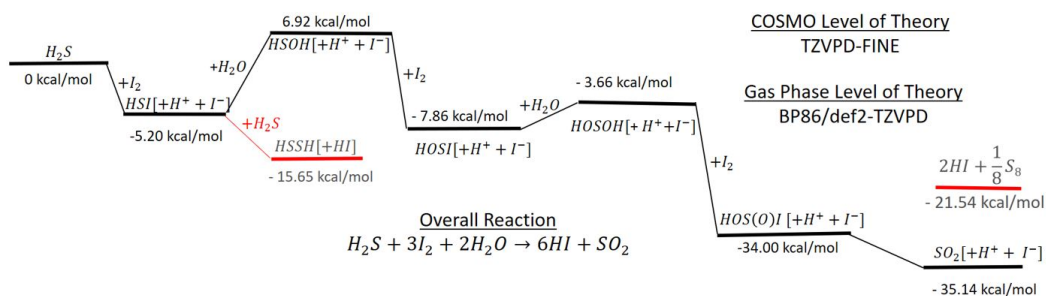


Figure B-19: The first and the last steps of the alternative pathway in aqueous phase is represented in the above figure, after the formation of the first intermediate, HSI using BP86/def2-TZVPD level of theory. One mole of HI is formed in each intermediate step and is not considered to react in the subsequent step. All the energies are zeroed with respect to H_2S and calculated at 298.15 K. A complete energy diagram at this level of theory can be seen in the supporting information.

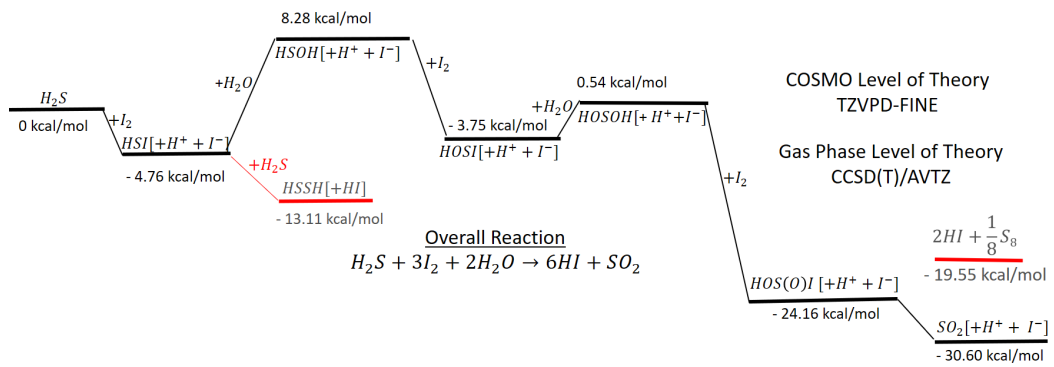


Figure B-20: The first and the last steps of the alternative pathway in aqueous phase is represented in the above figure, after the formation of the first intermediate, HSI using CCSD(T)/AVTZ level of theory. One mole of HI is formed in each intermediate step and is not considered to react in the subsequent step. All the energies are zeroed with respect to H_2S and calculated at 298.15 K.

Bibliography

- [1] China V Gasoline and Diesel Fuel Quality Standards. *ICCT Policy Update*, International Council on Clean Transportation, 2014.
- [2] Sulfur. 2015 minerals yearbook, U.S. Geological Society, U.S. Department of the Interior., January 2017.
- [3] A Breath of Fresh Air: Taking bold action to clean up shipping emissions by reducing sulphur. *International Maritime Organization*, 2020.
- [4] Average Price of Electricity by End Use - March 2020. *Electric Power Monthly*, U.S. Energy Information Administration, 2020.
- [5] Global Petroleum and Other Liquid Fuels Consumption. *Short-Term Energy Outlook*, U.S. Energy Information Administration, 2020.
- [6] R. Ahlrichs, M. Bar, M. Haser, H. Horn, and C. Kolmel. Electronic structure calculations on workstation computers: The program system turbomole. *Chem. Phys. Lett.*, 3(162):165–169, 1989.
- [7] M Albu, Ian Barnes, K H. Becker, Iulia Patroescu-Klotz, Thorsten Benter, and Raluca Mocanu. FT-IR product study on the OH radical initiated oxidation of dimethyl sulfide: Temperature and O_2 partial pressure dependence. In *NATO Security through Science Series C: Environmental Security*, pages 501–513. 01 2008.
- [8] Jr. Alred H. Taylor and R. H. Crist. Rate and equilibrium studies on the thermal reaction of hydrogen and iodine. *Journal of the American Chemical Society*, 63:1377–1385, 1941.
- [9] Frank Eckert Andreas Klamt and Wolfgang Arlt. COSMO-RS: An alternative to simulation for calculating thermodynamic properties of liquid mixtures. *Annual Review of Chemical and Biomolecular Engineering*, 1:101–122, 2010.
- [10] Thorsten Burger Andreas Klamt, Volker Jonas and John C. W. Lohrenz. Refinement and parametrization of COSMO-RS. *J. Phys. Chem. A.*, 26(102):5074–5085, 1998.
- [11] Lori E. Apodaca. Sulfur. *2017 Minerals Yearbook*, U.S. Geologic Survey, 2020.

- [12] Cecilia Arsene, Ian Barnes, and Karl H. Becker. FT-IR product study of the photo-oxidation of dimethyl sulfide: Temperature and O_2 partial pressure dependence. *Phys. Chem. Chem. Phys.*, 1:5463–5470, 1999.
- [13] R. Atkinson, D. L. Baulch, R. A. Cox, R. F. Hampson, J. A. Kerr, M. J. Rossi, and J. Troe. Evaluated kinetic and photochemical data for atmospheric chemistry: Supplement vi. iupac subcommittee on gas kinetic data evaluation for atmospheric chemistry. *Journal of Physical and Chemical Reference Data*, 26(6):1329–1499, 1997.
- [14] J. A. Barnard. The pyrolysis of isopropanol. *Trans. Faraday Soc.*, 56:72–79, 1960.
- [15] Ian Barnes, Jens Hjorth, and Nikos Mihalopoulos. Dimethyl sulfide and dimethyl sulfoxide and their oxidation in the atmosphere. *Chemical Reviews*, 106(3):940–975, 2006.
- [16] A. D. Becke. Density-functional exchange-energy approximation with correct asymptotic behavior. *Phys. Rev. A*, 38:3098–3100, Sep 1988.
- [17] S. W. Benson and Norman Cohen. *Current Status of Group Additivity*, chapter 2, pages 20–46.
- [18] C. Berndhauser and K. Knoche. Experimental investigations of thermal HI decomposition from $H_2O/HI/I_2$ solutions. *Int. J. Hydrogen Energy*, 19(3):239–244, March 1994.
- [19] Torsten Berndt and S Richters. Products of the reaction of OH radicals with dimethyl sulphide in the absence of NO_x : Experiment and simulation. *Atmospheric Environment*, 47:316–322, 02 2012.
- [20] Andre M. Braun, Laurent Jakob, Esther Oliveros, and Claudio A. Oller do Nascimento. *Up-scaling Photochemical Reactions*, chapter 3, pages 235–315. 1993.
- [21] W. F. J. Burgers, P. S. Northrop, H. S. Kheshgi, and J. A. Valencia. Worldwide development potential for sour gas. *Energy Procedia*, 4:2178–2184, January 2011.
- [22] W. K. Busfield, H. Mackle, and P. A. G. O'Hare. Studies in the thermochemistry of sulphones. part 2. the standard heats of formation of sulphones of the type RSO_2CH_3 . *Trans. Faraday Soc.*, 57:1054–1057, 1961.
- [23] W.K. Busfield and K.J. Ivin. The thermochemistry of some sulphones. part 1. the kinetics of decomposition of dimethyl sulphone, benzyl methyl sulphone and allyl methyl sulphone. *Trans. Faraday Soc.*, 57:1044–1053, 1961.
- [24] M.W. Chase. *NIST-JANAF Thermochemical Tables, 4th Edition*. American Institute of Physics, 1998.

- [25] Nilima S. Chaudhari, Bharat B. Kale, et al. Ecofriendly hydrogen production from abundant hydrogen sulfide using solar light-driven hierarchical nanostructured $ZnIn_2S_4$ photocatalyst. *Green Chemistry*, 13:2500–2506, 2011.
- [26] T. Chivers, J.B. Hyne, and C. Lau. THE THERMAL DECOMPOSITION OF HYDROGEN SULFIDE OVER TRANSITION METAL SULFIDES. *Int. J. Hydrogen Energy*, 5:499–506, 1980.
- [27] Caleb A. Class, Jorge Aguilera-Iparraguirre, and William H. Green. A kinetic and thermochemical database for organic sulfur and oxygen compounds. *Phys. Chem. Chem. Phys.*, 17:13625–13639, 2015.
- [28] Caleb A. Class, Mengjie Liu, and William H. Green. Automatic mechanism generation for pyrolysis of di-tert-butyl sulfide. *Physical Chemistry Chemical Physics*, 31:21651–21658, 2016.
- [29] J.D. Cox, D.D. Wagmand, and V.A. Medvedev. *CODATA key values for thermodynamics*. New York: Hemisphere Publishing Corp., 1989.
- [30] Kyle N. Crabtree, Oscar Martinez, Lou Barreau, Sven Thorwirth, and Michael C. McCarthy. Microwave detection of sulfoxylic acid (hosoh). *The Journal of Physical Chemistry A*, 117(17):3608–3613, 2013.
- [31] T. A. Czuppon and L. J. Buividas. *Hydrogen for Ammonia Production and the Economics of Alternate Feedstocks*, chapter 4, pages 47–66.
- [32] Meng Dan, Shiqian Wei, Dmitry E. Doronkin, Yi Li, Ziyan Zhao, Shan Yu, Jan-Dierk Grunwaldt, Yuanhua Lin, and Ying Zhou. Novel mns/(inxcu1-x)2s3 composite for robust solar hydrogen sulphide splitting via the synergy of solid solution and heterojunction. *Applied Catalysis B: Environmental*, 243:790 – 800, 2019.
- [33] James P. Danehy, Brendan T. Doherty, and Catherine P. Egan. Oxidation of organic divalent sulfur by iodine. ii. equilibrating thiol-iodine-disulfide-hydrogen iodide system in acetic acid and evidence for sulfenyl iodide intermediates. *The Journal of Organic Chemistry*, 36(17):2525–2530, 1971.
- [34] James P. Danehy, Catherine P. Egan, and Jurgen Switalski. Oxidation of organic divalent sulfur by iodine. iii. further evidence for sulfenyl iodides as intermediates and for the influence of structure on the occurrence of cyclic intermediates in the oxidation of thiols. *The Journal of Organic Chemistry*, 36(17):2530–2534, 1971.
- [35] James P. Danehy and Michael Y. Oester. The oxidation of organic divalent sulfur by iodine. i. alternative pathways for thiols as determined by structure. *The Journal of Organic Chemistry*, 32(5):1491–1495, 1966.

- [36] Viet Quang Dang and Khalid Al-Ali. The synthesis and investigation of the reversible conversion of layered zrs2 and zrs3. *New J. Chem.*, 44:7583–7590, 2020.
- [37] Richard Dawes, Phalgun Lolur, Jianyi Ma, and Hua Guo. Communication: Highly accurate ozone formation potential and implications for kinetics. *The Journal of Chemical Physics*, 135(8):081102, 2011.
- [38] S.S. Devush, Prisyazhnyuk Z.P., and Koval'skaya A.M. Kinetics of the thermal gas phase decomposition of C1-C4 organic peracids. *Kinet. Catal.*, 24:1098, 1983.
- [39] Ibrahim Dincer and Canan Acar. Review and evaluation of hydrogen production methods for better sustainability. *International Journal of Hydrogen Energy*, 40(34):11094 – 11111, 2015.
- [40] A. J. Downs and C. J. Adams. *The Chemistry of Chlorine, Bromine, Iodine and Astatine*. 1973.
- [41] Hadi Ebrahimi, Akbar Zamaniyan, Alireza B. Sarand, and S. Joda. CO₂ emission in industrial hydrogen plants. *2nd European Process Intensification Conference, 2009*.
- [42] Carl Eckart. The penetration of a potential barrier by electrons. *Phys. Rev.*, 35:1303–1309, Jun 1930.
- [43] Frank Eckert and Andreas Klamt. Fast solvent screening via quantum chemistry: COSMO-RS approach. *AICHE Journal*, 48(2):369–385, 2002.
- [44] JS Edwards and BO Palsson. The escherichia coli mg1655 in silico metabolic genotype: Its definition, characteristics, and capabilities. *Proceedings of the National Academy of Sciences of the United States of America*, 97(10):5528–5533, 2000.
- [45] R.W.J Edwards and M.A. Celia. Infrastructure to enable deployment of carbon capture, utilization, and storage in the united states. *PNAS*, page Supplementary Information, 2018.
- [46] P. Favuzza, C. Felici, M. Lanchi, R. Liberatore, C. V. Mazzocchia, A. Spadoni, P. Tarquini, and A. C. Tito. Decomposition of hydrogen iodide in the *S – I* thermochemical cycle over *Ni* catalyst systems. *Int. J. Hydrogen Energy*, 34(9):4049–4056, 2009.
- [47] P. Favuzza, C. Felici, L. Nardi, P. Tarquini, and A. Tito. Kinetics of hydrogen iodide decomposition over activated carbon catalysts in pellets. *Appl. Catal. B Environ.*, 105:30 – 40, 2011.

- [48] Aaron J. Frank and Frantisek Turecek. Methylsulfonyl and methoxysulfinyl radicals and cations in the gas phase. a variable-time and photoexcitation neutralization-reionization mass spectrometric and ab initio/rrkm study. *The Journal of Physical Chemistry A*, 103(27):5348–5361, 1999.
- [49] M. J. Frisch, G. W. Trucks, H. B. Schlegel, G. E. Scuseria, M. A. Robb, J. R. Cheeseman, J. A. Montgomery, Jr., T. Vreven, K. N. Kudin, J. C. Burant, J. M. Millam, S. S. Iyengar, J. Tomasi, V. Barone, B. Mennucci, M. Cossi, G. Scalmani, N. Rega, G. A. Petersson, H. Nakatsuji, M. Hada, M. Ehara, K. Toyota, R. Fukuda, J. Hasegawa, M. Ishida, T. Nakajima, Y. Honda, O. Kitao, H. Nakai, M. Klene, X. Li, J. E. Knox, H. P. Hratchian, J. B. Cross, V. Bakken, C. Adamo, J. Jaramillo, R. Gomperts, R. E. Stratmann, O. Yazyev, A. J. Austin, R. Cammi, C. Pomelli, J. W. Ochterski, P. Y. Ayala, K. Morokuma, G. A. Voth, P. Salvador, J. J. Dannenberg, V. G. Zakrzewski, S. Dapprich, A. D. Daniels, M. C. Strain, O. Farkas, D. K. Malick, A. D. Rabuck, K. Raghavachari, J. B. Foresman, J. V. Ortiz, Q. Cui, A. G. Baboul, S. Clifford, J. Cioslowski, B. B. Stefanov, G. Liu, A. Liashenko, P. Piskorz, I. Komaromi, R. L. Martin, D. J. Fox, T. Keith, M. A. Al-Laham, C. Y. Peng, A. Nanayakkara, M. Chalacombe, P. M. W. Gill, B. Johnson, W. Chen, M. W. Wong, C. Gonzalez, and J. A. Pople. Gaussian 03. Gaussian, Inc., Wallingford, CT, 2004.
- [50] M. J. Frisch, G. W. Trucks, H. B. Schlegel, G. E. Scuseria, M. A. Robb, J. R. Cheeseman, G. Scalmani, V. Barone, B. Mennucci, G. A. Petersson, H. Nakatsuji, M. Caricato, X. Li, H. P. Hratchian, A. F. Izmaylov, J. Bloino, G. Zheng, J. L. Sonnenberg, M. Hada, M. Ehara, K. Toyota, R. Fukuda, J. Hasegawa, M. Ishida, T. Nakajima, Y. Honda, O. Kitao, H. Nakai, T. Vreven, J. A. Montgomery, Jr., J. E. Peralta, F. Ogliaro, M. Bearpark, J. J. Heyd, E. Brothers, K. N. Kudin, V. N. Staroverov, R. Kobayashi, J. Normand, K. Raghavachari, A. Rendell, J. C. Burant, S. S. Iyengar, J. Tomasi, M. Cossi, N. Rega, J. M. Millam, M. Klene, J. E. Knox, J. B. Cross, V. Bakken, C. Adamo, J. Jaramillo, R. Gomperts, R. E. Stratmann, O. Yazyev, A. J. Austin, R. Cammi, C. Pomelli, J. W. Ochterski, R. L. Martin, K. Morokuma, V. G. Zakrzewski, G. A. Voth, P. Salvador, J. J. Dannenberg, S. Dapprich, A. D. Daniels, Ö. Farkas, J. B. Foresman, J. V. Ortiz, J. Cioslowski, and D. J. Fox. Gaussian 09, 2009. Gaussian Inc. Wallingford CT.
- [51] M. J. Frisch, G. W. Trucks, H. B. Schlegel, G. E. Scuseria, M. A. Robb, J. R. Cheeseman, G. Scalmani, V. Barone, G. A. Petersson, H. Nakatsuji, X. Li, M. Caricato, A. V. Marenich, J. Bloino, B. G. Janesko, R. Gomperts, B. Mennucci, H. P. Hratchian, J. V. Ortiz, A. F. Izmaylov, J. L. Sonnenberg, D. Williams-Young, F. Ding, F. Lipparini, F. Egidi, J. Goings, B. Peng, A. Petrone, T. Henderson, D. Ranasinghe, V. G. Zakrzewski, J. Gao, N. Rega, G. Zheng, W. Liang, M. Hada, M. Ehara, K. Toyota, R. Fukuda, J. Hasegawa, M. Ishida, T. Nakajima, Y. Honda, O. Kitao, H. Nakai, T. Vreven, K. Throssell, J. A. Montgomery, Jr., J. E. Peralta, F. Ogliaro, M. J. Bearpark, J. J. Heyd, E. N. Brothers, K. N. Kudin, V. N. Staroverov, T. A. Keith, R. Kobayashi,

J. Normand, K. Raghavachari, A. P. Rendell, J. C. Burant, S. S. Iyengar, J. Tomasi, M. Cossi, J. M. Millam, M. Klene, C. Adamo, R. Cammi, J. W. Ochterski, R. L. Martin, K. Morokuma, O. Farkas, J. B. Foresman, and D. J. Fox. Gaussian 16, 2016. Gaussian Inc. Wallingford CT.

- [52] Dirk Fulle, Hendrik F. Hamann, and Horst Hippler. The pressure and temperature dependence of the recombination reaction $HO + SO_2 + MHOSO_2 + M$. *Phys. Chem. Chem. Phys.*, 1:2695–2702, 1999.
- [53] Connie W. Gao, Aaron G. Vandeputte, Nathan W. Yee, William H. Green, Robin E. Bonomi, Gregory R. Magoon, Hsi-Wu Wong, Oluwayemisi O. Oluwole, David K. Lewis, Nick M. Vandewiele, and Kevin M. Van Geem. Jp-10 combustion studied with shock tube experiments and modeled with automatic reaction mechanism generation. *Combustion and Flame*, 162(8):3115 – 3129, 2015.
- [54] C.W. Gao, J.W. Allen, W.H. Green, and R.H. West. Automatic construction of chemical kinetic mechanisms. *Computer Physics Communications*, 203:212–225, 2016.
- [55] H.G. Gilbert. *Encyclopedia of Biological Chemistry*. 2 edition, 2013.
- [56] Ryan J. Gillis, Khalid Al-Ali, and William H. Green. Thermochemical production of hydrogen from hydrogen sulfide with iodine thermochemical cycles. *International Journal of Hydrogen Energy*, 43(29):12939–12947, 2018.
- [57] Nuria Gonzalez-Garcia, Angels Gonzalez-Lafont, and Jose M. Lluch. Kinetic study on the reaction of OH radical with dimethyl sulfide in the absence of oxygen. *Chem. Phys. Chem.*, 8(2):255–263, 2007.
- [58] David A. Good, Jaron Hanson, Joseph S. Francisco, Zhuangjie Li, and Gill-Ran Jeong. Kinetics and reaction mechanism of hydroxyl radical reaction with methyl formate. *The Journal of Physical Chemistry A*, 103(50):10893–10898, 1999.
- [59] W.D. Good, J.L. Lacina, and J.P. McCullough. Methanethiol and carbon disulfide: Heats of combustion and formation by rotating-bomb calorimetry. *J. Phys. Chem.*, 65(12):2229–2231, 1961.
- [60] N. O. Guldal, H. E. Figen, and S. Z. Baykara. New catalysts for hydrogen production from H_2S : Preliminary results. *Int. J. Hydrogen Energy*, 40:7452–7458, 2015.
- [61] J.A. Hawari, D. Griller, and Lossing F.P. Thermochemistry of perthiyl radicals. *J. Am. Chem. Soc.*, 108(12):3273–3275, 1986.
- [62] Willian Hermoso and Fernando R. Ornellas. Predicting new molecular species of potential interest to atmospheric chemistry: The isomers {HSI} and {HIS}. *Chemical Physics Letters*, 459(1–6):77 – 81, 2008.

- [63] Ward N. Hubbard and Guy Waddington. The heats of combustion, formation and isomerization of propanethiol-1, propane-thiol-2 and 2-thiabutane. *Recueil des Travaux Chimiques des Pays-Bas*, 73(11):910–923, 1954.
- [64] W.N. Hubbard, W.D. Good, and G. Waddington. The heats of combustion, formation and isomerization of the seven isomeric C₄H₁₀S alkane thiols and sulfides. *J. Phys. Chem.*, 62:614–617, 1958.
- [65] R.J. Hwang and S.W. Benson. Thermochemistry of the reaction of hydrogen sulfide with iodine and the heat of formation of HSI - a new sulfur compound. *J. Am. Chem. Soc.*, 101(10):2615–2617, 1979.
- [66] R. Javadli and A. de Klerk. Desulfurization of heavy oil. *Appl. Petrochemical Res.*, 1(1):3–19, 2012.
- [67] B. B. Kale, J. O. Baeg, K. J. Kong, S. J. Moon, S. M. Lee, and W. W. So. Synthesis and structural analysis of visible light photocatalyst, ZnBiGaO₄ for photocatalytic solar hydrogen production. 34:404–411, 2010.
- [68] D. W. Kalina and E. T. Maas. Indirect hydrogen sulfide conversion - I. an acidic electrochemical process. *Int. J. Hydrogen Energy*, 10(3):157–162, 1985.
- [69] D. W. Kalina and E. T. Maas. Indirect hydrogen sulfide conversion - II. a basic electrochemical process. *Int. J. Hydrogen Energy*, 10(3):163–167, 1985.
- [70] V. E. Kaloidas and N. G. Papayannakos. Hydrogen production from the decomposition of hydrogen sulphide equilibrium studies on the system H₂S/H₂/S_i (i=1-8) in the gas phase. *Int. J. Hydrogen Energy*, 12(6):403–409, 1987.
- [71] Yu Kamiji, Kaoru Onuki, and Shinji Kubo. Corrosion resistance of nickel-based alloy to gaseous hydrogen iodide decomposition environment in thermochemical water-splitting iodine-sulfur process. *International Journal of Chemical Engineering and Applications*, pages 167 – 170, 2018.
- [72] John L. Kice. *Progress in Inorganic Chemistry*. John Wiley & Sons, 1972.
- [73] J. M. Kim, J. E. Park, Y. H. Kim, K. S. Kang, C. H. Kim, C. S. Park, and K. K. Bae. Decomposition of hydrogen iodide on Pt/C-based catalysts for hydrogen production. *Int. J. Hydrogen Energy*, 33(19):4974–4980, 2008.
- [74] H. Kiuchi, K. Funaki, Y. Nakai, and T. Tanaka. THERMOCHEMICAL DECOMPOSITION CYCLE OF H₂S WITH NICKEL SULFIDE. *Int. J. Hydrogen Energy*, 9(8):701–705, 1984.
- [75] A. Klamt and G. Schuurmann. COSMO: a new approach to dielectric screening in solvents with explicit expressions for the screening energy and its gradient. *J. Chem. Soc., Perkin Trans. 2*, pages 799–805, 1993.

- [76] Andreas Klamt. Conductor-like screening model for real solvents: A new approach to the quantitative calculation of solvation phenomena. *J. Phys. Chem.*, 7(99):2224–2235, 1995.
- [77] L.C. Koch, Paul Marshall, and A.R. Ravishankara. An investigation of the reaction of CH₃S with CO. *J. Phys. Chem. A*, 108(24):5205–5212, 2004.
- [78] Arthus L. Kohl and Richard B. Nielsen. *Gas Purification*. 5 edition, 1997.
- [79] V. Krey, O. Masera, G. Blanford, T. Bruckner, R. Cooke, K. Fisher-Vanden, H. Haberl, E. Hertwich, E. Kriegler, D. Mueller, S. Paltsev, L. Price, S. Schlammer, D. Urge-Vorsatz, D. van Vuuren, and T. Zwickel. Contribution of working group iii to the fifth assessment report. *Intergovernmental Panel on Climate Change*, 2014.
- [80] Kenneth Kroenlein, Andrei F. Kazakov Chris D. Muzny, Vladimir Diky, Robert D. Chirico, Joseph W. Magee, Ilmutdin Abdulagatov, and Michael Frenkel. NIST Standard Reference Subscription Database. *Thermodynamic Research Center*, 2012.
- [81] Lawrence Lai, Sarah Khanniche, and William H. Green. Thermochemistry and group additivity values for fused two-ring species and radicals. *The Journal of Physical Chemistry A*, 123(15):3418–3428, 2019.
- [82] Tsan H. Lay, Joseph W. Bozzelli, Anthony M. Dean, and Edward R. Ritter. Hydrogen atom bond increments for calculation of thermodynamic properties of hydrocarbon radical species. *The Journal of Physical Chemistry*, 99(39):14514–14527, 1995.
- [83] Samuel H. Lebowitz. A demonstration working model of the frasch process for mining sulfur. *Journal of the American Chemical Society*, pages 1630 – 1633, 1931.
- [84] Timothy J. Lee, Martin Head-Gordon, and Alistair P. Rendell. Investigation of a diagnostic for perturbation theory. comparison to the t1 diagnostic of coupled-cluster theory. *Chemical Physics Letters*, 243(5):402 – 408, 1995.
- [85] Ji Li, Armin Moniri, and Hui Wang. Apparent kinetics of a gas-liquid-liquid system of bunsen reaction with iodine-toluene solution for hydrogen production through H₂S splitting cycle. *Int. J. Hydrogen Energy*, 40:2912–2920, 2015.
- [86] Yi-Pei Li, Kehang Han, Colin A. Grambow, and William H. Green. Self-evolving machine: A continuously improving model for molecular thermochemistry. *The Journal of Physical Chemistry A*, 123(10):2142–2152, 2019.
- [87] C. A. Linkous, T. E. Mingo, and N. Z. Muradov. Aspects of solar hydrogen production from hydrogen sulfide using semiconductor particulates. *Int. J. Hydrot. Energy*, 19(3):203–208, 1994.

- [88] C. A. Linkous, T. E. Mingo, and N. Z. Muradov. Aspects of solar hydrogen production from hydrogen sulfide using semiconductor particulates. *Int. J. Hydrogen Energy*, 19:203 – 208, 1994.
- [89] Alan E. Long, Raymond L. Speth, and William H. Green. Ember: An open-source, transient solver for 1d reacting flow using large kinetic models, applied to strained extinction. *Combustion and Flame*, 195:105–116, 2018.
- [90] H. Mackle, D. V. McNally, and W. V. Steele. Studies in the thermochemistry of sulphones. part 10. heats of combustion and formation of several $\alpha\beta$ -unsaturated sulphones. *Trans. Faraday Soc.*, 65:2060–2068, 1969.
- [91] H. Mackle and P. A. G. O'Hare. Studies in the thermochemistry of sulphones. part 6. heats of combustion, fusion, vaporization and atomization of six aromatic and two allylic sulphones. *Trans. Faraday Soc.*, 57:1521–1526, 1961.
- [92] H. Mackle and P. A. G. O'Hare. Studies in the thermochemistry of sulphoxides. part 1. the gas-phase heats of formation of diethyl, di-n-propyl, t-butyl ethyl, allyl ethyl and diphenyl sulphoxides. *Trans. Faraday Soc.*, 57:2119–2124, 1961.
- [93] H. Mackle and W. V. Steele. Studies in the thermochemistry of organic sulphites and sulphates. part 1. heats of combustion and formation of some dialkyl sulphites and sulphates. *Trans. Faraday Soc.*, 65:2053–2059, 1969.
- [94] E. Magnusson. Hypercoordinate molecules of second-row elements: d functions or d orbitals? *J. Am. Chem. Soc.*, 112:7940 – 7951, 1990.
- [95] Iamir E. Maloka, S.M. Aliwi, and S.A. Naman. Thermal decomposition of hydrogen sulphide by cadmium chalcogens. *Petroleum Science and Technology*, 24(1):103–112, 2006.
- [96] Nick M. Marinov. A detailed chemical kinetic model for high temperature ethanol oxidation. *International Journal of Chemical Kinetics*, 31(3):183–220, 1999.
- [97] Naomi Masuda, Yatsuhisa Nagano, and Minoru Sakiyama. Standard molar enthalpy of formation of $(CH_3)_2SO$, dimethylsulfoxide, by combustion calorimetry. *The Journal of Chemical Thermodynamics*, 26(9):971 – 975, 1994.
- [98] J.P. McCullough, W.N. Hubbard, F.R. Frow, I.A. Hossenlopp, and G. Waddington. Ethanethiol and 2-thiapropane: Heats of formation and isomerization; the chemical thermodynamic properties from 0 to 1000 deg k. *J. Am. Chem. Soc.*, 79:561–566, 1957.
- [99] A. Mehra and M. M. Sharma. Absorption of hydrogen sulfide in aqueous solutions of iodides containing dissolved iodine: Enhancements in rates due to precipitated sulfur. *Chem. Eng. Sci.*, 43(5):1071–1081, 1988.

- [100] Fukuzo Tohdo Motonari Adachi, Wataru Eguchi and Minoru Yoneda. Reactions of iodine in aqueous solutions containing sodium hydroxide. *Journal of Chemical Engineering of Japan*, 7(5):360–363, 1974.
- [101] Koichiro Nakanishi and Soto Asakura. Solubility of iodine in mixed solvents. a case study of preferential solvation in nonpolar and associated solutions. *J. Phys. Chem.*, 18(81):1745–1750, 1977.
- [102] NIST Thermodynamics Research Center. NIST/TRC Table Database. *CD-ROM*, 2004.
- [103] William D. Nordhaus. Revisiting the social cost of carbon. *Proceedings of the National Academy of Sciences*, 114(7):1518–1523, 2017.
- [104] K. Onuki, S. Kubo, A. Terada, N. Sakaba, and R. Hino. Thermochemical water-splitting cycle using iodine and sulfur. *Energy Environ. Sci.*, 2(5):491, 2009.
- [105] Y. Oosawa, R. Takahashi, M. Yonemura, and T. Sekine. Proposal of a new H_2S decomposition process using solar energy. *Sol. Energy*, 39(5):429–431, 1987.
- [106] Clive Oppenheimer. Sulphur eruptions at volcán poás, costa rica. *Journal of Volcanology and Geothermal Research*, 49(1):1 – 21, 1992.
- [107] Paschalis D. Paraskevas, Maarten K. Sabbe, Marie-Françoise Reyniers, Nikos Papayannakos, and Guy B. Marin. Group additive values for the gas-phase standard enthalpy of formation, entropy and heat capacity of oxygenates. *Chemistry – A European Journal*, 19(48):16431–16452, 2013.
- [108] Laura A. Pellegrini, Giorgio Soave, Simone Gamba, and Stefano Lange. Economic analysis of a combined energy - methanol production plant. *Applied Energy*, 88(12):4891 – 4897, 2011.
- [109] John P. Perdew. Density-functional approximation for the correlation energy of the inhomogeneous electron gas. *Phys. Rev. B*, 33:8822–8824, Jun 1986.
- [110] Kirk A. Peterson. Systematically convergent basis sets with relativistic pseudopotentials. i. correlation consistent basis sets for the post-d group 13-15 elements. *The Journal of Chemical Physics*, 119(21):11099–11112, 2003.
- [111] Kirk A. Peterson, Detlev Figgen, Erich Goll, Hermann Stoll, and Michael Dolg. Systematically convergent basis sets with relativistic pseudopotentials. ii. small-core pseudopotentials and correlation consistent basis sets for the post-d group 16-18 elements. *The Journal of Chemical Physics*, 119(21):11113–11123, 2003.
- [112] Gautam Rajpal and Peter Arvan. *Handbook of Biologically Active Peptides*. 2 edition, 2013.

- [113] R.W. Ramette and Jr. R.W. Sandford. Thermodynamics of iodine solubility and triiodide ion formation in water and in deuterium oxide. *Journal of the American Chemical Society*, 22(87):5001–5005, 1965.
- [114] Stephen A. Ramsey, Jennifer J. Smith, David Orrell, Marcello Marelli, Timothy W. Petersen, Pedro de Atauri, Hamid Bolouri, and John D. Aitchison. Dual feedback loops in the GAL regulon suppress cellular heterogeneity in yeast. *Nature Genetics*, 38(9):1082–1087, SEP 2006.
- [115] A.P. Reverberi, Jiri Klemes, Petar Varbanov, and B Fabiano. A review on hydrogen production from hydrogen sulfide by chemical and photochemical methods. *Journal of Cleaner Production*, 136:72–80, May 2016.
- [116] BRIAN K. RICHARDS, FREDERICK G. HERNDON, WILLIAM J. JEWELL, ROBERT J. CUMMINGS, and THOMAS E. WHITE. In situ methane enrichment in methanogenic energy crop digesters. *Biomass and Bioenergy*, 6:275 – 282, 1994.
- [117] H Richter and JB Howard. Formation of polycyclic aromatic hydrocarbons and their growth to soot - a review of chemical reaction pathways. *Progress in Energy and Combustion Science*, 26(4-6):565–608, 2000. 1st Mediterranean Combustion Symposium (MCS-99), Antalya, Turkey, JUN 20-25, 1999.
- [118] Matthias Rupp, Alexandre Tkatchenko, Klaus-Robert Mueller, and O. Anatole von Lilienfeld. Fast and Accurate Modeling of Molecular Atomization Energies with Machine Learning. *Physical Review Letters*, 108(5):058301, JAN 31 2012.
- [119] Ramakanta Sahu, Byung Jin Song, Ji Sun Im, Young-Pyo Jeon, and Chul Wee Lee. A review of recent advances in catalytic hydrocracking of heavy residues. *Journal of Industrial and Engineering Chemistry*, 27:12 – 24, 2015.
- [120] S. Satyapal. Hydrogen and fuel cells progress overview. Technical report, U.S. Department of Energy, May 2017.
- [121] Sandeep Sharma, Sumathy Raman, and William H. Green. Intramolecular hydrogen migration in alkylperoxy and hydroperoxyalkylperoxy radicals: Accurate treatment of hindered rotors. *J. Phys. Chem. A*, 114:5689–5701, 2010.
- [122] Y. Shindo, N. Ito, K. Haraya, T. Hakuta, and H. Yoshitome. Kinetics of the catalytic decomposition of hydrogen iodide in the thermochemical hydrogen production. *International Journal of Hydrogen Energy*, 9(8):695 – 700, 1984.
- [123] Rüdiger Siebert, Reinhard Schinke, and Martina Bittererová. Spectroscopy of ozone at the dissociation threshold: Quantum calculations of bound and resonance states on a new global potential energy surface. *Phys. Chem. Chem. Phys.*, 3:1795–1798, 2001.
- [124] JM Simmie. Detailed chemical kinetic models for the combustion of hydrocarbon fuels. *Progress in Energy and Combustion Science*, 29(6):599–634, 2003.

- [125] William H. Smith. *Encyclopedia of Biodiversity*. 2001.
- [126] R. Soltani, M.A. Rosen, and I. Dincer. Assessment of CO₂ capture options from various points in steam methane reforming for hydrogen production. *International Journal of Hydrogen Energy*, 39(35):20266 – 20275, 2014.
- [127] James G. Speight. *Natural Gas*. 2 edition, 2019.
- [128] W. M. Stewart, D. W. Dibb, A. E. Johnston, and T. J. Smyth. The contribution of commercial fertilizer nutrients to food production. *Agronomy Journal*, 97:1 – 6, 2005.
- [129] Supriya V. Tambwekar and M. Subrahmanyam. Photocatalytic generation of hydrogen from hydrogen sulfide: An energy bargain. *International Journal of Hydrogen Energy*, 22(10):959 – 965, 1997.
- [130] Abdulkadir Tanimu and Khalid Alhooshani. Advanced hydrodesulfurization catalysts: A review of design and synthesis. *Energy Fuels*, 33:2810 – 2838, 2019.
- [131] J. C. J. Thynne. Reactions of alkyl radicals. part 1. methyl radical photosensitized decomposition of ethyl formate. *Trans. Faraday Soc.*, 58:676–684, 1962.
- [132] Cammi R. Tomasi J., Mennucci B. Quantum mechanical continuum solvation models. *Chem. Rev.*, 8(105):2999–3093, 2005.
- [133] WC Trogler. Physical properties and mechanisms of formation of nitrous oxide. *Coordination Chemistry Reviews*, 187:303–327, JUN 1999.
- [134] A Trummal, L. Lipping, I. Kaljurand, I.A. Koppel, and I. Leito. Acidity of strong acids in water and dimethyl sulfoxide. *J. Phys. Chem. A.*, 120:3663–3669, 2016.
- [135] Turbomole GmbH. TURBOMOLE V6.2 2010, a development of University of Karlsruhe and Forschungszentrum Karlsruhe GmbH.
- [136] F Turecek, L. Brabec, T. Vondrak, V. Hanus, J. Hajicek, and Z. Havlas. Sulfenic acids in the gas phase. preparation, ionization energies and heats of formation of methane-, ethene-, ethyne- and benzenesulfenic acid. *Collect. Czech. Chem. Commun.*, 53:2140–2158, 1988.
- [137] Andrew A. Turnipseed, Stephen B. Barone, and A. R. Ravishankara. Reaction of OH with dimethyl sulfide. 2. products and mechanisms. *The Journal of Physical Chemistry*, 100(35):14703–14713, 1996.
- [138] Oystein Ulleberg and Ragnhild Hancke. Techno-economic calculations of small scale hydrogen supply systems for zero emission transport in norway. *Int. Jnl. of Hyd. Energy*, pages 1201 – 1211, 2020.

- [139] Peter J. Valdez, Vincent J. Tocco, and Phillip E. Savage. A general kinetic model for the hydrothermal liquefaction of microalgae. *Bioresource Technology*, 163:123–127, JUL 2014.
- [140] Leonardus Volkert van der Ham and Earl Lawrence Vincent Goetheer. Hydrogen sulfide conversion. Patent: EP 2883834, 05 2015.
- [141] Aaron G. Vandeputte, Maarten K. Sabbe, Marie-Francoise Reyniers, and Guy B. Marin. Modeling the gas-phase thermochemistry of organosulfur compounds. *Chemistry - A European Journal*, 17(27):7656–7673, 2011.
- [142] A. I. Vogel. *Practical Organic Chemistry*. 1978.
- [143] M.G. Voronkov, V.A. Klyuchnikov, S.N Kolabin, G.N. Shvets, P.I. Varusin, E.N. Deryagina, N.A. Korchevin, and S.I. Tsvetnitskaya. Thermochemical properties of dialkyl chalcogenides and dichalcogenides RMnR ($m =$ sulfur, selenium, tellurium; $n=1,2$). *Dokl. Akad. Nauk SSSR, Phys. Chem.*, 307(5):1139, 1989.
- [144] R. Walsh and S. W. Benson. Kinetics and mechanism of the gas phase reaction between iodine and isopropyl alcohol and the tertiary carbon-hydrogen bond strength in isopropyl alcohol. *Journal of the American Chemical Society*, 88(15):3480–3485, 1966.
- [145] Hui Wang. Hydrogen production from a chemical cycle of H_2S splitting. *Int. J. Hydrogen Energy*, 32:3907–3914, 2007.
- [146] Hui Wang, Ivo G. Dalla Lana, and Karl T. Chuang. Kinetics and oxidation of hydrogen sulfide by concentrated sulfuric acid. *Ind. Eng. Chem.*, 41:6656–6662, 2002.
- [147] Z. Wang, L. Wang, S. Chen, P. Zhang, J. Xu, and J. Chen. Decomposition of hydrogen iodide over Pt–Ir/C bimetallic catalyst. *Int. J. Hydrogen Energy*, 35(17):8862–8867, 2010.
- [148] Motonari Adachi Wataru Eguchi and Minoru Yoneda. Dependency of partition equilibrium of iodine between air and aqueous solution containing sodium hydroxide upon temperature and concentration. *Journal of Chemical Engineering of Japan*, 6(5):389–396, 1973.
- [149] F. Weigend and R. Ahlrichs. Balanced basis sets of split valence, triple zeta valence and quadruple zeta valence quality for h to rn: Design and assessment of accuracy. *Phys. Chem. Chem. Phys.*, 18(7):3297–3305, 2005.
- [150] Hans-Joachim Werner, Peter J. Knowles, Gerald Knizia, Frederick R. Manby, and Martin Schütz. Molpro: a general-purpose quantum chemistry program package. *Wiley Interdisciplinary Reviews: Computational Molecular Science*, 2(2):242–253, 2012.
- [151] Egon Wiberg and Arnold Frederick Holleman. *Inorganic Chemistry*. 2001.

- [152] J. Zaman and A. Chakma. Production of hydrogen and sulfur from hydrogen sulfide. *Fuel Processing Technology*, 41(2):159–198, January 1995.
- [153] Ke Zhang, Weiren Bao, Liping Chang, and Hui Wang. A review of recent researches on bunsen reaction for hydrogen production via si water and h₂s splitting cycles. *Journal of Energy Chemistry*, 33:46 – 58, 2019.
- [154] Peng Zhang, Nathan W. Yee, Sorin V. Filip, Casey E. Hetrick, Bin Yang, and William H. Green. Modeling study of the anti-knock tendency of substituted phenols as additives: an application of the reaction mechanism generator (RMG). *Phys. Chem. Chem. Phys.*, 20:10637–10649, 2018.
- [155] Y. Zhang, Z. Wang, J. Zhou, J. Liu, and K. Cen. Catalytic decomposition of hydrogen iodide over pre-treated Ni/CeO_2 catalysts for hydrogen production in the sulfur–iodine cycle. *Int. J. Hydrogen Energy*, 34(21):8792–8798, 2009.
- [156] Yanwei Zhang, Pingan Peng, Zhi Ying, Qiaoqiao Zhu, Junhu Zhou, Zhihua Wang, Jianzhong Liu, and Kefa Cen. Experimental investigation on multi-phase bunsen reaction in the thermochemical sulfur–iodine cycle. *Industrial & Engineering Chemistry Research*, 53(8):3021–3028, 2014.
- [157] Li Zhu and Joseph W. Bozzelli. Kinetics of the multichannel reaction of methanethiyl radical CH_3S with O_2 . *The Journal of Physical Chemistry A*, 110(21):6923–6937, 2006.
- [158] X. Zong, J. Han, B. Seger, H. Chen, G. Lu, C. Li, and L. Wang. An integrated photoelectrochemical-chemical loop for solar-driven overall splitting of hydrogen sulfide. *Angew. Chemie - Int. Edition*, 126:4488–4492, 2014.